

Crop load estimation in orchards: the potential of single RGB images from unmanned aerial vehicles

Chenglong Zhang



Propositions

1. Real-time orchard management tasks can be accomplished by the use of single raw images derived from unmanned aerial vehicles.
(this thesis)
2. Unmanned aerial vehicles are the key to establish orchard digital twins.
(this thesis)
3. A well-written introduction is already halfway to have a manuscript accepted by a scientific journal.
4. Business models should not steer sciences.
5. Robots should not have the attributes of a human-like appearance but need to maintain the characteristics of a functional machine.
6. Meditation and yoga can ease the negative emotions caused by the fast life pace but not solve them.

Propositions belonging to the thesis, entitled

Crop load estimation in orchards: the potential of single RGB images from unmanned aerial vehicles

Chenglong Zhang

Defence date 28 February 2024

Crop load estimation in orchards: the potential of single RGB images from unmanned aerial vehicles

Chenglong Zhang

Thesis committee

Promotor

Prof. Dr Lammert Kooistra

Personal chair at the Laboratory of Geo-information Science and Remote Sensing
Wageningen University & Research

Co-promotors

Prof. Dr Wensheng Wang

Professor, Agricultural Information Institute
Chinese Academy of Agriculture Science, Beijing, China

Dr Joao Valente

Assistant professor, Information Technology Group
Wageningen University & Research

Dr Leifeng Guo

Assistant professor, Agricultural Information Institute
Chinese Academy of Agriculture Science, Beijing, China

Other members

Prof. Dr Ricardo da Silva Torres, Wageningen University and Research

Dr Peter Lootens, Institute for Agricultural, Fisheries and Food Research, Merelbeke Belgium

Dr Mariana Belgiu, University of Twente, Enschede

Dr Alexandre Escolà Agustí, Universitat de Lleida, Spain

This research was conducted under the auspices of the C. T. de Wit Graduate School for Production Ecology and Resource Conservation (PE&RC).

Crop load estimation in orchards: the potential of single RGB images from unmanned aerial vehicles

Chenglong Zhang

Thesis

submitted in fulfillment of the requirements for the degree of doctor at Wageningen University

by the authority of the Rector Magnificus,

Prof. Dr A.P.J. Mol,

in the presence of the

Thesis Committee appointed by the Academic Board

to be defended in public

on Wednesday 28 February 2024

at 11 am in the Omnia Auditorium.

Chenglong Zhang

Crop load estimation in orchards: the potential of single RGB images from unmanned aerial vehicles,
242 pages.

PhD thesis, Wageningen University, Wageningen, the Netherlands (2023)


With references, with summary in English

ISBN: 978-94-6447-871-6

DOI: <https://doi.org/10.18174/637786>

Contents

Chapter 1 Introduction	2
Chapter 2 Orchard management with small unmanned aerial vehicles: a survey of sensing and analysis approaches	16
Chapter 3 Automatic flower cluster estimation in apple orchards using aerial and ground-based point clouds	64
Chapter 4 Feasibility assessment of tree-level flower intensity quantification from UAV RGB imagery: A triennial study in an apple orchard	96
Chapter 5 Orchard fruit load estimation in multi-temporal high-resolution UAV imagery using deep learning	134
Chapter 6 Synthesis	176
References	197
Summary	222
Acknowledgments	226
About the author	231
PE&RC Training and Education Statement	234

A large, stylized white letter 'I' is centered on a dark, textured, splattered background. The background consists of various shades of gray and black, with irregular, splattered edges and some small black dots scattered throughout. The letter 'I' is a simple, bold, sans-serif font with a slight curve at the top and bottom. The overall composition is high-contrast and abstract.

Chapter I

Introduction

1.1. Site-specific orchard management to advance sustainable agro-production

Agriculture maintains the function of providing sufficient food and nutrition for human beings. Confronting the projected 11.4 billion global population by 2050, the food demand, in global scenarios, is required to increase by 35% to 56% between 2010 and 2050 (Bebber and Gurr, 2015; van Dijk et al., 2021). Over the same period, -91% to +8% of the population at risk of hunger is expected. If natural resource constraints and climate change are taken into consideration, the projected situation will be more challenging for global food security.

Horticulture, *hortus and cultura* (garden culture), mainly hold the task of nutrition supply for humans and suffer comparable or even more challenges as other agricultural domains to ensure food security. It generally comprises ornamental plants like flowers and ornamental trees, and food plants like vegetables and fruits. These high-value crops are intensively cultivated in a small but well-designed space which is different from field crops like corn that are usually grown in an expansive field. Intensive and individualized crop management is the main characteristic of horticulture. Yet current horticultural practice still highly relies on manual efforts which are tedious and costly and the precision of decision-making is hard to guarantee (Zhang et al., 2021). Faced with global food security challenges, precise and automatic site-specific management of horticulture is greatly in demand.

Site-specific management requires decisions on the use of resources and the practical actions closely match the requirements of individual crops (Mendez-Vazquez et al., 2019). Consequently, the production of individual crops is maximized while conserving resources and mitigating environmental impacts. Orchards as a special horticultural section, in this context, should also implement site-specific management. Within a complete life-cycle of fruit trees, various activities are engaged. Within this time frame the fruit tree develops from flower buds, and flower clusters, to fruitlets and mature fruits, till tree dormancy period (Zhang et al., 2019a). Correspondingly, different actions are conducted for individual trees to sustain tree health for a respectable yield. As an example, during the blooming period only, diverse management activities have already been implemented. Firstly, it is crucial to quantify the flower cluster per tree to guide flower thinning. Excessive flower load may lead to harvested fruits like apples holding suboptimal sugar levels and even reduced storage life (Forshey, 1986). Growers need the exact flower cluster amount per tree to decide how many flowers to remove. On the other hand, a precise estimation of flower load on the tree also benefits the optimization of chemicals usage which is friendly to natural environments. Next, the flowering intensity crossing a whole orchard needs to be continuously monitored over a complete blooming season which usually lasts 2-3 weeks (Wang et al., 2021b). This information is used to identify the full blooming date (Zhou et al., 2023) and assist the growers to organize the upcoming activities at an earlier stage, such as pollination management (Chen et al., 2019a). In addition, spatio-temporal flowering monitoring also aids the breeding program.

However, currently, these management decisions are still banking on growers' empirical judgment. Though a few investigations have already explored potential solutions, in general, the resulting performance is still far from satisfactory (Tubau Comas et al., 2019; Vanbrabant et al., 2020a).

Orchard management, during the harvesting period, retains a major part of the total cost. For example, in the case of citrus production, it can reach 35%-45% of the total cost which reveals the importance of optimizing the current harvesting chain (Sanders, 2005). In the early stage of fruit maturation, fruit counts per tree primarily benefit from the management of irrigation, fertilization and variable spraying strategy (Bargoti and Underwood, 2016; Wang and He, 2021). At a more advanced maturation stage, yield estimation supports market-related decision-making and logistics optimization, such as labor force and harvest containers (Xia et al., 2022). Both stages require precise information on the fruit-bearing status of individual trees for the optimization of resource usage like labor, water and chemicals. Moreover, a variety of other management activities is also duty-bound to be employed throughout the whole growing season. To track the growth of fruit trees and evaluate the effects of different pruning strategies, geometric characteristics such as canopy volume and tree height need to be measured (Ganz et al., 2019). This is also the central difference between orchards and other horticultural crops like strawberries (Chen et al., 2019b). As fruit and nut trees in orchards hold a more complicated tree structure which leads to additional data demand in the 3-dimensional (3D) space. Monitoring water stress of individual trees directs precision irrigation (Ballester et al., 2018). While the inspection of fruit-tree nutrition status (Garza et al., 2020) and diagnosis of the potential disease (Choosumrong et al., 2023) are necessary to keep the orchard sustainable. In summary, multiple aspects of fruit and nut trees (e.g., physical and biological characteristics) impact and steer decision-making in orchards which discloses the urgency of automatic and precise monitoring.

1.2. UAVs are reforming site-specific orchard management

Since the projection that unmanned aerial vehicles (UAVs) were poised to depart as powerful platforms for scientific research (Marris, 2013), the use of UAVs in supporting orchard management has been progressively investigated in the past decade (Lucena et al., 2022; Yuan et al., 2023). Sensor miniaturization is also increasing UAVs popularity in terms of the diversity of data sources, the quality of sensing data, and the efficiency of data collection. Recent studies indicate that UAVs would be indispensable in horticultural (Vinci et al., 2023) and other agricultural applications (Liu et al., 2023).

Orchard sensing data, in the data-driven age, is normally produced by ground-based (Tsoulas et al., 2023), aerial (Tang et al., 2023) and space-based monitoring platforms (Sandonis-Pozo et al., 2022) which construct a complete space-air-ground observation network. Distance between the target fruit trees and cameras onboard these platforms are dissimilar, and thus, this distance difference further

creates orchard data with various resolutions. On the other hand, the difference among the running tracks of these platforms makes them desirable in different survey scales. For these two aspects, each one of the orchard monitoring platforms is dominant in certain application scenarios (Zhang et al., 2021).

Handheld cameras are one of the earliest emerging inspection platforms in the orchards (Srivastava and Sadistap, 2018). Device portability, ease of use and high-resolution make it a strong sensing approach. Rapid development in the smartphone industry limits handheld cameras to RGB sensors. With the extremely high-resolution RGB images, the adjustable distance between the camera and target fruit trees enable this approach to capture the entire tree structure for tree height calculation and on-tree fruit detection (Zhao et al., 2023b), and to diagnose fruit disease like scab and rust with a zoom-in camera view (Ozden, 2021). However, the methods developed from handheld cameras, in some cases, are unrepeatable because of uncertainties derived from different sensing distances (Xia et al., 2022). Another widely used terrestrial monitoring system is ground vehicles. Compared with handheld cameras, one ground vehicle is capable to carry multiple sensors like RGB (Koirala et al., 2020a) and multispectral cameras providing orchard data derived from abundant spectral segments. Thus this sensing approach holds a wider range of applications. For example, ground vehicles with RGB-D cameras (Gene-Mola et al., 2019b) or a laser scanner have been applied for apple detection (Gene-Mola et al., 2019a). Fruit shape like apple diameter is also feasible when LiDAR was employed (Tsoulas et al., 2020). Ground vehicle-based sensing platforms are more efficient in data collection than handheld approaches and the data quality is more unified. However, overall, observational terrestrial systems are labor-intensive which is greatly time- and labor-cost for time-series orchard data. And they are more feasible for small size orchard monitoring. Current advancements in robotic automation still cannot fully meet the requirements of unmanned ground self-driving vehicles in modern orchards (Lyu et al., 2018). And the complex environment in modern high-density orchards (Zine-El-Abidine et al., 2021) makes it more challenging. In addition, though these terrestrial systems are regarded as non-destructive sensing approaches (Srivastava and Sadistap, 2018), they are only non-destructive for the surveyed fruit trees. The effects derived from the operators and vehicles on the orchard like the soil are an attention point.

Conventional remote sensing mainly comprises airborne and satellite-based observations. Airborne imaging holds a relatively comparable resolution to that of the terrestrial systems but it is more powerful for large-size orchards and regional surveys. For example, an area of 17 ha can be mapped in 0.5 h with an airborne platform (Garcia-Ruiz et al., 2013). Flying altitude of airborne platforms can reach 1km which takes into account the image resolution while improving sensing efficiency (Sepulcre-Canto et al., 2007). This characteristic enables airborne platforms to survey not only orchards but the surrounding landscape like forests as well (Hycza and Kupidura, 2021). Similar to the capability of ground vehicles, airborne platforms equipped with multiple sensors are feasible in fruit quality estimation (e.g., peach

and olive water content) (Sepulcre-Canto et al., 2007), fruit disease detection (e.g., the Huanglongbing in citrus production) (Garcia-Ruiz et al., 2013) and water stress monitoring by using time-series data of photochemical reflectance index (PRI) (Suarez et al., 2010). Yet constraints related to data accessibility, platform availability and weather conditions result that airborne observation is uncommon in operational orchard management.

By contrast, the public availability of satellite images makes space-based observations also practicable in supporting orchard monitoring. Satellite images embrace mainly optical multi-spectral images which would allow the physical characterization of the temporal development of fruit trees feasible. For example, Sentinel-2 derived vegetation indices like normalized difference vegetation index (NDVI) and the green normalized difference vegetation index (GNDVI) can be applied for almond-tree geometric characteristics estimation such as width and cross-sectional area (Sandonis-Pozo et al., 2022). The canopy chlorophyll content index (CCCI) produced by WorldView-2 is feasible for macadamia leaf nitrogen estimation and can further assist variable fertilizer spraying (Felderhof and Gillieson, 2011). In addition, the planting year of apple orchard (Zhu et al., 2020), kiwifruit dry matter content estimation (Mills et al., 2019) and water stress monitoring (Van Beek et al., 2013) has also been predicted by space-based multispectral imagery. This type of approach is powerful in regional, national (Brinkhoff and Robson, 2020) or even continental-level orchard-related monitoring. Its disadvantage can be suboptimal spatial and spectral resolutions, and an unfavorable re-visit time. With the increasing spatial resolution of images from satellite-based platforms (e.g., satellites from Maxar Technologies and Planet Labs), space-based observations are becoming a viable complementary source for orchard management.

UAVs, as relatively new sensing platforms, have been proven a dominant and complementary tool in the space-air-ground orchard observation network that was introduced above (Zhang et al., 2021). It integrates the high-resolution characteristic of proximal terrestrial sensing systems and the spatial-temporal mapping efficiency of airborne and space-based observations. Its capability of employing various optical cameras makes it fast expanding to diverse orchard application scenarios ranging from resource efficiency monitoring (Ballester et al., 2018), to yield estimation (Tang et al., 2023) and disease detection (Ali et al., 2023), and to fruit-tree geometric characteristics calculation (Vinci et al., 2023).

Extensive research induced the UAVs equipped with RGB cameras to be the most prevailing in orchard management (Zhang et al., 2019a). There are, in general, three ways that have been incorporated into the analysis of the geotagged RGB images. The first one is direct use which means image processing is conducted on the raw images directly. This approach mostly is suitable for on-tree fruit load detection by using advanced object detection algorithms. For example, it can be used for yield estimation of the late-autumn shoots of litchi (Liang et al., 2023) and pear (Li et al., 2023b). Since the UAVs were fully manual-controlled during the flights and usually the flying altitude is low, such as less than 9m. The

resulting performance normally was high, for instance, the correlation between the deep learning algorithm YOLOv4 detected chestnut burs and the ground truth collected in situ can reach an R^2 of 0.83 (Arakawa et al., 2023).

The other two ways of RGB image analysis were on the basis of the structure from motion (SfM) technique. The SfM-derived methods retrieved the nadir-view and 3D structure of fruit trees by producing orthomosaics and colored point clouds. With RGB orthomosaics, projected canopy area, potential fruit tree location and counting can be detected with object detection methods like Faster-RCNN (Neupane et al., 2019). While colored point clouds are well-known for the geometric characteristics calculation, such as canopy volume (Jimenez-Brenes et al., 2017), canopy perimeter and area (Johansen et al., 2018). Its main advantage is the reconstructed 3D information and, in comparison with LiDAR point clouds, unique color information. In summary, the introduced RGB image-based methods are affected by illumination conditions, and the orthomosaic and colored point clouds normally require certain computational sources for reconstruction.

Multispectral cameras are the other more general UAV-equipped sensor adopted in orchard management. With the aid of additional spectral bands compared to RGB imagery like red-edge (RE) and near-infrared (NIR) (Catania et al., 2023), aerial multispectral imaging has a wider range of applications. The produced spectral indices are capable to accomplish monitoring tasks like production (Chen et al., 2019a) and water stress estimation (Zhao et al., 2017), and disease detection (Pourazar et al., 2019). For instance, the aerial modified ratio vegetation index (RVI) was proven to be most sensitive to apple fire blight (Mahmud et al., 2023). Applied methods, in general, are based on the correlation between aerial vegetation indices and the pre-measured biological status like stem water potential and stomatal conductance. With high-resolution multispectral images, in addition, geometric traits like canopy area can also be calculated from orthomosaics (Catania et al., 2023). Compared to multispectral cameras, hyperspectral and thermal cameras have drawn much less attention in assisting UAVs for orchard management. Aerial thermal imagery is mostly used for water stress monitoring since temperature correlates to the photosynthesis of fruit trees and affects the stomatal conductance directly (Egea et al., 2017; Ortega-Farías et al., 2016). Regarding hyperspectral cameras, the complexity of spectral analysis and high-cost traits severely limit their application in orchards. But they provide continuous spectra covering a large part of the optical range. This makes hyperspectral advantageous in the diagnosis of serious fruit diseases like Huanglongbing in citrus (Garcia-Ruiz et al., 2013).

LiDAR is the last widely used sensor for UAVs in supporting orchard management (Tsoulias et al., 2023; Zhang et al., 2021). Recent development in the miniaturization and lightweight of LiDAR enable UAV-based LiDAR measurements to become popular. It contributes to the precise delineation of fruit-tree geometric traits like crown volume and main trunk (Lombardi et al., 2022) because of the high-

density point clouds, in comparison with colored point clouds. And LiDAR-derived point clouds are not affected by illumination conditions. Currently, more and more comparisons between aerial LiDAR- and RGB images-based point clouds were conducted (Ganz et al., 2019; Lombardi et al., 2022). It reveals that the use of point clouds in orchards is already moving toward data source optimization. In a nutshell, with the last piece (LiDAR) of the puzzle (UAV-derived orchard management) complete, it is believed that the use of UAVs will reform orchard management in the near future.

1.3. Opportunities of UAVs in crop load estimation

Crop load initially is an industrial parameter defined as fruits per trunk cross-sectional area (Racskó, 2006). Later it was extended to a broader denotation – quantifying the number of fruits per tree (Gongal et al., 2016; Suo et al., 2016). In this thesis, crop load comprises the number of flowers per fruit tree (flower load) and the number or weight of fruits per tree (fruit load).

Crop load estimation is fundamental in orchard management as this information directly correlates to the harvested yield and its quality. Fruit load estimation benefits the decision-making for the market. Yet fruit yield at row level or plot level can also contribute to this purpose. By contrast, flower load estimation holds a more strict standard for accuracy. Because this information guides the flower thinning, and the operators, either a thinning robot or a technician, need this estimation to quantify the exact number of flowers required to be removed for individual trees (Zhang et al., 2022b).

Traditional fruit load estimation is conducted in an indirect way. It explores the correlation between optical sensor-derived indices and the exact yield harvested or recorded in the field. These indices consist of Vegetation indices (VI) and fruit-tree geometric characteristics. For example, the NDVI derived from UAVs can be used for banana yield estimation (Machovina et al., 2016). Yet, the correlation of these indices to the fruit amount is poorly understood. Investigated geometric characteristics comprise canopy projected area (CPA) (Sola-Guirado et al., 2017), tree height (Sarron et al., 2018a) and canopy perimeter (Uribeetxebarria et al., 2019). 3D morphological characteristics such as crown volume can also be good yield predictors (Lopez-Granados et al., 2019b). The correlation of estimated crown volume from aerial imagery to actual yield can be higher than 0.7 (R^2) for some almond varieties. In addition, VI and geometric traits can also be combined for a yield model development using methods like ensemble learning (Chen et al., 2022b).

Fruit yield, in orchards, correlates to the exact fruit number and size (Mitchell, 1986; Stajanko et al., 2009b). Thus, fruit counting is a potential approach to provide more accurate yield estimation than traditional methods. From current achievements of robotics and sensing approaches, however, it is impossible to automatically obtain the exact fruit or flower load. Because fruit trees suffer heavily from

occlusion produced by leaves, branches and other fruits (Zine-El-Abidine et al., 2021). Even so, it is believed that the flower or fruit counting derived from the external feature of fruit trees highly correlates to the actual yield and can be regarded as a yield indicator (Apolo-Apolo et al., 2020b).

Advances of object detection in computer vision community make fruit or flower amount can be well quantified in the images. Conventional object detection is mostly conducted at pixel level. Color thresholding is the most famous (Horton et al., 2017). Yet it is significantly affected by illumination conditions. More advanced machine learning methods are support vector machines (SVM) (Dias et al., 2018b), clustering methods (Tubau Comas et al., 2019) and convolutional neural networks (Dias et al., 2018a). Such approaches, in the case of CNN combined with SVM, can reach a precision and recall rates of 90%. By contrast, object-based deep learning algorithms are proven to be the most powerful. It generally comprises one-stage detectors and two-stage detectors. Algorithms like fast R-CNN, faster R-CNN (Fu et al., 2020) and mask R-CNN (Jia et al., 2022) are two-stage detectors. They normally hold more accurate fruit detections than one-stage detector but are more time-consuming. Lightweight one-stage detectors such as single shot multibox detector (SSD), YOLO series (Li et al., 2023b; Zhang et al., 2022d) and RetinaNet have drawn more attention in fruit and flower detections. These achievements, in general, were based on terrestrial images. But they are transferable to the use of RGB images derived from UAVs. Yet, the variability of fruit size and shape in UAV images can be challenging. In addition, previous studies demonstrated fruit or fruit flower counting at image level only which means those algorithms only recognize the number of visible fruits in the image (Liu et al., 2021). The link between these detections to the actual fruit count in the field is still not fully investigated. A few studies used terrestrial sensing approaches like ground vehicles and handheld cameras to build up this link. Yet strict manual control was involved either during the data collection stage or the postponed data processing. In the first case, the purpose was to ensure each image covered one tree (Hocevar et al., 2014). While, in the later, manual segmentation was applied for individual trees. From this aspect, the geotagged RGB images derived from UAVs potentially provide a good solution for crop load estimation.

1.4. Underlying problems and motivations for the use of UAVs in orchard management

The use of UAVs in supporting orchard management is still in its infancy but it has been receiving considerable attention (Zhang et al., 2019b). It is crucial, in this context, to conduct a systematic analysis for the identification of current achievements and research gaps, and for searching potential opportunities. In application scenarios, unbalanced development in various orchard-related fields was observed. As an example, the monitoring of water stress (Ballester et al., 2018; Zhao et al., 2017) and the calculation of fruit-tree geometric characteristics (Sun et al., 2019; Tu et al., 2019) have been investigated by extensive research. Yet yield estimation and disease detection should also be given more attention. From a methodology aspect, the majority of current practices applied a single method to

survey one single fruit species under certain environmental and weather conditions (Hobart et al., 2020; Osco et al., 2020b). It is essential to explore the generalization or scalability of these methods which enhance the recognition of an optimal and robust UAV-based solution. In addition, because of the unique way of UAV-derived sensing, the effects of different flying parameters on monitoring performance are also one of the most frequently stated questions (Hou et al., 2019; Meng et al., 2020). Overall, a systematic field campaign design or a systematic review is required at the current stage.

UAVs were introduced to the space-air-ground orchard monitoring network at a relatively late phase. Though high accuracy of UAV-derived predictions was demonstrated by broad studies (Vélez et al., 2023; Vinci et al., 2023), for a specific case, the fair comparison between UAV- and other platform-based performance was still not fully answered. The complexity of orchard circumstances (Zine-El-Abidine et al., 2021), the unevenness of data quality produced by different monitoring platforms and variability of adopted methods lead to a poor understanding of the pros and cons of each individual system in the space-air-ground network. Thus, with consistent settings of these aspects, a systematic comparison is suggested. For example, it is essential to identify the difference in disease detection derived from UAVs (Ali et al., 2023) and ground-based platforms (Bleasdale et al., 2022) to recognize the optimal solution. Moreover, terrestrial colored point clouds were capable of in-situ apple detection (Gené-Mola et al., 2020). In a same scene, the performance of aerial colored point clouds in apple detection also needs to be examined.

Existing orchard monitoring produced by UAVs mostly focuses on tree-level predictions where individual trees are regarded as the minimum units, such as the identification of disease-infected trees (Selvaraj et al., 2020), the counting of trees (Osco et al., 2020b) and the canopy volume of individual trees. This meets the requirement of site-specific management. Such approaches, however, have failed to monitor the intra-canopy information like flower and fruit amount. Current achievements, in computer vision community, are proven potent in fruit detection using advanced deep learning algorithms (Zhao et al., 2023b). The performance of fruit load estimation derived from ground vehicles is already satisfactory. For example, rotational region CNN can produce an F1-score of 82% for on-tree mango panicle classification (Koirala et al., 2020c). Yet this knowledge has not been fully transferred to UAV-based aerial images for orchard management. Though flower load estimation can be conducted with RGB-derived orthophoto, it was confirmed that information from nadir-view canopy only is not sufficient (Tubau Comas et al., 2019). Raw UAV RGB images comprise both the nadir-view and side-view of fruit trees which are a potential source for crop load estimation. But its performance is still unclear. One reason can be the heavy fruit occlusion found in UAV images due to the aerial camera view. Overall, further research should be carried out to test the feasibility of aerial images-based crop load estimation.

Individual tree identification is fundamental for orchard spatial mapping. Each of the introduced orchard applications requires this information to further achieve tree-level analysis. Previous research mainly established tree detection methods for orthomosaic-based applications (Šandric et al., 2022; Vélez et al., 2023). Yet, the complexity of modern high-density orchards limits the adoption of computer vision technology. For example, the tree space in a modern orchard can reach 1 m which induces fruit trees in the same row to suffer the issue of interlacing and touching branches (Zhang et al., 2022b). This complicated situation within a row further makes the segmentation or even identification of individual trees impossible. This relates to both orthomosaics (Apolo-Apolo et al., 2020b) and point clouds (Zine-El-Abidine et al., 2021). To enhance the use of UAVs in site-specific orchard management, therefore, there is an urgent need to establish a new approach to solve individual tree identification problems.

1.5. Research objectives

The main objective of this thesis is to optimize the use of single raw aerial RGB image source to enhance UAV application in monitoring agricultural production which is required to make management decisions, especially in horticulture. To identify the research gaps and examine the potential technologies of UAVs in orchard management, current status of UAV-derived practice was first reviewed (RQ1). Inevitably, the core focus was determined as crop load estimation in an apple orchard which comprises apple flower intensity estimation and yield estimation. Next, as a benchmark, conventional photogrammetric measurement (structure from motion (SfM)) was applied to UAV- and ground-based images to evaluate the potential of colored point clouds in flower intensity estimation (RQ2). For comparison, the feasibility of estimating flower intensity with single raw UAV images was evaluated (RQ3). Finally, the use of single raw aerial RGB images was further examined and optimized in another other orchard application - apple yield mapping (RQ4).

RQ1: What are the research gaps and opportunities of UAV-derived monitoring in orchard management?

RQ2: How can apple flower load be spatially mapped from UAV-based colored point clouds?

RQ3: What is the feasibility of estimating the spatial distribution of flower load in apple orchards with single raw UAV images only?

RQ4: How can a deep learning approach using single raw UAV images support the automatization of apple yield spatial mapping?

1.6. Thesis outline

Taking the underlying problems identified in section 1.4 as starting points, and to further investigate the use of UAVs in orchard management, the present thesis was organized as follows:

Chapter 2: A comprehensive literature review was conducted firstly to identify the current status of UAVs in orchard management. Opportunities of UAVs were investigated by searching research gaps and examining the potential technologies.

Chapter 3: In the case study of apple flowering intensity estimation, the performance of a conventional UAV photogrammetry method, based on colored point cloud, was evaluated and taken as a benchmark. Its performance against ground vehicle-derived point clouds was also compared and discussed.

Chapter 4: In comparison with the benchmark established in Chapter 3, the feasibility of flower load estimation with single raw aerial images was examined first. Next, the effects of vertical (nadir) and horizontal (angular) overlapping of flower clusters within the canopy were investigated.

Chapter 5: To further improve the single raw UAV RGB images-based methods demonstrated in Chapter 4, an automatic fruit load estimation method was developed. The performance of YOLOv5s in aerial image-based fruit detection was tested. And fruit load estimation was accomplished by using a proposed pixel-geolocate method.

Chapter 6: Finally, the main findings of the present thesis were discussed. Based on these findings, projections for future research were also made, in parallel with the latest research that is relevant to this thesis project.



A large, stylized white number '2' is centered on a dark, textured, ink-like background. The background consists of various shades of gray and black, with a rough, splattered appearance, suggesting a watercolor or ink wash effect. The number '2' is a simple, clean, sans-serif font, standing out prominently against the dark, mottled background.

2

Chapter 2

Orchard management with small unmanned aerial vehicles: a survey of sensing and analysis approaches

This chapter is based on:

Zhang, C., Valente, J., Kooistra, L., Guo, L., Wang, W., 2021. Orchard management with small unmanned aerial vehicles: A survey of sensing and analysis approaches. *Precision Agriculture* 22, 2007-2052.

Abstract

Advances in sensor miniaturization are increasing the global popularity of unmanned aerial vehicle (UAV)-based remote sensing applications in many domains of agriculture. Fruit orchards (the source of the fruit industry chain) require site-specific or even individual-tree-specific management throughout the growing season – from flowering, fruitlet development, ripening, and harvest – to tree dormancy. The recent increase in research on deploying UAV in orchard management has yielded new insights but challenges relating to determining the optimal approach (e.g., image-processing methods) are hampering widespread adoption, largely because there is no standard workflow for the application of UAVs in orchard management. This chapter provides a comprehensive literature review focused on UAV-based orchard management: the survey includes achievements to date and shortcomings to be addressed. Sensing system architecture focusing on UAVs and sensors is summarized. Then up-to-date applications supported by UAVs in orchard management are described, focusing on the diversity of data-processing techniques, including monitoring efficiency and accuracy. With the goal of identifying the gaps and examining the opportunities for UAV-based orchard management, this chapter also discusses the performance of emerging technologies and compare similar research providing technical and comprehensive support for the further exploitation of UAVs and a revolution in orchard management.

2.1. Introduction

Faced with the challenges of a growing global population, rural poverty, and natural resource management, public awareness about sustainable practices in food production has become prominent. Food productivity, e.g., in fruit crops, and the economics of cultivation and irrigated agriculture are important topics in precision agriculture that relate to these challenges. In the case of fruit orchard management, the challenges also concern processes. Within the context of precision agriculture, site-specific management is key to reducing environmental impact and enhancing agricultural economics. Such management includes the general stages of collecting data, mapping orchard variability, and making decisions (Zhang and Kovacs, 2012) and enables each aspect of crop cultivation (e.g., physical, biological, chemical factors) to be understood.

Throughout the growing cycle of fruit crops, a variety of management activities are employed (Fig. 2.1). Different activities focus on the management of fruit trees at specific growth stages, and some activities are not limited to one growth stage. For instance, thinning generally occurs during the flowering and fruitlet stages. The management activities attracting most research attention have been fruit thinning, fruit-tree pruning, and the assessment of irrigation strategy. Apple-flower number strongly correlates with the final yield (Aggelopoulou et al., 2009). Improving fruit size and quality will bring more economic benefits because of the higher market prices (Bound, 2018). However, without precise management, an excessive number of flowers per tree might lead to poor fruit quality and size. Overload of fruits also threatens the trees (Dennis, 2000). For example, only 7% of apple flowers are necessary for final harvest, which means that flower thinning should be conducted regularly (Greene and Costa, 2013). In some cases, manual thinning represents 31% of all cultural costs (costs of activities carried out during an entire fruit-tree growing cycle) (Glozer and Hasey, 2006). Though mechanical thinning effectively reduces labor input, the bottleneck is the precise estimation related to flower intensity. Changes in fruit-tree structural properties can be used to monitor tree crop growth status, and site-specific treatments with fungicides and water can be implemented with the aid of a spatial structural variation map (Mu et al., 2018). Fruit tree physical structure, such as canopy volume, affects fruit quality and yield by intercepting light (Rom, 1991). Trees in fruit orchards are therefore pruned at certain fruit-growing stages, following a pruning strategy. Geometric characteristics like canopy area are the main way of assessing the pruning effects. By measuring this parameter, optimal pruning type and intensity can be selected and applied, to help guarantee the final income of local growers (Castillo-Ruiz et al., 2015; Miranda-Fuentes et al., 2015). In addition, because of the global water shortage, agricultural irrigation is a relevant topic. In the context of deficit irrigation, the water inputs for orchards should meet the realistic demands of individual fruit trees. Mild water stress is often employed to maintain or improve fruit quality and yield in orchards. Thus, to optimize water resources usage, appropriate monitoring is necessary. In summary, projecting into the future, precision orchard management not only

saves labor resources and increases the income of growers, but also has great significance in improving resource utilization.

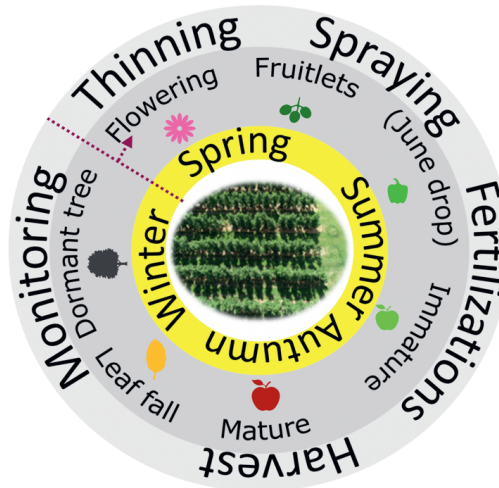


Fig. 2.1. Natural yearly cycle of fruit crops and associated management activities (outer ring) during the seasons of a year (yellow ring).

Broadly, remote sensing (RS) describes a group of techniques that from a distance collect sensor data on the target of interest. This involves sensing, recording, processing, analyzing, and applying reflected or emitted energy by employing various sensing devices, such as imaging sensors, radar, and sonar and satellite sensor arrays (Usha and Singh, 2013). Recently, a considerable amount of research has demonstrated the applicability of RS in orchard management for processing the data derived from various platforms (Barbagallo et al., 2009; Garcia-Ruiz et al., 2013; Salgadoe et al., 2018). The methods, which vary according to monitoring scale, are manual observation (MO), handheld detection (HD), sensor networks (SN), ground vehicle (GV), unmanned aerial vehicles (UAVs), aerial sensing (AS), and spectral satellite sensing (SSS). These methods can be adopted for data collection relating to specific orchard management activities (e.g. thinning assessment, spraying, disease detection and yield estimation and prediction) throughout the whole fruit-trees growing cycle. Each monitoring method has its own pros and cons, depending on the application scenarios (Table 2.1) (Dias et al., 2018a; Shakoore et al., 2017). Although tedious, visual assessment of a limited number of trees, is the basis of a relatively accurate management strategy that depends on manual efforts to achieve the assessments (Sarron et al., 2018a). Handheld detection has a similar detection range, it can provide a more accurate evaluation, and requires less expertise on fruit-tree growing on the part of the operator (Aggelopoulou et al., 2010). Compared with these two monitoring methods, ground vehicle platforms are more efficient, and extensive research on these has been conducted in the domain of orchard management (Colaco et al., 2018; Escolà et al., 2016; Wang et al., 2018a).



All three methods mentioned above are employed at ground level, and their major advantage is the quality of datasets collected – i.e., due to the close sensing distance, high-resolution data are easily accessed. However, it has now been well established in a variety of studies that remote sensing technology is of great interest within orchard management, especially when it comes to the monitoring scale and data acquisition efficiency (Salamí et al., 2019; Sola-Guirado et al., 2017; Tu et al., 2018). Conventional remote sensing technology, aerial sensing, and spectral satellite sensing have been applied in orchard management, with promising performance. However, all are limited by weather conditions and monitoring costs (Calderon et al., 2013; Panda et al., 2010). In addition, spectral satellite sensing is also limited by the lack of imagery with optimum spatial and spectral resolutions, and an unfavorable re-visit time (Berni et al., 2009b).

Table 2.1.

Relevant monitoring methods for fruit orchard management and their attributes*.

Attributes	MO	HD	SN	GV	UAVs	AS	SSS
Scale	+/++	+	+/++	+/++	+/+++	+/+++	+/+++
Sensor Payload Size		+	+/++	+/+++	+	+++	+++
Autonomous		✘	✓	✘	✘	✘	✓
Data Post-Processing Level		+	++	++	++	++	+++
Platform Accessibility	+++	++	++	++	+++	++	+/++

* - The qualification scale +, ++ and +++ represent “small, medium, and large”, or “light, moderate and high”, respectively. Symbols “✓” and “✘” represent automated and non-automated, respectively. Methods: manual observation (MO), handheld detection (HD), sensor network (SN), ground vehicle (GV), unmanned aerial vehicles (UAVs), aerial sensing (AS), spectral satellite sensing (SSS).

Thanks to recent advances in sensor miniaturization, UAVs have become increasingly available to meet the need for quick and real-time monitoring turnaround times for orchard management at usable spatial, spectral, and temporal resolutions (Berni et al., 2009a; Caruso et al., 2019; Torres-Sanchez et al., 2018b; Valente et al., 2019). Thermal sensors, multispectral sensors, and light detection and ranging (LiDAR) systems are data acquisition resources for the direct monitoring of fruit trees. However, there are various factors to consider when choosing a UAV to carry these sensors and achieve the required time frequency and spatial resolution for orchard management. Ground-based platforms are difficult to transport from

one location to another, and it may not be easy to generate field maps in real time. These limitations can be overcome by using a suitable UAV to obtain data with the required time frequency and spatial resolution (Campos et al., 2019; Matese et al., 2019). Compared with satellite-based remote sensing, using UAVs for monitoring is less dependent on weather conditions. For the monitoring of regions covered by significant cloud, UAV yielded a data-acquisition probability of 45-70%, while the probability based on satellite was around 20% (van der Wal et al., 2013). UAVs have been found to have many other advantages: they can be deployed in high-risk situations, data acquisition is fast, and images are geo-referenced (Handique et al., 2017; Saldana Ochoa and Guo, 2019). The limitations of UAVs are the battery life and operational speed. Battery life enables UAVs to operate in relatively small or medium-sized orchards. Their operational speed is lower than that of manned airborne platforms (Garcia-Ruiz et al., 2013). In order to collect data of high quality, a good balance between flying speed and data quality should be maintained during data collection.

Given the increasing need for site-specific and precise management information in orchards, the current status of UAV-based monitoring activities and research, and the potential opportunities for new applications and technologies, this chapter aims to: (1) provide a detailed overview of the state of art, including UAV types, sensor types, and the analysis methodologies that have been applied, (2) identify the research gaps for fruit orchard management applications by evaluating and comparing relevant research, and (3) examine the potential technologies of UAVs for achieving precision orchard management. The hypothesis of this study is that the use of UAVs in orchard management is in its early stage and not widely investigated yet. Recent publications can provide insights in common methods and future points for development. The study is divided into three main sections. The section 'Selection and analysis of the reviewed papers' describes the review and analysis approach which was adopted. Next, the results section provides a detailed description of the selected literature sources using the application of UAV based monitoring approaches for orchard management as starting point, and comparing aspects related to UAV systems, camera types, analysis approaches and management indicators among literature sources. The last section, summarizes latest developments, discusses main research gaps and provides recommendations for further investigation on UAV-based acquisition approaches and orchard management oriented analysis methods.

2.2. Selection and analysis of the reviewed papers

For this review, 84 related papers from the Web of Science (WoS) database either published or available online before 1st January 2020 were found and evaluated using keyword combinations (Fig. 2.2). The reproducible review approach in this study is comparable to previous approaches (Leroux and Tisseyre, 2019; Pathak et al., 2019) but does not follow the strict criteria (e.g., meta-analysis) of other systematic review methods (Methley et al., 2014). Although for a selection of papers a quantitative comparison

was made in this study, a complete meta-analysis could not be made because the adopted experimental designs in the studies differed too much to allow pooling of results. In order to make a sharp analysis and to avoid non reviewed references (or inaccurate information), the analysis of literature only considered scientific studies that received external review as are covered within the WoS database. This motivation is in light that the WoS core collection has been used officially by organizations as a quality standard for longer time and provides weekly updates (Falagas et al., 2008). The database of Web of Science Core Collection, which is composed of four citation indexes (Science Citation Index Expanded (SCI-EXPANDED), Social Sciences Citation Index (SSCI), Arts & Humanities Citation Index (A&HCI), and Emerging Sources Citation Index (ESCI)), was selected. The internal WoS search function was adopted to cover the following searching fields: the title, abstract, author keywords and Keywords Plus of each record. Timespan, language, and searching model were set for 1945-2019, English and basic search, respectively. The search string consists of two components, “monitoring platforms” and “monitored objects”, which were combined with AND:

- (1) Monitoring platforms (UAV OR unmanned aerial vehicle OR UAS OR unmanned aerial system OR remotely piloted aircraft systems OR drone)
AND
- (2) Monitored objects (orchard* OR fruit trees OR fruit crops OR pome fruits OR stone fruits OR apple OR citrus OR orange OR mandarin OR lemon OR olive OR pear OR almond OR peach OR banana OR mango OR apricot OR chestnut OR nectarine OR lychee OR coconut OR persimmon OR kiwi fruit OR avocado OR apricot)

As noted in component (2), specific fruit species were explicitly included to ensure that the survey would not miss any related research. This search function totally generated 155 articles, which were further examined. The survey focused on the orchards planted with fruit trees such as apple, citrus, or olive. As orchards can be broadly defined as the cultivation for commercial food production of fruit crops growing as shrubs of a size between herbaceous plants and trees, or as trees, the search also yielded a considerable amount of literature on UAV-based investigation in vineyard crops (de Castro et al., 2018; Di Gennaro et al., 2019; Jimenez-Brenes et al., 2019; Matese et al., 2019; Pichon et al., 2019). But grapes fall into the category of climbing shrubs, which differ significantly biologically and geometrically from the fruit trees which form the focus of this study, so they were discarded. Similarly, articles focus on watermelon, blueberry, tomatoes, macadamia and coffee were also discarded. After removing other irrelevant ones, 80 articles remained. Among the 80 articles, one article is a meeting abstract and was discard as well (Garza et al. 2018), because not all information can be extracted. Besides these 79 articles, 4 relevant articles cited by the ones among this 79 articles were found and added to the survey (Berni et al., 2009b; Ishida et al., 2018; Torres-Sanchez et al., 2015; Zarco-Tejada

et al., 2013). One article was actually published in 2019 but its publication year in WoS system was 2020 (Martinez-Guanter et al., 2019). It was also included.

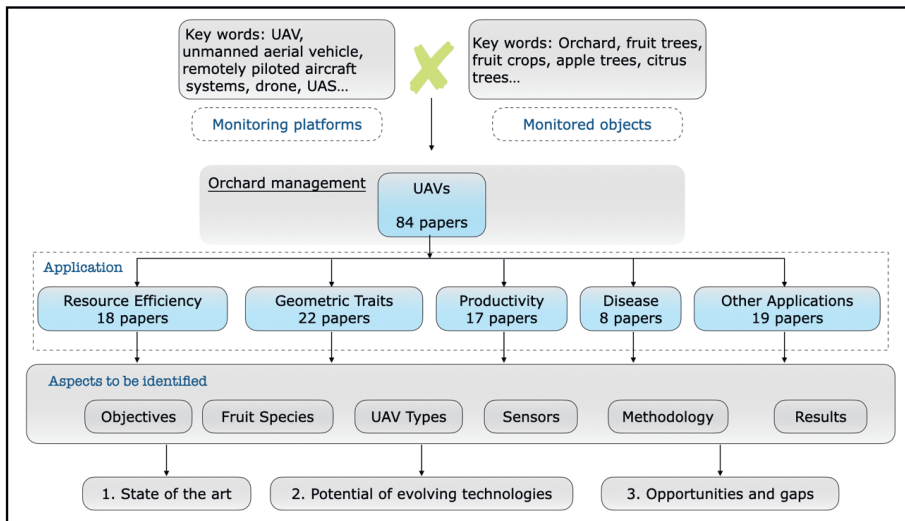


Fig. 2.2. Overview of the criteria and categories investigated for the papers (84 in total) selected from the Web of Science for the survey.

For every paper, specifications of the study (e.g., sensors applied, study regions) were derived and compared (Fig. 2. 2). First, the selected papers were classified into five categories on the basis of their main focus: resource efficiency, geometric traits, productivity, disease, and other applications. In each category, relevant papers were analyzed in relation to the following aspects: research objectives, UAV type(s), sensors uploaded, analysis methods applied, and results in relation to orchard management. To identify factors that affect the research performance, comparisons among fruit species were also made. As a result, this chapter is concluded by summarizing the state of art, potential of new technology, research gaps, and opportunities for UAVs in orchard management.

2.3. Results

2.3.1. General status

The trend in UAV-based orchard management publications and citations of these articles is illustrated in Fig. 2.3. Publications on UAV-based orchard management show a steady increase over the period from 2009 to 2019, in spite of a small drop around 2015. As can be seen from the citation statistics (3.b), UAV-based orchard management has attracted significant interest, hence the need for comprehensive analysis and summary at this stage. The publications originate from and report fieldwork in a large

variety of countries throughout the world (Fig. 2.4), and they deal with different fruit species, mainly depending on climatic and geographic conditions.

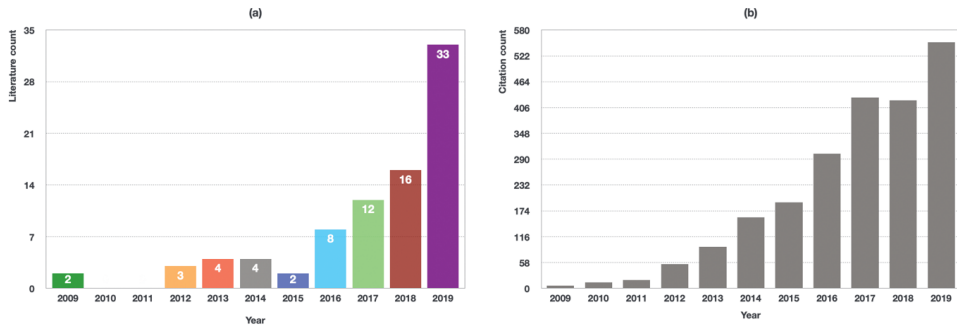


Fig. 2.3. (a) Number of publications per year for the period 2009-2019 and (b) Annual cumulative citation frequency. The search was conducted on January 01, 2020 (Source: Web of Science).

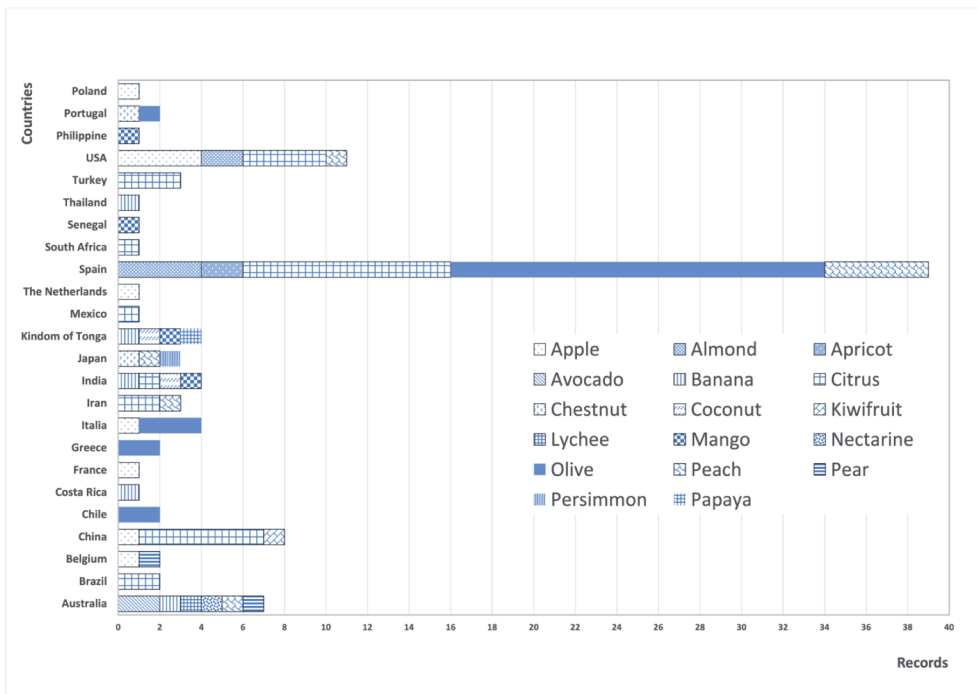


Fig. 2.4. Distribution of fruit species involved in the 84 research conducted in different countries. Citrus includes the fruit species of orange, mandarin and lemon.

The articles reviewed were classified into five classes on the basis of the orchard management application of the UAV and the objective of the application (Fig. 2.5):

- Resource efficiency: To optimize the efficiency of the inputs: e.g., water, site-specific status, or even status of individual trees is monitored and subsequently used to devise an irrigation strategy.
- Fruit-crop geometric traits: To monitor the dynamics of fruit tree growth and potential yield, geometric traits such as tree height, canopy volume, and area are evaluated. The measured data can further be used for pruning effect assessment or pruning planning.
- Fruit-crop productivity: In order to maximize economic benefits, the spatial yield estimation and prediction of final yield at final harvest are investigated.
- Fruit-crop disease: In regular monitoring of the health status of fruit crops, disease classification and assessment should be timely, in order to provide basic protection.
- Other applications: A few studies focused on UAV-based pesticide spraying, others reported research on agricultural resource management and food quality tracking.

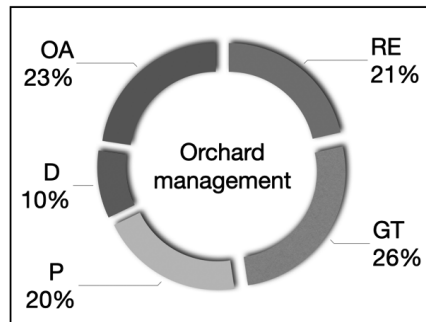


Fig. 2.5. Distribution of the five application categories in the selected 84 papers. RE: resource efficiency; GT: geometric traits; P: productivity; D: disease; OA: other applications.






Aspects for the entire fruit-crop growing cycle (Fig. 2.1) were covered, but there were significant differences in the focus: the three main categories – resource efficiency, geometric traits and productivity – account for 67% of the research conducted in orchard management. Below, all five application fields will be used as a starting point for further comparison and synthesis of the selected papers.

2.3.2. UAV platforms

An aircraft flying in a set direction and at a set speed and controlled remotely is referred to as an unmanned aerial vehicle (UAV) or drone. In recent years, the availability of UAVs has rapidly increased, and there are now many types, from multi-rotor to fixed-wing. According to the literature reviewed in

this chapter, three types of UAVs are currently used for orchard management: fixed-wing, rotary-wing, and multi-rotors (Table 2.2).

Table 2.2. Typical types of UAVs used for orchard management in five of the 84 papers.

	Multi-rotors				
	Fixed-wing	Rotary-wing	Quadcopter	Hexacopter	Octocopter
			(4-rotor)	(6-rotor)	(8-rotor)
Picture					
Model	Classic	Benzin Acrobatic	MD4-1000	Matrice 600	ARF OktoXL 6S12
Manufacturer	SenseFly, Switzerland	Vario, Germany	Microdrones,GmbH, Germany	SZ DJI, China	HiSystems GmbH, Germany
Capacity/mAh	-	6000	-	5700	4500
Weight/kg ^a	Approx. 0.69	6.57	5.82	Approx. 9.4	<5
Cruise speed/m s ⁻¹	11-25	31.29	15	<18	-
Endurance/min	50	35	30-45	17	-
Wind resistance/m s ⁻¹	12	-	-	8	-
Ref.	(Vanbrabant et al., 2019)	(Berni et al., 2009b)	(Mesas-Carrascosa et al., 2018)	(Ishida et al., 2018)	(Jarolmasjed et al., 2019)

^a – Gross weight includes the supplied sensor and battery

The specific UAV type chosen for orchard management depends on the requirements and limitations of the application. The most widely used UAV types in orchards are multi-rotors. A multi-rotor is a helicopter that can fly at different altitudes; it can be driven by four to eight rotors. This platform has several advantages. It can hover over a given location, use global positioning system (GPS) - based navigation, fly horizontally and vertically, and only requires a small take-off and landing space. The ease of control and high maneuverability are also the benefit of it. In addition, a flight altitude of 70 m can enable the optical sensor to achieve a 3D resolution of centimeter level already (Caruso et al., 2019). Yet, the main limitations of rotor craft compared to fixed-wing craft are the lower speed and shorter flight time.

Compared to multi-rotor UAVs, fixed-wing UAVs have longer flight times and faster travel speeds. A major advantage of fixed wing UAVs is the capability of high payload though the cost of this UAV is

relatively higher than multi-rotor UAVs. However, they are not able to hover. The speed of this type of UAV can cause image blurring, which can be solved by using an imaging sensor with improved features, including fast shutter speeds. Moreover, recent developments in the field of UAV have led to an interest in the adoption of UAVs with vertical take off and landing (VTOL) system in orchard management (Mesas-Carrascosa et al., 2018; Torres-Sanchez et al., 2018b). VTOL UAVs are easy to maneuver and have the freedom from bad weather and even site condition restrictions. In addition to the UAVs mentioned above, customized UAVs have also emerged in order to meet particular requirements in some case studies (Stefas et al., 2019). These UAVs are regarded as imaging and remote sensing platforms in orchard management. Still, UAVs also play an active role, such as the UAVs applied for spraying, which provide a new solution for the safety of conventionally manual pesticide spraying (Gao et al., 2019).

2.3.3. Sensors

UAVs have been equipped with various sensors and have been able to collect data on the color, spectral, temperature, and geometric traits of fruits or fruit trees. So far, the main sensors used for UAV-based orchard management (UAV-OM) are RGB and multispectral. Hyperspectral and thermal sensors are used in a relatively small range of applications in UAV-OM (Fig. 2.6). In the literature reviewed, research using LiDAR only was described in one paper, which focused on the geometric traits measurement of apple trees (Hadas et al., 2019). The application of LiDAR is limited by cost and power consumption, especially in the case of lightweight UAVs (Stefas et al., 2019). Depending on the application scenario, the five main sensor types play different roles in different orchard management activities (Fig. 2. 6).

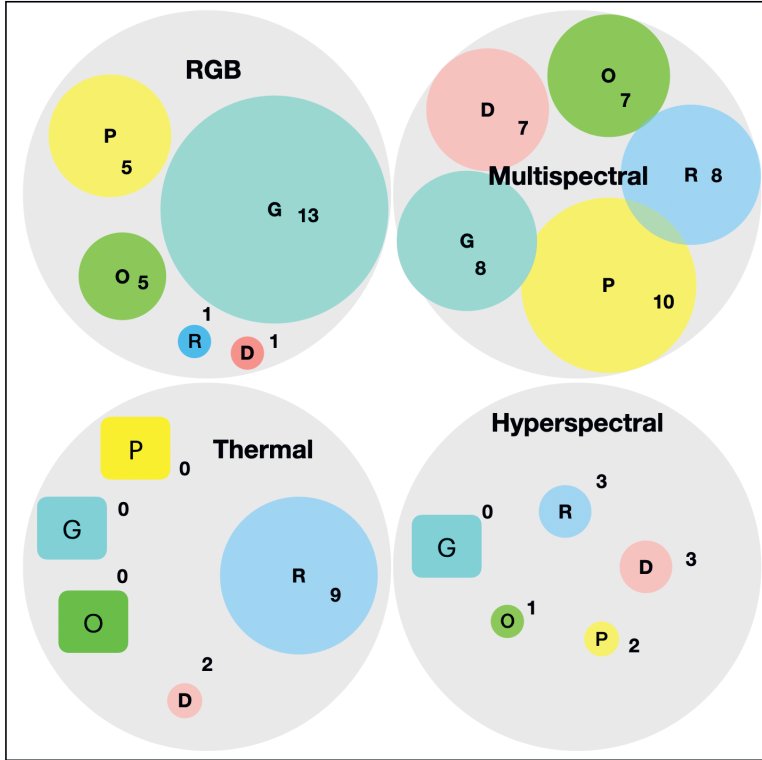


Fig. 2.6. Sensors for UAV-based orchard management as mentioned in the 84 papers selected for this survey.*

*- The areas of the brightly colored circles in the figure represent the proportion used in similar applications; specific number of relevant articles are also marked; rounded rectangles represent zero. The abbreviations are the initials of the application category: “R” stands for Resource efficiency in orchards (dark blue), “G” for Geometric and biophysical traits (light blue), “P” for the applications in Productivity (yellow), “D” for Disease detection (orange), and “O” for Other applications (green). Because LiDAR was employed only once in the literature reviewed, it is not included in the figure.

UAVs equipped with RGB imaging sensors have the widest range of applications in visible characterization, such as fruit-tree geometric trait assessment using grayscale or color images (Ok and Ozdarici-Ok, 2018a; Xue et al., 2019). RGB sensors, also referred to as “point-and-shoot cameras” and “consumer-grade cameras”, are the most commonly used sensors in orchard research. Their advantages are low cost and simple operation. The high-resolution RGB sensor in particular is capable of providing detailed information for a wide range of orchard management applications (Gao et al., 2019). For example, the sensor provides sufficient detail for analyzing the physiological characteristics of peach trees when ground resolution of RGB images fell into the range of 0 ~ 1 cm/pixel. The correlation

between orthogonal crown widths derived from UAV imagery and measured in the field yielded an R^2 value of 0.91 (Mu et al., 2018). Normally, users can obtain high-quality images by adjusting the exposure parameters of the sensor according to weather conditions. In the domain of UAV-OM, orthophotos or digital surface models (DSMs) / digital elevation models (DEMs) indirectly obtained from RGB are of most interest to researchers (Jimenez-Brenes et al., 2017; Ok and Ozdarici-Ok, 2018b). First, in order to obtain high-quality orthophotos, to minimize the influence of camera distortion RGB images need to undergo deformation processing based on the specific model of sensor used. Then, algorithms are used for image matching and optimization processing. Finally, automatic processing software such as Agisoft Photoscan software (Uribeetxebarria et al., 2019) is used to stitch the acquired images into a complete ortho-mosaic.

Depending on the spectral resolution, multispectral and hyperspectral sensors have been used in a variety of UAV-OM applications, from water status assessment to disease detection (Calderon et al., 2013; Ishida et al., 2018; Romero-Trigueros et al., 2017). The primary imaging principle of these sensors is based on differences in spectral absorption and reflection characteristics of different objects or different parts of the same object. The image processing for the spectral sensor mainly includes radiometric and geometric pre-processing with subsequent statistical analysis. Compared with RGB sensors, datasets generated from hyperspectral and multispectral sensors have increased processing effort, and standardized processing chains are still being developed. Processing the hyperspectral data is a complex task, and the hybrid spectral decomposition model has certain limitations in practical research (Guillen-Climent et al., 2012). In terms of the cost, multispectral sensors are relatively affordable for the growers in orchard but, it acquires spectral information in lower bands than do hyperspectral sensors – and hyperspectral sensors have an advantage in terms of spectral detail: they can record continuous spectra, covering a large part of the optical range. This feature enables hyperspectral sensors to perceive the spectral characteristics and spectral differences of fruit trees, making them ideal for applications where specific traits need to be derived (Abdulridha et al., 2019).

With their combination of an infrared detector and an optical lens, thermal sensors can receive infrared radiation energy in the emissive part of the spectrum. The temperature differences that can be derived from these thermal radiance observations are especially useful for the assessment of water status (Gomez-Candon et al., 2016; Park et al., 2017). The primary sensor for assessments of water status is the thermal sensor, as there is a close relationship between transpiration rate and canopy temperature due to photosynthesis (Zarco-Tejada et al., 2012). In the measurement of crop canopy temperature, the selection of the region of interest varies and influences the estimation accuracy (Stagakis et al., 2012). UAVs equipped with thermal sensors are capable of recording fruit-tree canopy temperatures which reveal the temperature differences in canopies under different conditions. However, during this process, solar radiation, air temperature, and wind speed around the canopy also have an impact on data

collection, making the final assessment results uncertain. In addition, in order to simulate the overall energy balance of the working environment, it is also important to create models which are relevant, such as the tree canopy conductance model proposed in previous research, which incorporates simulations of net radiation and aerodynamic resistance (Berni et al., 2009a). Meanwhile, sensor correction and processing of mixed pixels are still a problem that cannot be ignored (Gomez-Candon et al., 2016). Fortunately, data fusion, such as the fusion of thermal and RGB images, shows potential for providing a solution.

2.3.4. Advances in UAV-based remote sensing in orchard management

To enable the comparison among studies with the same or similar objective, a UAV-based orchard management framework was proposed (Fig. 2. 7). The selected literature fell into the proposed five categories according to their research objectives in terms of the management activities introduced in Fig. 2.1. Various data sources were acquired for different management scenario showing notable difference. LiDAR sensor was applied for geometric traits estimation only. Next, decision indicators were extracted or calculated from the collected datasets utilizing advanced methodologies. Each “orchard management” sub-category contains important aspects of the management activities, such as thermal drift correction which aims to improve the accuracy of assessment of water stress. In each application scenario, different studies share the same main focus.

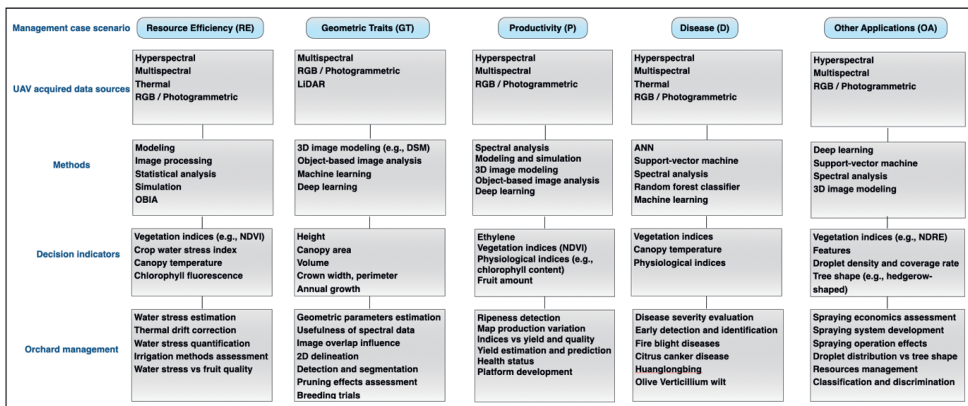


Fig. 2.7. Data-decision framework in orchard management using UAV technology, based on the selected 84 papers.

2.3.4.1. Fruit-tree geometric traits

Geometric characteristics such as the shape and size of trees have emerged as important indices for a wide range of activities for managing the growth process of fruit trees. In breeding trials, information on olive tree crown dimensions provides a benchmark for developing suitable cultivars in a given training system, e.g., open vase configuration or hedgerow (Ben Sadok et al., 2012; De la Rosa et al., 2007). Here, a training system means the management model for growing the fruit trees to a desired size and form, which is accomplished by pruning. Furthermore, traits like canopy area and crown volume are decisive when assessing pruning impact. By mapping these traits, optimal pruning type and intensity can be selected and applied (Castillo-Ruiz et al., 2015; Miranda-Fuentes et al., 2015). In general, structural properties monitoring is capable of elucidating tree crop growth status. Further, these geometric traits are useful for developing site-specific treatments involving water, and for ameliorating the management problems caused by soil heterogeneity. Acquiring conventional measurements manually requires intensive effort and is associated with much uncertainty due to the irregularity of tree crowns. First, the primary dimensions (e.g., the tree height) are measured and empirical models or equations that represent the trees as regular polygons are applied for the characterization of the trees (e.g., the canopy area or crown volume) (West, 2009). In-situ measurements of large orchard plots are more inefficient and costly. The estimation from terrestrial platforms show promising performance; they include active RS technology and LiDAR laser scanners, which have been found to be able to achieve an R^2 value of 0.97 for the tree height estimation (Moorthy et al., 2011). Though UAVs equipped with LiDAR have not been properly explored for geometric measurement in the domain of orchard management, UAVs installed with other sensors, e.g., RGB and multispectral, have been shown to be reliable alternatives for fruit-tree geometric measurements (Anifantis et al., 2019; Hadas et al., 2019).

Recent studies have described UAV-based quantification of geometric features in fruit trees, focusing on automated 3D reconstruction technique. 3D reconstruction of trees is the one of challenges in the domain of remote sensing, whereas 2D delineation quality affects the estimation based on the 3D digital models (Ok and Ozdarici-Ok, 2018a). Without the use of height thresholds, a delineation method for citrus-tree canopies that employs orientation-based radial symmetry transform (OBRS) resulted in an overall F1-score of 91.2% (Ok and Ozdarici-Ok, 2018a). OBRS transform locates the circular objects directly and improves the accuracy of the subsequent extraction of regions of interest. Circular Hough transform algorithms are also suitable for the extraction of fruit trees. Research has indicated that an approach combining this algorithm with sequential thresholding and canny edge detection resulted a delineation accuracy exceeding 80% (Koc-San et al., 2018). Neural network based methods are also capable of classifying fruit trees (Ampatzidis et al., 2019). For instance, (Kestur et al., 2018) compared the K-means method with an extreme learning machine (ELM) approach that uses a single hidden layer feed forward neural network (SLFN) for the classification of different fruit-tree crowns (banana, mango,

and coconut). In this case study, ELM performed better than the unsupervised K-means method: the classification accuracies were 96.0% and 85.5%, respectively.

In general, the combination of geographic object-based image analysis (GEOBIA) and DSMs derived from the structure from motion (SfM) method is a well-established approach for fruit-tree classification and geometric index calculation in which the indices consist of tree height, and crown width and perimeter (Jimenez-Brenes et al., 2017; Johansen et al., 2018; Ok and Ozdarici-Ok, 2018b; Torres-Sanchez et al., 2015). In a case study of height estimation, a GEOBIA method treating points between 1 and 1.5 m as the crown center was first applied in photogrammetric point cloud analysis, yielding an R^2 value of 0.94 (Torres-Sanchez et al., 2018a). This indicates that dense 3D point clouds are sufficiently representative to be used for geometric measurements. With the use of similar method, the differences in the quality of tree crown 3D reconstruction derived from two training system, intensive and hedgerow system, was observed (de Castro et al., 2019). Furthermore, when a random forest classifier was trained on the basis of GEOBIA, the estimation of crown height and plant projective cover (PPC) yielded a R^2 value of 0.65 and 0.62, respectively (Tu et al., 2019). In the case of peach trees, (Mu et al., 2018) reported that a combination of adaptive threshold and watershed segmentation methods was suitable for measurements of crown width and crown projection area (CPA, m^2) (Eq.1). Based on this, the spatial and temporal data on growth rate based on CPA was observed. An adaptive threshold is also appropriate for filtering non-fruit trees, particularly the threshold related to tree height (Xue et al., 2019).

$$CPA = 0.65 \times W_1 \times W_2 \quad (1)$$

Where the equation is based on local experience, and W_1 , W_2 represent the crown widths parallel and perpendicular to the tree rows.

Additionally, the UAV data collection design has a significant impact on the estimation results for different application scenarios. (Torres-Sanchez et al., 2018b) indicated that the best configuration for olive-tree volume estimation is the combination of 95% forward overlap and 60% side overlap while the flight altitude, the ground sampling distance (GSD) and image footprint was 100m, 0.038 m/pixel and 124×94 m, respectively, which could achieve an estimation accuracy of 95% and save 85% computing time compared to applying maximum overlap (97%). The effects of flight height on the tree height estimation was also validated. It showed that the R^2 value changed from 0.79 to 0.86 when the GSD decreased from 16 cm to 3 cm (Marques et al., 2019). GSD value affects the point cloud density directly. Research indicated that the row detection accuracy could reach 100% when the GSD ranged from 2.13 to 6.69 cm/px (Sun et al., 2019). A approach in order to enable automatic estimation of geometric parameters has been to develop valuable processing tools in QGIS software. One new plugin was capable of achieving automatic detection of trees by integrating several external algorithms and had a classification accuracy of 92.84% (Duarte et al., 2018). Different spatial resolutions produced DSMs of inconsistent quality. For one study, a stable relationship between spatial resolution and DSMs

quality was found when resolution fell in the range of 5 to 30 cm/pixel (Zarco-Tejada et al., 2014). To date, limited attention has been paid to the feasibility of upscaling methods, and several methods have only been evaluated for a given training situation (Torres-Sanchez et al., 2018a). The methods should be tested in other circumstances, e.g., related fruit species, other data collection strategies. Focusing on the isolation of error sources in the full process of estimating the geometric traits of fruit trees can likely identify the critical steps in workflow. For instance, methods based solely on morphological traits such as shape are ineffective if the background contains objects of no interest that have the same morphological traits.

2.3.4.2. Fruit-tree productivity traits

Productivity estimation is frequently prescribed for orchard management practices as it provides key information for growers and other stakeholders in market supply and exports. Detailed spatial explicit information in particular is key for growers to facilitate efficient utilization of resources and to optimize and streamline their harvest process (Suo et al., 2019; Woodward and Clearwater, 2012). In addition, estimation of essential elements such as the nitrogen status and chlorophyll content and of the fraction of intercepted photosynthetically active radiation (fIPAR) during the growing season also benefits the estimation of potential final yield and fruit-crop performance (Guillen-Climent et al., 2012; Perry et al., 2018; Vanbrabant et al., 2019). Traditional in-situ estimation of productivity variables is time-demanding and uncertain. It entails visual inspection of number, color, shape, size, and other information on fruits or fruit trees according to the grower's own experience (Srivastava and Sadistap, 2017). This results in limited samples and repetitions, which are insufficient to account for the spatial and temporal variability within and between orchards (Aggelopoulou et al., 2009; Perry et al., 2009). Most studies, however, have been conducted under special conditions (e.g., using light-shielding cover to collect data), or at ground-scale level, which also shows the limitations for operational management (Nguyen et al., 2016). A recent study has examined yield estimation based on satellite imagery, but the method was shown to have low feasibility for different orchards (Rahman et al., 2018a). Despite the timeliness and low monitoring cost of satellite-based methods, they do not satisfy all the requirements of yield-related management in orchards.

It is now well established from a variety of studies that UAV-based imaging has potential to support data-driven yield estimation algorithms. In general, counting flowers/fruits on trees is the direct and precise solution using UAV imagery technology (Horton et al., 2017). Yet, the occlusion of flowers/fruits by branches, leaves and/or other fruits, variable outdoor lighting conditions, and color similarity seriously affect the direct estimation. Fruit trees need to be accurately thinned during flowering stage in order to gain better yield and fruits with good quality. Thus the basis is the precise estimation of the flowering status in orchards. In this context, an enhanced bloom index (EBI) (Eq. 2)

was proposed for quantifying floral phenology in an almond orchard. The EBI is capable to enhance flower signals and reduce the noise produced by soil and green vegetation. Robust information on floral phenology was provided by the EBI, showing an agreement with the bloom coverage (with a R^2 of 0.72) (Chen et al., 2019a). Flower numbers is difficult to accurately count with aerial images due to the high density and occlusion of flowers. To deal with this, flowering density calculated from 3D point clouds was proved to monitor the flowering dynamics at field scale using SfM and OBIA approaches (Lopez-Granados et al., 2019b). To further improve the feasibility of UAV in yield mapping, a vision-based UAV system was suggested (Stefas et al., 2019). Its capability of avoiding obstacle in high density orchards enable increasing spatial resolution navigating autonomously among apple rows and trees.

$$EBI = \frac{\text{Brightness}}{\text{Greenness} \cdot \text{Soil} \cdot \text{Signature}} = \frac{R + G + B}{\frac{G}{B} \cdot (R - B + \epsilon)} \quad (2)$$

Where the ϵ is an adjusting constant to make the denominator non-negative, and R, G, B are the reflectance of red, green and blue bands, respectively.

In addition to direct measurements, alternative parameters (such as geometric traits and vegetation indices) for indirect productivity estimation or prediction are of interest. Canopy projected area (CPA) and canopy perimeter have been proved to be correlated with the fruit load of peach trees (Uribeetxebarria et al., 2019). CPA yielded a higher correlation, with an R value of 0.85. Olive yield can be forecast from individual crown area estimated from UAV images (Sola-Guirado et al., 2017), and a high agreement between the crown volume and yield was also observed in some almond varieties (Lopez-Granados et al., 2019b). In the case of banana productivity, normalized difference vegetation index (NDVI) was positively correlated with several metrics regarding the yield and fruit quality (e.g., bunch weight, length of the longest finger), and negatively correlated with fruit loss (Machovina et al., 2016). Further, an attempt to demonstrate the influence of soil heterogeneity on fruit productivity found no relationship between NDVI and physical soil quality. In addition, predictive models for mango yield based on geometric parameters have provided an R^2 value greater than 0.77 using GEOBIA, without counting numbers (Sarron et al., 2018a). Meanwhile, research exploring whether the methods proposed have universal application is interesting. One source of weakness in estimation using structure indices is that vegetation dynamics related to short-term physiological processes cannot be captured. To deal with this, chlorophyll content related index - TCARI/OSAVI, light use efficiency related index - PRI570, and canopy chlorophyll fluorescence can be alternatives. Research suggests that these three indices yielded values of R^2 in the range between 0.75-0.84 when estimating the gross primary production (GPP) (Zarco-Tejada et al., 2013). Productivity estimation related to physiological is largely based on data derived from multispectral or hyperspectral sensors. In this context, there are still operational challenges

in employing fixed-wing UAVs (two hours' preparation time: set up, camera calibration, safety check, and launch) and in application scale (Machovina et al., 2016).

In order to optimize fruit productivity and harvest activities, it has been advised to focus on harvesting time optimization, fruit tree vitality and health status monitoring (Vanbrabant et al., 2019). Fruit ripeness is the key element to determine the harvest time; it affects fruit quality directly during transport to markets. Preliminary efforts on ethylene detection via ethylene-sensitive sensors attached to UAVs have shown the effects of flying height and sensing wind speed when assessing apple maturity (Valente et al., 2019). This demonstration provides a novel method for harvest time optimization, though the modeling and simulation results indicated a short detection margin for the ethylene. In one study in the domain of radiation interception estimation, vegetation indices mostly related to tree crop structure were regarded as a proxy for fraction of absorbed photosynthetically active radiation (fAPAR) (Zarco-Tejada et al., 2013). On the other hand, fIPAR at crop canopy scale also proved mappable via airborne imagery, especially in peach and citrus orchards (Guillen-Climent et al., 2012). Similar fIPAR estimation results were found when methods employing the combination of 3D radiative transfer model and scaling-up were compared with a model inversion method: RMSE values were 0.09 and 0.10, respectively. It was shown that row orientation affected the relationship between NDVI and fIPAR. Further, fIPAR quantification was also validated via Mahalanobis distance supervised classification method, which resulted in a RMSE of 0.06 (Guillen-Climent et al., 2014). In order to achieve higher productivity, regular nutritional status monitoring is the main requirement for fruit species like citrus (Osco et al., 2019a). Evidence was found that nitrogen contents prediction accuracy for citrus depends on the sub-tree areas where the spectral data extracted from. Nitrogen prediction accuracy based on the spectral data from the whole canopy and the young leaves was found lower than that from the mature leaves, while the effects of sub-tree areas on the prediction accuracy of soluble sugar and starch in the leaves were not clear (Liu et al., 2016). Instead of using conventional indices for nitrogen status assessment, (Perry et al., 2018) applied a new index, the modified canopy chlorophyll content index (M3CI) (Eq.3), for the assessment at canopy level, resulting in an R^2 value of 0.67. Machine learning algorithms currently performed well in the monitoring of fruit tree conditions such as chlorophyll content (Vanbrabant et al., 2019), nitrogen content. Compared with SVM, ANN and decision tree (DT) machine learning algorithms, random forests (RF) was the optimal one for the prediction in canopy nitrogen content of orange trees. R^2 value reached 0.9 while the mean squared error (MSE) was 0.307 g/kg (Osco et al., 2019b).

$$M3CI = \frac{R_{NIR} + R_{Red} - R_{RE}}{R_{NIR} - R_{Red} + R_{RE}} \quad (3)$$

Where the R_{NIR} was measured in the band of 810-nm, the measured reflectance of R_{Red} and R_{RE} were in the 660-nm and 710-nm band, respectively.

The aforementioned papers still reveal limitations in the data-processing time (Sarron et al., 2018a), the robustness of methods proposed, and experimental design in terms of sample size (Perry et al., 2018). Finally, nearly all of the research was conducted at a certain period of time and few comparative studies report results of estimations at different fruit-growing stages throughout the entire growth cycle.

2.3.4.3. Resource efficiency in orchards

The water used for irrigation in agriculture accounts for 85% of the total water managed at a global scale. Because of the water shortage worldwide, precise water management in orchards is a crucial practice, particularly in semi-arid areas where water inputs require higher economic investment. Climate change is also becoming a problem for the fruit industry, as some geographic areas are experiencing long periods of drought (Gomez-Candon et al., 2016). An efficient irrigation strategy is key to minimizing this negative impact on orchard managers' profit. Sufficient water input is closely related to fruit production and quality. Even some drought-tolerant species like olive (*Olea europaea* L.) can benefit from irrigation, i.e., the promotion of growth, yield and fruit quality (olive oil), especially when grown in high-density training systems (Caruso et al., 2019; Egea et al., 2017). Within the definition of deficit irrigation, water inputs should meet the realistic requirement of the trees. Site-specific water management is thus of great importance to track the variability of water needs in orchards. More specifically, it solves the variability problem caused by soil heterogeneity and canopy-cover differences (Couvreur et al., 2016). The use of remote sensing technology for fast assessment of the water status in orchards aims to improve productivity and water use efficiency in irrigation. For instance, the normalized difference red-edge (NDRE), derived from UAV imagery is capable for monitoring the irrigation inhomogeneities and may further identify the growth inhomogeneities (Jorge et al., 2019).

When water supply from the soil cannot meet the demand for transpiration of plants, water deficits occur. These short-term deficits may hamper the growth of fruit trees and will affect the productivity. As most fruit trees are sensitive to water deficits, information related to optimizing irrigation is critical. Water stress monitoring benefits the application of deficit irrigation, allowing water resources to be saved and fruit yield and quality to be maintained (Girona, 2002; Zarco-Tejada et al., 2012).

In the late 1970s, canopy temperature was identified as a proxy for water status monitoring, with the concept of crop water stress index (CWSI) (Idso et al., 1978; Jackson et al., 1981). The CWSI normalizes the difference between air (T_a) and canopy temperature (T_c), and lower (LL) and upper limit (UL) (transpiration of a leaf at potential rate and no transpiration, respectively), demonstrating the evaporative demand (Eq.4).

$$CWSI = \frac{(T_c - T_a) - (T_c - T_a)_{LL}}{(T_c - T_a)_{UL} - (T_c - T_a)_{LL}} \quad (4)$$

UAV imagery has shown to be potentially more efficient for canopy temperature assessment than traditional field measurement (Gonzalez-Dugo et al., 2014). When it comes to the exploration of canopy temperature, stomatal aperture is key to understanding the fluctuations, i.e., stomatal closure can lead to a decrease of evaporative cooling and rise in leaf temperature. The impacts of environmental conditions on stomatal response vary for different fruit species, which should be borne in mind, especially when the temperature of the fruit-tree canopy is taken as an indicator (Ballester et al., 2013). CWSI applications are mainly restricted by two aspects: necessary spatial resolution and the site-dependent equation of non-water-stressed baseline (NWSB). Without the use of reference surfaces, a high-resolution CWSI map was achieved by combining energy balance equations based on physical models with thermal imagery (Berni et al., 2009a). This reveals the capability of CWSI for quantifying the spatial variability too. However, if the targeted orchard contains different species or the same fruit species with different training systems, the thermal response is affected and a single set of reference values may lead to errors. In a study investigating this case (Park et al., 2017), an adaptive CWSI yielded an agreement with stem water potential (ψ_s) and stomatal conductance (g_s) with determination coefficients (R^2) of 0.72 and 0.82, respectively, employing temperature thresholds. This was in contrast to the conventional CWSI, which yielded R^2 values of 0.27 and 0.34, respectively. The orchard had been divided into four sub-areas according to the fruit species and training systems and the adaptive thresholds of the lower and upper reference were estimated for the adaptive CWSI calculation. The CWSI algorithm applied is shown in Eq. (5). Here, the canopy temperature derived from aerial imagery was applied instead of the difference between canopy and air temperature (Jones, 2013).

$$\text{CWSI} = \frac{T_c - (T_c - T_a)_{LL}}{(T_c - T_a)_{UL} - (T_c - T_a)_{LL}} \quad (5)$$

Where T_c is the aerial canopy temperature measured, T_a is the air temperature, LL represents the temperature of a leaf at full transpiration and UL is non-transpiring temperature.

It is widely accepted that ψ_s is a reliable parameter which is closely related to plant response to water stress. ψ_s not only reveals the water status in the plant–soil–atmosphere continuum but integrates the effects from soil moisture and evapotranspiration. However, obtaining ψ_s values with a field measurement method is a labor-intensive and inefficient process (Zhao et al., 2017); alternative indices derived from aerial imagery are therefore needed. Thus, in addition to CWSI, research on comparing vegetation indices derived from the UAVs with ground-collected data, such as ψ_s and g_s , is currently of interest (Gonzalez-Dugo et al., 2013; Stagakis et al., 2012; Zarco-Tejada et al., 2012).

To explore suitable indicators for the assessment of water stress, a variety of reflectance indices derived from UAVs have been calculated, analyzed, and compared with water-stress-related measurement methods conducted on the ground, e.g., g_s (Table 2.3). Indices integrating data from different spectral ranges such as the NDVI have shown potential for inferring water status in several types of orchards

(Caruso et al., 2019). Indices such as chlorophyll and fluorescence indices (leaf-level), green ratio (GR), enhanced normalized difference vegetation index (ENDVI), normalized difference green near infrared index (NDGNI), and saturation (S) have also proved to be sensitive to water status (Bulanon et al., 2016; Zarco-Tejada et al., 2012). Intensity (I) did not provide reliable results in the case of apple orchards. Additionally, two formulations of photochemical reflectance index (PRI), PRI₅₇₀ and PRI₅₁₅, were correlated with water stress and showed promise for fruit quality assessment in an orange orchard (Stagakis et al., 2012). NDVI calculated at canopy level in almond trees decreased within areas with high water stress when the blue band was employed (Eq.6), which indicates that the canopy NDVI could be a water stress indicator for some fruit crops (Zhao et al., 2017).

$$NDVI_B = \frac{\rho_{NIR} - \rho_B}{\rho_{NIR} + \rho_B} \quad (6)$$

On the other hand, as a canopy structure parameter, the leaf area index (LAI) is sensitive to water stress. Studies of LAI indirect measurement showed that the NDVI calculated from UAV images also correlated with the LAI measured on the ground (R^2 value ranged from 0.78 to 0.88) (Berni et al., 2009b; Caruso et al., 2019).

Table 2.3.

List of spectral vegetation indices used in the assessment of water stress and its associated equations and applied for UAV-acquired datasets in fruit orchards.

Aerial Reflectance Indices	Equation	Ref.
Enhanced Normalized Difference Vegetation Index (ENDVI)	$ENDVI = \frac{NIR + G - 2(B)}{NIR + G + 2(B)}$	(Bulanon et al., 2016)
Intensity (I)	$I = NIR + G + B$	(Bulanon et al., 2016)
Normalized Difference Green Near Infrared Index (NDGNI)	$NDGNI = \frac{NIR - G}{NIR + G}$	(Bulanon et al., 2016)
Saturation (S)	$S = \frac{I - 3(B)}{I}$	(Bulanon et al., 2016)
Normalized Difference Vegetation Index (NDVI)	$NDVI = \frac{NIR - RED}{NIR + RED}$	(Ballester et al., 2018; Berni et al., 2009b; Caruso et al., 2019; Delalieux et al., 2014; Romero-Trigueros et al., 2017; Stagakis et al., 2012; Zarco-Tejada et al., 2012; Zhao et al., 2017)
Renormalized Difference Vegetation Index (RDVI)	$RDVI = \frac{R_{800} - R_{670}}{\sqrt{R_{800} + R_{670}}}$	(Delalieux et al., 2014; Stagakis et al., 2012; Zarco-Tejada et al., 2012)

OSAVI Index	$(1 + 0.16) * \frac{R_{800} - R_{670}}{R_{800} + R_{670} + 0.16}$	(Delalieux et al., 2014; Zarco-Tejada et al., 2012)
Simple Ratio (SR)	$SR = R_{800} / R_{670}$	(Delalieux et al., 2014; Zarco-Tejada et al., 2012)
Modified Simple Ratio (MSR)	$MSR = \frac{R_{800}/R_{670} - 1}{(R_{800}/R_{670})^{0.5} + 1}$	(Delalieux et al., 2014; Zarco-Tejada et al., 2012)
Triangular Vegetation Index (TVI)	$TVI = 0.5 * [120 * (R_{750} - R_{550}) - 200 * (R_{670} - R_{550})]$	(Stagakis et al., 2012; Zarco-Tejada et al., 2012)
Modified TVI (MTVI)	$MTVI = 1.2 * [1.2 * (R_{800} - R_{550}) - 2.5 * (R_{670} - R_{550})]$	(Zarco-Tejada et al., 2012)
Xanthophyll Indices		
Photochemical Reflectance Index (PRI ₅₇₀)	$PRI_{570} = \frac{R_{570} - R_{531}}{R_{570} + R_{531}}$	(Ballester et al., 2018; Delalieux et al., 2014; Stagakis et al., 2012; Zarco-Tejada et al., 2012)
Modified Photochemical Reflectance Index (PRI ₅₁₅)	$PRI_{515} = \frac{R_{515} - R_{531}}{R_{515} + R_{531}}$	(Ballester et al., 2018; Delalieux et al., 2014; Stagakis et al., 2012; Zarco-Tejada et al., 2012)
Chlorophyll a b Indices		
ZM	$ZM = R_{750}/R_{710}$	(Delalieux et al., 2014; Stagakis et al., 2012; Zarco-Tejada et al., 2012)
Vogelmann (VOG1)	$VOG1 = R_{740}/R_{720}$	(Delalieux et al., 2014; Zarco-Tejada et al., 2012)
Transform Chlorophyll Absorption in Reflectance Index (TCARI)	$TCARI = 3 * [(R_{700} - R_{670}) - 0.2 * (R_{700} - R_{550}) * (R_{700}/R_{670})]$	(Ballester et al., 2018; Delalieux et al., 2014; Zarco-Tejada et al., 2012)
TCARI/OSAVI	$TCARI / OSAVI$	(Ballester et al., 2018; Zarco-Tejada et al., 2012)
Blues/Green/Red Ratio Indices		
GR	$GR = R_{550}/R_{670}$	(Bulanon et al., 2016; Gonzalez-Dugo et al., 2013; Zarco-Tejada et al., 2012)
BGI1	$BGI1 = R_{400}/R_{550}$	

Chapter 2

BGI2	$BGI2 = R_{450}/R_{550}$	(Zarco-Tejada et al., 2012) (Zarco-Tejada et al., 2012)
Blue/Red Indices		
BRI1	$BRI1 = R_{400}/R_{690}$	(Zarco-Tejada et al., 2012)
BRI2	$BRI2 = R_{450}/R_{690}$	(Delalieux et al., 2014; Zarco-Tejada et al., 2012)
Lichtenthaler Index		
LIC3	$LIC3 = R_{440}/R_{740}$	(Zarco-Tejada et al., 2012)
Carotenoid Indices		
	R_{520}/R_{500}	(Delalieux et al., 2014; Zarco-Tejada et al., 2012)
	R_{515}/R_{570}	(Delalieux et al., 2014; Zarco-Tejada et al., 2012)
	R_{515}/R_{670}	(Delalieux et al., 2014; Zarco-Tejada et al., 2012)
Fluorescence Indices		
	$L_{747} - L_{762}$	(Zarco-Tejada et al., 2012)
	$L_{780} - L_{762}$	(Zarco-Tejada et al., 2012)
	L_{747} / L_{762}	(Zarco-Tejada et al., 2012)
	L_{780} / L_{762}	(Zarco-Tejada et al., 2012)
	$((L_{747} + L_{780}) / 2) - L_{762}$	(Zarco-Tejada et al., 2012)
	FLD2 (747; 762)	(Zarco-Tejada et al., 2012)
	FLD2 (780; 762)	(Zarco-Tejada et al., 2012)
	FLD3 (747; 762 780)	(Zarco-Tejada et al., 2012)
	$\int [747, 780]$	(Zarco-Tejada et al., 2012)

However, not all the pixels within the canopy area yield the water status: these are non-leaves or shaded areas. Besides the multispectral indices mentioned in Table 2.3, monthly canopy volume increment correlated well with daily water stress integral (WSI), with an R^2 of 0.99 (Caruso et al., 2019). WSI reduces the impact of the fluctuations in water status. The slope of $(T_c - T_a)$ over time was found to be another novel indicator (Gonzalez-Dugo et al., 2013). Generally, research focused more on the indices

related to canopy structural changes than on diurnal physiology changes (Romero-Trigueros et al., 2017). In the case of orchards with several fruit species, using one single index could dramatically simplify management. Because different species vary in their canopy architectures and nutrient status, diverse water status indicators are needed (Ballester et al., 2018). Suitable indices should not be determined by numerous specific conditions, such as fruit species, irrigation methods, and geographic conditions (Bulanon et al., 2016; Caruso et al., 2019). For particular applications, varying experimental comparisons are required, and a general case study per application may provide insight into the bottlenecks. For example, in order to explore the universal vegetable index for water status assessment, the performance of methods proposed for different fruit species should be tested.

Generally, two thermal sensor systems are available for temperature imaging: cooled systems, which are loaded on satellite and aerial platforms, and uncooled systems, which are used on UAV payloads with less power consumption. However, the temperature drift that occurs in uncooled systems affects the rate of error, causing offset non-uniformity of the acquired data (Gomez-Candon et al., 2016). Some drift correction strategies for thermal sensors need additional flying time, which means higher requirements for on-board batteries, though the accuracy is greater than 1 °C. Maintaining the same correction accuracy and using the methods based on redundant information, the cubic drift model enables more efficient drift correction (Mesas-Carrascosa et al., 2018). Even during data collection prior to this operation, the final estimation of water status can be adversely affected by factors such as: the effects of solar motion when aiming at calculating canopy NDVI; the data collection interval, which may reduce the influence of fluctuation; and the flight altitude, which affects subjective interference. Fruit orchard properties (e.g., cultivars and training systems) should be taken into account in order to achieve a comprehensive analysis of the images. Conducting edge extraction prior to modeling enhanced the mapping accuracy of stem water potential (Park et al., 2017). Yet approaches on increasing the efficiency of image extraction and radiometric correction should also be considered for use in the statistical analysis or image processing (Gomez-Candon et al., 2016). In addition, it is not uncommon for pixels to be mixed together in image areas, e.g., areas contain canopy and non-interested pixels, the soil pixels, and methodologies need to be further developed to reduce the associated error. Though in most cases the fine-resolution imagery necessary for pure crown extraction or intra-canopy variability investigation is available, more quantification studies are needed for precise water management in orchards.

2.3.4.4. Detection of diseased fruit trees

Different types of diseases may occur throughout the fruit-growing season – from flowering to harvest, and even in the dormant tree period during winter. In terms of their cause, diseases in orchards fall into two categories: biotic and abiotic. Biotic diseases are caused by living pathogens, which could be

bacteria, fungi, viruses, or insects. A well-known apple bacterial disease is fire blight, which leads to significant losses in fruit production by infecting the fruits and rootstock of fruit trees (Jarolmasjed et al., 2019). Apple scab and pear black necrotic leaf spot belong to fungal and viral diseases, respectively (Belfanti et al., 2004; Shim et al., 2004). Abiotic stress is caused by the interaction of fruit trees and other factors in the planting environment, such as water pollution, overwatering, and extremes of light and nutrients. Treating abiotic stress as abiotic disorders may predispose fruit trees to infectious diseases, and abiotic and biotic diseases can also occur in the same trees. Diseases significantly affect the fruit quality and final yield by infecting fruits, trees, and other areas, such as twigs and leaves. Many diseases show mild effects, resulting in limited to no harm at some point. But some diseases even cause tree mortality. Huanglongbing (HLB), or citrus greening, and phytophthora root rot disease can be lethal to fruit trees worldwide and attract growers' attention because of their significant economic impacts (Salgadoe et al., 2018; Sankaran et al., 2011). The most effective management to deal with fruit trees diseases is to detect the infected trees as early as possible. In addition, specific treatment can be taken, i.e., removing diseased trees, applying dedicated pest protection measures, and planting resistant species. Some diseases are hard to diagnose from visual symptoms at the early infected stage, with the result that no effective action can be taken to deal with the disease when the serious symptoms are recognized at a late stage. Traditional methods for diagnosing fruit-tree diseases are visual observations in the field combined with laboratory analysis and have limitations relating to reliable evaluation and time–cost efficiency (Khan et al., 2018; Pan et al., 2014; Srivastava and Sadistap, 2017). UAV-based fruit-crop disease monitoring has been employed for a few types of disease, but it is still critical to investigate its applicability for monitoring severe diseases like Panama disease in banana (O'Neill et al., 2016). Additionally, disease detection based on aerial images from UAVs can provide orchard scouting over a larger area and is low-cost in terms of both time and equipment.

Disease identification is the first step for practical control. The complexity of disease diagnosis and diversity of fruit species hampers the transfer of research findings to other methods of fruit-tree disease detection. Different symptoms of diseases have been classified with different sensors, deriving valuable indicators from aerial images. The capability of UAVs equipped with hyperspectral and multispectral sensors to classify citrus trees infected by two types of biotic diseases, bacterial canker and HLB, respectively, has been described (Abdulridha et al., 2019; Garcia-Ruiz et al., 2013). Machine learning has shown promise for exploring the complex sensitivity of an indicator for a specific disease diagnosis issue. Citrus bacterial canker (symptoms are yellow halos on fruit and twigs) is a disease with serious implications (Duan et al., 2018). (Abdulridha et al., 2019) explored detection techniques for this disease under laboratory conditions and in an orchard, utilizing hyperspectral imaging and machine learning. In total, 31 vegetation indices were evaluated for the disease detection; also studied was the classification of disease development stages – asymptomatic (infected but with no symptoms), early (tiny lesions), and late symptoms (brown lesions). Two machine learning methods were compared for

the indoor detection: neural network radial basis function (RBF), which is regarded as a powerful classifier for spectral reflectance data, and K-nearest neighbor (KNN). Overall, RBF performed better than KNN in different stages of the disease. The water index (WI) (Eq.7) and anthocyanin reflectance index (ARI) (Eq.8) and TCARI (Table 2.3) were the optimal indices for laboratory conditions and UAV-based diagnosis of infected trees, respectively. Identification accuracy of healthy and non-healthy trees from UAV-based detection was good, and the classification accuracy achieved for the late stage detection under laboratory conditions was 92%. But the authors also noted that immature fruit could not be used for early detection.

$$WI = \frac{R_{900}}{R_{970}} \quad (7)$$

$$ARI = \left(\frac{1}{R_{550}} \right) - \left(\frac{1}{R_{700}} \right) \quad (8)$$

Detection on the deadly disease HLB, for which the only treatment option is to cut down and remove the infected trees, has long been a research topic of great interest. A comparison between a UAV-based and an aircraft-based system for identifying HLB was conducted using multispectral imagery (Garcia-Ruiz et al., 2013). Compared to earlier case studies, the opportunities for using platforms with different spatial resolutions for disease classification were demonstrated. Resolutions of 0.5m and 5.45cm per pixel were employed for the aircraft and UAV, respectively. More indices were analyzed: 6 spectral bands and 7 vegetation indices. For the classification methods, support vector machine (SVM) with kernel performed better than linear SVM, linear discriminant analysis (LDA), and quadratic discriminant analysis (QDA). Results showed that the identification accuracy from the UAV was 67-85%, while aircraft-based yielded 61-74%. The authors suggested that future studies should focus on algorithm development, image acquisition, and the temporal effect of aerial identification of HLB. Similarly, a HLB detection accuracy of 81.75% was achieved when 16 vegetation indices were extracted for the classification based on SVM method (DadrasJavan et al., 2019). The study also found that the registration errors between bands of multispectral sensors could lead to a lower classification accuracy when the errors were larger than one pixel, especially for the application of UAV technology. In general, radiometric calibration complicates the process of HLB detection. However, the study showed insignificant effects of radiometric calibration on the discrimination of HLB-infected and healthy trees when the data were collected consistently with similar illumination and atmospheric condition (Pourazar et al., 2019). Disease scouting contributes to the control of disease. With the help of UAV-based platforms, the scouting efficiency was improved. However, UAV-based scouting is influenced by flying time, due to the limitation resulting from the payload.

In addition to disease identification, the main concerns investigated by researchers are early disease detection and severity evaluation, especially in the application of fruit breeding programs. A type of fungal disease, verticillium wilt (VW) in olive, greatly impacts the final yield and even leads to tree

mortality. By analyzing thermal, multispectral, and hyperspectral datasets derived from UAV, (Calderon et al., 2013) aimed at the early detection of VW and discrimination among different VW severity levels. They analyzed different indices, e.g., physiological indices, and other indicators. Based on the finding that VW can cause water stress changes in olive trees, the investigation demonstrated that the reduction in g_s was associated with an increase in PRI_{570} and a decrease in fluorescence. Based on this, not only the early detection of VW was achieved, but also the discrimination of severity levels. Olive orchards with different agronomic characteristics were compared, which enhances the flexibility of the detection method proposed. The carotenoid reflectance index 2 (CRI2) and NDVI were also validated for detecting the early and advanced VW-infected trees (Iatrou et al., 2016). Apart from this, changes in the NDVI rate was found sensitive for monitoring the effects of plant growth enhancer formulation (PGEF) on the recovery of the trees, which can further enhance the management of VM in olive orchard.

Apple scab significantly affects the yield and quality of apple fruit and has become a major problem in apple orchard. It is caused by the Ascomycete fungus, *Venturia Inaequalis*. Research has shown the potential of making a risk evaluation model on the monitoring of apple scab in orchard using UAV technology (Stella et al., 2017). Apple scab can be indirectly monitored by acquiring leaf wetness data. On the basis of this, data extracted from UAV provided precise inputs to the evaluation model for the risk prediction based on the output of the model, the leaf wetness data. Detection methods based on thermal or spectral sensors make up for the shortcomings of classical detection methods that rely on visual observation by orchard experts. RGB sensors might also be used to detect diseases with apparent visual traits. Fire blight of apple is caused by the pathogen *Erwinia amylovora* infecting apple flowers, fruits, and the rootstock. Typical visual symptoms are the blackened shoots. This disease particularly threatens the production of commercial orchards (Salm and Geider, 2004). A recent study employed multispectral, hyperspectral, and RGB sensors to evaluate fire blight severity and found that detection from features derived from RGB and multispectral images was inferior to detection derived from hyperspectral images (Jarolmasjed et al., 2019). The index of normalized difference spectral indices, computed from hyperspectral datasets, showed moderate to high classification accuracy, ranging from 71 to 93%. Spectral bands between 710-2340 nm proved relevant for the classification.

2.3.4.5. Other applications

Pesticides can be used to support protection from pests, especially in the case of economic products, such as fruit trees. The usual management measure to deal with infestation with citrus leafminer (CLM) which threatens the production of citrus is chemical control (Qureshi et al., 2017). However, the uncontrolled and inappropriate use of pesticides affects biological systems, polluting preserved areas and damaging ecosystems. In addition, manual spraying exposes workers to a high-risk setting full of harmful chemicals. In the precision agriculture literature focusing on pesticide spraying systems in

orchards, solutions based on UAVs are proposed to be safer, more precise, and more affordable than manual spraying or manned agricultural aircraft (Martinez-Guanter et al., 2019; Zhang et al., 2017). Nonetheless, aerial spraying can be inefficient in practice without a reasonable spraying strategy and detailed and precise information support, e.g., the identification of tree crown areas that are regarded as target spraying areas. Compared with other UAV-based management activities, there are more restricted operational parameters for sprayer UAVs, such as spray nozzle control, flying height, and speed. A deviation from the flight route or a change in wind direction will significantly impact on the droplet deposition distribution uniformity. Tree shape should also be taken into account even under the same spraying system (Zhang et al., 2016). For example, in the case of inverted triangle-shaped citrus trees, the lower layer was found to be the part with the most uniform distribution ($CV = 32.44\%$), and they received higher droplet density than triangle-shaped trees (Tang et al., 2018). Other plant shapes, i.e., hedgerow and open-center-shaped, show different performance and optimal operation parameters. While the optimal control parameters of droplet density for the inverted triangle-shaped citrus tree was determined using Taguchi method, the spraying height was 1.4 m and the flight speed was 1.0 m/s (Hou et al., 2019). In terms of control effect against pests like CLM, a case study showed that a UAV-based system could achieve 65-75% of the control effect of manual spraying. But high efficiency and low cost of UAV-based spraying was observed at the same time (Zhang et al., 2017).

A limited number of earlier studies focus on intelligent and real-time application of sprayer UAVs which, with the help of machine learning and powerful computation support, have high potential for precision work. Using the mutual subspace method, an intelligent spraying UAV system could achieve an average recognition accuracy of 70% for spray or non-spray areas (Gao et al., 2019). This result falls within the requirements of precision agriculture, efficiently utilizing chemical inputs while reducing the environmental damage. However, the bottlenecks include limited battery capacity, the large volumes of liquid that must be carried, and the difficulty of reconciling high spraying speed and computation speed with promising recognition accuracy. For further study, deep learning methods should be tested against the machine learning-based recognition (Saldana Ochoa and Guo, 2019), in order to deal with the noise in the datasets and the negative impacts from the changing lighting conditions. Additionally, a pesticide spraying system based on multi-sensor data fusion algorithms may help bring about a high-efficiency revolution in the use of pesticides by accurately identifying and locating target trees and controlling pesticides.

Apart from research on sprayer UAV, several studies have used longitudinal UAV data for agro-environmental monitoring in orchards, such as the analysis of landslide evolution affecting the olive orchard (Fernandez et al., 2016) and the delineation of management zones for pest control (Mendez-Vazquez et al., 2019). Vegetation ground cover (VGC), the vegetation cover spontaneously grows on the surface of the ground, is an important component in the ecological system. A vegetation index

derived from UAV, inverse ratio vegetation index (IRVI), was suggested to be the most sensitive index for the quantification of the density of VGC, and IRVI and ratio vegetation index (RVI) (Table 2.4) could most accurately distinguish the VGC densities > 80 in a cover interval range of 10% ($p < 0.001$) and VGC densities $< 30\%$ in a cover interval range of 15% ($p < 0.01$), respectively (Lima-Cueto et al., 2019). Monitoring tasks in orchards are different from other agricultural activities. Cost-effective monitoring approaches are always the classic problem not only for the growers in the orchard but also the researchers. On the basis of this, a study focus on the development of customized sensor capable to be mounted on the UAV show several advantages (Barrows and Bulanon, 2017). The customized low-cost multispectral sensor, for which the original internal infrared filter was replaced with a special dual-band filter, was proved to be comparable with the commercial grade sensor in the estimation of NDVI in orchards.

Table 2.4. Vegetation indices applied in the quantification of VGC.

Index	Formula ^a
Inverse ratio vegetation index (IRVI)	$IRVI = RED/NIR$
Ratio vegetation index (RVI)	$RVI = NIR/RED$

^a Wavelength band values RED (660nm centre, 40nm bandwidth), NIR (790nm centre, 40nm band width).

Fruit tree detection or classification is fundamental to the majority of UAV-based site-specific management in orchards. In general, machine learning and OBIA methods are currently the most popular methods for the detection and classification (Neupane et al., 2019). For instance, in a case study of agricultural resource management (Saldana Ochoa and Guo, 2019), a deep convolutional neural network (CNN) was employed. The processing chain proposed needs long-time and large datasets for training, which reveals the important need to strengthen the input requirements of CNN, although a significant classification accuracy was observed, with an F1 score of 0.89. Semantic segmentation may be a vital dimension in extracting crop classification from complex information. SVM performed well in the classification of both RGB and hyperspectral datasets. To segment citrus trees from the background in RGB images, an SVM model established by the calculation of 14 color features and 5 statistical texture features could result in an accuracy of $85.27 \pm 9.43\%$ (Chen et al., 2019c). For the later case, misclassification of sunlit and shaded areas could be overcome with the help of SVM, achieving a classification accuracy of 94.5% of mango trees (Ishida et al., 2018). This classification capability can be further improved if the effects of wind on the data collection can be reduced, as wind deforms the flexible fruit-tree structure, thereby affecting image overlapping. Within the classification chain of an OBIA-based olive mapping study, dividing the original UAV image capturing a large plantation into

subsets was suggested to speed up and facilitate the calibration (Karydas et al., 2017). Apart from these two popular methods, vegetation indices like NDRE, and the DSM could also be applied in fruit-crop discrimination (Handique et al., 2017). Most studies focus on the classification between fruit trees and other plantation while a combination of univariate and multivariate statistical approaches was applied for olive cultivar recognition. Results suggested that the classification accuracy between scions was 90.9%, however, 68.2% of the discrimination cases between rootstocks failed (Avola et al., 2019).

In addition to the standard applications discussed above, UAV-based management in the domains of regular crop monitoring and food quality tracking also have considerable impact on the development of UAVs in orchard management. In some cases, studies on these aspects have focused on fruit trees at a smaller scale than the standard orchard, or on fragmented land holdings. (Handique et al., 2017) reported on the collection of crop statistics in hilly terrain or terrace cultivation systems, such as in the northeast of India, where UAVs were used for crop discrimination for farming systems in hilly landscapes. The possibility of discriminating banana, orange, plum and bamboo with vegetation indices such as NDVI, NDRE and GNDVI was validated. Among countries located in the Pacific region, bananas, coconut and sweet potato are major food crops (Halavatau and Halavatau, 2001). However, high-risk disasters such as cyclones and storm surge occur here frequently and threaten food security. In this context, UAVs enable robust food assessments and the localizing of security and classification of diverse crops, especially of targeted fruits like mango, papaya, and coconut (Saldana Ochoa and Guo, 2019).

2.4. Discussion

In this survey, the research on UAV-assisted orchard management literature has been discussed in terms of five categories: fruit-crop resource efficiency, geometric traits, productivity, disease, and other applications. The first three categories account for 67% of the publications reviewed (Fig. 2. 5), while the other two categories merit highlighting. Gaps and potential of evolving technologies in the domain of UAV-OM have been explored, ranging from application scenarios and UAV platform development to aerial data processing methodologies. In summary, UAV-based monitoring has very broad application prospects in orchard management because of its advantages related to flexibility, high efficiency, and low monitoring costs. In the following subsections, research gaps and opportunities in the near future are discussed.

2.4.1. Geometric traits of fruit trees

Different geometric traits of fruit trees have been measured using UAV imagery technology. To determine the state of art of the outputs, general geometric measurement performance was analyzed per year of article publication for four validation parameters: coefficient of determination (R^2),

classification accuracy, root mean square error (RMSE), and F1-score (Fig. 2. 8). The general performance of the selected geometric traits assessment from UAV imagery improved significantly in the last two years surveyed: 2018 and 2019. The reasons could be the advancements in sensor precision and data processing methodologies. Nevertheless, algorithm development needs further improvement in case studies on, e.g., the estimation of crown diameter, which shows a low R^2 . Within the analysis of estimation accuracy (Fig. 2. 8), the latest accuracy achieved for fruit-tree detection and counting is 99.9%, thanks to the employment of machine learning and deep learning (Ampatzidis et al., 2019). The overall trend in development is positive, but the compatibility of models needs further testing against different fruit species.



Fig. 2.8. Comparison of performance for geometric trait estimation in the 22 articles on the application of fruit-tree geometric traits. CPA: crown projection area, PPC: plant projective cover. Note: If an article described the results with two validation dimensions, both were included in this figure.

Studies over the past five years demonstrated the positive role of UAVs in fruit tree geometric measurement. To further enhance the adoption of UAVs for this application, the following developments can be identified:

- 3D representation: A realistic 3D representation of fruit trees is fundamental to the monitoring of geometric traits (Fig. 2.8). To deal with the problem of improving 3D reconstruction accuracy, investigation on the effect of flying speed, data capture view, GSD value and image overlapping parameter should be conducted, as demonstrated in earlier studies (Torres-Sanchez et al., 2018b; Xue et al., 2019).

- **Model generalization:** As found in the literature on geometric measurements the validation of the algorithm was based on one fruit species only (Johansen et al., 2018; Mu et al., 2018), more universal models should be developed and tested. Fruit varieties, orchard areas, irregular or other planting patterns and various climatic conditions (Fig. 2.4) should be extended to validate the robustness of the algorithms proposed.
- **Data processing efficiency:** Time-consuming issue is intimately tied to ortho-mosaic image processing and DSM generation as shown in previous studies (Sun et al., 2019). Thus there is an urgent need to further develop SfM method and faster algorithm for DSM generation and ortho-mosaic processing.
- **Automation:** Current measurements are semi-automated (Marques et al., 2019), and manual interference even leads to subjective errors. Further experimentation into automatic fruit tree identification and geo-referencing is strongly recommended. More sampled trees and the employment of artificial intelligence, e.g., machine learning, would provide more definitive evidence in automated and simultaneous identification.
- **LiDAR sensor:** Most of the research used passive sensors, e.g., RGB and multispectral sensors (Fig. 2.6). Only one article used a laser scanner (Hadas et al., 2019), which significantly yielded an apple-trees identification accuracy of 99% (shown as the second case scatter point in 2019 in Fig. 2.8). The potential of LiDAR application in estimating fruit-tree geometry deserves special attention due to its advantages in point cloud analysis. In addition, comparison between RGB and LiDAR-based aerial geometric measurement would also be a fruitful topic.

2.4.2. Resource efficiency

Stem water potential (ψ_s), stomatal conductance (g_s), and crop water stress index (CWSI) have been regarded as useful indicators for water status monitoring and irrigation strategy support in orchards (Ballester et al., 2018; Shackel et al., 1997). CWSI and alternative indices derived from UAV observations show promising results for water status assessment in orchards (Bulanon et al., 2016; Zhao et al., 2017). To date, a variety of indices have been compared against the commonly accepted indicators, ψ_s and g_s , and the reliable indicator CWSI (Table 2.3).

The correlation between remote sensing indices derived from UAV imagery and the three indicators mentioned above was analyzed (Fig. 2.9) based on the validation results for the coefficient of determination (R^2). In total, five fruit species, almond, citrus, apricot, peach and olive, were included. To clearly visualize the distribution of performance of each index, samples used for validation were divided into two categories, fruit species mixture and individual species. Because some research validated the performance of the method developed on an orchard with several fruit species instead of on a mono-species orchard (Park et al., 2017), mixed species was added to the analysis. On the other

hand, the 11 studies on which Fig. 2. 9 is based indicated that in UAV-based orchard management the tendency is to develop monitoring models or algorithms applicable for diverse fruit species. If an article compared indices against different species under different irrigation treatments, the best performance of each index toward a specific fruit species was selected for inclusion in Fig. 2. 9. In addition, as some indices belong to the same spectral family and are of less interest, or rarely selected by researchers, the one in the same family with relatively high correlation was included in Fig. 2.9. Several data in the figure were obtained from the same experiment.

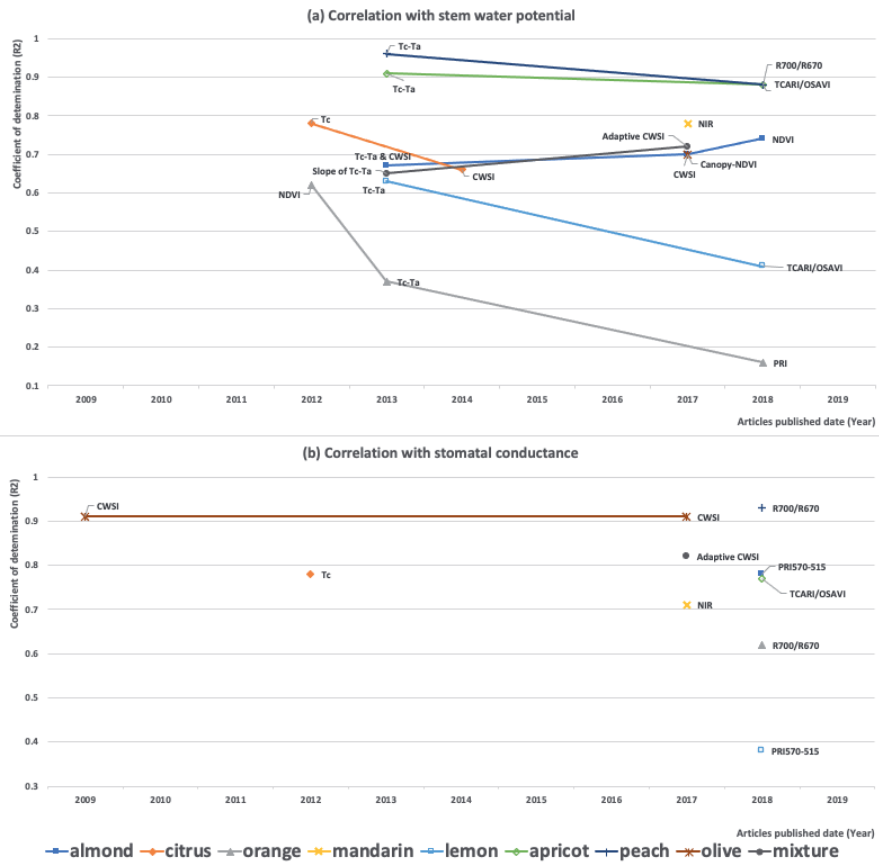


Fig. 2.9. Performance of diverse remote sensing indices for water status assessment in 11 articles: (a) Correlation with stem water potential (ψ_s) (b) Correlation with stomatal conductance (g_s) NOTE: The vegetation indices presented are described in Table 2.3.

When it comes to the correlation with ψ_s it was found that CWSI and the difference between Tc and Ta were generally relatively highly correlated with ψ_s (Fig. 2. 9). Some indices show high correlation with ψ_s for specific fruit species, e.g., PRI₍₅₇₀₋₅₁₅₎ and TCARI/OSAVI, while some indices level out at a low correlation, e.g., MTVI1 and Xanthophyll indices. An optimal estimation index for specific fruit species

can be determined, e.g., the difference between T_c and T_a is the best for peach tree water status assessment. Similar to the analysis of ψ_s , the correlation between the indices derived from UAVs against g_s showed that the most investigated indices were canopy NDVI, TCARI/OSAVI, and PRI, and that these indices performed differently for different species. TCARI/OSAVI and canopy NDVI showed relatively high correlation with g_s for several fruit species, so have potential as a universal index to be employed in diverse orchards. The plant-based indicator CWSI is regarded as a reliable tool for irrigation strategy support (Gonzalez-Dugo et al., 2014). The correlation between remote sensing indices and CWSI was explored among five fruit species in relation to water status assessment. Canopy NDVI showed high correlation with CWSI in three fruit species, almond, apricot, and peach, while PRI generally showed a relatively low correlation in most fruit species. In orange species, all the indices showed low correlation with CWSI. It is very important to compare variable indices with CWSI in order to determine alternatives for water stress assessment. More fruit species and indices should be tested in the near future, to enable optimal indicators to be determined for specific fruits.

The majority of research focus on the resource efficiency in orchard, especially on the estimation of water status, has yield promising results. Further research should focus on the following scope:

- **Model generalization:** Most research were conducted under specific conditions, which makes the methods proposed low-range applications (Caruso et al., 2019; Park et al., 2017). To establish an accurate and reproducible model, methods (Fig. 2.9) should be established and validated in various conditions, e.g., different weather, crop phenological stages, crop fields and management conditions.
- **Data calibration:** Assessment of fruit tree water status mainly relies on temperature information derived from thermal images (Fig. 2.6). Yet, the reduction of effects from solar motion, atmospheric thermal path radiation and transmittance on the indices calculation is a problem (Berni et al., 2009b; Zhao et al., 2017). Ensuring consistent relationship analysis performance and high assessment accuracy, the optimization of calibration strategy and the management of thermal drift effect to thermal sensors are necessary.
- **Intra-canopy variability of water stress:** Current research focused on the estimation of water stress at tree scale (Ballester et al., 2018). Investigation of the variability at intra-canopy level is needed, especially for the analysis of fruit tree genotypic response to the water constraints.
- **Periodic mapping:** Previous studies developed their methods by doing UAV flight one time only (Jorge et al., 2019). By contrast, periodic mapping of water status in orchards can not only test and enhance the robustness of methods proposed but also facilitate the adoption of UAVs in irrigation management for growers.

2.4.3. Productivity and disease monitoring

Although most of the research focused on resource efficiency monitoring and geometric traits estimation, other aspects of orchard management were also covered, such as nutritional status and yield monitoring. For these aspects, crop physiological changes need to be understood and reliably modeled. Interdisciplinary investigation is a challenge for researchers in the domain of UAV-OM. UAVs are still generally underused and more comprehensive and in-depth exploration are needed. The research on the nutritional status monitoring of fruit trees shows an increasing trend, which is important not only for improving the output of fruit industry, but also for guiding the use of chemical fertilizers and pesticides. Yield estimation and prediction is then key for decision-making, especially for harvest strategy. As the costs of RGB sensors fall, the use of sensors to determine the optimal harvesting period for orchard production will increase. Yield estimation entails estimating flowering, which benefits the thinning activities. The complex structural traits of fruit crops may force UAVs to fly between tree rows in order to achieve an optimal inspection angle and a fine spatial resolution. Further investigation and experimentation are strongly recommended in the following aspects:

- Yield estimation at the tree or fruit level: A study applied ANN and yield an apple segmentation accuracy of 99.12% showed the great potential of UAV in fruit yield estimation, though the data was manually collected by emulating UAV capture conditions (Sabzi et al., 2018). Unfortunately, no research focused on yield estimation at fruit level was conducted (Fig. 2.7). Thus real-time direct estimation of fruits is encouraged.
- Method generalization: Current achievements in indirect yield estimation and health status monitoring are positive, as introduced in fruit-tree productivity traits section. However, there is abundant room for further progress in enhancing the robustness of the methods proposed (Fig. 2.7). Periodic mapping, as demonstrated by the study (Perry et al., 2018), is encouraged. Yet performance for different crops and growing stages remain unanswered at present.
- Machine learning: Methods and models proposed in some research (Fig. 2.7) need to be adjusted when apply them into a new case (Horton et al., 2017). Advanced machine learning algorithm can solve this problem, but also issues from the complexity of lighting intensity and conditions need to be taken into account.

In regular management, an outbreak of fruit-tree disease cannot be ignored. So far, the research on early warning monitoring of fruit-tree diseases has not shown an increasing trend, though a few studies have suggested the feasibility of UAVs in detecting biotic diseases in orchards. One reason may be that most fruit-tree diseases are not lethal, while HLB disease has attracted more attention because of its globally lethal effect on citrus crops (Arredondo Valdés et al., 2016). The complexity of pathological analysis for disease detection is also an important factor restricting related research. In other words, the development of UAV-OM for disease diagnosis is limited by laboratory detection or pathological

research in particular cases. Future efforts could focus on the changes caused by disease, ranging from apparent external traits, such as color and texture, to fruit-tree photosynthesis. In addition, the substantially reduced spatial resolution of UAV is another issue can not be addressed and affect the disease monitoring. For example, wheat yellow rust can be detected in inoculation stage by analyzing the spectral reflectance differences, but it is difficult to monitor with the UAV though advanced sensor and low flight altitude, 16m, were designed (Su et al., 2018). Further studies should focus as follows:

- Timely and localized diagnose models: Differing from other UAV applications in orchards (Fig. 2.7), disease monitoring is regional (Stella et al., 2017). Thus statistical study is encouraged to build timely, robust and localized disease detection models.
- Machine learning: Current studies extracted too many features for the disease monitoring (DadrasJavan et al., 2019), which makes the reduction of the features used the tendency. Though SVM, random forest classifier and ANN have been deployed (Fig. 2.7) and yielded promising results, advanced machine learning algorithms needed to be explored for improving disease detection efficiency and even monitoring the diseases undetectable currently.

2.4.4. Other applications

Inspection in orchards leads to the implementation of management operations such as pesticide or nutrient spraying using UAV sprayers (Tang et al., 2018). Currently, research is mainly exploring the selection of the spraying parameters, e.g., operation height, and the whole process is remotely controlled. Intelligent spraying requires the spraying system to automatically identify objects to be sprayed and to have automatic variable-spraying ability. On the basis of precise information sensed by sensor-equipped UAVs (Gao et al., 2019), operational systems could achieve precision spraying in orchards. The combination of remote sensing and automation deserves to be highlighted. Apart from this, fruit-tree classification and identification has been the subject of current research. Promising results become the basis for further investigation of fruit-tree at individual level. The UAVs developed for orchard management could be applied to related agricultural domains, e.g., the food supply chain (Saldana Ochoa and Guo, 2019). And the monitoring technology in orchards could also be used to improve the performance of agricultural monitoring on a large scale. Further research topics identified are the following:

- Spraying automation: Optimization of UAV control parameters for ideal pesticide spraying has been the subject of many research (Hou et al., 2019; Tang et al., 2018). However there is a still unanswered question about the effects of deviated flight routes caused by manual control. Thus validation with automatic spraying process is recommended, especially for facilitating real-time precision spraying.
- Statistical study: To develop robust fruit-tree classification methods, statistical studies will be needed for the isolation of error sources, thus determine the limitations of the proposed solutions



(Ishida et al., 2018). On the other hand, optimal parameters for the implement of proposed methods can be highlighted, such as the optimal flying height during data acquisition.

- **Deep learning:** Machine learning and OBIA has been widely deployed in tree detection and classification (Karydas et al., 2017; Saldana Ochoa and Guo, 2019). Despite the promising results, further progress in improving the performance of proposed methods in various environmental and agronomic conditions with advanced deep learning algorithm need to be undertaken. And the first issue is the availability of larger training datasets with multiple fruit tree species.
- **Automation:** Automatic classification and identification of trees is still challenging. The complexity of orchard environment, e.g., the changing solar illumination, seasonal vegetation in high density modern orchard, makes semi-automated methods (Chen et al., 2019c) the optimal solution for current orchard management tasks. Studies with more focus on the automated and simultaneous classification are therefore recommended.
- **UAV versus ground vehicles:** The differences of imagery capture angle and spatial resolution between UAV and ground vehicle significantly effects their performance in orchard management (Zhang et al., 2019b). Combining UAV and ground vehicle, or even other platforms (Table 2.1), could be an advantage, in different applications.
- **UAV customization:** Current commercial UAVs can not meet all the requirements in orchard management. Customization of sensor deployed or UAV system provides new insights in the adoptability of UAVs, as demonstrated in one case study (Barrows and Bulanon, 2017). For example, a UAV system with the capability of upward image acquisition or acquiring datasets at specific fruit-tree organs scale will make unique spatial resolution or details of fruit-tree structure available for many research.

2.4.5. UAV platforms

Almost all the research in UAV-OM employed commercial UAVs due to the cost-effectiveness compared to handcrafted or industrial UAVs. Multi-rotor UAVs is the most widely used. While the complicated operation of fixed-wing UAVs make it less popular, such as the requirement of minimum flight speed before they stall. UAVs with VTOL system have emerged as new powerful platform. Its freedom from site condition restrictions make it capable work even on steep orchards (Torres-Sanchez et al., 2018b). RTK GNSS is becoming standard resulting in increased geometrical quality in SfM processing (Xue et al., 2019) and derived products like ortho-mosaic and 3D point clouds (Marques et al., 2019) of fruit trees in orchard. This would allow comparison of changes in geometrical properties of trees within growing season and over years as indicator for productivity. The fundamental constraint to developing technology applications is the hardware system. The current limitations to the adoption of UAV platforms to orchards are the payload and endurance (Garcia-Ruiz et al., 2013), especially for

UAV-based pesticide sprayers and LiDAR UAVs. Increasing the battery capacities increases the payload, yet the payload of UAVs significantly affects the endurance performance. With the improvement of capacity of batteries, all types of UAVs flight duration will be extended, and VTOL will be more suitable for the mapping task in large surface fruit orchards and plantations. Powerful UAVs capable of carrying multiple sensing systems are generally more costly and not affordable for applications, especially in developing countries. Data collection opportunities and timing in orchards are limited and restricted. To ensure resistant flight in various weather and environmental conditions, the design of UAVs with weather-proofing capability is needed. In addition, platform vibration affects the accuracy of aerial indices and image quality. This could be resolved by improving UAV design and the post data-processing procedure. When deployed optimally in orchard management, UAVs are currently operated by persons with the skills of professional pilots. In the near future, the human-UAV interaction and ease of operation are expected to be further improved.

The articles reviewed revealed a shortage of customized UAV platforms. Various outdoor agricultural operations are very complex. For investigations on UAV-OM, requirements related to aspects such as image capture parameters and sensor automatic adjustment differ from each other. To set up datasets of optimal quality, researchers should clearly understand the theory underlying the data collection systems. The first basic step is to assess the suitability of the platform employed and whether it can be customized to meet the unique demands for the specific problem to be addressed. Although platform customization has drawn attention in studies on water status assessment and spraying (Ortega-Farias et al., 2016), it should also be considered in other scenarios.

Despite UAVs have been proved effective in assisting growers for orchard management, current development of UAVs is still far from meeting the requirements of precision agriculture in orchards. Futuristic development of UAVs should cover the following heads:

- LiDAR UAVs: UAVs with RGB, thermal, multispectral, and hyperspectral sensors have been explored in orchard management (Fig. 2.6), yet UAVs with LiDAR are undervalued. The weight of LiDAR sensors and their high power consumption pose a challenge for LiDAR UAVs, though significant advantages of it in geometric traits measurement has been demonstrated (Hadas et al., 2019).
- Onboard processing: By reducing the requirements of network bandwidth, commercial UAVs with onboard processing capabilities may benefit its controllability. On the other hand, with the advent of the 5G era, it would also enable the efficient communication among UAVs and other platforms which are used to execute management operations. In this way, so-called swarm intelligence (SI) can be achieved in orchards where detection and actuation is divided among different platforms (Zhang et al., 2019b).

- Active management platform: Current function of UAVs are mainly imaging and sensing (Fig. 2.6). However, more active involvement in orchards is required. Besides the UAVs with recognition capability for automatic and precise spraying (Gao et al., 2019), development in active visual scouting in orchards, e.g., searching for the trees with low nutritional status and even pests, will also be of interest.
- Obstacle avoidance: The complexity of horticultural environment limits the application of UAVs in orchard. Compared with conventional remote sensing, UAV automatic scouting between rows of fruit trees has potential of collecting data with higher resolution and yielding better performance (Das et al., 2015). To deal with this, UAVs with accurate obstacle avoidance system are needed to lessen the threat from trees and even birds to the flight safety.
- Night vision: Previously published studies have shown the feasibility of UAVs for monitoring various fruit tree traits that are directly related to the aerial imagery or spectral information and achieved promising results. Yet, for the complex traits that are indirectly related, e.g., the aerial indicator of Fusarium wilt of banana, few achievements were reported. UAVs with night working model may provide new insights to UAV-OM. Additionally, experiments from ground vehicles also indicated the potential of UAVs with night vision in improving the yield estimation accuracy (Chen et al., 2017; Wang et al., 2018a).

2.4.6. Sensor payload

Promising performance for various applications has been shown for five types of sensors that can be used on UAVs, namely RGB, thermal, multispectral, and hyperspectral sensors, and LiDAR. Based on the analysis of the sensors deployed, further analysis of the development of various sensors in different management applications was conducted (Table 2.5). Besides further explorations within orchard management, the blank area indicates potential for a “new” sensor more capable in a specific domain, such as utilizing LiDAR in yield estimation. All five sensors need to be corrected or calibrated within the process of aerial data processing in order to improve the monitoring accuracy. However, current RGB sensors lack the function of camera calibration and radiometric calibration, which can affect the sensor performance, especially for geometric estimation. Meanwhile the impacts of filters, optical defects, and sensor lenses, and even the selection of radiometric correction approaches for calculating the accuracy of remote sensing indices should also be kept in mind (Tu et al., 2018). Hyperspectral sensors gained the attention of the scholars in UAV-OM. Besides the reason of its size and less affordable characteristic, the geometric calibration accuracy also seriously affect the popularity. Though the sensor is capable to provide centimeter level spatial resolution, the geometric calibration accuracy is difficult to reach the same level. The application of LiDAR for fruit orchard management is relatively unexplored (Díaz-Varela et al., 2015); upcoming research areas may demonstrate the potential of LiDAR in orchard management, especially for geometric traits measurement. Regarding the pros and

cons of each sensor type, the tendency is for imagery or information fusion (Delalieux et al., 2014; Kestur et al., 2018). The basic principle of this multi-modal sensing approaches is combing different sensos on the same UAV platform. Datasets collected from different sensors contain unique fruit-tree traits, and imagery fusion can achieve the goals of getting these traits to complement each other and improving the detection accuracy. The development of UAV platforms is the basis of information fusion technology.

Table 2.5. Potential of UAV-based monitoring sensors for diverse orchard management activities.*

	Resource efficiency	Geometric traits	Productivity	Disease	Others
RGB	Horizontal pattern, down arrow	Vertical pattern, up arrow	Horizontal arrow, left	Down arrow	Vertical pattern, down arrow
Thermal	Vertical pattern, up arrow	Horizontal pattern, down arrow	Down arrow	Horizontal arrow, left	Horizontal pattern, down arrow
Multispectral	Vertical pattern, up arrow	Vertical pattern, up arrow	Horizontal arrow, left	Vertical pattern, left arrow	Down arrow
Hyperspectral	Vertical pattern, up arrow	Down arrow	Vertical pattern, left arrow	Vertical pattern, up arrow	Down arrow
LiDAR	Horizontal pattern, down arrow	Vertical pattern, left arrow	Horizontal pattern, down arrow	Down arrow	Horizontal pattern, down arrow

*- Cell patterns indicates application potential: Horizontal patterns: unknown potential; No patterns: suitable; and Vertical patterns: optimal selection. Arrow direction indicates current use: Up arrow: well exploited; Horizontal arrow: reasonably exploited; and, down arrow: unexploited.

As the basis of the adoptability of UAVs in orchard management, current limitations and perspectives of sensors deployed are as follows:

- Development in size and weight: The selection and cost of UAVs are limited by the size and the weight of sensors to be deployed e.g., the LiDAR sensor has more weight, which makes the UAV-derived LiDAR data largely unexplored (Hadas et al., 2019). What is now needed is the further miniaturization of sensors, especially for hyperspectral sensors. On the other hand, it is also intimately tied to the application of multi-modal sensing approaches.
- Development in imaging capability: The existing sensors limits the quantitative investigations due to the difficulty of extracting quantitative information from the data collected. Advanced sensors capable to obtain quantitative information in complex orchard environments are needed.
- Integration of sensor and UAV control systems: The vibration of UAVs during data acquisition process affect the performance of sensors payload, e.g., the geometric distortion occurs in hyperspectral data (Vanbrabant et al., 2019). The integration of the two control systems enable the dynamical control of the imaging sensors and further improve the data quality.



2.4.7. Data collection strategy

There are potential research areas in the design of fieldwork strategy. In some areas, continuous cloud cover greatly restricts the use of satellites for most of the year, making the potential of alternative sensing platforms like UAVs attractive. However, the aerial surveys should be postponed in windy conditions or light rain. Next, the trade-off between flying altitude and required image resolution deserves attention. A higher flying altitude produces lower spatial resolution. The differences of spatial resolution may affect the validation of the method developed. As a satellite maintains a constant altitude, effects of this are rarely observed. Many investigations produced a suitable solution for a specific problem by employing a strict set of operational parameters, e.g., flying height and angle of capture. Next, the effects of these parameters on the estimation accuracy should be studied, in order to expand the practical scope of approaches developed and to determine the optimal setting for the operational parameters.

Most research focused on specific fruit species at a certain growing stage under certain conditions. In other words, the achievements were attained under specific circumstances. The ideal situation is to develop approaches capable of monitoring various species or different growing stages of the same fruit species. Comparison between different species or certain growing stages provides a better algorithms validation strategy. Subsequently, various training systems or planting patterns could also be tested.

2.4.8. Development of methodology

Compared with conventional direct measurements, UAV-OM requires empirical statistics, reverse modeling, and image-processing technologies for effective, automatic, and precise management in orchards (Ballester et al., 2018; Saldana Ochoa and Guo, 2019). In the general workflow for UAV data processing, key steps are geometric correction and radiometric calibration. To deal with effects like solar motion, further calibration study is needed. Many monitoring methods have been proposed as being usable for similar case studies (Chen et al., 2017). However, the outdoor environment is far more complex than the indoor environment. Thus, problems in outdoor practice demand more sophisticated solutions. It is not surprising that existing algorithms are being applied to deal with certain problems, but researchers tend to overlook the need to refine the algorithms. This also explains why the developed algorithms prove unsuitable when tested under irregular conditions and why the classification performance is easily affected by background objects with characteristics similar to those of the target objects. Moreover, techniques like machine learning and deep learning have not been properly employed in UAV-OM. Focusing on the theory underlying the tools applied can overcome the limitations resulting from established techniques, especially in the case of application in a real agricultural environment. Finally, using large UAV datasets, efforts should be made to improve the

efficiency of image processing (Saldana Ochoa and Guo, 2019). And statistical studies aimed at verifying the robustness of methods developed deserve more attention.

2.5. Conclusion

This review has provided an overview of different applications employing UAVs with multiple sensors for fruit orchard management. The majority of the research was conducted in the past 4 years. UAVs generally yield a fine monitoring efficiency and accuracy, which indicates their potential as novel remote sensing platforms. Yet, UAVs currently are mainly used by experts and there is still a need to make this technology directly benefit the crop producers providing them with precise information on the operational application of UAV technology in day-to-day operations.

UAV-OM investigation is yet in its infancy. The applications for resource efficiency and geometric traits are relatively mature, while yield estimation, especially the estimation at fruit level, disease monitoring and UAV-based sprayer will becoming increasingly important area. Results have demonstrated high correlations between various UAV-derived indices and target physiological traits measured manually. Yet new indices correlated to the complex traits which are difficult to directly assess remain undiscovered at present. Model generalization, data processing efficiency and automation are still challenging. Further studies, which take these three issues into account, will need to be undertaken. As a next step, the combination of artificial intelligence and remote sensing sciences will be able to close the gap between current research and precision orchard management. UAVs have promising application prospects in precision orchard management because of their fast and efficient monitoring. Real-time monitoring is the key trait of UAV-based remote sensing that makes up for the long periodic intervals of satellite monitoring. Timely fruit-crop-growing information like this will enable healthy crop growth to be assured and economic loss to be avoided. Further, growers may obtain real-time growth information from web or mobile applications using cloud computing and wireless transmission technology (Salami et al., 2019).

In recent years, multi-rotor UAV is the most widely used UAV in orchard management and the majority is the commercial UAV. In the trend of continuous miniaturization of sensors, the limitation to UAV-OM is mainly the flying time due to current state-of-the-art in battery capacity. Different types of UAV sensors have their own place for specific monitoring activities but share the pros and cons. Thus, multi-sensor data fusion could be promising although was not yet investigated. In the case of LiDAR, despite its notable advantages for measuring geometric parameters, it is not commonly exploited due to its significant operational costs and the limited UAV flight time (Friedli et al., 2016; Garcia-Ruiz et al., 2013). Additionally, pre-flight flying parameter settings, such as UAV speed and field of view, affect the monitoring performance. Thus, statistical study to determine the optimal data acquisition parameters and understand the effects for specific research is encouraged.

Global orchard production is especially significant at regional scale. This diversity is attributed to the local climate and soil, geographic and topographic conditions, and high number of fruit species. The lack of publicly available datasets requires researchers to develop their own datasets although it could be more efficient to reuse images already acquired. At some point, growers will be encouraged to share the data gathered with their own UAVs and in situ observations to boost the advances in UAV-OM.



Chapter 3

Automatic flower cluster estimation in apple orchards using aerial and ground-based point clouds

This chapter is based on:

Zhang, C., Mouton, C., Valente, J., Kooistra, L., van Ooteghem, R., de Hoog, D., van Dalssen, P., Frans de Jong, P., 2022. Automatic flower cluster estimation in apple orchards using aerial and ground based point clouds. *Biosystems Engineering* 221, 164-180.

ABSTRACT

Chemical and mechanical thinning processes have long been used in the practice of stone and pome fruit production. During the thinning process of apple flowers, growers use chemicals to regulate the tree load. Moreover, hand thinning is applied after June drop to trim trees with excess crop load. The process of thinning can be an unpredictable process especially in biennial bearing cultivars. Incentives to optimize chemical usage and to lower expensive manual labour is ever increasing. Ground based machine vision systems have grown in popularity in orchard management due to the level of detail as well as plant coverage they can inspect with. Additionally, Unmanned Aerial Vehicles (UAV) based remote sensing is an increasingly popular non-invasive quality inspection tool. This chapter proposes a framework for combining UAV and ground based RGB image data to detect flowering intensity in a Dutch Elstar apple orchard. The framework, based on point cloud reconstruction, presents automatic point cloud handling techniques as well as automated unsupervised flowering intensity estimation methods. Two linear regression models based on unsupervised machine learning methods were trained and validated from the framework that estimate flowering intensity in the orchard with both models having $R^2 > 0.65$, $RRMSE < 20\%$ and $p\text{-stat} < 0.005$ for the correlation between the image derived flower index and the flower cluster number counted in field. The proposed methods provide a novel strategy for guiding flower thinning using simple RGB images and location data only. Moreover, the proposed methods also reveal the flexibility of intra-tree inspection by checking its sub-volumes.

Nomenclature				
UAV	Unmanned aerial vehicles	I_U		Images taken from a UAV (.jpg)
RGB	Red, green, blue	GV		Ground vehicle sensing platform
SVM	Support vector machines	PC_E		Point cloud constructed from I_E only
CNN	Convolutional neural networks	PC_W		Point cloud constructed from I_W only
SD_{bio}^2	Biological standard deviation	PC_U		Point cloud constructed with I_U only
SD_{obs}^2	Observed variance	SOM		Spatial orientation model
SE	Standard error	PCA		Principle component analysis
WT	West-top observation volume of a tree	MSAC		M-estimator sample consensus
WM	West-middle observation volume of a tree	RANSAC		Random sample consensus
WB	West-bottom observation volume of a tree	FDM		Flower detection model
ET	East-top observation volume of a tree	PC_{Hyb}		Hybrid point cloud constructed by merging PC_E and PC_W
EM	East-middle observation volume of a tree	LOOCV		Leave-one-out cross validation method
EB	East-bottom observation volume of a tree	UI		User interface
RTK	Real time kinematic positioning	Model-T		Flower cluster prediction model for the top volume of a tree
GPS	Global positioning system	Model-MB		Flower cluster prediction model for the sum of the middle and bottom volumes of a tree
PC	Point cloud	R^2		Coefficient of determination
I_E	Images taken from Eastern side using a ground vehicle (.tiff)	RMSE		Root mean square error
I_W	Images taken from Western side using a ground vehicle (.tiff)	RRMSE		RMSE relative to mean

3.1. Introduction

During the process of growing apple trees, the trees undergo an annual flowering phase in spring. During this phase, the quantity of flowers can be an indicator to the fruit set (the number of flowers successfully pollinated and becoming fruits) and ultimately the resulting yield. At this stage of the cycle the grower would like to perform tree load management to guarantee desired fruit set, which is the management of, in this case, the number of flowers per tree (Zhang et al., 2021). This is where the process of thinning, mechanical and chemical thinning, is performed - to control the number of flowers per tree and ultimately the fruit set. Thinning is usually carried out over a rather large period including bloom and post bloom (Greene & Costa, 2013). It is an established method used to control the tree load in order to ensure fruits of a marketable size on a regular basis. A higher than optimal tree load results in higher quantity of fruit, but fruits of a smaller size - which is unfavourable for the grower as it leads to less sellable product. Excessive fruit load in apple trees may also result in suboptimal sugar levels, fruit colour and even storage life (Forshey, 1986). Thinning is implemented usually up to the point where fruits are at 18mm diameter in size. According to Greene & Costa (2013), manual and chemical thinning techniques are used nowadays for stone and pome fruits, but in the case of pome-fruits, specifically apples, the method of choice is mostly chemical thinning to lower labour costs for manual thinning.

Flower and fruit thinning remains an unpredictable process, especially in biennial bearing apple species that alternate irregularly between high and low bearing seasons (Greene & Costa, 2013). Add to the irregular annual flowering the fact that individual trees in the orchard vary in flowering intensity, and the unpredictability is understandable. Since this variation in flowering intensity occurs often, hand thinning (in addition to mechanical spraying machines) is still necessary to ensure the correct dosage per tree. It is the unpredictability, manual estimation errors and manual labour that holds great potential for improvement. It is therefore beneficial to the grower to know exactly how the intensity of tree flowering or, if possible, how many flower clusters are present per tree. The grower could with this information for instance optimise the fruit set per tree, optimise the amount of chemicals used and reduce significantly the manual labour involved in estimating the clusters during flowering and thinning labour. If flower intensity information of individual trees can accurately be accumulated, flowering in terms of spatial variability could also be mapped (allocating for instance each tree with a flower intensity score) and used to make better thinning decisions for individual trees (Farjon et al., 2020). These tree load maps could for instance be used in conjunction with a variable rate sprayer for the thinning process (Krikeb et al., 2017).

Rapid technological advancements have made it more accessible to gather flowering and other plant information in orchards, such as water stress, nutritional status and tree height, in a non-destructive way

with the use of machine vision systems on a range of platforms, such as handheld devices, ground vehicles and Unmanned Aerial Vehicles (UAV) (Aggelopoulou et al., 2011; Bargoti & Underwood, 2017; Lopez-Granados et al., 2019; Zhang et al., 2021). With regard to the sensors equipped to the platform within the research focusing on flowers in orchard, only RGB and multispectral sensors have been employed, due to the distinct colour feature of flowers against the background (Liakos et al., 2017; Tubau Comas et al., 2019). These platforms have their own pros and cons depending on specific application scenario. Though the monitoring conducted with handheld devices is inferior to others when it comes to the data collection efficiency, the data quality, especially the image resolution, enable more features available (Wu et al., 2020). Ground vehicle platforms are often used in orchard management because of convenience and data collection efficiency (Dias et al., 2018a, 2018b). For a particular research purpose, ground vehicle platforms can also provide a unique circumstance that benefits the data collection. For instance, with the help of the artificial lights equipped on the ground vehicle, image collection at night is available which reduces the effects of sunlight significantly (Wang et al., 2021). Current achievements in sensor miniaturization enable successful use of UAVs for orchard management, however, only a few researchers have conducted systematic research into flowering intensity estimation (Zhang et al., 2021). UAVs can not only provide efficient and reliable monitoring for orchards but also a detailed spatial and temporal solution. Research has demonstrated the use of UAVs in flowering intensity estimation and the ground vehicle in flower detection (Horton et al., 2017; Sun et al., 2021). Yet the comparison of these two platforms has been subject to considerable discussion. For example, when the spatial information of fruit trees is retrieved, such as the flower cluster number per tree, with 3D point clouds derived from UAV and ground vehicles, the two platforms often show different spatial scales and occlusions because of the different data acquisition locations. Thus there remains a paucity of evidence on which platform is more suitable for flowering intensity estimation in orchards.

Extensive research has been carried out on flower detection, classification and estimation in orchards with machine vision technology. Flower estimation studies have been mostly restricted to estimation at picture level rather than at tree level (Dias et al., 2018a, 2018b; Wu et al., 2020). In recent studies, the detection of flowers has been investigated in two ways, pixel-based and object-based detection methods (Vanbrabant et al., 2020). For pixel-based methods, the first step is the extraction of the pixels of interest. Once these pixels are extracted, flower detection is conducted by the calculation of flower pixel amount or a different fraction. Thresholding techniques are most commonly used within pixel-based methods, where the targeted objects are segmented by transforming a grayscale images into a binary one (Aggelopoulou et al., 2011). This is effective for images with high levels of contrast, and significant outcomes have been observed from previous studies (Horton et al., 2017). Krikeb et al. (2017) reported a R^2 of 0.97 for the correlation between the threshold derived flower areas to the flowering intensity scored given by an expert. A R^2 of 0.86 was observed between the flower intensity and the apple yield for both RGB and multispectral image based detection (Liakos et al., 2017). One disadvantage of

thresholding is that the threshold adjustment is needed for a new environment or dataset. By contrast, more advanced machine learning techniques are more robust and have attracted interest in the flower detection community. More specific, the machine learning derived pixel-based methods consist of support vector machines (SVM) (Dias et al., 2018b; Xiao et al., 2014), K-means (Tubau Comas et al., 2019), convolutional neural networks (CNN) (Dias et al., 2018b). For example, a model based on the combination of CNN and SVM proved to be successful with precision and recall rates of 90% (Dias et al., 2018b). Object-based detection is generally conducted with two steps, image segmentation and object classification. Image segmentation algorithms first aggregate pixels into spectrally homogenous objects, and then each of the objects is classified to accomplish the detection (Dias et al., 2018a; Vanbrabant et al., 2020). For the object-based CNN, an image patch is evaluated directly to detect if there is a flower (Chen et al., 2019; Yuan & Choi, 2021). Since object-based methods do the classification at object level, different classes of targeted objects can be determined and labelled during image annotation process. Based on this approach, not only flowers can be detected, but also the specific flowering stage can also be classified (Koirala et al., 2020; Yuan & Choi, 2021).

Earlier studies have demonstrated the capability of using machine vision technology for flower detection at picture level. To assist the growers to decide how many flowers needed to be removed for each individual tree, flower quantification at tree level is required to support flower management within the orchard. To our knowledge, there are only five studies focussing on the correlation between the flower estimation derived from image and the exact flower number counted in situ. Three studies were conducted with ground vehicles (Hočevár et al., 2014; Koirala et al., 2020; Wang et al., 2021) and two with UAVs (Tubau Comas et al., 2019; Vanbrabant et al., 2020). Two reported R^2 values of the correlation between the image based flower index and the exact cluster number counted in situ were 0.56 and 0.59 because of the camera capture view, using only top-view and one-side view of the trees, respectively (Hočevár et al., 2014; Tubau Comas et al., 2019). Simple capture view limits the estimation ability of machine vision, especially for the complex-structured fruit trees with more flower occlusion. Fruit trees are larger and have a more complex architecture compared to common agricultural crops, such as cotton, i.e., plant height and flower numbers for fruit trees and cotton, respectively, are 3-4m versus <1m and 350-2100 flowers versus 15-20 flowers (Vanbrabant et al., 2020). By contrast, Koirala et al. (2020) employed a dual-view imaging approach for mango panicle estimation at tree level capturing two images from each side of the trees to represent the total number of flowers per tree. Although the highest R^2 of the correlation between the panicle count on images and in-field human counts per tree yielded from the rotational region CNN was 0.86, a high bias was also observed. In addition, the proposed method could not be applied to the flower estimation of apple or pear trees since apple flower estimation suffers from higher flower occlusion and it is much more difficult to label each apple flower cluster in the picture. Wang et al. (2021) reported a CNN-based apple flower estimation, but the ground truth used was part of the tree where a coloured square section marker was used to

delineate and limit one counting area from a tree. RGB dense point cloud datasets derived from multi-view images have potential to retrieve tree spatial information, such as the geometric traits, as shown in several studies (Lopez-Granados et al., 2019; G. Sun et al., 2019; Torres-Sánchez et al., 2018). Vanbrabant et al. (2020) has demonstrated its performance of addressing the pear flower occlusion problems, but the errors in their study could not be explained because of the limitation in ground truth.

This chapter aims to develop and evaluate an approach for automated apple flower cluster estimation at tree level. The presented research contributes to the following:

1. Comparison of the capability of four conventional classification algorithms, manual threshold, Otsu segmentation, K-means and Hierarchical clustering, for flower cluster segmentation;
2. Comparison of the accuracy of UAV and ground vehicle derived point clouds for flowering intensity estimation;
3. Examine the effects of point cloud density on the flowering intensity estimation accuracy;
4. Evaluate the possibility of combining UAV and ground vehicle derived point clouds for flowering intensity estimation.

3.2. Materials and methods

3.2.1. Study area and field data

The study area for this project is an apple orchard in Randwijk, Netherlands (51.938, 5.7068 in WGS84 UTM 31U) (Fig. 3. 1). Apple trees in this orchard were planted in 2007 with four-years trees. In total 14 rows were designed, while for each row 101 trees were planted. The average tree height was around 2.3m in 2018. Row 5 (100 trees) of the orchard is unique from the rest of the orchard with the aim being to intensely monitor the phenotypical change in the row. Hand thinning is needed each year, but the amount of mechanical thinning is very variable. Detailed information about the orchard can be found in Table 3.1. Ground truth data, flower cluster and floridity, for Row 5 was established by an expert in the orchard. Flower cluster number was counted and recorded manually for 31 random trees in row5. More specific, for each individual tree, the exact flower cluster number was counted in the top, middle and bottom parts of the tree and documented accordingly. Floridity was determined by giving each tree a flowering intensity rating between 1 and 9 where 1 being no flowers and 9 being extreme flowering intensity. Floridity refers to the intensity at which the tree is flowering while flower clusters are the clustered arrangement of inflorescence.



Fig. 3.1. The study area and the subject row of this study (row 5). The orchard is delineated with red line and the row 5 is marked with a blue rectangle.

Table 3.1. Orchard information and management activities for 2018

Size	0.47 ha
Variety	Elstar
Rootstock	M9
Row spacing	3.0 m
Tree spacing	1.1 m
Flower thinning chemical	ATS (ammonium thiosulphate)
Fruit hand thinning threshold	110 fruits/tree
Rows	14

High within-sample variability can be observed in an orchard with high natural or biological variability (Anderson et al., 2021). To illustrate the within-sample variability in this study, the biological or intrinsic variability, biological standard deviation (SD_{bio}^2), was calculated by decomposing the estimator variance:

$$\text{Var} = SD_{obs}^2 = SD_{bio}^2 + SE^2 \quad (1)$$

Where SD_{obs}^2 represents the observed variance within the collected samples, and SE represents the standard error.

The ground truth, cluster number and floridity, was acquired on the 24th of May 2018 when trees were fully blooming. And the trees generally scored floridity between 5 and 8.5. Afterwards, an inventory of the collected ground truth was created (Table 3.2), based on Eq.1. As mentioned before, floridity is a manually assessed score and was given by the expert in the orchard. The variability within the samples can not reflect the natural variability. Thus no biological variability, SD_{bio}^2 , was calculated for floridity, but the standard deviation and the standard error were provided.

Table 3.2. Calculated floridity and cluster variance within trees.

	N	Average	SD_{obs}	SD_{bio}	SE
	(#trees)*	(# or #cluster/tree)	(# or # cluster/tree)	(#cluster/tree)	(#cluster/tree)
Floridity	100	6.8	0.7	-*	0.1
Total cluster	32	194	64	63	11

*“#” represents number; “-” represents no value.

100 trees in row 5 of the Randwijk orchard were equipped with observation tape (Fig. 3.), which was used by the expert as a frame of reference to compartmentalize trees and ground truth flower count. The observation tape runs throughout the entire row and serves the purpose of maintaining consistency in the counting of flower clusters and floridity of the tree. The tape divides trees into a Top, Middle and Bottom observation window. The tape was placed through the middle of the tree as to additionally divide the trees into East and West halves. Each tree in the row therefore has six observation volumes namely west-top, west-middle, west-bottom, east-top, east-middle and east-bottom (Fig. 3. 2, C). The expert used these observation volumes as a guide for assigning floridity and flower clusters scores to the trees and to be able to compare results of different instances and the changes that occur. Only cluster number was counted in detail for these observation volumes. Floridity was assessed from East and West sides and the average was marked as the flowering intensity for each tree. The inventory of the cluster variability within sub-observation volumes was calculated in Table 3.3.

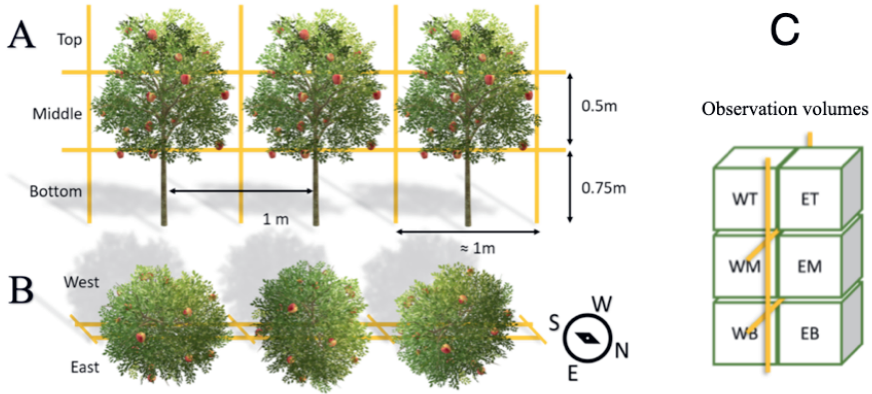


Fig. 3.2. Yellow observation tape used for counting purposes. A. Front view; B. Top view; C. Observation volumes. WT: West-top volume of a tree, WM: West-middle volume, WB: West-bottom volume, ET: East-top volume, EM: East-middle volume, EB: East-bottom volume. Note: Directional indicator is valid for B only.

Table 3.3. Calculated cluster variance within different sub-observation volumes.

	N (#volumes)*	Average (#cluster/volume)	SD _{obs} (#cluster/volume)	SD _{bio} (#cluster/volume)	SE (#cluster/volume)
Top	32	56	30	29	5
Middle	32	75	23	22	4
Bottom	32	62	21	21	4
Total	96	65	26	26	3

* “#” represents number.

3.2.2. Platforms and image acquisition

Images of row 5 were acquired using two platforms with onboard cameras. A ground vehicle equipped with three RGB cameras as well as a real time kinematic positioning (RTK) system, drove through row 5 taking pictures (1m from the trees) at three different heights (0.75m, 1.30m and 1.85m from the ground respectively). These three cameras were equally spaced vertically to capture, in combination, the full height variation of the trees. The images were taken at a rate of 11 frames per second. The ground vehicle drove through the orchard on the East and West side of row 5. This platform path allowed pictures to be taken from the Eastern and Western side of the trees. The second camera platform was a UAV equipped with a camera and a global positioning system (GPS), taking images of the orchard at a height of approximately 10 meters above the orchard canopy. This camera setup offered multiple

vantage points of any given tree in the row. Refer to Table 3.4 for more details regarding the platforms and Fig. 3.3 for a summary of the data collected. At the time of data acquisition (24 April 2018), weather conditions were cloudy.

Table 3.4. Camera platform specifications and data size

	Aerial vehicle	Ground vehicle
Vehicle type	DJI™ Phantom 3 PRO, Shenzhen, China (quad-rotor)	Tractor (generic)
Camera type	FC300X, Shenzhen, China (RGB)	Intel® RealSense™ Depth Camera D435 (RGB-Depth)
Sensor resolution	4000x3000	1920 × 1080
Frequency	Variable	11 fps
Positioning system	GPS (geotag per image)	RTK (10Hz)
Acquired images	362	10,355

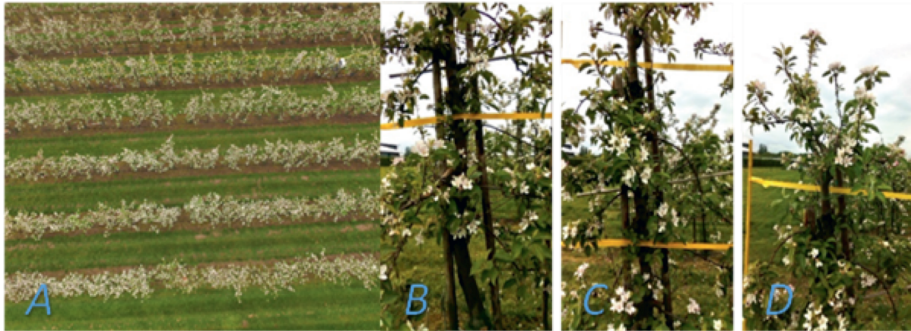


Fig. 3.3. Example image data. A: UAV imagery. B: Ground vehicle imagery, camera position: 0.75m. C: Ground vehicle imagery, camera position: 1.30m. D: Ground vehicle imagery, camera position: 1.85m.

3.2.3. Methods

The approach proposed follows the methodology presented in Fig. 3.4. To utilise both data sources and merge them, it was decided to assess the trees through the use of photogrammetric point clouds (PCs). It was decided that a PC of row 5 could offer great insight into the spatial variability of the flowering intensity of the trees by allowing not only inter-tree analysis but also intra-tree analysis. This approach proposes to create three separate PCs from three vantage points, handle and analyse them separately and ultimately combine their results at the statistical analysis stage of the framework. Two software, Agisoft Metashape Professional (Agisoft LLC, St. Petersburg, Russia) version 1.6.2 build 10247 and MATLAB R2019b (MathWorks Inc., Natick, MA, USA), were used for the manual and automatic analysis indicated in the framework. This approach allows all three PCs to undergo the same empirical

operations without any spatial or colour-space differences influencing their results. It also allowed for the trees in the three PCs to be subdivided and therefore inspected in a more flexible way.

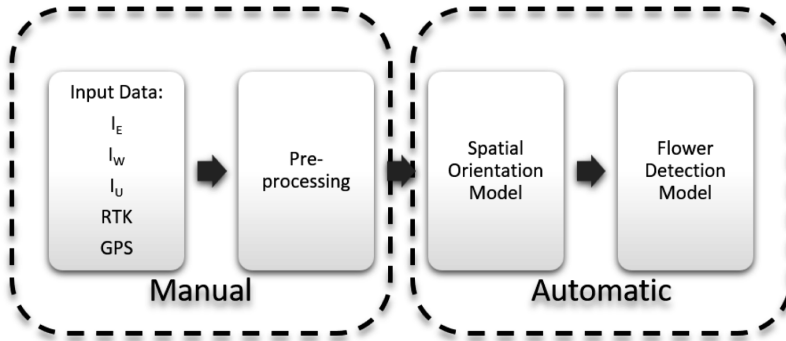


Fig. 3.4. Schematic of the proposed framework. I_E and I_W : ground vehicle derived images taken from Eastern and Western side of a tree, respectively; I_U : images taken from the UAV

3.2.3.1. Image pre-processing

During the pre-processing phase, raw images and positioning data from the respective camera platforms were manually processed. The altitude of the images was determined by the altitude of the study area and adjusted according to the known height the image was taken. The location data (RTK & GPS) along with the images were loaded into Agisoft Metashape software. Using Agisoft Metashape, location data and image data were used to create point clouds of the row of trees. Two main stages were involved in this process: aligning the images and building the dense cloud. Aligning the photos automatically identifies image features, creates image pairs and reconstructs camera locations. Moreover the 3D structure of the scene is initialized. Based on the tie points, the images were loaded again and the geometry between the tie points was calculated during the second stage. Detailed processing parameters applied during these two stages were summarized in Table 3.5. From Fig. 3.5 it can be seen that the output of the pre-processing phase consists of three versions of point clouds of the same row of trees. Then these point clouds were transferred to .ply format, which is compatible with MATLAB, for the automatic processing in the following two models, spatial orientation model and flower detection model. Density information per point cloud can be found in Table 3.5. Density difference between the GV and UAV point clouds can be described as considerable.

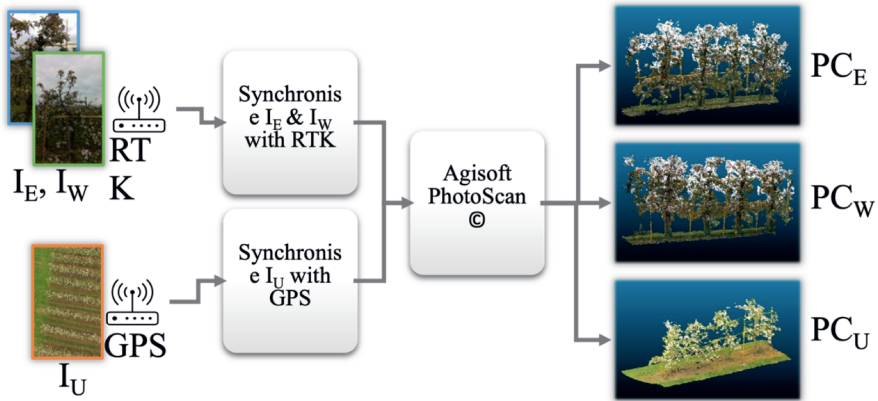


Fig. 3.5. Schematic of pre-processing phase with three point clouds as output. I_E and I_W : ground vehicle derived images taken from Eastern and Western side of a tree, respectively; I_U : images taken from the UAV; PC_E : point cloud constructed from I_E only; PC_W : point cloud constructed from I_W only; PC_U : point cloud constructed from I_U only.

Table 3.5. Parameters of the point cloud generation in Agisoft Metashape and the yielded point cloud density.

	PC_E^*	PC_W	PC_U
Align photos			
Accuracy		High	
Generic preselection		Disabled	
Key point limit		40,000	
Tie point limit		4,000	
Build dense cloud			
Quality		High	
Depth filtering		Mild	
Calculate point colours		Enabled	
Coordinate system	WGS 84 / UTM zone 31N (EPSG: 32631)		
Data points per tree	$3.90 * 10^5$	$3.30 * 10^5$	$0.30 * 10^5$
Tie points per image	158	141	71

* PC_E and PC_W : point cloud constructed from the ground vehicle derived Eastern and Western side images of the trees, respectively; PC_U : point cloud constructed from the UAV imagery.

3.2.3.2. Spatial orientation model

The input to the spatial orientation model (SOM) (Fig. 3. 6), three point clouds, undergo a process whereby the main goal was to divide each tree in the point clouds into six observation volumes. These volumes and their properties can then be used to detect the floridity and flower cluster counts. As previously mentioned, the aim was to empirically handle the PCs and fuse the results of the flower detection model. The spatial orientation model therefore prepared the observation volumes to be used in the detection phase later in the process.

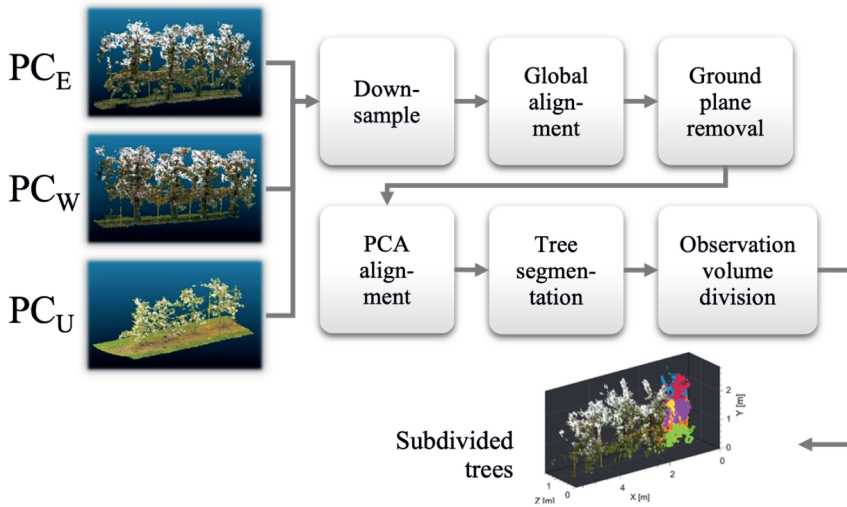


Fig. 3.6. Schematic of the spatial orientation model (SOM). PC_E and PC_W : point cloud constructed from the ground vehicle derived Eastern and Western side images of the trees, respectively; PC_U : point cloud constructed from the UAV imagery.

The first function in the SOM was to downsample the PCs in order to limit computational time and allow for the PCs to be handled more computationally efficient by the succeeding algorithms. The PCs were downsampled randomly from their original count as to not influence the spatial distribution of the input data. To further smooth the point cloud from outliers and reduce the amount of measurement errors and density variations a statistical outlier removal filter was applied (Rodríguez et al., 2018; Sultani & Ghani, 2015). More specific, all points inconsistent with all neighbours were trimmed out by calculating and comparing the mean distances with the interval defined by mean and standard deviation. The global orientation of the PC entering the SOM might be distorted. In a similar fashion to Dong et al. (2020), the global alignment function made use of principle component analysis (PCA) to align the component of highest spatial variance (in this case the length of the PC) to the X-axis. An important function of the SOM was removing the ground beneath the trees (Fig. 3. 7). The ground data points that fall within a specified distance from the ground plane were removed from the PC to leave only the trees

remaining. This improves the accuracy of succeeding operations by eliminating the possibility of taking irrelevant data, ground data points, into account.

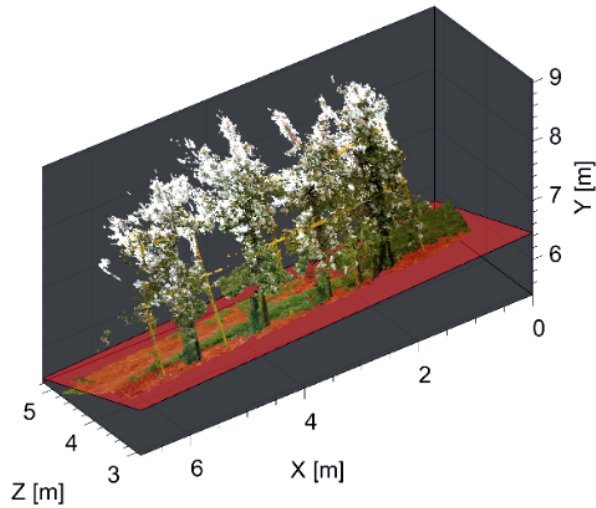


Fig. 3.7. Illustration of the ground plane removal function. The red plane represents the ground plane.

With ground data points being removed and only trees left the PC now served as input to the PCA alignment function. During this function the PC was aligned in all three spatial dimensions for the second time to offset the result of the first PCA alignment due to ground points. Using PCA, the component with the highest spatial variance (length) was re-aligned to the X-axis. The component with the second highest variance (height) was aligned to the Y-axis. Finally, the component with the least spatial variance (depth) was aligned to the Z-axis (Fig. 3. 8). At this stage of the model, all three input PCs were aligned in the same coordinate system and orientation. Equally important is the distribution of spatial data start from the origin (0) after this function was applied.

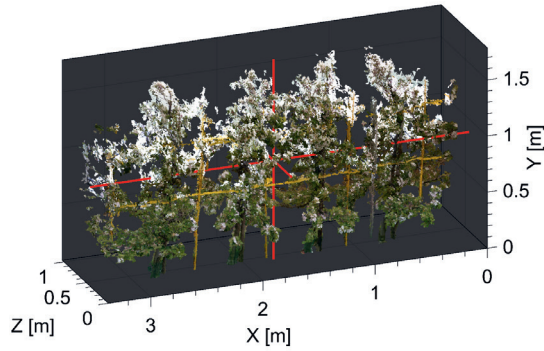


Fig. 3.8. Trees fully aligned by PCA alignment function. The red lines indicate the direction of each principle component.

The segmentation function automatically isolated all trees based on the vertical observation tape in between trees using a MSAC (Fischler & Bolles, 1981) algorithm, a variant of the random sample consensus (RANSAC). The MSAC was used to fit rectangular planes to the observation tape horizontally and vertically (Fig. 3. 9). Four planes isolated a tree from the rest of the row as well as divide the tree into a bottom, middle and top volume based on the observation tape. The size of these volumes vary from tree to tree depending on how the observation tape was installed in the orchard. The resulting individually segmented trees then passed through to the final function of the SOM. The subject tree enters the final function of the SOM where the tree was divided into six observation volumes (Fig. 3. 10). Every tree in the three input PCs, PC_E , PC_W and PC_U , was processed. The height layers were defined for every tree and the data points that fall within those height layers were divided in an East and West part of the tree. Therefore, at this stage of the framework, for any given tree in row 5, there were three versions with each six subsections.

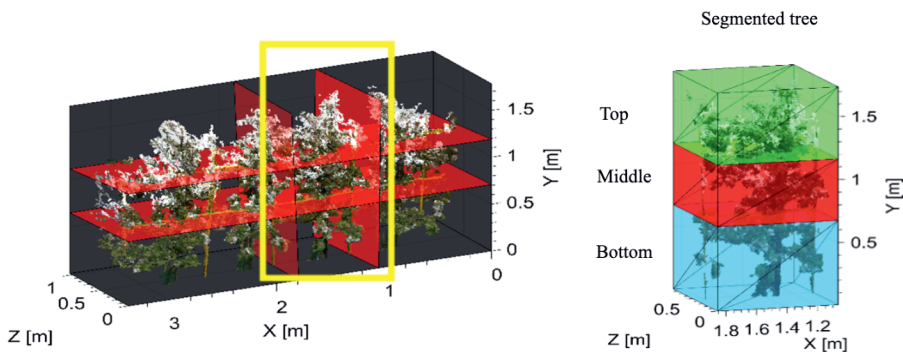


Fig. 3.9. Individual tree segmented from row 5. The height layers, defined by observation tape, of the tree in the yellow window is shown on the right.

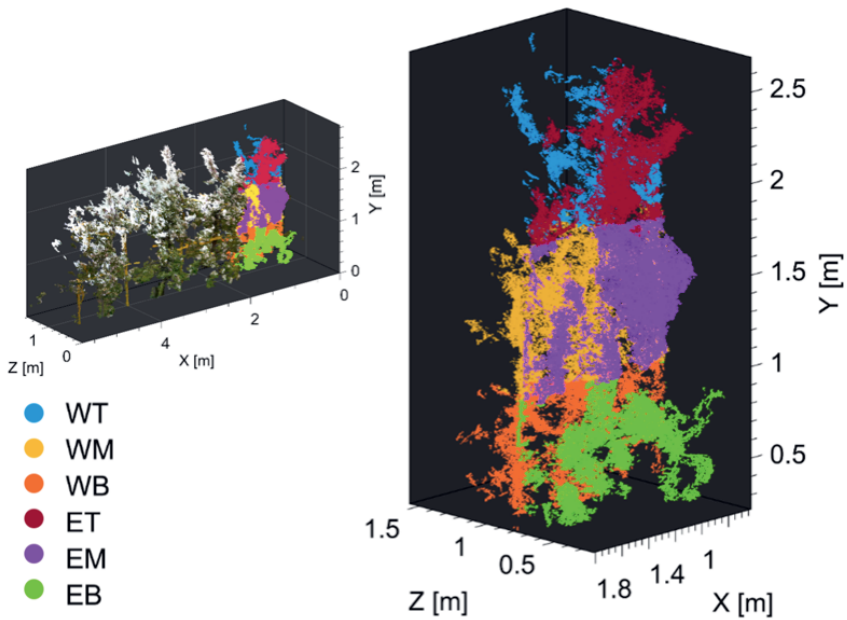


Fig. 3.10. Outcome of the SOM model. For each tree, tree points in the six observation volumes are highlighted in different colour. WT: West-top volume of a tree, WM: West-middle volume, WB: West-bottom volume, ET: East-top volume, EM: East-middle volume, EB: East-bottom volume.

3.2.3.3. Flower detection model

The aim of the flower detection model (FDM) (Fig. 3.11) was to extract data points, based on their colour properties, that belong to flower clusters. These data points can then be used to find a correlation between the amount of white data points and the ground truth flower clusters in the various subsections of the trees.

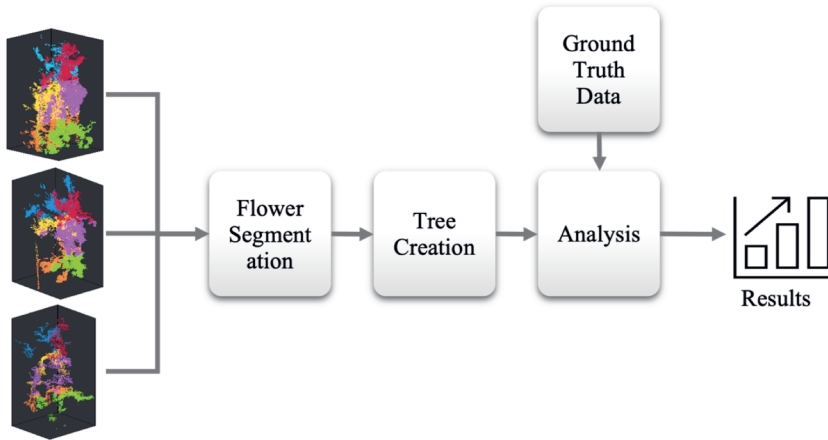


Fig. 3.11. Schematic of the flower detection model.

To segment the data points that belong to white flower clusters in the flower segmentation function, four different methods were used:

1. Manual thresholding
2. K-Means clustering
3. Otsu segmentation
4. Hierarchical clustering

Manual threshold segmentation was achieved by manually inspecting a collection of images (45 from GV and 40 from UAV) from random trees in the orchard. By segmenting all the images manually, average lower and upper thresholds were determined for red, green and blue colour bands that explain the flower cluster pixels. These thresholds were used to segment data points in the point clouds that belong to flower clusters by extracting data points that have the colour properties which match the criteria.

The blue colour band was used for the three automatic methods to prevent the influence of the yellow observation tape on the segmentation result. The flower clusters could not be segmented without including the observation tape when using the red colour band. The blue and green colour band showed some collinearity in segmentation and therefore only blue was used. Using only one colour band also reduces the computation time for more computationally intense algorithms such as Hierarchical clustering.

K-Means clustering is an unsupervised machine learning algorithm that finds clusters in data by maximizing inter-class variance while minimizing intra-class variance. It is also a popular point cloud

clustering technique that uses features or attributes from the point clouds (Grilli et al., 2017). The algorithm finds k number of clusters, where k is predetermined. K-means clustering was implemented on the colour properties of the data points from the various subsections to cluster the data points into classes based on the blue colour band. By manual inspecting a collection of images, flower colour feature were found distinguishable in the blue channel. Moreover, flower points in the point cloud showed highest brightness compared with the background, in UAV coloured point clouds. For ground-based point clouds, four components showed significantly different sensitivity to the changes of threshold in blue channel, they are the sky, the flowers, the ground with no vegetation and the green objects(leaves and the grass). Therefore, $k=2$ was set for PC_U , and $k=4$ was determined for ground-based point clouds.

Otsu segmentation is an algorithm that automatically segments data into two parts by automatically defining a threshold between two classes. It has also been proven successful in segmenting point clouds based on RGB information (Jia et al., 2019). Otsu segmentation method divides the data by maximizing the inter-class variance.

Hierarchical clustering is a machine learning algorithm that finds a predefined number of clusters in the data set. It is an unsupervised clustering method that iteratively splits the data set into smaller subsets until every subset contains only one object (Ng & Han, 1994). The Hierarchical clustering algorithm iteratively splits the blue colour band data of the subject point cloud to find distinct classes in the data. With the same approach to the determination of k for K-means method, Hierarchical cluster number was predefined as 4 and 2 for ground vehicle and UAV data respectively.

The outcome of flower segmentation consists of only data points belonging to flower blossoms (Fig. 3. 12). The count of data points in the resultant subsections is known as the white index and will be used in the analysis function.

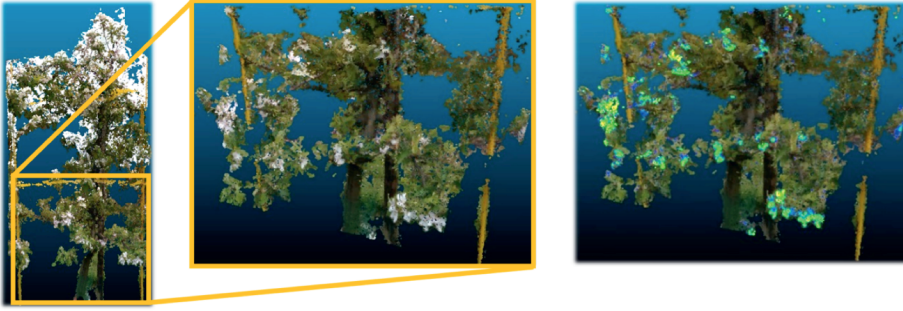


Fig. 3.12. Left: colored point cloud of tree 14. Middle: bottom section of tree 14 with clear flower blossoms present. Right: flower clusters detected from the middle volume using the Otsu segmentation method.

The sub volumes of the trees created in the SOM allow any combination of sub volumes to be used as “puzzle pieces” to build a tree comprising of different point cloud origins. The conclusion can also be made that the Eastern side of PC_E was of higher quality than the Western side since the exposure to the camera was greater and occluding branches and leaves prevent the camera from potentially capturing flower blossoms on the Western side. The same can be said for PC_W . The tree creation function combined the best sides of PC_E and PC_W to create a hybrid combination tree. Therefore, the three eastern segmented subsections from PC_E (East-top, East-middle and East-bottom) and the three western segmented subsections from PC_W (West-top, West-middle and West-bottom) were combined for every tree. Each sub volumes had flower data points only. The output of the tree creation function is explained in a tabulated form (Table 3.6).

Table 3.6. Composition of a tree resulting from the tree creation function.

	PC_U^*	PC_{Hyb}
Top volume	$ET_{PC_U} + WT_{PC_U}$	$ET_{PC_E} + WT_{PC_W}$
Middle volume	$EM_{PC_U} + WM_{PC_U}$	$EM_{PC_E} + WM_{PC_W}$
Bottom volume	$EB_{PC_U} + WB_{PC_U}$	$EB_{PC_E} + WB_{PC_W}$

* WT = West-top volume of a tree, WM = West-middle, WB = West bottom, ET = East-top, EM = East-middle, EB = East-bottom, PC_E = East side of ground vehicle point cloud, PC_W = West side of ground vehicle point cloud, PC_U = UAV point cloud, PC_{Hyb} = the hybrid point cloud constructed from PC_E and PC_W .

The analysis function used the PC_U and PC_{Hyb} trees as well as ground truth data as inputs to compare the count of the trees to the floridity and the flower cluster ground truth. The aim was to find which segmentation algorithm results in the highest correlation between the white index and ground truth data.

Evaluating if the white index of the trees should have a linear relation to the floridity and amount of flower clusters, linear regression was used as the statistical model to find correlation. The combination of data source, flower segmentation method and section of the tree with the highest correlation was used to train and validate a linear regression model for predicting flowering intensity. Due to the limited size of the model, a leave-one-out cross validation (LOOCV) method was used to validate the models. LOOCV is a special case of the resampling procedure K-fold cross validation. It is used to evaluate the performance of machine learning models with small data sets. LOOCV is the case where the fold number equals to the number of observations.

3.3. Results

Two main outcomes of the SOM are the point clouds of individual trees and their subdivided observation volumes. The performance of the individual trees and their subdivided observation volumes segmentation was validated for 107 trees (Fig. 3. 13) and 186 observation volumes (Fig. 3. 14), respectively, by comparing the segmented data points to manually annotated ground truth counts. Outliers are determined for both results. These are trees and observation volumes that could not be spatially segmented properly. Only trees with spatial segmentation accuracy higher than the 25th percentile were used for correlation analysis. A simple user interface (UI) enables the user to select a single tree or its six observation volumes in the row to inspect visually. With this UI, performance of the proposed method on a series of adjacent trees stretching from 17 to 21 was also demonstrated (Fig. 3. 13). In the case of tree17, inconsistent segmentation results are observed, where the segmentation of East-side is better than that of the West-side. For the result of tree subdivided observation volume segmentation (Fig. 3. 14), it is clear that trees created from GV data can be divided more accurately. This can be attributed to the poor visibility, in the PC_U , of the horizontal yellow observation tape running through the trees. As this is the feature used to segment the observation volumes, it makes sense that the performance for PC_U is inferior.

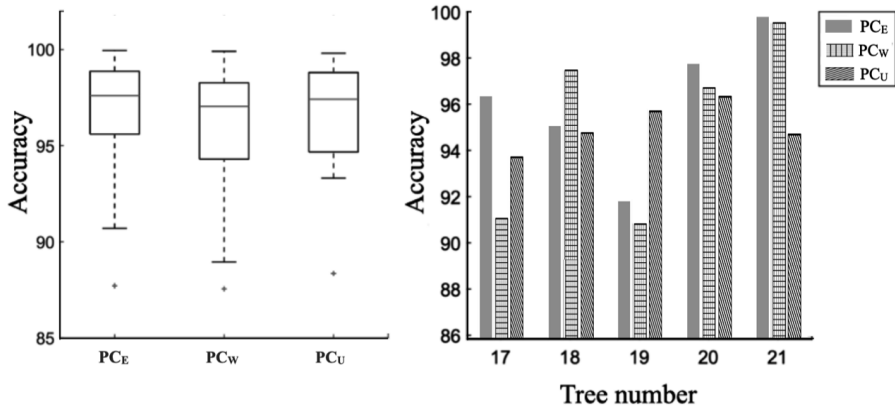


Fig. 3.13. Accuracy of the tree segmentation. Left: validation for 107 trees. Right: accuracy of the segmentation to trees ranging from tree17 to tree21. PC_E = East side of ground vehicle derived point cloud; PC_W = West side of ground vehicle derived point cloud; PC_U = UAV derived point cloud.

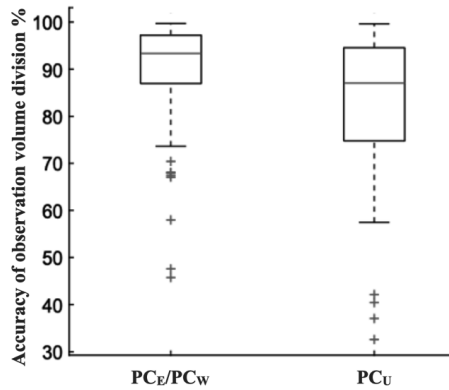


Fig. 3.14. Accuracy of the observation volume segmentation. PC_E = East side of ground vehicle derived point cloud; PC_W = West side of ground vehicle derived point cloud; PC_U = UAV derived point cloud.

Correlations between white index derived from different segmentation methods and ground truth, flower cluster number and floridity, for PC_{Hyb} and PC_u trees are shown in Table 3.7. It suggests clearly that for trees in PC_{Hyb} the most effective way to segment flower blossoms from the trees is with Hierarchical Clustering, with the only exception being in the top part of the tree where manual thresholding ($R^2 = 0.67$) supersedes the automatic methods ($R^2 = 0.24$). For PC_U, as hypothesised, optimal method proved to be Otsu segmentation in the blue colour band. However, when the segmentation of the top-middle combination is evaluated, Hierarchical method has a significant performance, with R^2 of 0.78 (Table 3.7). Floridity is a subjective score given by the expert in the

orchards, which is used to describe how intensive the flowering situation is. In general, there is less room for the improvement of the floridity estimation based on PC_U , where no positive correlation is found. And the segmentation performance at tree level is also poor, with a mean R^2 of 0.4. But the PC_U evaluation at upper sub-volumes is significantly good, for example, R^2 for the top and top-middle sub-volume is 0.7 and 0.78, respectively (Table 3.7).

Table 3.7. The correlation results for different segmentation algorithms on both PC_U and PC_{Hyb} .

R^2 (White index VS)	Manual threshold		Otsu segmentation (Blue band)		K-means clustering (Blue band)		Hierarchical clustering (Blue band)	
	PC_U	PC_{Hyb}	PC_U	PC_{Hyb}	PC_U	PC_{Hyb}	PC_U	PC_{Hyb}
	Floridity	-	0.60	-	0.23	-	0.61	0.21
Total cluster	0.41	0.50	0.43	0.28	0.20	0.52	0.46	0.61
Top	0.67	0.41	0.70	-	0.33	0.31	0.35	0.24
Middle	-	0.40	-	0.20	0.30	0.15	-	0.66
Bottom	-	0.51	-	0.36	-	-	-	0.50
Top + Middle	0.67	0.46	0.67	0.19	0.22	0.44	0.78	0.53
Middle + Bottom	-	0.51	-	0.27	-	0.47	-	0.70

Note: Only the first row shows the correlation between white index and floridity, the rest is the correlation with flower cluster number. Cells highlighted with shading represent the highest correlation yielded in this study, while cells with no data indicate no positive correlation ($R^2 < 0.1$). PC_U = UAV point cloud. PC_{Hyb} = Ground-based hybrid point clouds.

Results indicate that using Otsu segmentation in the top of the trees with UAV data gives a higher correlation while using Hierarchical clustering with ground vehicle data gives the highest correlation for the middle and bottom of the tree combined. The high correlation can also be checked in details with plots (Fig. 3. 15). For both figures, data points evenly distributed on both sides of the regression line.

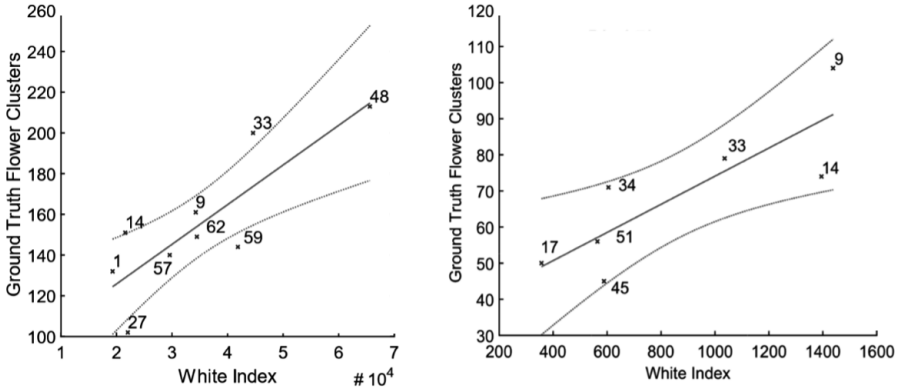


Fig. 3.15. Correlation between white index and flower cluster number. Left: white index calculated from bottom + middle volumes of PC_{Hyb} using Hierarchical clustering ($R^2=0.70$, $RMSE=17.4$). Right: white index calculated from top volume of PC_U using Otsu segmentation ($R^2=0.70$, $RMSE=10.3$). Blue crosses indicate tree numbers, dotted red lines indicate 95% confidence bounds and solid red line indicates line of best fit. PC_U = UAV point cloud. PC_{Hyb} = hybrid point clouds constructed from ground vehicle derived point clouds.

To filter out the optimal segmentation methods for flowering intensity estimation, the methods yield the highest correlation with the flowering data, such as the flower estimation at the top volume of the trees, were summarized (Table 3.8). Additional metrics were calculated for further analysis, such as RMSE and bias. In order to make a comprehensive comparison between PC_U and PC_{Hyb} , the Hierarchical based method was also included. According to the definition of floridity, RMSE 0.4 meet the requirement of practical application when PC_{Hyb} -based Hierarchical method was applied. As the correlation between White index and flower cluster, Otsu and Hierarchical method generally yielded a promising results, though a poor correlation was demonstrated for the cluster estimation at tree level. In addition, small bias was achieved for each units to be estimated. PC_U based estimation provided better performance for the flowers from upper sub-volumes, such as top and top-middle, than that of the PC_{Hyb} based.

Table 3.8. Correlation between white index and in-situ flowering data, floridity and flower cluster number.

	Methods	PC _U /PC _{Hyb}	R ²	RMSE	bias
Floridity	Hierarchical	PC _{Hyb}	0.65	0.4	0.004
Total cluster	Hierarchical	PC _{Hyb}	0.61	35.3	-1.082
	Hierarchical	PC _U	0.46	29.5	-0.039
Top	Otsu	PC _U	0.70	10.3	-0.026
Middle	Hierarchical	PC _{Hyb}	0.66	9.2	0.769
Bottom	Hierarchical	PC _{Hyb}	0.50	13.9	0.063
Top + Middle	Hierarchical	PC _U	0.78	12.0	0.003
Middle + Bottom	Hierarchical	PC _{Hyb}	0.70	17.4	1.653

Note: Only the first row shows the correlation between white index and floridity, the rest is the correlation with flower cluster number. PC_U = UAV point cloud. PC_{Hyb} = hybrid point clouds constructed from ground vehicle derived point clouds.

The flower cluster prediction model was developed using linear regression as the statistical model. Analysing the results above, two prediction models were developed: one model for the middle+bottom of the tree (Model-MB) and one model for the top of the tree (Model-T). The best performing method for flower cluster detection in the combined middle and bottom part of trees proved to be Hierarchical clustering segmentation in combination with the GV data (PC_{Hyb}). Thus, a linear regression model using Hierarchical clustering was trained and validated (Model-MB). Similarly, a linear regression model using Otsu segmentation was trained and validated for the top of the tree with UAV data (Model-T). The validation results of both models are shown in Table 3.9.

Table 3.9. Validation of linear regression models for flower cluster predictions.

Model – middle + bottom (Model-MB)						
Y = a*X + b	Estimate	Standard error	t-statistic	p-statistic	RMSE	
b	87.907	19.72	4.458	0.003	RRMSE	21.7
a	0.002	5.27e-04	3.649	0.008	R ²	14.03 (%)
					R ²	0.66
					adjusted P-statistic	0.61
						0.0082
Model – top (Model-T)						
Y = a*X + b	Estimate	Standard error	t-statistic	p-statistic	RMSE	
b	35.032	11.621	3.015	0.029	RRMSE	13.1
a	0.0392	12.3e-03	3.185	0.024	R ²	19.12 (%)
					R ²	0.67
					adjusted P-statistic	0.60
						0.024

Although the data sets for both models in Table 3.9 are limited, the validation suggests that they are statistically significant with P-statistic for both models, lower than 0.05. In terms of relative root mean squared error (RRMSE) both models perform good with values between 10% and 20%. Therefore, an important statistical data fusion was made. Model-MB and Model-T was developed to be used in combination to predict flowering intensity by using each model in a different section of the tree. The validation correlation graph of the two models can be seen in Fig. 3. 16. Within the validation result, three prediction cases yielded a significantly high accuracy, one from the prediction for the middle+bottom volume and two from the top volume. In general, a promising performance was observed for the combination of Model-T and Model-MB.

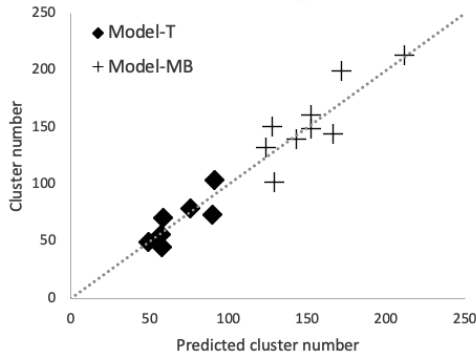


Fig. 3.16. Validation of the two flower cluster prediction models. Model-T: flower cluster prediction model for the top volume of a tree; Model-MB: prediction model for the middle + bottom volumes. The grey trendline is a reference line for ideal situation (prediction accuracy = 100%).

3.4. Discussion

In terms of flowering intensity estimation at tree level, this study compared the performance of coloured point clouds derived from two platforms, ground vehicle and UAV. We applied different flower segmentation methods and demonstrated the feasibility of combining UAV and GV imagery to estimate the apple flower clusters. By comparing the flower estimation performance at sub-volume level, the pros and cons of the two point clouds were explored (Table 3.7). The potential of improving the estimation performance with advanced segmentation methods and larger datasets was also demonstrated.

The major bottleneck for the use of PC_{Hyb} in the pre-processing phase was attributed to the noise in the middle and top part of the trees respectively. The ambiguity that exists in distinguishing similarly coloured flower blossoms from clouds in the sky proved challenging. This is also revealed in Table 3.7, in which the results concerning the top volume of PC_{Hyb} (R^2 : 0.24-0.41) are relatively lower than that of the bottom volume (R^2 : 0.36-0.51). Because of the camera view, white data points of white clouds in the sky exist in the PC_{Hyb} , by which the white flower data points could not be extracted precisely. Advanced algorithms need to be tested in follow-up research to deal with this problem (Xu et al., 2018). In addition, a potential solution could be segmenting images firstly rather than a point cloud and using the location of the segmented pixels to determine the location of the data points in the point cloud. These data points can then be labelled as flower points. For the method proposed, however, detailed documentation of camera parameters and setup is required.

In PC_U , on average 71 tie points are present per image compared to 141-158 for the GV images (Table 3.5). This resulted in a lower quality or less dense point cloud from the UAV data. This explains the

inferior performance of the various segmentation models on the UAV data compared to GV data in Table 3.7. The results of the top of the tree (R^2 : 0.33-0.70) compared to the middle ($R^2=0.30$) and bottom (no positive correlation, $R^2<0.1$) respectively can be attributed to the same reasons. The tie points in the top of the trees generated with UAV data are far more dense than in the middle and bottom.

This study has shown the potential of flower intensity estimation at tree level with a combination of PC_U and PC_{Hyb} (Fig. 3. 16). Yet, merging point clouds from multiple views required semantic features to be visible and accurately created in 3D space for both point clouds. Using semantic features such as tree trunks is limited in this study since tree trunks are hard to recognize or even not visible in UAV images. Manually inserting reference features in the orchard, visible to both UAV and GV cameras could be useful in spatially merging the two point clouds. An alternative approach to fuse the data between UAV and GV is to use images from both data sources to build a 3D model by feeding image data along with location data from both sources into Agisoft. Yet, tie points should be found between pairs of images of both sources. And the feature matching algorithms should be able to detect enough features to create tie points between image pairs. In this study, the SURF algorithm could not positively identify matching features between the UAV image and the GV image of the same tree, but has shown good performance for GV images only (Fig. 3. 17). This visually explains the limitation of using both datasets, UAV and ground vehicles datasets, in combination for creating a 3D model in this chapter.

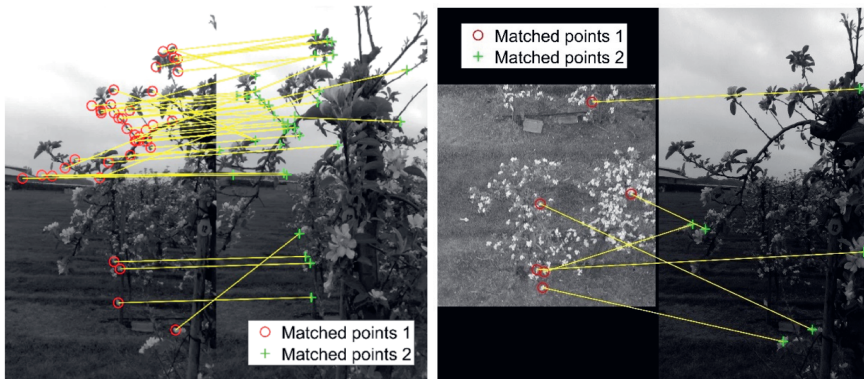


Fig. 3.17. SURF algorithm for feature matching in tree1. Left: Feature matching in ground-based images. Right: Feature matching between UAV and ground-based images.

Flowering intensity estimation in orchards is still in its infancy. The majority of pre-existing study focus on the estimation at picture level, which lack the information of the real flowers in tree and make it difficult to compare the achievement in this study with. Despite this fact, this study first collected a unique ground truth with not only the total cluster number per tree but also the cluster number in sub-volumes of a tree, overcoming the problems raised by Wang et al. (2021), and further demonstrated the

flower estimation at tree level. Compared with the relevant research as mentioned before, the approach proposed is more comparable to Vanbrabant et al. (2020), though the image data used in this study is more complex against them by comparing the average cluster number per tree (198 vs 150). As they mentioned, heavy flowering provides more flower occlusion problems and thus affects the estimation accuracy. The point clouds derived from UAV showed a decrease in the density from the top to the bottom. Whereas the method proposed in this study enable the inspection of the influence of PCs density to the estimation accuracy by comparing the performance from different sub-volumes (Table 3.7), which further enhance the use of point clouds for fruit tree monitoring. A relative improvement was achieved in this study, while the highest R^2 of the correlation between the image based flower index and the in-field counts of the cluster number achieved by Tubau Comas et al. (2019) and Hočevar et al. (2014) was 0.56 and 0.50 respectively, compared to 0.7 in this study.

The investigated four flower segmentation methods, manual threshold, Otsu, K-means and Hierarchical clustering, have been applied in a variety of flower detection studies (Bhattarai et al., 2020; Dias et al., 2018b; Liakos et al., 2017; Tubau Comas et al., 2019). A comparison of these methods was made and the segmentation results reported from this study were also proved to be reasonably capable of segmenting the flower blossoms (Table 3.7). In general, the results also returned low bias (Table 3.8). Otsu segmentation and Hierarchical clustering reported a better performance compared to the other two methods. Because of the camera view, top volume of PC_U is more representative for the flower number in top section of the tree (Table 3.7). Thus the significant correlation returned from Otsu segmentation, with a R^2 of 0.7, indicates the capability of it for flower point segmentation. Hierarchical clustering shows a stable performance, even for the detection from the bottom volume of PC_{Hyb} , with a R^2 of 0.5. However, unsupervised clustering methods enable the model to be robust against lighting and illumination changes. Different image acquisition locations enable PC_U and PC_{Hyb} show different spatial scales and occlusions. This explain the difference between the floridity and flower cluster estimation performance based on the two type PCs (Table 3.7). Since floridity was scored by the expert whose view is more close to the camera equipped on the ground vehicle, the floridity estimation from PC_{Hyb} is much better than that of PC_U , with a highest R^2 of 0.65 (Table 3.7). While a comparable performance of these two PCs was observed for the estimation of flower cluster.

The approach followed in this chapter provides a novel solution to estimate the flowering intensity at tree level and yielded a relatively good results (Table 3.8). It relies on high-quality multi-view imaging, combining UAV and ground based RGB images, and point cloud reconstruction to facilitate the estimation. By constructing point clouds and having GPS/location information available, spatial and even temporal information is readily available. The final products, 3D point cloud representations, provide an understanding of the flowering variability of the whole orchard from not only tree level but also a height based level (Fig. 3. 9 and Table 3.7). Creating point clouds from two data sources allows

flexibility in selecting the best 3D represented regions of trees and analyse them with different segmentation methods based on the height of the tree (Fig. 3. 10). To further validate the approach proposed in this study, higher image resolution will be tested when it comes to the experiment design. Higher resolution RGB cameras could perhaps result in more tie points per image, which contributes to solving the point cloud merging issue discussed above, and therefore point clouds with higher quality will become available. Though aerial images from this study yield a 4000×3000 resolution, it is far from the advanced RGB camera capable for UAVs. In addition, data size would also be expanded to test the robustness of the method proposed. As shown in Table 3.2 and 3, the cluster variance within the orchard is relatively high which limits the robustness of flowering intensity estimation based on small data size. With larger data size, more advanced machine learning technique would also be suitable to test for further improvement of flower estimation, such as the CNN worked on dense point cloud has been reported for cotton bloom detection (Xu et al., 2018).

3.5. Conclusions

In our work, a novel framework based on point clouds derived from UAV and GV images was designed to automatically estimate flowering intensity in an apple orchard during the full blooming phase of the growth season. The possibility of combining UAV and GV to precisely assess flowering intensity among apple trees, including the spatial variability of flowering intensity in the orchard and even within an individual tree, was demonstrated. Multiple camera angles can in this way be used to complement each other in terms of coverage of certain parts of a tree. Automatic flower cluster estimation at the tree level yielded a R^2 of 0.7, and RMSE lower than 20 for the correlation between the image derived flower index, the white index, and the in-field counts of the cluster number.

The automatic SOM performed well, and high accuracy was achieved in handling the point clouds and spatially segmenting trees and observation volumes. Four flower extraction methods, manual thresholding, Otsu segmentation, K-means and Hierarchical clustering, were explored. Otsu Segmentation and Hierarchical clustering method performed the best for the segmentation in GV and UAV point clouds, respectively. Both models can however be improved with a larger data set. Higher diversity in Floridity scores would also make the linear regression approach for floridity detection more significant.

UAV imagery can be applied for studying less detailed features of the fruit trees. But to analyse detailed features, such as flowering intensity, strict requirements are needed to guarantee the point cloud quality. Depth information can be helpful in improving the accuracy of surface reconstructions in the point cloud, as proven in the study by Dong et al. (2020). For future studies, flying lower and closer to the tree canopy could result in higher quality images for the same resolution and more tie points per point cloud. We expect that this could also benefit in matching features between the GV images and UAV images and perhaps enable spatial merging of point clouds, if a proper parametrical setup is made for the respective cameras. Grey reference strategies could be implemented to make the model even more robust against illumination differences between UAV and GV data.

A large, bold, white number '4' is centered on a dark, textured, splattered background. The background consists of various shades of gray and black, with a rough, ink-splattered appearance. The number '4' is a simple, sans-serif font with a thick stroke. The overall composition is high-contrast and abstract.

Chapter 4

Feasibility assessment of tree-level flower intensity quantification from UAV RGB imagery: A triennial study in an apple orchard

This chapter is based on:

Zhang, C., Valente, J., Wang, W., Guo, L., Tubau Comas, A., van Dalssen, P., Rijk, B., Kooistra, L., 2023. Feasibility assessment of tree-level flower intensity quantification from UAV RGB imagery: A triennial study in an apple orchard. *ISPRS Journal of Photogrammetry and Remote Sensing* 197, 256-273.

Abstract

A timely and accurate spatial inventory of flowering characteristics benefits both the floral phenology monitoring in ecology and various crop management activities in agricultural systems. Recent advancement has proven the superiority of computer vision in flower classification at image level. Yet progress in the flowering intensity estimation at tree level is much less and still far from satisfactory. To tackle this problem, a novel approach was designed for the use of single raw aerial images to quantify flower intensity. With pre-prepared dataset, flower-associated pixels were extracted for individual trees using a pixel-based classification method, the color thresholding. Next, three flowering indices retrieved from unmanned aerial vehicle (UAV) were evaluated, the index percentage (IPG), index pixel (IP), and index area (IA). Finally, linear correlation of the flowering indices to flower cluster number and expert-assessed floridity recorded in the field were calculated. Results indicated that IPG yielded the highest correlation to flower cluster ($R^2 = 0.93$, RMSE = 8) and floridity estimation ($R^2 = 0.78$, RMSE = 0.9). A UAV-based floridity scoring method was also designed for automatic estimation tasks in practice, and a comparable and even better performance to the expert-based approach was demonstrated. Furthermore, effects of vertical (nadir) and horizontal (angular) overlapping of flower clusters within the canopy were evaluated, showing excellent potential to improve the estimation accuracy.

4.1. Introduction

Floral phenology is highly sensitive to climate change. Evidence from the ecological community suggests that changes in floral phenology, such as flowering time and duration, may alter processes at species and community level (Hovenden et al., 2008), and reshape regional ecological communities (CaraDonna et al., 2014). In agricultural systems, floral phenology also plays a crucial role in various crop management activities during the entire growing cycle, especially for fruit and nut trees. Floral phenology of fruit trees covers a short life cycle starting from small green buds to falling flower petals. The complete cycle of apple flower development has a duration of 2-3 weeks (Wang et al., 2021a). Within this period, the following flowering stages are identified: tight cluster, balloon blossom, king bloom, and full bloom. Quantification of flowering intensity contributes directly to decision-making in orchards, such as pollination management (Chen et al., 2019a), flower thinning (Wang et al., 2021a) and determination of heating requirements (Yuan and Choi, 2021). In the community of plant breeding, this information also contributes to breeding line identification and cultivar selection (Lopez-Granados et al., 2019a). Additionally, regional observation-based investigations have shown that flowering distribution in apple orchards may provide a final yield prediction at an early stage (Aggelopoulou et al., 2011; Liakos et al., 2017). Yet, in the context of precision agriculture, a timely and accurate temporal inventory of flowering characteristics at the tree level is highly required.

Research on flowering characteristics in orchards has experienced a two-stage evolution in the past ten years. First, the capability of flower detection and classification with computer vision, and as a follow-up, the adoption of computer vision-derived tree-level flowering inventory. Within this first stage, both classification-based and spectral index-based methods have been applied, which mainly rely on high-resolution imagery and multispectral observations, respectively. Earlier studies have shown evidence that classification-based methods are able to detect flowers and classify flowering stages (Dias et al., 2018a; Tian et al., 2020; Wang et al., 2021a). Flower color features are distinct from the background in the orchard scene. Thus several studies employing these methods were conducted by thresholding at pixel level (Hocevar et al., 2014; Liakos et al., 2017; Sun et al., 2021; Wouters et al., 2015). Thresholding methods are prone to over-fitting and are sensitive to varying backgrounds and illumination. In specific environments, the thresholding method followed by support vector machine (SVM) can improve performance (Wang et al., 2018b). Additionally, thresholding methods can be regarded as a baseline approach for understanding and improving more complex detection algorithms, e.g., deep learning-based object detection (Farjon et al., 2020). Conventional classification methods at pixel level, such as SVM (Lin et al., 2020), K-means and other clustering methods (Lu et al., 2021; Tubau Comas et al., 2019; Vanbrabant et al., 2020a), and convolutional neural networks (CNN) (Cibuk et al., 2019; Wang et al., 2020) have also been adopted, and proved to be more robust. These methods

usually are hybrid, combining the pixel-based flower classification with further flower pixel analysis for flower number or flower cluster number counting purposes.

Another group of classification-based methods has been conducted at object level. These algorithms evaluate the small object pattern directly to classify if the object is a flower or not. Deep neural networks with various feature extraction modules have been demonstrated for this aspect, such as VGG16 (Wang et al., 2021a), DeepLab-ResNet (Sun et al., 2021; Tian et al., 2020), YOLOv4 (Koirala et al., 2020b; Wu et al., 2020a). One advantage of neural networks is the ability to classify flowers at different stages, which is superior to the classification at pixel level (Tian et al., 2020; Wang et al., 2021a; Yuan and Choi, 2021). The ResNeSt50 network achieved an identification accuracy of 92.4% within a two-classes testing set: apple bud and leave bud (Xia et al., 2021). Apart from the classification-based methods, also spectral index-based methods are able to track the flowering characteristics, especially for the flowering time and flowering spatial variation (Chen et al., 2019a). This method contributes to the reduction of the noise from the soil and green vegetation and is more suitable for efficient floral phenology monitoring at the regional scale.

The first stage evolution of flowering characteristic studies already provides sufficient support for the adoption of advanced techniques in practice. Quantification of flower cluster and flowering intensity at tree level is the basis of floral phenology monitoring, and of subsequent site-specific management. Yet this area of research is still challenging and current flower quantification methods are still far from satisfactory. One challenge is related to the complex agricultural environment, such as the outdoor illumination variation, flower occlusion, and the large internal variance of the flowers (Farjon et al., 2020). Another aspect is related to uncertainties in flower cluster reference data collection (Wang et al., 2021a), especially for the stone fruits like apples and pears. Normally stone fruit trees bloom 50-300 flower clusters with a total of 350-2100 flowers per tree in comparison with 15-20 flowers per plant for cotton (Vanbrabant et al., 2020a). Thus far, nine flower quantification studies were conducted in orchards, with a practical focus on the estimation at the tree level. Six studies describe ground vehicle-based investigations (Hocevar et al., 2014; Koirala et al., 2020b; Lee et al., 2022; Scalisi et al., 2021; Wang et al., 2021a; Wang et al., 2018b) and three are based on unmanned aerial vehicles (UAV) (Tubau Comas et al., 2019; Vanbrabant et al., 2020a; Zhang et al., 2022b). Mainly RGB sensors were employed within the six studies, and three fruit types were covered: apple, pear, and mango. (Koirala et al., 2020b) and (Wang et al., 2018b) indicated the highest flower cluster estimation accuracy for mango panicles, giving an R^2 of 0.86 and 0.84, respectively. Both of them utilized a ground-based dual-view imaging approach at night-time in order to achieve a more accurate and high-contrast flower cluster representation in two-dimensional (2D) RGB images. By contrast, the remaining research which focused on the stone fruit cluster estimation generally achieved lower accuracy. This could be attributed to the fact that apple or pear trees suffer a significantly higher cluster occlusion problem, and their

flower sizes are much smaller than that of mango panicles complicating the detection task. The highest flower cluster estimation accuracy achieved for stone fruits was an R^2 of 0.61 which was obtained from a regression-based estimation (Zhang et al., 2022b).

Camera view is an important factor in flower cluster estimation with 2D imagery. One-perspective scanning estimates tree-level flower clusters based on the detected flowers in images captured from one side of the trees. It provided a minimum percentage error of 13.49% for apple flower cluster estimation (Lee et al., 2022). When a regression-based method was applied, the accuracy reached 0.56 (R^2) (Hocevar et al., 2014). Dual view has been proven to improve the proximal sensing system (Koirala et al., 2020b). The resulting error (RMSE) was 5 clusters per image (Scalisi et al., 2021). Earlier studies adopting a top-view approach from aerial imagery achieved accuracies of apple flower cluster estimation at the tree level of 0.44 (R^2) (Vanbrabant et al., 2020a) and 0.53 (R^2) (Tubau Comas et al., 2019). (Vanbrabant et al., 2020a) showed that only 50%-76% of the in-situ flowering variability can be represented within a top-view image. Vertical (nadir) and horizontal (angular) overlapping of flower clusters within the canopy exist in original RGB images captured from the aerial sensing system. This makes it more challenging to estimate the flowering intensity at tree level. 3D point clouds-based estimation at tree level can be a potential solution (Lopez-Granados et al., 2019a), accuracies of 0.46 (R^2) (Vanbrabant et al., 2020a) and 0.61 (R^2) (Zhang et al., 2022b) were observed. Apart from this focus, improved results were demonstrated for the flower cluster estimation at plot level (Vanbrabant et al., 2020a) or partial-tree level (Wang et al., 2021a). However, it does not meet the requirement of precise horticulture management, where accurate flower characteristics at tree level are in high demand.

With increasing concern for practical adoption of advanced UAV imagery technology in orchard management, a novel approach was designed adopting aerial geotagged RGB images to quantify flower intensity. In the case study of apple flowering intensity estimation, flower-associated pixels were extracted from individual-tree datasets using a pixel-based classification method, i.e. color thresholding method. Next, three well-established flowering intensity indices were evaluated, e.g., the index percentage (IPG), index pixel (IP), and index area (IA). Finally, the possibility of flowering intensity estimation using UAV imagery was validated by calculating the linear correlation of the flowering indices to the flower cluster number and floridity score recorded in the field. In addition, a UAV-based floridity scoring method was also designed for automatic flowering intensity estimation tasks in practice. To further evaluate this approach, the effects of vertical and horizontal overlapping were demonstrated which provides potential to improve the flowering intensity estimation accuracy. The given approach provides a new image analysis strategy for UAVs and the derived flower cluster estimation method shows the potential to promote the advancement of precision orchard management during the flowering period.

Faced with gaps demonstrated above, this study takes an apple orchard as case study to estimate the flowering intensity at tree level based on a three-consecutive-year bloom dataset. The following points will be elaborated:

- Evaluate the feasibility of tree-level flower cluster and floridity estimation with single raw UAV images;
- Compare the performance of visual field observations and UAV-derived flowering floridity estimations;
- Examine the effects of structural overlapping, i.e. vertical (nadir) and horizontal (angular) overlapping, on flowering intensity estimation accuracy in aerial imagery.

4.2. Study area and datasets

4.2.1. Study area

The research was conducted within an apple orchard located in Randwijk, Overbetuwe, The Netherlands (51.938, 5.7068 in WGS84 UTM 31U) (Fig. 4.1). The orchard of 0.47 ha, contains 14 rows of the apple variety Elstar, *Malus pumila* 'Elstar', with tree and row spacing of 1.1m and 3.0m, respectively. The orchard was planted in 2007 with 4-years old trees, and the rootstock is M9. For every row in the orchard, trees are numbered from 1, starting from South to North. Per row, after each 10th tree, a pollinator tree is planted in between two Elstar trees (mostly Granny Smith). There were about 101 trees in each row before 2019. In 2020, nearly half of the trees were removed for other orchard management purposes. More specific, tree numbers ranging from 1 to 45 were removed for each row. Afterward, there are 56 trees in each of the 14 rows, and the orchard surface area changed to 0.26 ha. Among the regular orchard management, ammonium thiosulphate (ATS) is used for chemical thinning during the blooming stage. In case of high pollination and a high number of fruits, Brevis® is used for chemical thinning of fruits with a size between 8 and 16 mm. Brevis® is a thinning agent which contains metamitron and calcium. After June drop, trees are hand thinned until each tree has a maximum of 100 fruits.

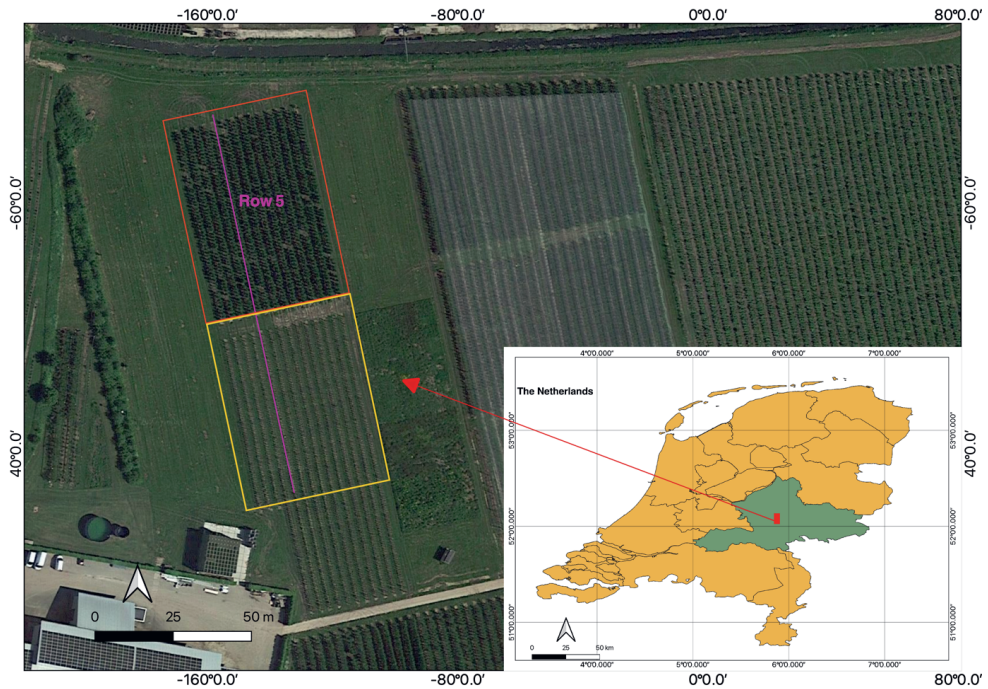


Fig. 4.1. The location of the apple orchard located in Randwijk, Overbetuwe, Gelderland in the Netherlands in 2020. The province of Gelderland is filled with green; the red rectangle delineates the present orchard; the yellow rectangle marks the removal area; the study tree row (row5) is highlighted in purple.

Within the orchard, the fifth row from the West, Row5, was given specific environmental settings for a trial of flower thinning optimization (Fig. 4.2). Easily identifiable yellow poles were set vertically between every two trees in this row, which delineates each individual tree. Meanwhile, yellow tapes were set horizontally for the whole row, which divide each tree into three parts: bottom, middle and top. Based on this construction, space between every two adjacent yellow poles forms a unique observation window (Fig. 4.2a) (Fig. 4.3). Because of the high-density planting system, vertical yellow poles are not able to segment one individual tree completely. Thus in an observation window, not only flowers from the tree inside the window can be observed, but often also flowers from the adjacent trees. In addition, since the tree shape is spindle-tree, the plane from the yellow poles and tapes divides each individual tree into two sections, the West section and the East section (Fig. 4.2b).

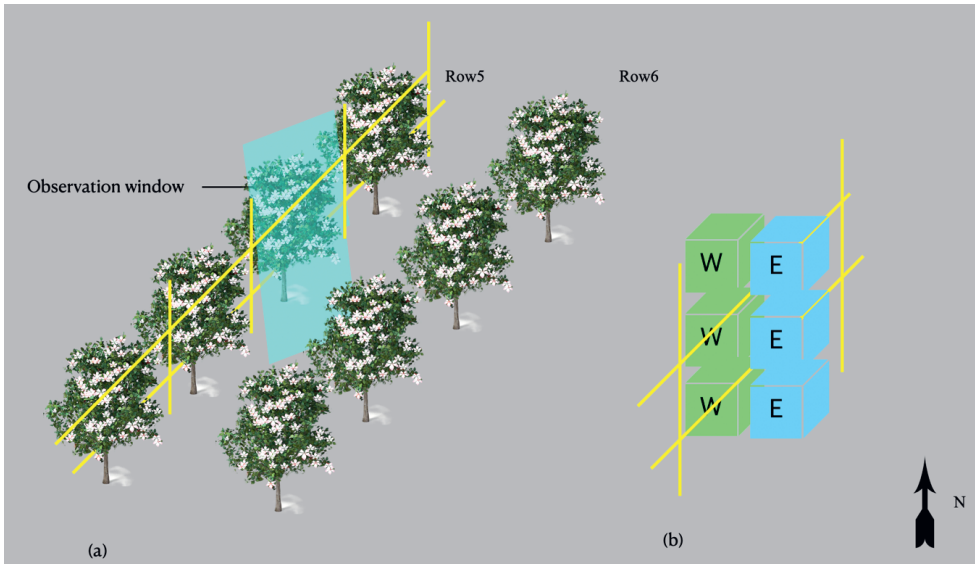


Fig. 4.2. Yellow tapes and poles applied in row5: (a) demonstration of the observation window with three parts: bottom, middle and top; (b) West side and the East side from the same tree.



Fig. 4.3. West view of trees and the yellow tapes in row5, cropped from original UAV imagery acquired in 2018, 2019, and 2020.

4.2.2. Aerial imagery from UAVs

In a continuous period of three years (2018, 2019 and 2020), three UAV platforms equipped with different RGB sensors were used for the collection of the flowering intensity dataset (Table 4.1). Three commercial UAVs provided compact and accurate low-altitude data collection. To correct for common geo-location errors in the systems of Phantom3 and Phantom4 the location of ground control points (GCP) was measured. A Topcon HiperHR receiver was used as an aid and the real-time kinematic (RTK) signal from 06-GPS/MoveRTK via VRS has a dynamic accuracy of 2 cm. Since a more advanced UAV platform, Phantom4 RTK, was used in 2020, no GCPs were employed. Regarding the cameras, two camera resolutions were used: 4000×3000 and 5472×3648 pixels. Camera settings were set to automatic mode to keep the image quality consistent with the illumination changes during the flights. As shown in Fig. 4.3, RGB sensors with different resolutions provide heterogenous data for the same orchard, which allows evaluation of robustness and generalization capability of the method under investigation.

During full blooming periods of apple trees, multiple flights were conducted with different flying altitudes: 15m, 20m, and 25m (Table 4.1). Oblique mission was applied to obtain the complete feature of each individual tree from the side-view. And the mapping mission was set to autonomous model. Specific data collection date is not completely the same due to changes in weather conditions over these three years. This also produced datasets with various illumination conditions (Fig. 4.3).



Table 4.1. Description of flight parameters for the UAV campaigns over the study area for the period 2018-2020.

	Data 2018	Data 2019	Data 2020
UAV platform	DJI Phantom 3 PRO, Shenzhen, China	DJI Phantom 4 PRO, Shenzhen, China	DJI Phantom 4 RTK, Shenzhen, China
Sensor	FC300X	FC6310S	FC6310R
Type	CMOS	CMOS	CMOS
Resolution	4000×3000	5472×3648	5472×3648
Focal length (mm)	3.61	8.8	8.8
F number	f/2.8	f/4.5	f/2.8
Exposure time	1/100	1/200	1/500
Overlap ratio	85%	85%	85%
Flying velocity (m/s)	2	1.9	2
Flying altitude (m)	15	20	25
Ground sample distance (GSD) (cm/pixel)	0.64	0.55	0.69
GCP amount	4	6	0
Data size	61	418	252
Collection date & time	24 th April, 11:30 am	23 rd April, 10:53 am	18 th April, 11:33 am
Weather	Overcast	Sunny	Sunny
Temperature (°)	11	17	13
Wind (km/h)	20 SW	20 E	15 NE

4.2.3. In situ flowering intensity measurement

In this study, two types of ground truth data were recorded for the trees in row5: flower cluster number and floridity. In apple orchards, one flower cluster consists of mostly five flowers that are developed from the same bud. In general, flower number within one cluster ranges from three to six. For flower cluster counting, 32, 101, and 19 trees in row5 were selected for the manual measurement in 2018, 2019, and 2020, respectively. The flower cluster number on both West side and East side of a tree were counted separately, and the sum of these two counts represent the total cluster number of a tree. In addition, flower cluster number values at observation window level was also recorded, including flower clusters from adjacent trees (Fig. 4.3). Apple species like ‘Elstar’ are sensitive to biennial bearing. So in case of a heavy fruit load in one year, the tree will form fewer flowers in the next year (Fig. 4.4). As shown in

Fig. 4.4, a comparable blooming level was observed in 2018 and 2019, however some trees in 2018 bear a heavy blooming. In 2020, the blooming level decreased significantly (Fig. 4.3). In addition, in 2019, the production on the West side was quite high and in the East part relatively low. As a result, relatively more flowers were observed on the East side in 2020.

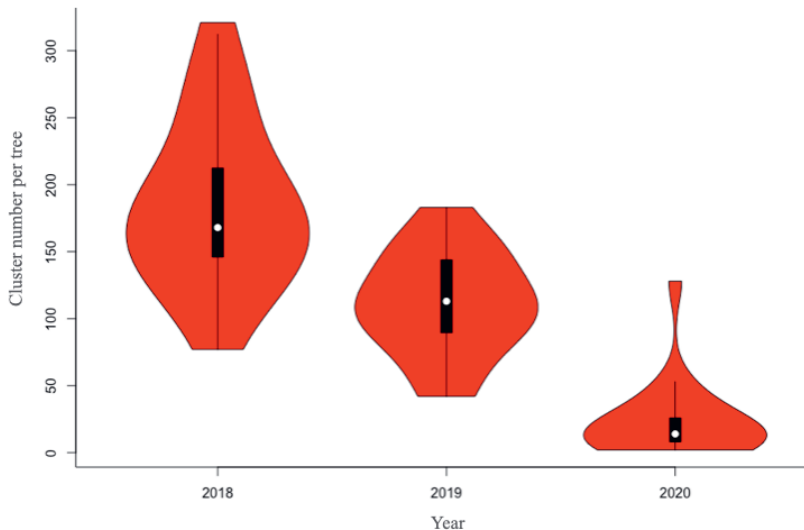


Fig. 4.4. Flower blooming level of a selection of trees in the apple orchard of Randwijk based on cluster number for the three study years. The cluster number presented here is the field-based flower cluster number counted at the observation window level.

The second ground truth measured in this study is floridity value. Flower floridity is an index used for representing the flowering level of apple trees. The field inspector gives each tree a floridity value based on observations on the overall flowering situation in the orchard. The index ranges from 1 to 9, where value 1 represents no flowers and 9 represents heavy blooming. The optimal floridity is intermediate bloom with a value of 5. More specific, the inspector evaluates every tree from West and East side separately, and the mean value of these two sides is the floridity value of the observed trees. All trees in row 5 were marked with floridity by an experienced expert over three years. Goodness of fit of the regression between floridity and flower clusters was evaluated, resulting in R^2 values from 0.64 to 0.94 (Fig. 4. 5). A discontinuous performance of visual floridity judgement was observed, indicating the disadvantage of subjective assessment. Between years a difference in the relation can be observed as shown by varying slopes of the regression lines. In 2018 with high flower cluster counts, the regression line is steeper. While for 2019 and 2020 with a comparable cluster range the steepness of slopes of the regression lines is comparable. This shows that visual observation of floridity is dependent on the range of flower clusters present within a year.

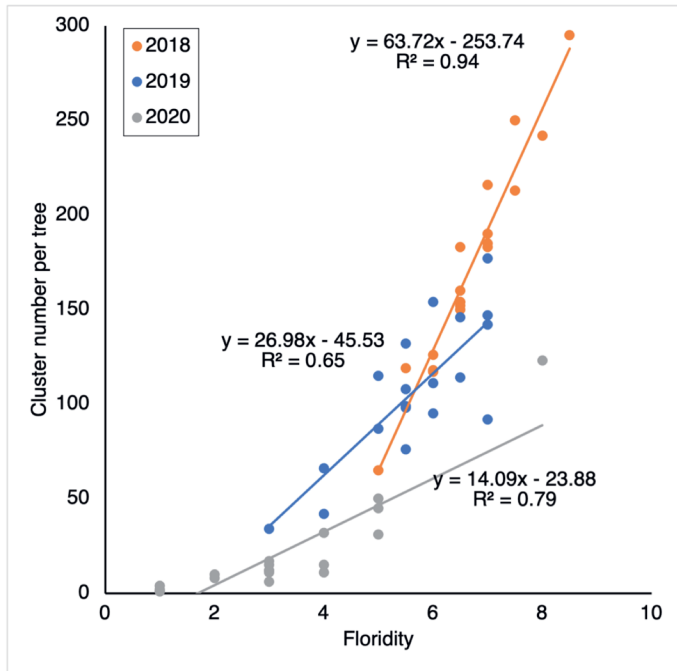


Fig. 4.5. Relationship between two ground truth datasets, the floridity and flower cluster number, for three years of field observations for a selection of trees within row 5 of the apple orchard in Randwijk.

4.3. Methods

4.3.1. Flowering intensity estimation

The proposed tree-level flowering intensity estimation approach consists of four stages as shown in Fig. 4.6. First, UAV images are grouped in two datasets with the orchard trees East-view and the West-view using a new image selection procedure. Second, individual trees were labeled and cropped from these two datasets. Third, a segmentation method was applied to extract the flower pixels from each individual tree. Fourth, characteristics of the region of interest (ROI) and the segmented flower pixels were used for calculation of flowering indices. Finally, correlation of the examined aerial flowering indices to the observed flower cluster number and floridity assessed in field (ground truth) was evaluated.

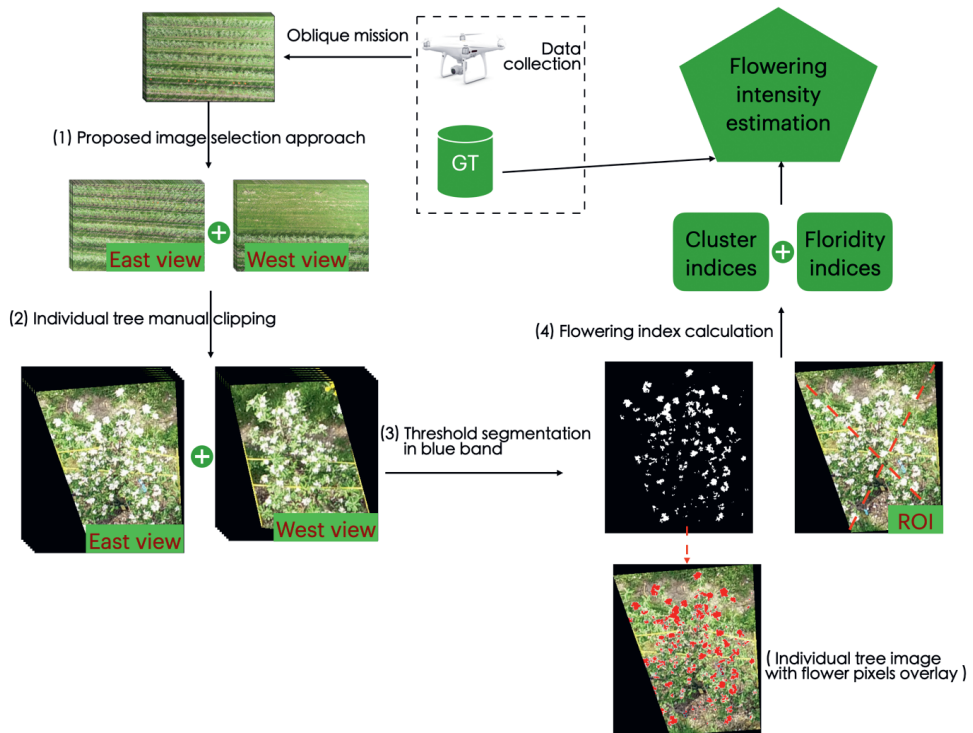


Fig. 4.6. Overview of the tree-level flowering intensity estimation method based on proposed UAV image analysis strategy: (1) select the images containing row5 in the orchard, (2) extract individual trees in row5 from the selected images, (3) perform color thresholding method to extract flower associated pixels, (4) calculate flowering indices by using the extracted features, the flower associated pixels and the ROI. GT: ground truth; ROI: region of interest.

4.3.1.1. Image selection

To make the proposed approach reproducible, an image selection procedure was designed. The procedure is carried out with support of Agisoft Metashape Pro (Agisoft LLC, St. Petersburg, Russia). First, raw UAV images were imported in Agisoft to ensure UAV image coordinates are visualized in the Ortho window within Agisoft. Each black hollow circle represents the coordinate of a single image acquired by the UAV (Fig. 4.7a). Based on this layout and associated image metadata, detailed information about the flying trajectory is retrieved. The first image captured is used to determine the starting point of the flight, indicated with the red mark in Fig. 4.7a. Successive image numbers indicate the flying trajectory of the drone, as the red arrows illustrate in Fig. 4.7a. Each tree row in the apple orchard is planted from South to North. Based on this orientation and the selected flight path, it was derived that uneven numbered image rows capture the East view of the (Fig. 4.7a). Images in the even

numbered image row capture the West view of the trees. Thus the whole dataset is divided into two groups: East-view and West-view images.

The next step is to divide the acquired UAV images into new East-view and West-view groups which are prepared for individual tree extraction. This division procedure follows the workflow as presented in Fig. 4.7b. For sake of providing an example, both the workflow content and follow-up introduction stick to image selection of the trees in row 5 indicated in Fig. 4.7a. As it shows, the first image taken in each IR is located at the largest distance to a tree or tree row in the orchard. Based on this, raw images with row5 are grouped in categories far, intermediate, close and vertical groups and are shown as blue, orange, grey, and black solid circles in Fig. 4.7a. For a fixed flying altitude, a higher side overlap produces more images in an IR, and as a result more image groups. Nadir-view images include heavy flower occlusion problems and lack the side-view feature of the trees. Thus vertical image groups were discarded in this study. Theoretically, the selected images within the same distance group should distribute on the same straight line perpendicular to the flying direction, as the image group of West-view group_far highlighted in green in Fig. 4.7a.

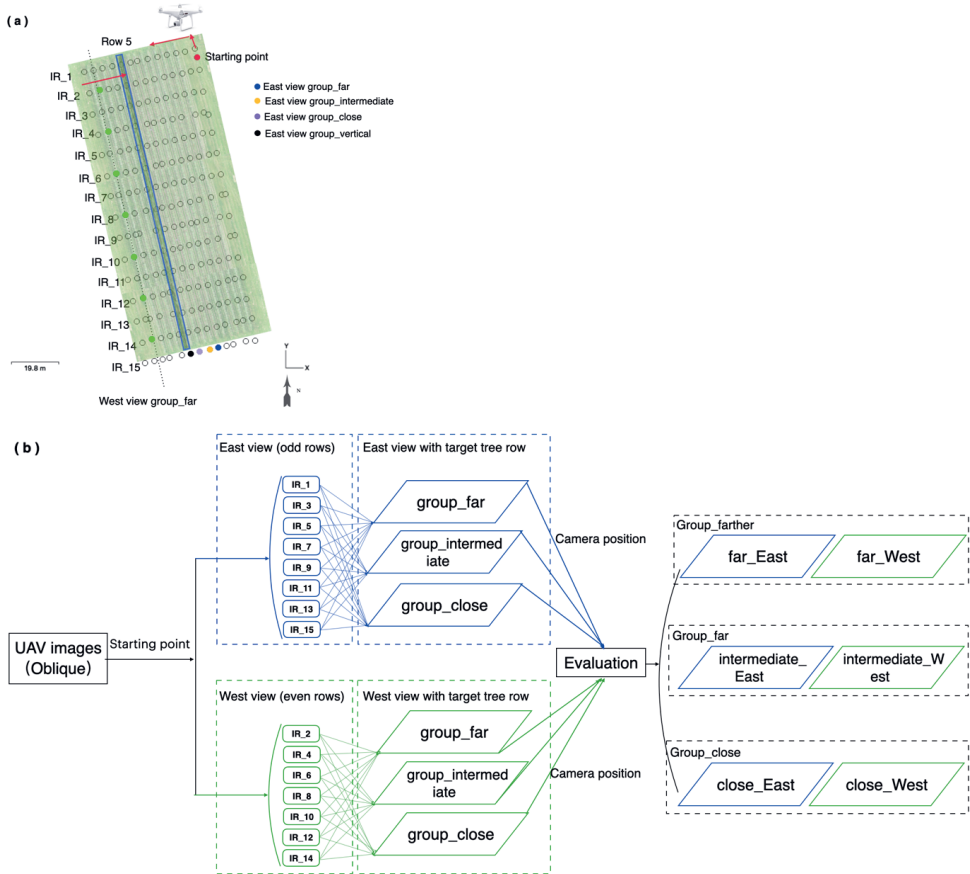


Fig. 4.7. Image selection strategy for aerial images captured at different distances to the trees in row 5, where ground truth is recorded in the field: (a) illustration based on the screenshot of Ortho window in Metashape, dataset 2019 was imported and processed. Black hollow circles represent UAV images; a blue rectangle delineates row 5 in the orthophoto. (b) Flow chart of the image selection. IR: image row.

Ideally, dual-view imaging conducted at same distance to targeted trees enables the flowering intensity estimation at tree level. Yet, effects of the distance between camera position and target row on the flowering intensity estimation accuracy introduce uncertainty. To examine this, the exact imaging distance of different image groups was measured in QGIS open source software, version 3.12). The vertical distance between every image and location of the trees in row5 was measured by the function measure line. The average distance calculated from the images within the same group represents the distance of the group. This measurement was conducted for three complete image groups derived from datasets 2019 and 2020 (Table 4.2), while only one image group from dataset 2018 was derived because of its limited data size.

Table 4.2. Seven groups of images selected for the three investigated years. The distance represents the distance between position of the image groups and the trees in row5.

Year	Image group	Distance_West(m)		Distance_East(m)		Average (m)	Difference (m)
		Average (m)	SD ^a (m)	Average (m)	SD (m)		
2018	Far	11.8	1.6	16.1	2.3	13.9	4.3
2019	Far	10.8	0.2	11.2	0.1	11.0	0.4
	Intermediate	7.2	0.1	7.6	0.3	7.4	0.4
	Close	3.5	0.4	3.7	0.4	3.6	0.2
2020	Far	20.8	0.5	23.2	0.5	22.0	2.4
	Intermediate	14.0	0.6	16.0	0.5	15.0	2.0
	Close	7.9	0.5	10.1	0.4	9.0	2.2

^a SD is short for standard deviation.

4.3.1.2. Individual tree cropping

For every image in the selected groups (Fig. 4. 7a), the individual trees located in row 5 are manually segmented in observation window scenario. Faced with irregularity of the observation window size and shape (Fig. 4.3), an image crop procedure was developed. Four points are defined around a single tree in the image, then a quadrilateral area covering a complete tree is extracted and stored (Fig. 4. 8a, b). The yellow sticks located between trees were regarded as reference to assist the operator to determine four points for each tree to be segmented. More specific, top and bottom parts of each yellow stick provide two points for delineating the area to extract (Fig. 4.8a). As shown in Fig. 4.8a, the majority of the yellow sticks are lower than the trees. As a result the top part of the trees cannot be covered by the quadrilateral area determined by the four points derived from the sticks. Therefore two of the four points needed to be moved along the extension line where the yellow stick is until a complete tree is covered. To shape the extracted individual tree area into a normal rectangle shaped image format, the remaining area was filled with black pixels automatically (Fig. 4.8b). The segmented area is regarded as Region of Interest (ROI). In addition, to identify the cropped individual tree ID, the orange hat-shape ground markers were used as reference (Fig. 4.8a). This cropping operation and the follow-up analysis were programmed in Matlab_2019b (MathWorks Inc., Natick, MA, USA).



Fig. 4.8. Crop individual trees from the selected UAV images. (a) Define four points to determine the area to crop and store. Purple and orange digits are used for labeling the tree ID, and the red digits label the ground marker (b) Cropped individual tree (c) Original UAV image

4.3.1.3. Color thresholding segmentation

Conventional color thresholding segmentation was applied for the prepared individual tree dataset to achieve flower pixel extraction. Pixel-based classification method has been evaluated for flower detection in previous studies (Hocevar et al., 2014; Horton et al., 2017; Zhang et al., 2020b). These thresholding cases were conducted within different color space channels: HSL (Hocevar et al., 2014), Lab (Tubau Comas et al., 2019), and RGB (Zhang et al., 2020b). To select the optimal color model, dataset 2018 was used for a comparison of segmentations derived from different color model (Tubau Comas et al., 2019). According to the segmentation results, a threshold in the blue channel could separate the flower pixels from the background. Next, a similar thresholding procedure ((Horton et al., 2017) was used for the blue channel in RGB color model. Based on a collection of images from the same year, visual inspection and comparison against original images was made. If a pixel from the input RGB image does not have a corresponding pixel value specified in blue channel, it is set to 0 in output binary image, otherwise, it is set to 1 (Fig. 4.9b, f). The color thresholding method is sensitive to changes in illumination. One fixed threshold (optimized by the sample images from a specific year) is not able to segment flower pixels from the images collected from a different year. Thus three different thresholds in the blue (B) channel were determined for the datasets collected over the years of 2018 ($B > 100$), 2019 ($B > 227$), and 2020 ($B > 223$).

The number of areas consisting of flower pixels in binary image was also calculated, to assist the calculation of index area. Based on flower pixels extracted, morphological operations were conducted to reduce noise. Morphological opening and closing operations were applied to the binary image derived from blue channel. The structuring element used was a disk with a size of 1. Parameters of this

structuring element were determined by visual inspection of a set of 10 randomly selected images. Finally, flower areas detected within one image were numbered sequentially from 1 and labeled with red rectangle bounding boxes (Fig. 4.9c, g).

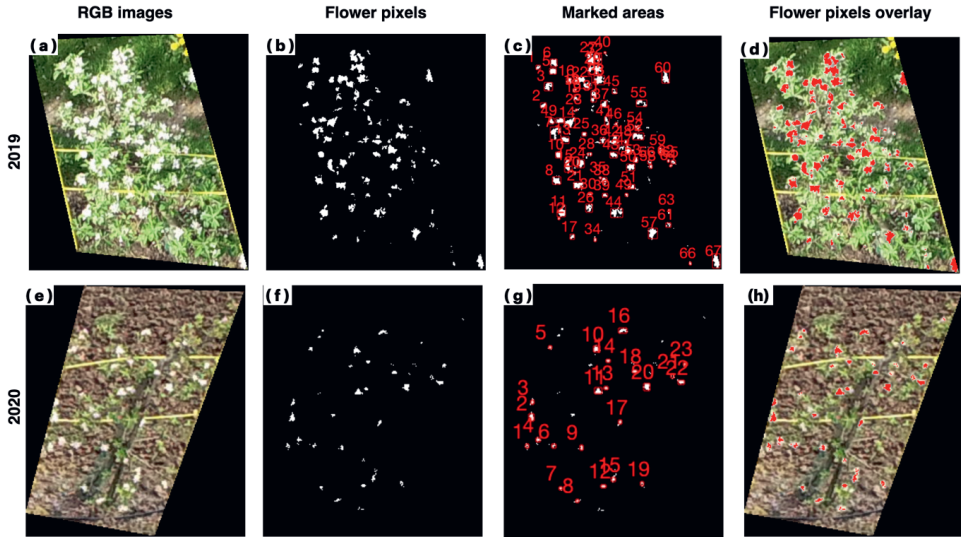


Fig. 4.9. Samples of the flower segmentation approach for two different years. (a and e) individual tree images, (b and f) perform color thresholding method, (c and g) perform morphological operations for flower area amount counting, (d and h) extracted flower associated pixels.

4.3.1.4. Flowering index calculation

There are four types of flowering indices used to monitor the flowering intensity in orchards. The first index is the counting of the absolute number of flowers in images, and it is also the only direct estimate. Majority of research employing this index is based on object-based classification (Wang et al., 2021a; Wu et al., 2020a). For pixel-based classification methods, three types of flowering index designs are well-established: (i) the number of the flower-associated pixels (Aggelopoulou et al., 2011); (ii) the ratio of flower to leaf or tree canopy-associated pixels (Wang et al., 2018b) or total image pixels (Chen et al., 2019a; Underwood et al., 2016); (iii) the number of flower associated areas in the image (Hocevar et al., 2014). These three indices and the direct counting of flower number have been applied in flower blooming variation monitoring (Hocevar et al., 2014), variable rate spray assistance (Wang et al., 2020), yield prediction (Aggelopoulou et al., 2011), and flowering peak time determination (Underwood et al., 2016). The number of white pixels in the image, flower pixels, should be able to describe the flowering intensity level of a specific tree. Thus, these three pixel-based indices were evaluated in this study.

The first examined index is based on the total number of flower-associated pixels within each of two images per tree (dual-view from aerial imaging). It is defined in Eq.1. As shown in Fig. 4.9b, f, the sum of the flower pixel number from each side of a specific tree is expected to be representative to the absolute cluster number counted on a whole tree.

$$\text{Index pixel (IP)} = \text{Flower pixel number}_{East} + \text{Flower pixel number}_{West} \quad (1)$$

Based on the flowering index used in (Hocevar et al., 2014), the second index is the number of flower-associated areas in an image corresponding to a specific tree. As the flower areas marked and counted in Fig. 4.9c, g, flower areas with different area sizes could represent the uncertainty that one apple flower cluster consists of three to six flowers. Similar to the interpretation from (Hocevar et al., 2014), a group of the neighboring pixels classified as independent objects should correspond to the flower cluster number. In addition, the filter of large objects was not applied in this study when the total flower-associated area number was calculated. Only the objects with too small sizes were filtered out as mentioned in section 3.4. Because they are the noise from the ground and yellow poles. The index area, is defined in Eq.2, which is the total number of white areas derived from each of the two images per tree, used to estimate the flower clusters directly.

$$\text{Index area (IA)} = \text{Flower areas number}_{East} + \text{Flower areas number}_{West} \quad (2)$$

The third flowering index which is a ratio of flower-associated pixels to leaf or canopy or total imaging scene pixels was also examined. Due to occlusion problem of flowers, the quantity of flowers from imagery is only a fraction of the absolute count on a whole tree, especially for quantitative methods based on IP and IA (Underwood et al., 2016). One advantage of this ratio-related index is that it can normalize the measurement with respect to the variation in image scales and overcomes issues related to different image capture distances (Wang et al., 2018b). The ratio-related index also mimics the context of the expert assessment of floridity, as introduced in section 2.3. While its potential merit in flower cluster estimation at tree level can also be proven by Fig. 4.5. In case of this study, the ratio of flower-associated pixels to the observation window pixels was designed (Eq.3). The observation window area was the ROI in pre-prepared dataset of individual trees (Fig. 4.6). Thus this index is defined by the ratio of flower pixels to ROI pixels.

$$\text{Index percentage (IPG)} = \frac{\text{Flower pixel numbers}}{\text{ROI pixel numbers}} \quad (3)$$

As can be seen in Eq.1 and Eq.2 index calculation consists of two steps: (1) the calculation on each side of a tree, which means the West-side and East-side; (2) the sum of the results from each side. Therefore,

there is only one way to do the calculation of IP and IA. For instance, the total IP equals the sum of IP calculated from the East side and that from the West side (Eq.1). But the calculation of IPG should be considered within two cases, as shown in Eq.4 and Eq.5. These two formulations share the same principle in theory. But the mathematical difference that exists in the formulation can provide different index values and further influence the estimation results. Thus both the two equations were calculated for analysis.

$$IPG = \frac{(Flower\ pixel\ number)_{East} + (Flower\ pixel\ number)_{West}}{(ROI\ pixel\ number)_{East} + (ROI\ pixel\ number)_{West}} \quad (4)$$

$$IPG2 = \left(\frac{(Flower\ pixel\ number)_{East}}{(ROI\ pixel\ number)_{East}} + \frac{(Flower\ pixel\ number)_{West}}{(ROI\ pixel\ number)_{West}} \right) / 2 \quad (5)$$

4.3.2. Accuracy assessment

To evaluate the accuracy of flower intensity estimation methods, relation between the flowering indices calculated from UAV images and field observation of flower cluster and floridity was evaluated. This relation was evaluated based on the coefficient of determination, R^2 (Eq.6), the root mean square error (RMSE) (Eq.7), and the mean absolute error (MAE) (Eq.8).

$$R^2 = 1 - \frac{\sum_{i=1}^k (y_i - \bar{y}_i)^2}{\sum_{i=1}^k (y_i - \hat{y}_i)^2} \quad (6)$$

$$RMSE = \sqrt{\frac{1}{k} \sum_{i=1}^k (y_i - \hat{y}_i)^2} \quad (7)$$

$$MAE = \frac{\sum_{i=1}^k |\hat{y}_i - y_i|}{k} \quad (8)$$

Where k is the sample size, y_i represents the ground truth value, the mean of ground truth value is \bar{y}_i and \hat{y}_i is the estimated flowering-related values derived from UAV imagery.

4.3.3. Comparison between expert- and UAV-based floridity estimations

Expert-based floridity estimation takes the overall flowering situation in an orchard as a reference and marks the trees bearing the lightest and most heavy blooming as 1 and 9, respectively. The flowering intensity of all the trees in the orchard thence is divided into 9 classes. To automate this visual expert-

based approach, a statistical UAV-derived method was developed where the same floridity scale scored by the expert was adopted. The nine floridity intervals or classes defined by the statistical method were the nine equal parts of the difference between the maximum and minimum flowering index values (Eq.9). These index values are derived from one complete dataset, e.g., group_Far 2018 (Table 4.2). This ensures that the flowering intensity distribution derived from the index is stable and precise. When floridity interval is identified for a flowering index, index value of each tree is classified as a certain floridity class.

$$\text{Floridity interval} = \frac{\text{Max}_{\text{Flowering index}} - \text{Min}_{\text{Flowering index}}}{9} \quad (9)$$

Where the flowering index is one of the two earlier described indices, IA and IPG. Max is the maximum of the flowering index value, Min is the minimum.

This UAV-derived floridity scoring method is applied to flowering indices IPG, IPG2 and IA directly. However, formulations of IA (Eq.2) and IPG2 (Eq.5) indicate that both indices were calculated from the two sides of one individual tree first. Only the sum or mean of the values determined from the two sides are used to represent the flowering intensity of a tree. Thus, an important concern is applying the scoring method to the intermediate values directly. For example, the Flower area number_{West} and Flower area number_{East} in Eq.2 are the intermediate values for IA calculation. Afterward, the mean of West and East-side floridity values is regarded as the final floridity of a tree. Since this process will produce different floridity values for a tree, it is important to examine its potential for floridity determination as well. Consequently, new UAV-derived floridity is produced from either IA or IPG2. They are named floridity IA2 and IPG3, respectively.

4.3.4. Magnitude of structural overlapping of flower cluster within the canopy on the flowering intensity estimation accuracy

To build up a benchmark framework for the use of single and raw UAV images in monitoring fruit tree 3D-phenotype traits, influential factors have been determined and validated in this study. The flower cluster number was manually counted which indicates that the ground truth data was collected in 3D circumstances. While the image data used in this study was single raw image. Thus the challenge becomes the flower occlusion in the images, though the data collected with crossing flight provides a dual side-view for the trees. The flower occlusion problem caused by the 3D structure of the tree is defined as structural overlapping in this study. There are two types of structural overlapping, vertical (nadir) and horizontal (angular) overlapping, based on the occlusion direction (Fig. 4.10b, c).

Vertical overlapping is noticeable in UAV imagery when a constant flying altitude is kept. As the example in Fig10.a shows, the variable vertical overlapping level can be observed for the same trees in

the images taken at position 1 (P1), position 2 (P2), and position 3 (P3). The samples of different vertical overlapping levels for one tree are displayed in Fig. 4.10b. From the image sample taken at P3, an approximate top-view of the tree is observed where the aerial camera stays at the closest position to a specific tree row or tree. In the UAV position closer to a tree, there is a larger chance of vertical overlap leading to occlusion of flower clusters from this view direction because fewer flowers from middle and bottom parts can be captured when a drone flies closer. Based on this, the distance from the image capture position to the target trees is regarded as the metric to describe the magnitude of vertical overlapping. To explore the effect of vertical overlapping on the flowering intensity estimation accuracy, six image groups with different image capture distance as presented in Table 4.2 are compared.

For orchard datasets collected with an oblique mission, horizontal overlapping also exists in each image. Assuming that trees in the same row, for example in row 5, are able to be captured at both P1 and P4 (Fig. 4.10a), but the surface feature of the same tree captured at these two positions can be quite different, as the sample images show in Fig. 4.10c. It shows that fewer flowers were recorded for tree65 in the image taken at P1 than that at P4. This shows the potential influence of horizontal overlapping on the flowering intensity estimation. One potential regular pattern of the horizontal overlapping is that, for the trees in the same row, the longer the distance between the tree and the capture position, the increased horizontal overlapping is taking place. This can also be observed in Fig. 4. 3 where trees with heavy horizontal overlapping have a big tilt in the image. In the prepared individual tree datasets, images with heavy horizontal overlapping were automatically filled with more black pixels (Fig. 4.9a, e), according to the developed tree extraction procedure introduced in section 3.1.2. Therefore, the metric used to describe the horizontal overlapping level is defined as follows:

$$\text{Horizontal overlapping level} = \frac{\text{Pixel number}_{\text{Black}}}{\text{Pixel number}_{\text{Total}}} \quad (10)$$

where the total pixel number is the total pixel number of the image and the black pixel number is the pixel number of the black area.

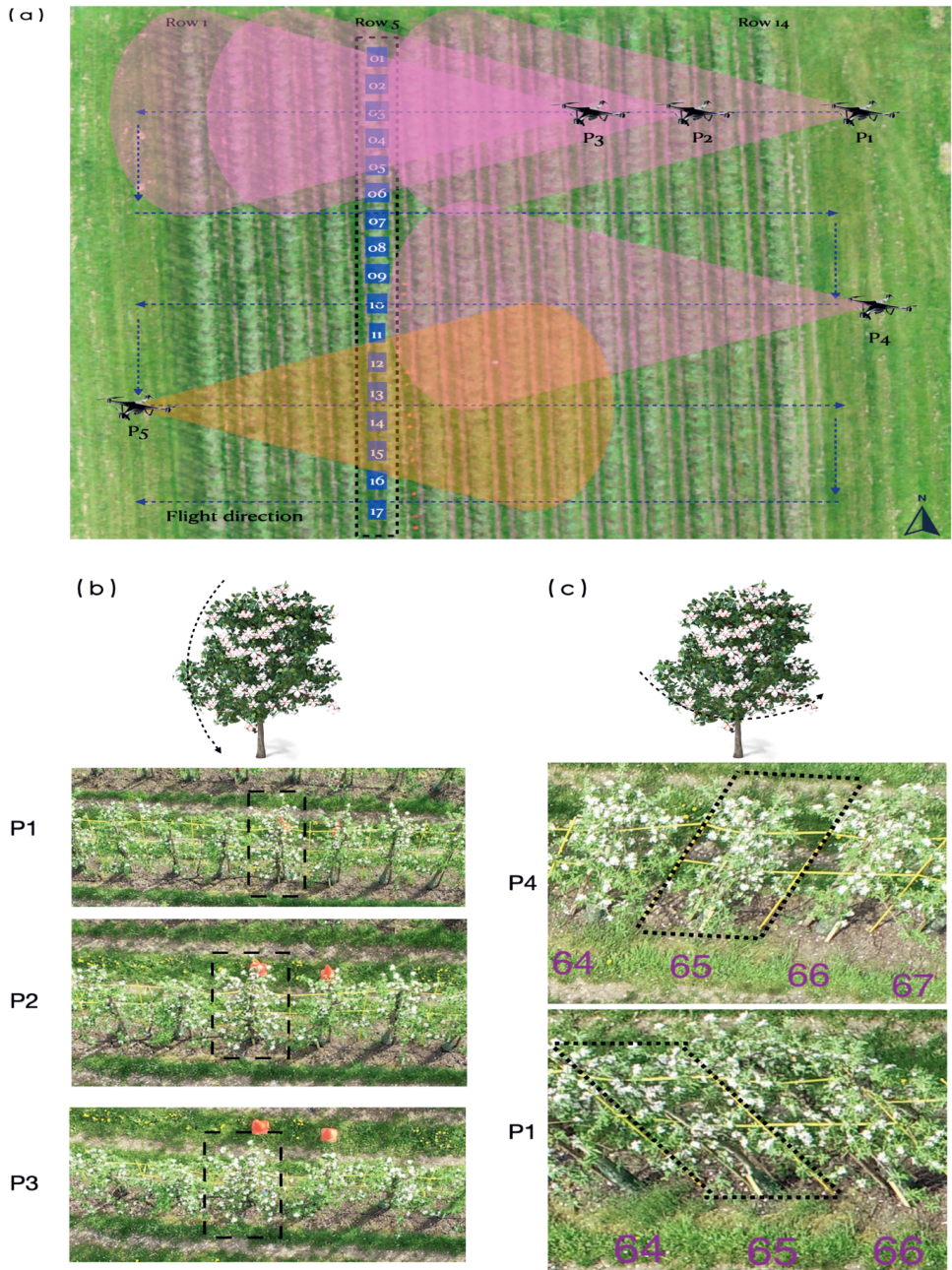


Fig. 4.10. Structural overlapping of flower clusters within the canopy: (a) demonstration of the structural overlapping. P1: position 1; P2: position 2; numbers in blue boxes: the numbered trees in row 5 (b) samples of the vertical overlapping effects to the trees in images collected in 2019, and (c) the visual effects of horizontal overlapping. The purple numbers mark the tree number.

4.4. Results

4.4.1. Flower cluster estimation

To analyze the ability of UAV-derived flowering indices for flower cluster estimation at tree level, the selected flowering indices (IPG, IP, IA) were related to the in-situ counted flower cluster number (Fig. 4.11). These results are based on the selected images of group_far from the three investigated years (Table 4.2). The individual tree images cropped during dataset preparation did not only include the tree but also background in the observation window. Therefore the ground truth used here was cluster number recorded at observation window level.

IPG and IA show a consistent relation over the three years (Fig. 4.11a, c). The data points for IPG center around the trendline (Fig. 4.11a) while the points for IP are more dispersed (Fig. 4.11b). The IPG index performs better than the other two regarding estimation generalization (Fig. 4.11). To understand the transferability of relation derived from the three indices between different years, performance of the indices was also calculated for each year (Table 4.3). In general, accuracy of two indices, IPG ($R^2=0.62$, RMSE=24) and IP ($R^2=0.48$, RMSE=28), derived from 2019 is higher than that of 2018 (with the lowest RMSE of 47). For these two years, IA shows the best performance. IP shows a less strong correlation to flower cluster number compared to the other two indices (Table 4.3). The relationship calculated from 2020 indicates higher results than those from 2018 and 2019, and the highest accuracy of $R^2 = 0.93$ (RMSE=8) was calculated from index IPG.

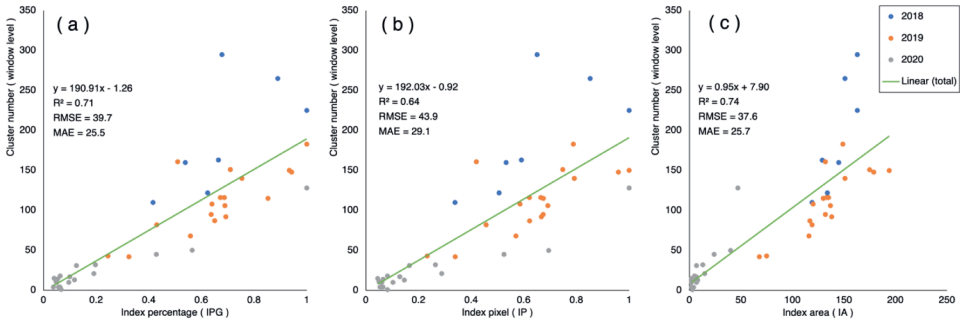


Fig. 4.11. Comparison of three indices, index percentage (IPG), index pixel (IP), and index area (IA), and their relation with the field observed cluster number for the datasets over three years. Linear correlation was calculated for the combination of the observations from 2018 (N=7), 2019 (N=18) and 2020 (N=18).

Table 4.3. Results of the relation of the three indices and the field observed cluster number per tree for the individual dataset per year.

Year	Index percentage (IPG)			Index pixel (IP)			Index area (IA)		
	R ²	RMSE	MAE	R ²	RMSE	MAE	R ²	RMSE	MAE
2018	0.43	50	38.6	0.50	47	36.1	0.74	33	31.4
2019	0.62	24	16.8	0.48	28	19.5	0.68	22	15.9
2020	0.93	8	6.5	0.88	10	7.8	0.81	12	8.9

4.4.2. Flower floridity estimation

The relationship of three indices, IPG, IPG2, and IA, and the field observed floridity score was compared (Fig. 4.12). The images from the image groups group_far from three different years (Table 4.2) were included. Results show that IA (R²=0.65, RMSE=1.0) performs worse compared to the other two indices (Fig. 4.12c). Though the mathematical difference between formulations of IPG and IPG2 was considered, results showed a high similarity for floridity estimation (Fig. 4.12a, b). In addition, it is noticeable that the three indices yielded a comparable RMSE value (Fig. 4.12).

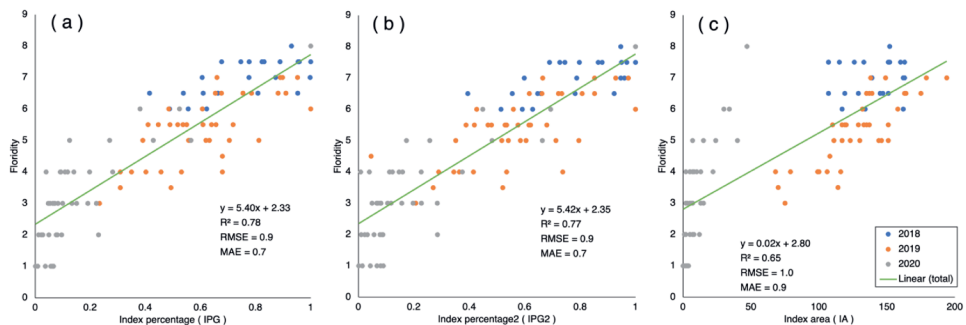


Fig. 4.12. The comparison of relationships between observed floridity and the three flowering indices, index percentage group (IPG, IPG2) and index area (IA), over three years. Linear correlation was calculated for the combination of the observations from 2018 (N=23), 2019 (N=40) and 2020 (N=40).

Results on transferability of the relation derived from the three indices among years (Table 4.4) indicate that no correlation was found between IA and floridity in 2018. But IA showed the highest estimation accuracy for the years 2019 (R²=0.67) and 2020 (R²=0.62)(Table 4.4). The other two indices, IPG and IPG2, showed similarity for the estimation in 2018 and 2019, while results from 2020 showed relatively higher accuracy, R² ranges from 0.61 to 0.63 and RMSE was 1 for both indices. In general, these three indices yielded RMSE at a similar level and relatively lower correlation to floridity, compared to their performance in flower cluster number estimation.

Table 4.4. Results of the relation of the three indices and the field floridity per tree for the individual dataset per year.

Year	Index percentage (IPG)			Index percentage2 (IPG2)			Index area (IA)		
	R ²	RMSE	MAE	R ²	RMSE	MAE	R ²	RMSE	MAE
2018	0.42	0.4	0.4	0.41	0.4	0.4	0.00	0.6	0.5
2019	0.52	0.7	0.6	0.46	0.8	0.7	0.67	0.6	0.5
2020	0.63	1	0.8	0.61	1	0.8	0.62	1	0.8

4.4.3. Comparison between expert-based and UAV-based floridity estimations

Comparison between the expert-based and UAV-derived floridity estimations was demonstrated by calculating the relationship between the scored floridity and the cluster number counted in-situ (Fig. 4.13). Visual floridity assessment was conducted at tree level by the expert while the UAV-derived estimate was at observation window level. Therefore the comparison was made at both tree level (Fig. 4.13a-c) and observation window level (Fig. 4.13d-f).

Performance of all the UAV-derived floridity at tree level (Fig. 4.13a-c) generally showed comparable accuracy to that at observation window level (Fig. 4.13d-f) over the three years. The maximum R² difference is 0.07, which happened in 2018, and the maximum RMSE difference is 2 (Table 4.5 and 6). Expert-based floridity shows a similar pattern when its performance at tree level (Fig. 4.13a-c) was compared with that at observation window level (Fig. 4.13d-f). Generally, there is a slight increase in estimation error when expert-based floridity estimation was demonstrated at observation window level (Table 4.5 and 4.6). This agrees with the fact that expert-based floridity was scored at tree level, where the expert scored the trees by visual inspection of individual trees rather than the observation windows. Expert floridity yielded the highest accuracy in 2018 but also the lowest accuracy in 2020. The six floridity estimation methods at tree level performed significantly different in 2018 (Table 4.5) where expert-based provided the highest accuracy. While the highest UAV-derived accuracy was produced by IA2 (R²=0.79, RMSE=28). However, the six indices performed comparably for the other two years, 2019 and 2020 (Table 4.5). Indices belonging to the same group, e.g., IA and IA2, yielded comparable accuracy for flowering intensity estimation although mathematical difference exists in their formulations. For instance, the tree-level results derived from IPG group in 2019 are comparable (Table 4.5). Transferability of the relation from indices crossing the three years showed a pattern that the average estimation accuracy of 2020 was higher than that of 2018 and 2019.

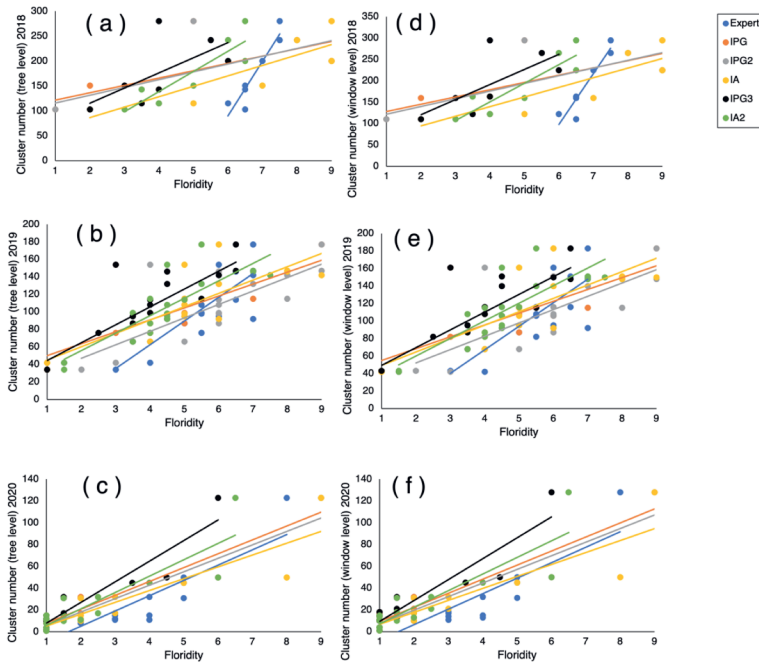


Fig. 4.13. Comparison between field-observed and UAV-based (IPG, IPG2, IA, IPG3, and IA2) floridity estimations for the three years by comparing these two types of estimations against the cluster number counted at tree level (a till c) and observation window level (d till f), respectively. IPG, IPG2 and IPG3: index percentage group; IA and IA2: index area group.

Table 4.5. Comparison of expert- and UAV-based floridity estimation at tree level. Index percentage group: IPG, IPG2 and IPG3; index area group: IA and IA2.

	Year 2018		Year 2019		Year 2020	
	R ²	RMSE	R ²	RMSE	R ²	RMSE
Expert	0.88	21	0.65	22	0.79	13
IPG	0.42	47	0.60	24	0.91	8
IPG2	0.43	46	0.58	24	0.90	9
IPG3	0.40	48	0.64	22	0.87	10
IA	0.72	33	0.67	22	0.82	12
IA2	0.79	28	0.70	21	0.79	13

Table 4.6. Comparison of expert- and UAV-based floridity estimation at observation window level. Index percentage group: IPG, IPG2 and IPG3; index area group: IA and IA2.

	Year 2018		Year 2019		Year 2020	
	R ²	RMSE	R ²	RMSE	R ²	RMSE
Expert	0.89	22	0.61	24	0.78	13
IPG	0.49	47	0.57	25	0.90	9
IPG2	0.50	47	0.54	26	0.89	9
IPG3	0.47	48	0.61	24	0.86	11
IA	0.72	35	0.65	23	0.81	12
IA2	0.79	30	0.68	22	0.78	13

4.4.4. Effect of structural overlapping on flower cluster estimation

Due to limited observations in 2018, evaluation of vertical overlapping effects on the flower cluster estimation could only be conducted for 2019 (Fig. 4.14a-c) and 2020 (Fig. 4.14d-f). In 2019, the three indices, IPG, IP, and IA, show different response patterns as the vertical overlapping parameter changed from 3.6m to 11m (Fig. 4.14a-c). There was less estimation accuracy difference observed when estimations at 7.4m and 11m were compared for the three indices. When the camera position changed to 3.6m, the vertical overlapping significantly affects the estimation accuracy for IPG (Fig. 4.14a) and IA (Fig. 4.14c). For instance, the maximum R² difference observed within the changes from 7.4m to 3.6m for IPG was 0.23, while for IA this was 0.45 (Table 4.7). Only IA-derived estimation accuracy showed deterioration when the overlapping parameter changed to 3.6m (Fig. 4.14c) (Table 4.7).

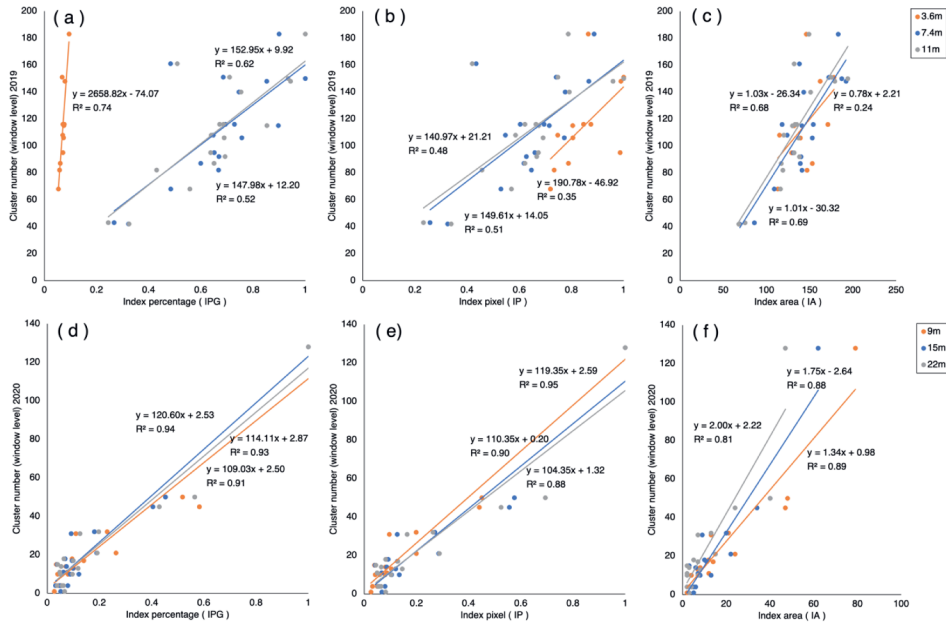


Fig. 4.14. Effects of vertical overlapping on cluster estimation accuracy in 2019 and 2020. It is evaluated for index percentage (IPG) (a and d); index pixel (IP) (b and e); index area (IA) (c and f). The distance from the image capture position to the target trees is regard as the metric to describe vertical overlapping magnitude, e.g., 3.6m.

Table 4.7. Results of cluster estimation derived from different vertical overlapping extent in 2019.

Overlapping extent	IPG		IP		IA	
	RMSE	MAE	RMSE	MAE	RMSE	MAE
Heavy (3.6m)	16	10.6	25	16.8	27	21.3
Moderate (7.4m)	27	20.0	27	20.3	21	17.6
Light (11m)	24	16.8	28	19.5	22	15.9

Concerning the contribution of vertical overlapping to the estimation conducted in 2020, a different pattern was seen (Fig. 4.14d-f). Insignificant effects of vertical overlapping were observed for all three estimations based on IPG, IP, and IA. The maximum R² difference was 0.08 for the estimation based on IP (Fig. 4.14e) (Table 4.8). Compared with IP and IA, IPG yielded the minimum R² difference of 0.04, which indicates a low sensitivity towards vertical overlapping (Fig. 4.14d) (Table 4.8). In addition, the error increased as the camera position changed from 9m to 22m, in the case of both IP and IA-derived estimation (Fig. 4.14e, f).

Table 4.8. Results of cluster estimation derived from different vertical overlapping extent in 2020.

Overlapping extent	IPG		IP		IA	
	RMSE	MAE	RMSE	MAE	RMSE	MAE
Heavy (9m)	9	6.5	6	5.1	9	6.7
Moderate (15m)	7	5.8	9	7.2	10	7.5
Light (22m)	8	6.5	10	7.8	12	8.9

Horizontal overlapping effect for flower cluster estimation was evaluated for the index IA. The evaluation was demonstrated on the datasets 2019 and 2020 separately (Fig. 4.15). Absolute error was calculated by the difference between cluster number observed in the field and cluster number predicted from IA. In 2019, a slightly increasing trend was observed along with the increasing horizontal level (Fig. 4.15a). Several outliers were also seen in the plot. Yet majority of the data points in 2020 were located at a comparable level (Fig. 4.15b), and no significant trend could be observed.

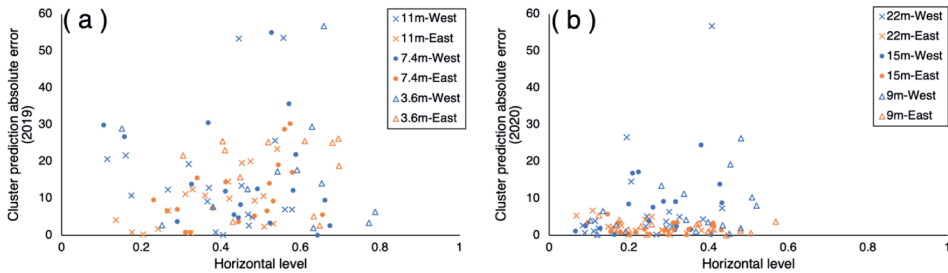


Fig. 4.15. Effects of the horizontal overlapping on the IA-derived cluster estimation accuracy for the years 2019 and 2020. Note: horizontal level is the ratio of the black pixel number to the total pixel number of the image (Eq.10). Cluster prediction absolute error = Observed cluster number – predicted cluster number.

4.5. Discussion

4.5.1. Flower cluster estimation

This study has demonstrated that single, raw UAV imagery can be adopted to estimate tree-level flower clusters in an apple orchard using two flowering indices: IPG and IA (Fig. 4.11). Three indices derived from UAV imagery, IPG, IP, and IA, were examined for flower cluster estimation. IPG proved to be the best index in relation to accuracy ($R^2 = 0.71$, RMSE = 39.7) (Fig. 4.11a) and robustness for flower cluster estimation over three years. Though a comparable performance for IA was also observed, performance for 2019 and 2020 was less promising (Fig. 4.11c) and over- and under-estimation was

observed, respectively. IPG was also applied in a previous study (Tubau Comas et al., 2019), where the IPG index was applied for the estimation based on UAV orthophoto. It yielded a maximum R^2 of 0.54, which is comparable to our results in 2018 and 2019, but lower than 2020 (Table 4.3). Transferability of the relation among three years indicated that IA was the best index for the estimation of individual years (R^2 : 0.68-0.81) (Table 4.3).

The validation result of IPG in apple flower cluster estimation was lower than that of mango panicles estimation demonstrated by a previous study, achieving an R^2 of 0.81 (Wang et al., 2018b). One reason is the difference in IPG formulations. In the same fashion as using color thresholding method for flower pixel segmentation, Wang et al. (2018) use the ratio of flower pixels to canopy pixels while the IPG in this study was the ratio to the observation window. The background in the ROI (Fig. 4.3), such as the grass, soil, and even flower clusters and branches from adjacent trees, results in additional estimation errors. Because these objects do not belong to the target tree. This point can be solved by applying an apple tree segmentation method during the individual tree cropping stage (Lee et al., 2022). Such a tree segmentation method could also automate the manual tree cropping method. Another reason is the fact that small apple flower cluster occludes more heavily than that of big mango panicles. This makes the tree-level estimation based on single and raw images more challenging. Because more flower clusters are not visible in the images. On the other hand, the mango images taken at night time suffer less from uneven illumination. It also benefits the adoption of color thresholding method for flower-associated pixels segmentation. However, compared with an image-level estimation study of apple flower cluster (Bhattarai and Karkee, 2022), even a slight improvement was achieved in this study (Table 4.3). They demonstrated a weakly-supervised approach with a result of 18.4 (RMSE) using a dataset that covers only 69 flower clusters per image.

A significant improvement was demonstrated in comparison with three previous studies focusing on UAV-derived apple flower cluster tree-level estimation, where an R^2 of 0.53 (Tubau Comas et al., 2019), an R^2 of 0.44 (Vanbrabant et al., 2020a) and an R^2 of 0.61 (Zhang et al., 2022b) were achieved. In the second study, the tree-level estimation based on 3D point clouds yielded the best model. Yet their plot-level estimation was comparable to the tree-level estimation in this study. UAV derived colored dense point cloud includes less features of the lower parts of trees in an orchard, while ground vehicle derived has lower density in the upper parts. This leads to low flower cluster estimation accuracy. A combination of these two point clouds is potential to improve the estimation accuracy (Zhang et al., 2022b). But estimation based on colored point clouds requires high computational resources. Apart from these methods, tree geometry parameters, such as cross-sectional leaf area (CSLA) also have the potential to estimate apple flowering intensity in an indirect way (Scalisi et al., 2021).

Weather conditions, flying altitudes of UAV, spatial resolution and blooming level of the orchard affect flowering intensity estimation accuracy. Direct sunlight in datasets of 2019 and 2020 decreased image contrast making part of the background more bright (Fig. 4.3). Thus leaves, chunks and soil clods were misclassified as apple flowers for some images. Yet images with homogeneous illumination in 2018 dataset suffer this problem less. A systematic experiment design is advised to further explore the effect of weather conditions. Image resolution for the dataset of 2019 was higher than that of 2018 (Table 4.1). This can explain the overall estimation accuracy improvement for all three indices in 2019 (Table 4.3), with the fact that flowering intensity in 2018 was higher than that of 2019 (Fig. 4.4). Spatial resolution refers to the feature richness of an individual object in aerial imagery. For the same drone, higher flying altitude produces images with larger ground sample distance (GSD)(Table 4.1). Lower flying altitude is recommended for apple flower detection. With the improved resolution, advanced flower detection techniques could be applied, such as faster R-CNN (Wang et al., 2018b), mask R-CNN (Mu et al., 2023) and YOLO (Chen et al., 2022c; Koirala et al., 2020b; Wang et al., 2022). For these approaches, larger datasets covering a larger range of environmental conditions are also needed and labeling individual flower cluster is difficult (Lee et al., 2022). However, utilizing aerial imagery to estimate flower number of the fruit crop with small flower size would be much more difficult (Lin et al., 2022). Trees with light blooming suffer less from flower occlusion. The blooming level of 2019 was significantly higher compared to 2020 (Fig. 4.4). This contributes to the significant accuracy improvement in 2020 and indicates that flower occlusion influences UAV-based flower cluster estimation accuracy (Table 4.3). In apple orchards, when blooming intensity was around 70 clusters per tree, estimation accuracy (RMSE) reached 5 clusters per image (Scalisi et al., 2021).

UAVs covering larger areas in one flight can be efficient platforms for flower cluster estimation in orchards. Inter-row views of fruit trees captured from proximal sensing platforms, such as handheld cameras, tripods, and ground vehicles like tractors, not always capture the entire tree (Chen et al., 2022c; Hocevar et al., 2014). Though GPS position can be recorded for tripod and ground vehicle-derived images, precise registration of individual trees is uncertain as tree branches prevent the RTK device from measuring exact positions. Yet, ground platform-derived images will experience less flower occlusion problems because of sensing view. Comparison of flower estimations from proximal sensing and UAV is encouraged in the near future. Apart from the selection of different monitoring platforms, the collection of ground truth is critical. The reference data was recorded by only one expert in this study. It does not provide insights into the uncertainty of manual counting. To quantify uncertainty within the ground truth of flowering intensity, flower cluster number, and floridity, two or three ground truth recordings from different persons are highly recommended (Farjon et al., 2020).

4.5.2. Flower floridity estimation

Floridity estimation results indicated that IPG group (IPG, IPG2) had best performance for the estimation crossing three years (Fig. 4.12a, b). Though these two indices were defined with different formulations, a comparable performance of them towards floridity estimation was demonstrated. A similar pattern with the IA-based flower cluster estimation was observed within the IA-based floridity estimation, where the index underestimated the floridity of 2018 and overestimated that of 2019 (Fig. 4.12c). The reason can be the usage of the camera with low resolution in 2018. This is demonstrated in Table 4.4, where no correlation between IA and floridity was observed in the case study of 2018. Moreover, IA yielded a comparable performance for the estimation in both 2019 ($R^2=0.67$) and 2020 ($R^2=0.62$) where the same image resolution was applied (Table 4.4). Related to the floridity estimation in individual years, the results from 2019 and 2020 proved that IA even had a comparable performance with the IPG indices when image resolution was the same (Table 4.4). In comparison to IA, the index percentage group, IPG and IPG2, was not sensitive to image resolution when comparing its accuracy in 2018 and 2019. But they were not superior to IA in the case that the trees were heavily blooming (in the years 2018 and 2019). For instance, the best performance yielded from the index percentage group in 2019 was from IPG ($R^2=0.52$), while IA showed a stable accuracy ($R^2=0.67$).

Flower floridity scored by experts contributes to the flower thinning strategy through spatial and temporal flowering intensity monitoring. For the first purpose, floridity is adopted to make decisions on whether a specific tree needs flower thinning. But in the context of precision agriculture, floridity can provide only an approximate flower number in assisting the growers to decide how many excess flower clusters to remove from a tree. Yet it has an advantage in the dynamic monitoring of flowering intensity, which benefits the breeding trials, fruit tree health status, and nutrition management (Chen et al., 2019a; Zhang et al., 2021). Currently, only two floridity estimation studies were conducted (Farjon et al., 2020; Zhang et al., 2022b). The flowering index IA tested in this study shows a similar performance to the point cloud-based method, where an R^2 of 0.65 was reported (Zhang et al., 2022b). But data processing efficiency of the IA-based method proposed in this study is higher. Since no complex and time-consuming pre-processing steps such as structure-from-motion were required. A high correlation between the image-derived and manually scored floridity was recorded in the other study, with an R^2 of 0.93 (Farjon et al., 2020). However, their floridity was judged by visual inspection of the images rather than scoring in the field. This can potentially result in a high agreement with the computer-vision derived estimation. In our study, the floridity was visually recorded independently in the field by an expert. Because of this difference, the accuracies of the two studies cannot directly be compared.

4.5.3. UAV-based and expert-based floridity estimations

As expected, results show that the manual assessment was year-variant (Fig. 4.13). By contrast, UAV-based ones were more robust on flowering intensity estimation. They were comparable and even better than the manual assessment. Both showed quite similar performance towards the flowering intensity estimation at tree and observation window level. This can be explained by the orchard training system in the study site. Because apple trees in the same row have a proper tree distance preventing highly branches overlapping from affecting flower thinning.

The index area group, IA and IA2, proved to be the optimal index for floridity estimation with minimum accuracy difference between IA and IA2 (Table 4.5, 6). The floridity assessment derived from the index percentage group (IPG) showed sensitivity to the flowering intensity, which agrees with its performance in floridity estimation. For example, its performance was significantly improved in 2020 and even slightly better than that of the index area group (Fig. 4.13). Low flowering intensity in 2020 corresponds to the fact that fewer flower clusters bloomed (Fig. 4.4). This entails light flower occlusion problems for flower cluster detection with RGB images. IA proved to have an advantage in this respect. A previous study only examined the agreement between the computer version derived and expert-based floridity estimation (Farjon et al., 2020). The question about which estimator is more representative of the real truth, the cluster number counted in the field, was not answered. Though results from this study provide insights into this comparison, advanced floridity estimation models, such as the linear regression model, are required to improve the UAV-based floridity estimation accuracy.

4.5.4. The effect of structural overlapping on flower cluster estimation

Results showed that vertical overlapping significantly influences cluster estimation accuracy (Fig. 4.14a-f). Different flowering indices examined in this study showed varying degrees of sensitivity to this, especially in 2019 (Fig. 4.14a-c). IPG and IA were the most sensitive, and the largest R^2 and RMSE differences were 0.45 and 11, respectively (Table 4.7). IPG and IA showed contrary responses with the distance increasing. As the distance between the camera position and trees increase, the IPG-derived cluster estimation accuracy decreased (Fig. 4.14a), but IA derived increased (Fig. 4.14c). No significant effect of vertical overlapping was demonstrated in 2020 (Fig. 4.14d-f). This can be explained by light flower occlusion. Because fewer flower clusters bloomed in that year. In addition, as shown in Table 4.2, the difference in the distance between the East and West side can also have an impact on the tendency observed in Fig. 4.14, though the distance difference in 2019 was smaller than 0.4m. It has been reported that visual countable pear flower clusters in the image captured with a top-view (orthomosaic) of the trees represent 50%-76% of the exact cluster number counted in field (Vanbrabant et al., 2020a). This calculation links to the overlapping magnitude directly. However, it is unrealistic to count the visible apple flower clusters in the aerial images collected in this study, especially for datasets

2018 and 2019, because of the heavy blooming and tree architecture. Even though, the proposed evaluation metric for overlapping magnitude, the distance between camera and trees, showed success in quantifying the effects of vertical overlapping on the flower cluster estimation accuracy.

The horizontal overlapping magnitude was evinced by the percentage of black pixels to whole image in this study (Eq.10). The ideal situation is when this metric value equals zero. Then the targeted tree is right in front of the camera, such as the tree3 to the drone position P1, or P2, or P3 (Fig. 4.10a). In other situations, the cropped individual trees can include flowers from adjacent neighboring trees which leads to inaccurate estimation at tree level. Such as the tree65 illustrated in Fig. 4.10c. Results in 2019 demonstrated that higher horizontal overlapping leads to an increased absolute error (Fig. 4.15a), which agrees with the initial hypothesis. No significant trend was observed in 2020 (Fig. 4.15b). But majority of the data dispersed in the range of 0 to 0.5, and the absolute error of the cluster number prediction was lower. This did not contradict the expectation in this study. On the hand, the results shown in Fig. 4.15 indicate that the higher the UAV flying altitude is, the fewer errors derived from horizontal overlapping can be achieved. In 2020, a relatively higher flying altitude was set (Table 4.1). Thus another case study conducted at 25m for the orchard with flowering intensity similar to 2019 is advised for future studies.

4.6. Conclusions

Flower characteristic monitoring in orchards is still in its infancy. In the case study of apple flowering intensity estimation, a novel framework that skips the conventional time-consuming photogrammetric approach such as structure-from-motion was designed, and the potential use of single and raw UAV images was evaluated. Tree-level flower cluster estimation derived from this approach shows an important potential. A well-established flowering index IPG yielded the highest accuracy for apple flower cluster estimation over three years, and a consistent relation was observed. For the estimation of flower clusters present within an individual year, a reliable index IA was demonstrated and yielded higher accuracy than the state-of-art methods. The IPG index group, IPG and IPG2, also proved to be capable of estimating flower floridity, while IA is the best flowering index for individual year floridity estimation.

Expert and UAV-derived floridity estimations showed comparable results. Among UAV-derived estimations, index group IA was the best one to automate the expert-based floridity estimation. This indicates that UAV-derived floridity estimation is capable to replace manual efforts with a robust performance. In addition, the three flowering indices, IPG, IP, and IA, evaluated for flower cluster estimation showed different sensitive patterns towards the effects of structural overlapping. It reveals that vertical and horizontal overlapping affects the accuracy of the flowering intensity estimation derived from single and raw UAV images.

5

Chapter 5

Orchard fruit load estimation in multi-temporal high-resolution UAV imagery using deep learning

This chapter is based on:

Zhang, C., Valente, J., Wang, W., Kooistra, L., 2023. Orchard fruit load estimation in multi-temporal high-resolution UAV imagery using deep learning (In preparation).

Abstract

Harvesting period in orchards accounts for the majority of total cost. Yet current development of fruit yield estimation still hinders management efficiency. Limited studies applied conventional UAV photogrammetry techniques that are based on structure from motion (SfM) in crop load estimation. They are generally resource-consuming and their performance is unsatisfactory. Faced with this, taking tree-level apple yield estimation as a case study, the present work proposed a novel approach using single raw UAV RGB images. First, apples were detected and localized with YOLOv5s. Next a fruit tree localization method was designed: (1) GPS positions of all the trees in the orchard were first predicted; (2) GPS positions of image-projected area corners were calculated by a great-circle-based method, and therefore, trees within the projected area were identified; (3) pixels in aerial images were registered in the real-world coordinate using a proposed convert method. Thus representative pixels of covered trees are recognized; (4) Finally, detected apples were assigned to predicted individual tree areas. Apple detection results showed that YOLOv5s is proficient in extreme small object detection in aerial images. mAP50 for datasets collected over three consecutive years ranging from 0.69 to 0.78. Model generalization tests across three years revealed that two temporal UAV RGB datasets are adequate for apple detection. Fruit tree identification achieved high accuracy in tree counting, with a maximum error of 1 tree per row. A good localization performance was observed as well. Additionally, a spatial pattern of predicted tree positions was summarized and indicated the optimal areas for tree-level yield estimation. Evidence showed great potential of proposed tree localization methods in supporting orchard management.

5.1. Introduction

Faced with the increasing nutrition and health needs of the growing world population, global apple production increased yearly from 2017 to 2021, while apple area harvested and production increased by 1.04 and 1.12 times respectively in 2021 (FAO, 2021). Efficient orchard management is fast becoming a key focus in agriculture.

The harvesting period accounts for the majority of total management cost, in citrus production, it takes up 35-45% of total cost (Sanders, 2005). Thus, the optimization of harvest process is fundamental. Broad apple yield estimation refers to the weight per tree. This estimation at a more advanced maturation stage directly benefits logistics optimization, such as labor force, harvest containers and gathering path (Osman et al., 2021; Xia et al., 2022). Growers utilize estimated yield to contract the receipt of fruits while other stakeholders within the fruit supply chain, such as storage and packing stations and processing companies also require a yield estimation (Janowski et al., 2021). A more narrow concept of apple yield estimation denotes fruit counting. This estimation at early stage proved a critical indicator in assisting precise irrigation, fertilization, crop growth monitoring and variable spraying strategy (Bargoti and Underwood, 2016; Wang and He, 2021).

Apple yield correlates to the exact fruit number and size (Mitchell, 1986; Stajanko et al., 2009a). Hence, fruit counting will also be key to broad yield estimation. Yet current practice of apple counting still relies on the traditional approach - labor-intensive manual counting, prone to errors and limits the application in large orchards. Manual counting systematically samples a certain percentage (e.g. 5%) of trees first, the total yield of an orchard is extrapolated from the samples afterward (Wulfsohn et al., 2012). Given the fact of labor shortage and high labor costs, automatic and precise apple yield mapping is of utmost importance.

Varying from the prediction scale, yield mapping comprises tree-level (Crtomir et al., 2012), row-level (Apolo-Apolo et al., 2020b) and plot-level estimation (Bai et al., 2021). Different application scenarios have their own requirement for this scale. For example, plot-level yield mapping is more adequate for a national yield inventory of fruits (Rahman et al., 2018b; Sarron et al., 2018b). Tree-level yield mapping facilitates the monitoring of individual trees aiming at maximizing orchard uniformity (Perry et al., 2010). It also benefits the analysis of individual trees in plant breeding. Tree-level yield mapping encompasses two tasks, fruit identification and fruit assignment. The identification of fruits links directly to fruit counting and correlates to the estimation of weights (Mitchell, 1986). While fruit assignment implies localizing the identified fruits, to recognize which tree the fruits belong to. Although extensive research has been carried out on the first task, fruit detection (Fu et al., 2020; Linker et al., 2012; Nguyen et al., 2016), a few published studies focus on the follow-up task, the fruit assignment.

Traditional fruit identification approaches use predefined hand-crafted features to extract fruit in the images. The features can be color (Zhou et al., 2012) and shape (Qian et al., 2018). Such approaches generally embrace color thresholding (Cheng et al., 2017) and Hough transform-based feature extractor (Kanwal et al., 2019). These approaches hold strict requirements on image acquisition conditions. In view of the fact that orchard images and complex illumination conditions and variation in fruit shape are always symbiotic (Zhang et al., 2022a), traditional approaches show great limitations in practice. Later, machine learning techniques such as support vector machines (SVM) (Peng et al., 2018), random forest and clustering (Nguyen et al., 2016) have also been adopted for facilitating fruit detection. They are more robust in fruit detection at pixel level. Yet they also hold constraints for fruit detection in 2 dimensional (2D) images. But both traditional and machine learning techniques can be widely used in 3D point cloud analysis of fruit trees aiming at fruit identification (Zine-El-Abidine et al., 2021).

Despite that the utilization of deep learning in agriculture, especially in horticulture, is nascent (Kamilaris and Prenafeta-Boldú, 2018), it has become commonplace in fruit detection and shows promising performance in comparison with conventional approaches. Early convolution neural network (CNN) applied a sliding window for fruit classification where the classifier is designed to scan spaced locations of an image first and detect fruits next. Thus, it renders this model slow. One typical model is the OverFeat network (Koirala et al., 2019). Though region-based CNN (R-CNN) replaces the sliding window with a heuristic selective search algorithm and improves the speed, it is still not efficient. In comparison with early methods, two-stage detectors, such as fast R-CNN and faster R-CNN (Fu et al., 2020), and mask R-CNN (Jia et al., 2022) are more efficient in terms of detection time and also more accurate. Considering the compromise between accuracy and efficiency, one-stage detectors show great advantages. Especially in practical scenarios of orchard management, the requirements for data processing efficiency are more important. In most recent studies, the lightweight one-stage detectors that draw more researcher attention embrace single shot multibox detectors (SSD), YOLO (Osman et al., 2021; Wang and He, 2021), and RetinaNet. Among these detectors, YOLO model family is more powerful. For instance, YOLOv3 can be 3.0 and 3.8 times faster than SSD and RetinaNet, respectively, with the same accuracy. Attention mechanism emerged in natural language processing (NLP) first, and great improvement was demonstrated over the neural machine translation system. Later, attention mechanisms and their variations were also introduced to computer vision community. The improvement it brings was also shown in fruit detection tasks (Jia et al., 2022; Liu et al., 2021). For example, a coordinate attention module can increase the mean average precision (mAP) of apple detection by 2.21% (Zhang et al., 2022a). However, current studies were based upon small datasets and small variations are observed within the dataset (Apolo-Apolo et al., 2020b; Ji et al., 2021). The universality of using the established deep learning models for fruit detection of another variety or weather conditions is still poorly understood (Liu et al., 2021; Xia et al., 2022).

As a follow-up task, fruit assignment is generally referred to as separating individual trees first and assigning detected fruits derived from the fruit identification stage to their bearing trees. Individual tree identification commonly comprises the detection of tree trunks and canopy areas (Zine-El-Abidine et al., 2021). Yet, the delineation of those is still technically challenging in dense orchards and forests where tree branches are occluded (Zhen et al., 2016). Tree trunks hold the most distinguishable structure in comparison with branches and leaves due to geometric size (Ho et al., 2022). This makes tree trunks a good reference for the identification of tree center position. Based on trunk position, detected fruits can be properly assigned to which trees they belong. In addition, tree trunks can also be used for fruit tracking in videos (Gao et al., 2022). It is feasible for the application based on ground vehicles. But tree trunk detection in aerial images is challenging because of the camera view and interlacing and touching tree structure, especially for modern high-density orchards. On the contrary, UAV imagery is advantageous in canopy delineation (Dong et al., 2020). Preferably, precise tree-level yield estimation requires the delineation of branches of individual trees to ensure accurate fruit assignment. However, heavy occlusion of leaves and branches in the harvesting period makes the delineation impracticable (Wu et al., 2020b).

There are also indirect approaches for the delineation of fruit trees which require more manual processing steps. This supervised approach normally sets a theoretical threshold for the tree shape, based on properly known tree positions in the images or the measured tree GPS coordinates in advance (Apolo-Apolo et al., 2020b). The supposed shape can be a circle (Apolo-Apolo et al., 2020b) or a rectangle (Apolo-Apolo et al., 2020a). It assumes that all the trees share the same size of canopy or tree area (Osco et al., 2020a). The fixed size can be determined by inspecting a set of tree samples in the target dataset. One way to generate the approximate tree positions is to make use of the GPS coordinates stored in geotagged images. While orthomosaics and point clouds derived from aerial images always have an advantage in localizing the tree positions based on a defined coordinate system (Dong et al., 2020; Raman et al., 2022). Compared with the direct tree delineation method, this supervised method inevitably produces errors. Because high variation exists among fruit trees in terms of canopy size. But it can be a relatively accurate solution for application in high-density modern orchards where trees in the same row are interlacing and touching each other making computer vision impossible to detect individual trees.

Besides the direct yield estimation approaches introduced above, spectral and geometric characteristics-based estimation are alternatives (Chen et al., 2022b; Sun et al., 2020). Earlier studies have shown that some vegetation indices (VI) are correlated with fruit tree photosynthetic activity and health status (Bai et al., 2019; Somers et al., 2010), such as normalized difference vegetation index (NDVI), normalized difference water index (NDWI) and photochemical reflectance index (PRI) (Van Beek et al., 2015). The

potential of using vegetation indices as indicators for fruit yield has also been demonstrated (Machovina et al., 2016). Yet, the correlation of these indices to the fruit amount is poorly understood (Rahman et al., 2018b). VI-based yield estimation requires more data from spectral bands than direct estimation. Generally, it encompasses data from visible, red-edge and infrared bands. Similar to the adoption of vegetation indices, existing research recognizes the correlation of another fruit tree characteristic, geometric features, to potential yield. Investigated geometric characteristics comprise canopy projected area (CPA) (Sola-Guirado et al., 2017), tree height (Sarron et al., 2018b) and canopy perimeter (Uribeetxebarria et al., 2019). 3D morphological characteristics such as crown volume are also good yield predictors (Lopez-Granados et al., 2019b). The correlation of estimated crown volume from aerial imagery to actual yield can be higher than 0.7 (R^2) for some almond varieties. UAVs equipped with RGB cameras are increasingly being used for the calculation of geometric features of fruit trees (Marques et al., 2019; Zhang et al., 2021). Advantages are the imaging view and promising estimation results derived from orthomosaics or point clouds. While the generation of point clouds is based on structure-from-motion (SfM) which requires high computational resources (Jimenez-Brenes et al., 2017).

Faced with the gaps above, the research presented in this chapter proposes a novel approach for tree-level yield mapping in an apple orchard from single raw UAV RGB images. Specifically, the following contributions will be elaborated:

- Evaluate the feasibility of using single raw and geotagged UAV images for tree-level apple yield estimation;
- Examine the generalization of deep learning models for apple detection in datasets across three years;
- Assess the accuracy of registering individual trees from single raw and geotagged aerial images;
- Investigate the effects of side-view and nadir-view of trees toward apple yield estimation accuracy.

5.2. Study area and datasets

5.2.1. Study area

The field survey area in this study is an apple orchard situated in Randwijk, Overbetuwe, Gelderland, The Netherlands (51.938, 5.7068 in WGS84 UTM 31U) (Fig. 5.1a). The planted apple variety is Elstar, *Malus pumila* 'Elstar', and the rootstock is M9. Totally, 1414 trees were planted in 2007, with a layout of 14 rows located from South to North. The tree and row spacing is 1.1m and 3.0m, respectively. To provide good pollinator habitat for Elstar apple trees, another apple variety, *Granny Smith*, was planted evenly over the whole orchard. In 2020, half of the apple trees were removed. As it is shown in Fig.

5.1.a, the red-dotted line delineates the whole orchard and the removed part is the bottom area. As a result, the orchard area decreased from 0.47 ha to 0.26 ha.

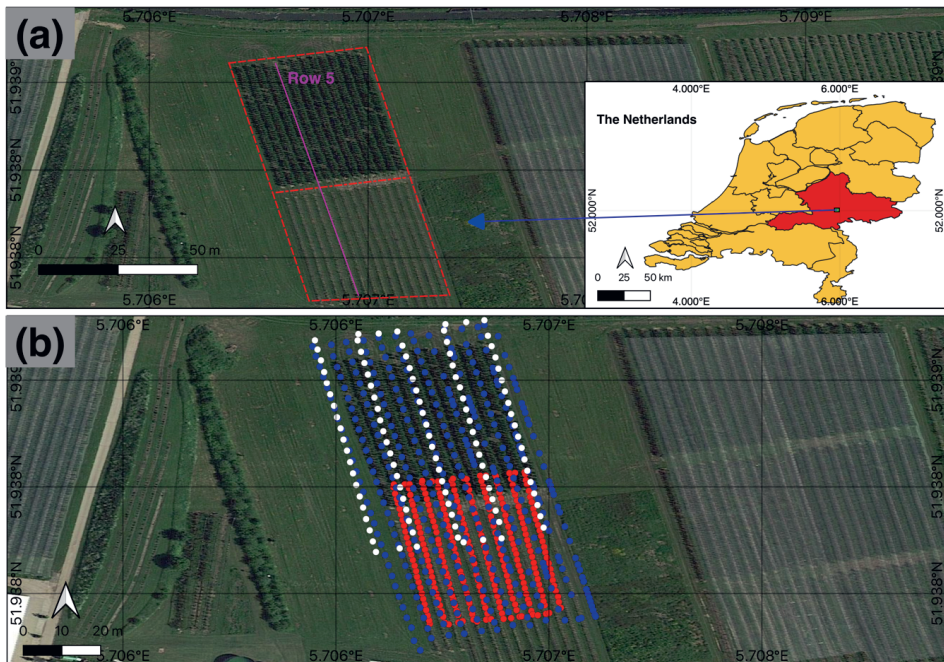


Fig. 5. 1. The experimental apple orchard in Randwijk, Overbetuwe, Gelderland in the Netherlands (a). The red dotted line delineates the apple orchard: trees in the lower area were removed in 2020. Pink line indicates the tree row with ground truth data. Province Gelderland is highlighted in red on the national map in the inset. (b) UAV flights over three consecutive years. Circles with different colors indicate the central location of geotagged UAV images. Red circle: 2018; blue circle: 2019; white circle: 2020.

5.2.2. Aerial images from UAVs

Starting in 2018, UAV-based field campaigns were conducted in the next two consecutive years, 2019 and 2020 (Table 5.1). Data collection dates were generally two weeks earlier than the final harvesting date while specific dates were different every year. Three UAV platforms were used for data collection, DJI Phantom 3 (2018) and DJI Phantom 4 (2019) and DJI Matrice 210 (2020). Only RGB cameras were adopted while associated sensor models were slightly different. During the three flights, a fixed gimbal pitch value was set to capture the nadir view of apple trees. Flights in 2018 and 2019 shared the same flying altitude, 15m, while flight 2020 adopted a higher altitude of 25m. Fig. 5.1b demonstrates these three flight paths in detail. The flight in 2018 covers the bottom area of the orchard (footprint with red

points) and flight 2020 covers the other part (white points). A complete orchard was mapped by flight 2019 (footprint with blue points). The three flights provided datasets covering various illumination conditions (Table 5.1).

Table 5.1

Description of UAV campaigns for the apple orchard during period 2018-2020.

	Data 2018	Data 2019	Data 2020
UAV platform	DJI Phantom 3 PRO, Shenzhen, China	DJI Phantom 4 PRO, Shenzhen, China	DJI Matrice 210, Shenzhen, China
Sensor	FC300X	FC6310S	FC6540
Type	CMOS	CMOS	CMOS
Sensor width (mm)	6.17	13.2	23.5
Resolution (inches)	4000×3000	5472×3648	6016 ×4008
Focal length (mm)	3.6	8.8	16
Shutter speed	1/100	1/200	1/640
Field of view (deg)	84	73.7	73.7
Gimbal pitch (deg)	-90	-90	-90
Flying velocity (m/s)	0.6	2.2	1.9
Flying altitude (m)	15	15	25
Ground sample distance (GSD) (cm/pixel)	0.64	0.41	0.61
Data size	277	353	103
Collection date & time	28 th August, 10:04 am	28 nd August, 12:12 pm	28 th August, 13:19 pm
Weather	Overcast	Sunny	Overcast

5.2.3. Ground truth data

To explore the correlation between apple amount visible in the aerial images and the exact apple yield (apple counting) recorded in the field, ground truth data were collected while the flight campaigns were conducted. For the three years, surveyed samples were the same apple trees in row 5, as it shows in Fig. 5.1a. An experienced agronomist counted the apple amount per tree and saved the records for later analysis. In 2020, the fruit load on-tree of 56 apple trees was collected due to the orchard management of tree removal. For the other two years, the number of trees was 101 (Fig. 5.2). *Malus pumila* 'Elstar' is a variety of biennial bearing which means that much less yield is harvestable every two years. This

coincides with the significant decrease in yield as it was observed in 2020 (Fig. 5.2). In addition, GPS positions of the trees located at the rectangle orchard corners were also measured.

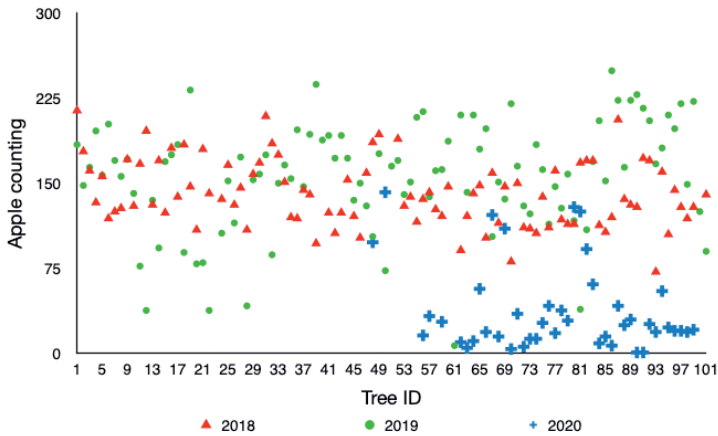


Fig. 5. 2. Ground truth data (apple amount per tree) collected over three years: 2018, 2019 and 2020.

5.3. Methodology

The proposed apple yield estimation mechanism mainly consists of two modules: apple detection and apple yield assignment model (Fig. 5.3). As a whole, it requires two inputs: 1) aerial images and metadata, 2) orchard boundary GPS coordinates. While ground truth data, was utilized to study efficiency of the models proposed. The apple detection and assignment model are presented in section 3.1 and section 3.2, respectively.

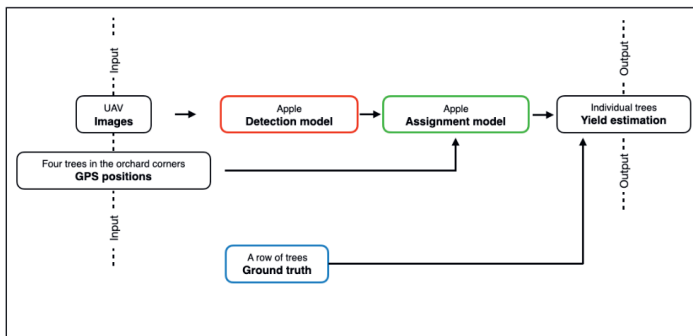


Fig. 5. 3. Overview of the tree-level fruit load estimation method proposed in this study consisting of two models: apple detection (red-borderline box) and apple assignment model (green-borderline box).



5.3.1. Apple detection model

The use of UAVs in supporting orchard management or other agricultural scenarios encompass higher requirement in data processing speed compared to ground vehicles-based monitoring. As discussed in the introduction section, out of several available deep learning-derived detectors, one-stage detectors have proven to be the optimal option for this study (Zhang et al., 2022d). YOLOv5 is one of the recent powerful one-stage detectors and both its detection accuracy and efficiency in fruit detection have also been validated (Li et al., 2023b; Liang et al., 2023). Thus YOLOv5 was selected as the apple detection model and used for a fair comparison with previous studies. In addition, in computer vision community, YOLO series were tested in the detection tasks of small objects derived from aerial images (K.R et al., 2023; Shen et al., 2022; Tian et al., 2022). Yet, its performance in extreme small object recognition such as the apple detection task in this study was not examined.

Of the YOLOv5 variations, the version YOLOv5s held similar performance as other variations such as YOLOv5m for detecting small fruits (Liang et al., 2023). Yet its architecture is lighter and faster to train. The YOLOv5s utilized in this study comprises the backbone of CSP-darknet53 and the neck consists of spatial pyramid pooling fast layer (SPPF) and cross stage partial connections-pyramid attention network (CSP-PAN). While it sustains the YOLOv3 head where bounding box loss function and non-maximum suppression (NMS) are integrated. The GIoU loss function was applied, which stands for Generalized Intersection over Union. And stochastic gradient descent (SGD) was used for optimizing objective functions.

5.3.1.1. Pre-processing

To ensure image variety for training YOLOv5s is representative for real-world orchard environment, selected UAV images should be spatio-temporal independent. Thus, for each dataset, five images were chosen from a whole dataset (Fig. 5.4). Ideally, they comprise the characteristics of apples growing at different locations across the orchard, such as apples from the upper left and center areas. To reduce false positives (FP), two to three images holding certain grass areas were designed to be added to the five images, as photos 117 and 132 shown in Fig. 5.4. The grass areas were regarded as background areas where no apples and labels were required. This is consistent with the design of COCO (Lin et al., 2014) from which 1% of the total images are background.

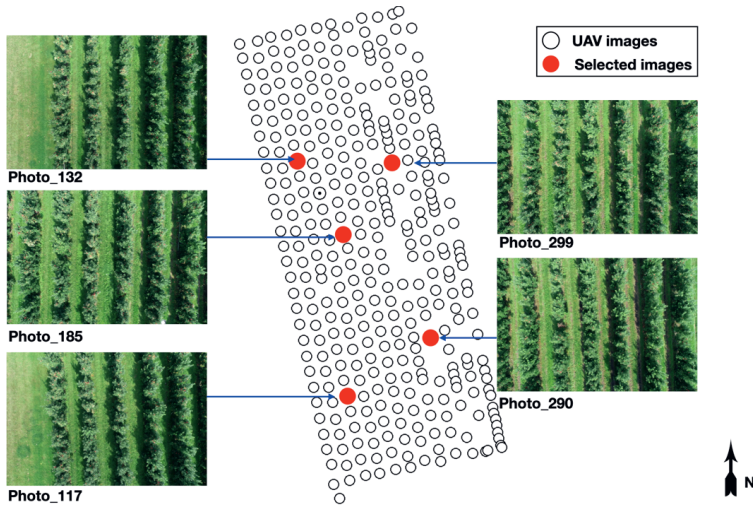


Fig. 5. 4. Image selection approach applied in this study. White circle represents UAV geotagged images collected in one flight; red circle represents the images selected for the development of apple detection model. Image selection for the dataset 2019 was illustrated in the figure. A comparable approach was adopted for the other two years.

Annotation was conducted on the original UAV images directly which is more flexible for model modifications in the late stages. The annotation tool was a free and open-source platform named Label Studio. It integrated a previously popular tool, LabelImg (Apolo-Apolo et al., 2020b). The main principle in labeling apples is to ensure the labels, based on bounding boxes, closely enclose each apple. Since apples are extremely small in the datasets, zoom-in and zoom-out operations were highly required during the annotation. To enhance the understanding of YOLOv5s in extreme object detection, apples in the UAV images were divided into four categories: apples, occluded apples, apples on the ground and difficult to identify apples (Fig. 5.5). Apples are defined as the apples within tree canopy and more than 50 percentage of its shape feature are visible in the image. By contrast, apples suffering heavy occlusion from leaves, branches and other apples and only small parts are visible (less than 50 percent) were regarded as occluded apples. During harvesting period, it is common to see apples falling on the ground. These apples were labeled as apples on the ground. Including this class is also expected to increase the model learning on what is actually an apple under the same operational conditions as the ones in the canopy. Concerning the class of difficult, it is the potential apples challenging the operator which could not be confirmed. Usually the leaves in dark areas or bearing strong illumination cause uncertainties. It is not necessary to classify these four classes for apple yield estimation. Yet examining how YOLOv5s functions to these classes assists model optimization and modifications in later stages. Labelling the extreme small apples in UAV images is challenging. For instance, it took 19.6 and 29.1 mins for finishing the annotation in one row in the datasets 2019 and 2018, respectively. In 2020, one

row even required 40 to 80 mins. Generally, for the images without background of grass, there are 6 and 8 tree rows in the datasets 2019 (Fig. 5.4) and 2018. While in 2020, it can be 13 to 14 rows per image.

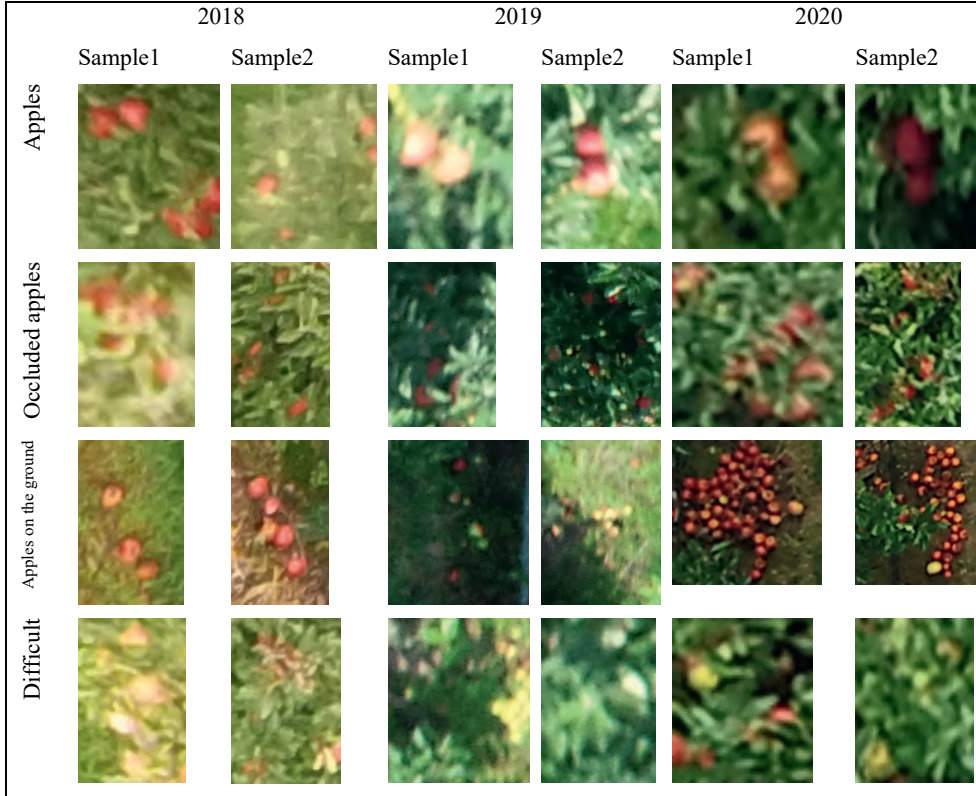


Fig. 5. 5. Image samples of the proposed four classes in the three years, apples, occluded apples, apples on the ground and difficult.

Original labeled UAV images were split into small tiles to improve the detection accuracy of YOLOv5s on small objects. Ideal input image resolution for YOLOv5s is 640×640 as suggested by previous studies (Li et al., 2022; Liang et al., 2023). To achieve this input requirement, different tile sizes were designed for the three datasets. Because they retained different resolutions over the years (Table 5.1). Stretching small images obscure YOLOv5s to learn the key features. Thus the produced tiles should hold a tile resolution slightly larger than 640×640 , such as a tile size of 684×729 . Next, to resize the tiles, tile aspect ratio was maintained, and the newly generated padding is a reflection of the tiles. To keep image display the same way as they are stored on disk, auto-orient was applied. Ratios of training, validation and test sets were set to 80%, 10% and 10%, respectively, for all the datasets. The inventory of prepared datasets is summarized in Table 5.2. Since classification of the four predefined apple classes

is not necessary in this study, these classes were modified to one class, apples, during the training and validation. The four classes were kept in the ground truth of manual labeling and used for visual inspection of the test performance. Generally, in the prepared datasets, the classes of occluded apples and apples on the ground hold the majority in the three datasets (Fig. 5.6).

Table 5.2

Description of the dataset composition.

	Tile resolution	Training set	Validation set	Test set	Null	Labels
2018	666×750	58	7	7	4	6,337
2019	684×729	160	20	20	11	5,515
2020	668×668	216	27	27	35	18,754

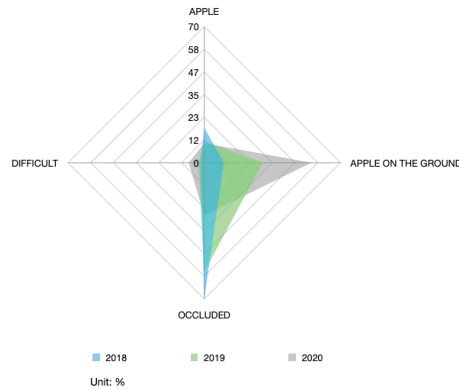


Fig. 5. 6. Distribution of the four annotation classes (%) over the three years, 2018, 2019 and 2020. The four classes are: apple, occluded apples, apples on the ground and difficult.

In addition, the feasibility of YOLOv5s in model generalization was tested across the three years. YOLOv5s was trained on mixed training sets in this section. The mixed sets are dataset 2018&19, 2018&20, 2019&20 and all the three years. The resulting models were tested on the three test sets separately to identify the problems hindering YOLOv5s generalization and find the optimal model generalization strategy.

5.3.2. Apple assignment model

As a follow-up step, to assign detected apples from the apple detection model to a specific bearing tree they belong to, core task is the apple tree identification and localization. In aerial remote sensing, each image samples a specific area namely the projection area. There are two routes for allocating trees on the field to each image collected by UAVs. One is directly detecting objects in the image by applying

segmentation and detection approaches. While the other is derived from geographic calculation using multi-source data. Yet trees in modern high-density orchards are interlacing and touching each other which induce serious canopy overlapping issue in 2D images, especially during the harvesting period. Therefore, geographic calculation is potential to be a better solution to geo-reference fruit trees in UAV images.

The apple assignment model proposed consists of five steps (Fig. 5.7). Firstly, to create a real-world reference, GPS coordinates of all the trees in the orchard were predicted based on the measured positions of trees located at the four corners of the orchard. Next, GPS coordinates of image-projected area corners are calculated using the raw image and metadata. With these first two steps, the trees within the projected area are identified. Third, all the pixels in the image were registered in the real-world coordinate using a coordinate conversion method proposed in this study. Based on the output of Step 3 and coordinates of the trees that are covered by the image (in the projected area), image pixels that can represent these covered trees are recognized. Thus coordinates of these pixels in the original image denote tree positions estimated in the image (Step 4). Finally, detected apples were assigned to individual trees employing the predicted tree positions.

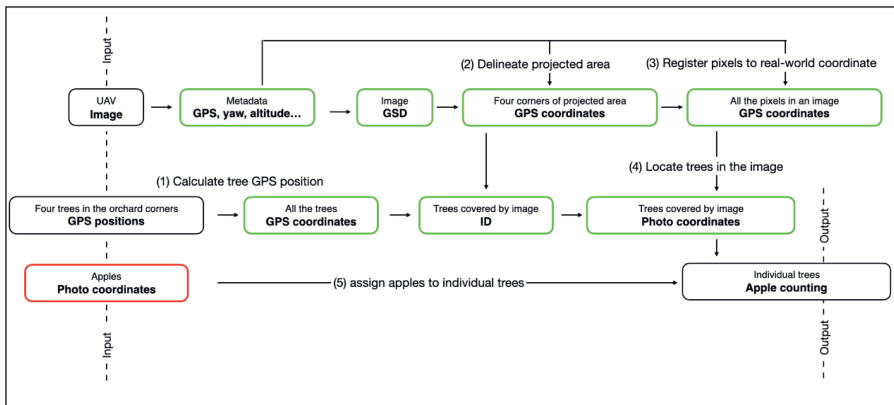


Fig. 5.7. Framework of the proposed apple assignment model. Color of the box borderline is consistent with Fig. 5.3. Box with red borderline: output from apple detection model; boxes with green borderline: data used and produced in the apple assignment model.

5.3.2.1. Calculate tree GPS coordinates

Calculation of tree GPS positions across the whole orchard is a pre-processing step. This inventory is built on the basis of four pre-measured tree positions, as the red points shown in Fig. 5.8. Given GPS positions of two points on the earth, the position of an intermediate point in between at any fraction can

be calculated. These points are along the great circle path where the distance between two points along this path is the shortest over the earth surface. Topographic changes between the two given points are ignored. Since the survey site in this study is a small orchard, only 0.47ha, this theory is applicable.

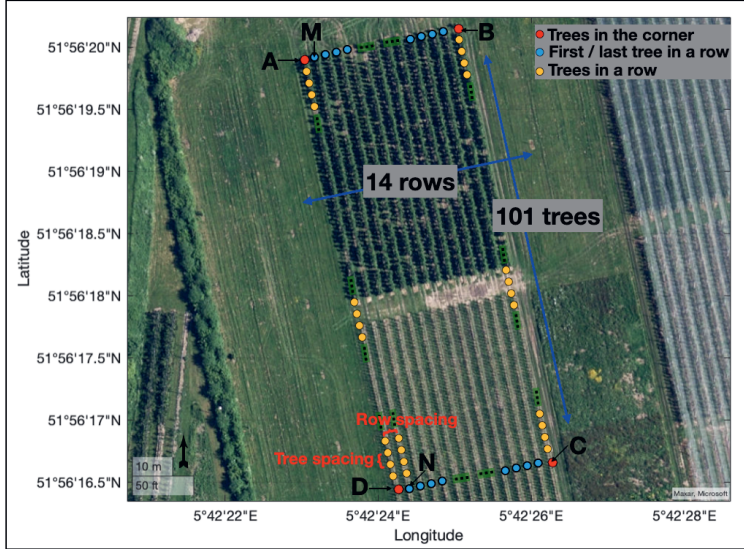


Fig. 5. 8. Illustration for the calculation of intermediate tree positions. A, B, C and D are the trees locate at upper left, upper right, bottom right and bottom left of the orchard, respectively, based on the ground truth data. M and N represent the last tree and the first tree (count from bottom to top) in row 2 (count from West to East), respectively. The satellite basemap is a tiled data set created using Natural Earth.

Given two points m and n (Fig. 5.8), formulations to calculate an intermediate point GPS position were the following:

$$\begin{aligned}
 a &= \sin((1-f) * \delta) / \sin \delta \\
 b &= \sin(f * \delta) / \sin \delta \\
 x &= a * \cos \varphi_1 * \cos \lambda_1 + b * \cos \varphi_2 * \cos \lambda_2 \\
 y &= a * \cos \varphi_1 * \sin \lambda_1 + b * \cos \varphi_2 * \sin \lambda_2 \\
 z &= a * \sin \varphi_1 + b * \sin \varphi_2 \\
 \varphi_i &= \text{atan2}(z, \sqrt{x^2 + y^2}) \\
 \lambda_i &= \text{atan2}(y, x)
 \end{aligned} \tag{1}$$

Where φ_1 and λ_1 is the latitude and longitude of point m; φ_2 and λ_2 is the latitude and longitude of point n; φ_i and λ_i is the latitude and longitude of an intermediate point n; δ is the angular distance d/R

(earth mean radius: 6371 km), f is the fraction (when $f = 0$, it is point m ; when $f = 1$, it is point n). It is based on a spherical earth model where ellipsoidal effects are ignored.

As introduced in section 2.1, 1414 apple trees were planted evenly in 14 rows where each row grows 101 trees. A fixed tree and row spacing was adopted. Based on the intermediate point calculation (Eq.1), GPS positions of the first and last trees (count from South to North) in the 14 rows (the blue points in Fig. 5.8) were determined first. The fraction was set to 13 for the calculation of both the first-tree and last-tree positions. For example, positions of the first trees were calculated based on pre-measured positions of tree C and D (Fig. 5.8). Next, intermediate tree positions (the yellow points in Fig. 5.8) in a row were estimated based on the pre-calculated tree positions of the first and last tree in the corresponding row. Here the fraction value was 100. Finally an inventory of GPS positions of all the apple trees in the orchard was created for further analysis.

5.3.2.2. Delineate image-projected area

To estimate GPS positions of each single pixel in an aerial image, the first step is to delineate the corresponding projection area. In particular, identification of the four corner points of the projection area is the key. A diagram describing the projection of an aerial image is shown in Fig. 5.9. where both the photo corners and image center pixel corresponding to projection area corners and center point on the plane of the ground, respectively. The GPS position stored in the raw image metadata is assumed to be the position of the center pixel, OI . According to GSD of the image, the length and width of the projection area are obtained. The distance of any projection area corners that travel from center O can also be calculated using geometric mathematics.

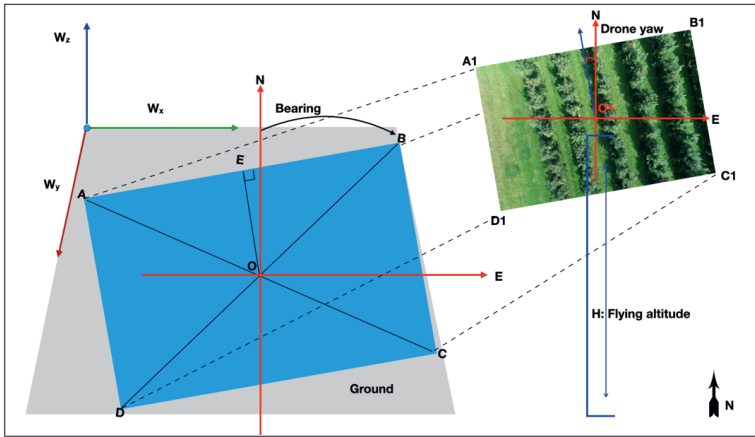


Fig. 5. 9. Illustration of calculating GPS coordinates of the four image-corners (A_1 , B_1 , C_1 and D_1). O_1 represents the center of the UAV image. Blue area is the projection area of the image. Four corners of the projection area are marked as A, B, C and D. O is the center. Line OE is perpendicular to line AB. W_x , W_y and W_z indicate the world (GPS) coordinates.

A bearing is the horizontal direction from or to a specific point which is usually measured by a clockwise angle from magnetic North (true North). For example, angle NOB is the bearing of point B that travels from point O (Fig. 5.9). Given the drone yaw that indicates angle EON , any bearing of the projection area corners can be calculated. Further, with a bearing and distance that a point travels from the center O along great-circle route on the ground plane, GPS positions of the projection area corners can be calculated by formulas as follows:

$$\begin{aligned} \varphi_2 &= \text{asin}(\sin\varphi_1 * \cos\delta + \cos\varphi_1 * \sin\delta * \cos\theta) \\ \lambda_2 &= \lambda_1 + \text{atan2}(\sin\theta * \sin\delta * \cos\varphi_1, \cos\delta - \sin\varphi_1 * \sin\varphi_2) \end{aligned} \quad (2)$$

Where φ is latitude, λ is longitude, θ is the bearing (clockwise from the North), δ is the angular distance.

5.3.2.3. Register image pixels to the real-world coordinate

Each pixel in an aerial image corresponds to a specific area cell in the projection area. Size of the area cell depends on GSD of the image. High GSD produces large area-cells for each image pixel. Derived from this, each single image pixel can be associated with a specific point in the real-world coordinate (W_x , W_y and W_z). This strict one-to-one relationship is demonstrated in Fig. 5.10, where the white points are image pixels and purple points are the corresponding points on the ground plane. When the

projection area is arranged in a 2-dimensional grid ($W \times H$ units) with the same resolution as the image ($W_1 \times H_1$ units), GPS position of any points on the projection area grid is representative of a specific image pixel. Thus the photo-coordinate of a pixel M_1 (I_x, I_y) can be converted to a real-world coordinate M (W_x, W_y), and vice versa.

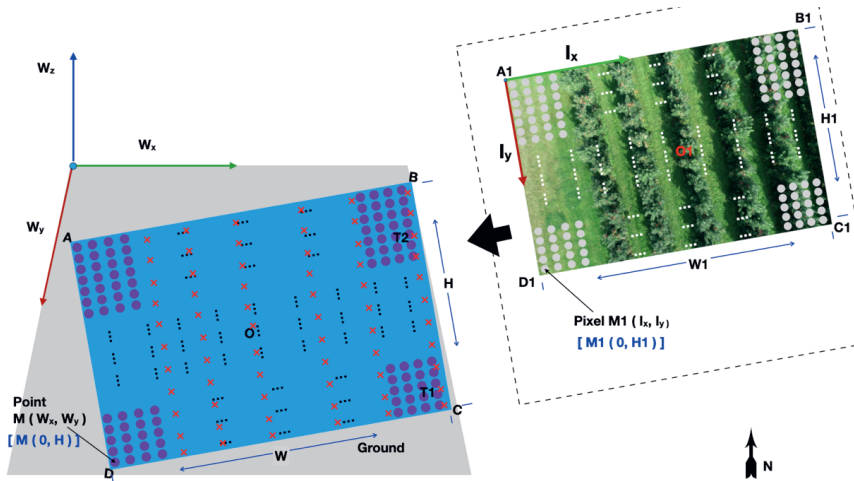


Fig. 5. 10. Illustration of converting pixel coordinates to GPS coordinates. Blue area ABCD is the projection area of a UAV image, with a width of W units and with a height of H units. O is the center. Grey points are image pixels. Purple points are the corresponding points of image pixels. Red cross represents trees within the projection area. M is the first point (count from bottom to top) in row 1 (count from West to East). W_x , W_y and W_z are the world coordinates. O_1 is the center of image $A_1B_1C_1D_1$. Image width is W_1 units and height is H_1 units. M_1 is a pixel in the photo coordinates of I_x and I_y .

GPS coordinates of the four projection area corners are pre-calculated in section 3.2.2. Thus GPS coordinates of other points on the projection area grid can be calculated using the same method introduced in section 3.2.1. Positions of the intermediate points lying on the side AB and DC were calculated first (Eq.1). The fraction value was set to $W-1$ for both sides (Fig. 5.10). Similarly, the positions of other points in the projection area were calculated based on positions of points on the sides AB and DC . The fraction was $H-1$.

5.3.2.4. Locate trees in the image

Given that GPS coordinate of any intersection points on the projection area grid can be converted to photo-coordinate position, as introduced in section 3.2.3, apple trees that are covered by the projection area (captured in the image) can be identified and localized in the corresponding image by comparing the known tree GPS positions with the grid intersection point positions. Positions of all the trees in the

orchard were recorded from section 3.2.1. Some trees can locate exactly on the intersection points of the projection area grid, then the photo-coordinate positions of the trees can be identified directly using the strict one-to-one relationship shown in Fig. 5.10. However the probability is small. Normally, pre-estimated positions of the trees in the orchard are among intersection points of the projection area grid, as points T1 and T2 shown in Fig. 5.10. For this reason, representatives of these trees need to be selected from the grid intersection points to present the real tree positions. To search representatives for trees that are covered by an image, the nearest points to these trees were queried from the intersection points. These nearest or closest points were measured in Euclidean distance. Then corresponding tree positions in the photo-coordinate were determined in an indirect way when the tree representatives are recognized.

5.3.2.5. Assign apples to individual trees

Apple assignment was conducted in the photo-coordinate space (I_x, I_y). A diagram of this process is shown in Fig. 5.11. It is assumed that apple trees in the image share the same canopy size and that a complete canopy area can be covered by a rectangle. Thus, with the help of the identified tree positions, the main task of apple assignment is delineation of the canopy areas. Specifically, it is to calculate the width (W) and height (H) of the small rectangle. Given that there are M trees in a row, the H of the small rectangle can be measured (Fig. 5.11). The first and last trees among the M trees were discarded first. Since it is hard to ensure that complete canopy areas of these two trees are captured by the image. Assuming the tree positions lie on a line through the center of the rectangle and perpendicular to the height line, the H of the small rectangle can be calculated by the following formula:

$$H = (y_2 - y_1)/(M - 3) \quad (3)$$

Where H is height of the small rectangle, y_2 and y_1 are the ordinates of the first and last tree positions (I_x, I_y), respectively (count from bottom to top), M is the total tree number in a row.

To test the feasibility of the apple assignment method proposed in this study, W of the small rectangle and the segment point $P(x_3, 0)$ were measured manually (Fig. 5.11). Further, top-left corner of the last tree canopy area (rectangle area) was identified, $Q(x_3, (y_1 - 0.5 \times H))$. And positions of all the tree canopy areas can be delineated. Finally, detected apples from the apple detection model were assigned to different small rectangle areas that represent individual trees.

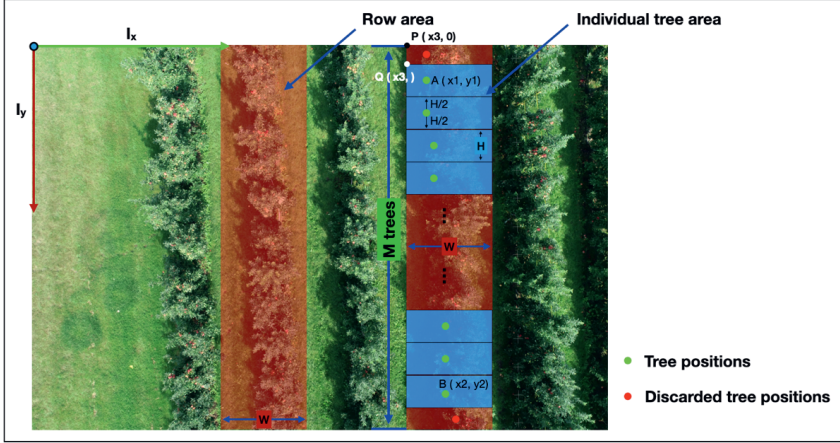


Fig. 5. 11. Illustration of mapping individual tree areas. I_x and I_y represent the photo coordinates. Each tree area is delineated with a blue rectangle. The width and height are W and H units, respectively. Tree area B and A are, respectively, the first and last areas in the same row (count from bottom to top).

5.3.3. Evaluation metrics

5.3.3.1. Apple detection

Three evaluation metrics were used to examine the performance of YOLOv5s in apple detection which comprise *precision*, *recall* and *mAP50*:

$$Precision = \frac{TP}{TP + FP} \tag{4}$$

$$Recall = \frac{TP}{TP + FN} \tag{5}$$

Where TP, FP, FN are true positive, false positive and false negative respectively. When one prediction produced from YOLOv5s holds an IoU that exceeds a defined IoU threshold to its corresponding target box, it is positive, otherwise negative. If the prediction is correct to manual labeling, it is true, otherwise false.

$$AP = \int_0^1 (precision * recall) dr \tag{6}$$

$$mAP = \frac{\sum_{c=1}^n AP_c}{n} \tag{7}$$

Where AP is the average precision which indicates the area below precision-recall curve when precision and recall are regarded as vertical and horizontal axis, respectively. mAP is the mean average precision

indicating the average of AP across various categories, c is a category, and n is the category number. mAP50 is the mAP of predictions that hold IoU greater than 0.5.

5.3.3.2. Apple assignment

The metric to evaluate tree GPS coordinate calculation was shown as follows:

$$\text{Mean relative error (MRE)} = \frac{\sum_{i=1}^n \frac{|y_i - \hat{y}_i|}{y_i}}{n} \quad (8)$$

Where n is the sample size, y_i represents the measured value and \hat{y}_i is the predicted value.

In addition, visual inspection was conducted to judge the quality of tree localization and apple assignment. In the first case, it is important to recognize how far a predicted tree position is to the bottom of the corresponding tree trunk. For apple assignment, the criterion is the integrity of the delineated canopy area.

5.3.3.3. Yield estimation

To verify the performance of proposed yield estimation mechanism, three metrics, R^2 , RMSE and MAE, were used. These metrics have been applied in previous studies (Zhang et al., 2021). Coefficient of determination (R^2) indicates how much of the variance of the dependent variable is explained by the independent variable. RMSE measures the deviation between the observed value and the true value. While MAE describes the actual situation of errors.

5.4. Results

5.4.1. Apple detection model

YOLOv5s was trained on different training sets and corresponding apple detection models were evaluated on the testsets of the three years separately. The different training sets comprise single training sets, i.e., training set 2018 (Table 5.2), and mixed training sets, i.e., the combination of training sets 2018 and 2019. The confidence and IOU thresholds were set to 0.25 and 0.6, respectively. Results showed that, overall, YOLOv5s yielded a similar detection performance for testset 2019 and 2020 while its performance in 2018 was slightly lower (Fig. 5.12). For each testset, the highest mAP50 proceed from models trained on datasets including the corresponding training set. For instance, during the evaluation on testset 2018, models with high accuracy were trained on either the single set of 2018 or mixed sets that including training set 2018, such as model 2018&19. And these models performed similarly. Specifics of models trained on the single-year and mixed training sets were reported in section 4.1.1 and 4.1.2, respectively.

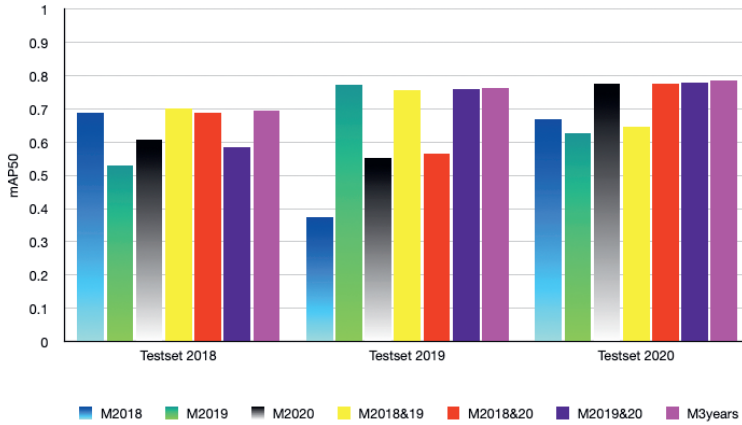


Fig. 5.12. Cross-test performance of YOLOv5s trained on different datasets. M2018 denotes the YOLOv5s model trained on dataset 2018. M3years is the model trained with a combination of datasets from all the three years, 2018, 2019 and 2020. Columns with gradient color indicate models trained with single datasets; normal columns with filled color are models trained with mixed datasets.

5.4.1.1. Apple detection on individual years

Detailed performance of YOLOv5s models trained on single-year datasets is given in Table 5.3. In general, YOLOv5s produced fine apple detection accuracy in aerial images. Its best performance for dataset 2019 and 2020 were similar. While its achievement in 2018 was relatively low where the highest mAP50 was 0.69 (Table 5.3). Model 2018 which was trained on training set 2018 provided similar performance for test set 2018 and 2020. Performance of other two models that were trained on single training set, i.e., M2019, decreased significantly when they were tested on datasets from a different year (Fig. 5.12).

Table 5.3

Cross-test results of the YOLOv5s trained on datasets from a single year.

		Testset 2018	Testset 2019	Testset 2020
Model 2018	Precision	0.707	0.454	0.739
	Recall	0.634	0.344	0.557
	mAP50	0.688	0.375	0.669
Model 2019	Precision	0.612	0.782	0.697
	Recall	0.484	0.694	0.561
	mAP50	0.530	0.774	0.628
Model 2020	Precision	0.701	0.627	0.839
	Recall	0.488	0.448	0.665
	mAP50	0.607	0.553	0.777

Qualitative evaluation indicates that multiple predictions, leaves with yellow-green areas and leaves in dark areas made YOLOv5s produce false positives (FP) in testset 2019 (Fig. 5.13). YOLOv5s performance in detecting green apples on the ground in the dark area was weak when they were tested in the same scenario (Fig. 5.A1). While model 2018 outperformed the other two models in detection of occluded apples in 2019. For dataset 2020, YOLOv5s reported good performance in occluded apple detection (Fig. 5.13). Yet one green apple in a test image from 2020 was undetected by model 2020. Model 2019 showed similar performance as other two models in the detection of red apples on the ground in dark areas (Fig. 5.13). The main FP in data2020 comes from the soil in dark areas. While model 2018 produced more FP with leaves. In testset 2018, model 2018 did not detect the apples on the ground with complete shapes but similar color as the ground. While model 2020 reported poor detections in occluded apples (Fig. 5.13). Leaves are the main FP detections. In addition, predicted bounding box size of model 2019 was bigger than 2018.

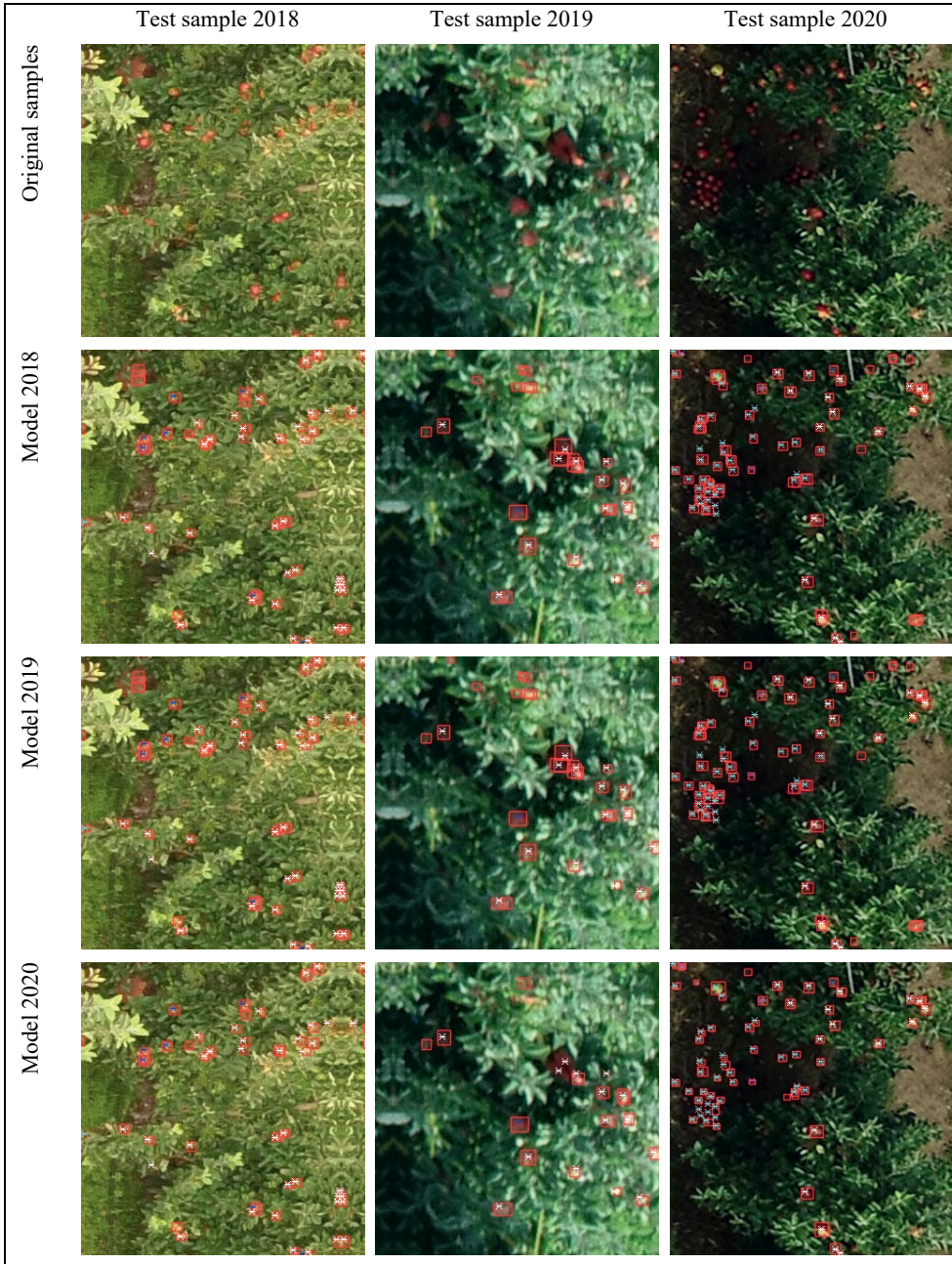


Fig. 5. 13. Apple detection performance of three YOLOv5s against manual annotation in various complex test set scenarios. Model2018: the YOLOv5s trained on dataset 2018. Red bounding box: detection results of YOLOv5s; star marker: manual annotation of the four apple classes. Star markers with blue color: apples; white: occluded apples; cyan: apples on the ground; magenta: difficult class.

5.4.1.2. Apple detection over three years

Performance of models that were trained on a dataset mixed from two years, i.e., Model 18&19, dropped to a certain extent when these models were tested on the dataset from a year not included for training (Table 5.4). As an illustration, model 2018&20 presented a lower accuracy on testset 2019 (mAP50: 0.57) than that on either testset 2018 or 2020. Highest accuracy of model 2018&19 and model 2018&20 was obtained in the evaluation on testset 2019 and 2020, respectively. While Model 2019&20 exhibited a similar achievement for testset 2019 and 2020, with a small mAP50 difference of 0.02. Model 3 years was one of the models that yielded the highest mAP50 for all the three testsets (Fig. 5.12). It showed similar detection performance for testsets 2019 and 2020. But its performance in testset 2018 was slightly lower where the reported mAP50 was 0.69 (Table 5.4).

Table 5.4

Cross-test results of YOLOv5s trained on datasets mixed from two or three years.

		Testset 2018	Testset 2019	Testset 2020
Model 2018 & 2019	Precision	0.733	0.820	0.712
	Recall	0.620	0.644	0.574
	mAP50	0.703	0.758	0.647
Model 2018 & 2020	Precision	0.722	0.570	0.828
	Recall	0.610	0.493	0.671
	mAP50	0.688	0.566	0.776
Model 2019 & 2020	Precision	0.656	0.829	0.818
	Recall	0.524	0.641	0.671
	mAP50	0.584	0.761	0.778
Model 2018 & 2019 & 2020	Precision	0.753	0.804	0.818
	Recall	0.609	0.651	0.679
	mAP50	0.694	0.765	0.785

Qualitative tests reported that the true negatives (TN) in test set 2018 caused by occluded apples decreased when only dataset 2020 was added for training (Fig. 5.14). Another type of TN, apples on the ground, also decreased when one additional training set was included. Models trained on datasets comprising dataset 2020 improved this issue dramatically such as model 2019&20. However, no improvement on this was observed for model 3 years. As FP in test set 2018 derived by multiple predictions, only model 2019&20 was favorable (Fig. 5.14). Model 3 year fixed the FP initiated by yellow-brown leaves. Conversely, model 2018&19 suffered more on this issue. During the test on

dataset 2019, hybrid models 2018&20 and 3 year produced more TN caused by occluded apples (Fig. 5.14). Generally hybrid models reported similar capability for the detection of apples on the ground. And these models endured the same FP as model 2019 such as multiple predictions. Regarding the evaluation on testset 2020, the four hybrid models produced slightly more TN of occluded apples than model 2020. Only model 2018&19 showed improvement on TN derived by apples on the ground (Fig. 5.14). And only it detected the missed green apple from model 2020 accurately. However, model 2018&19 reported more FP than other hybrid models. The FP mainly consists of the leaves and soil in dark areas (Fig. 5.14).

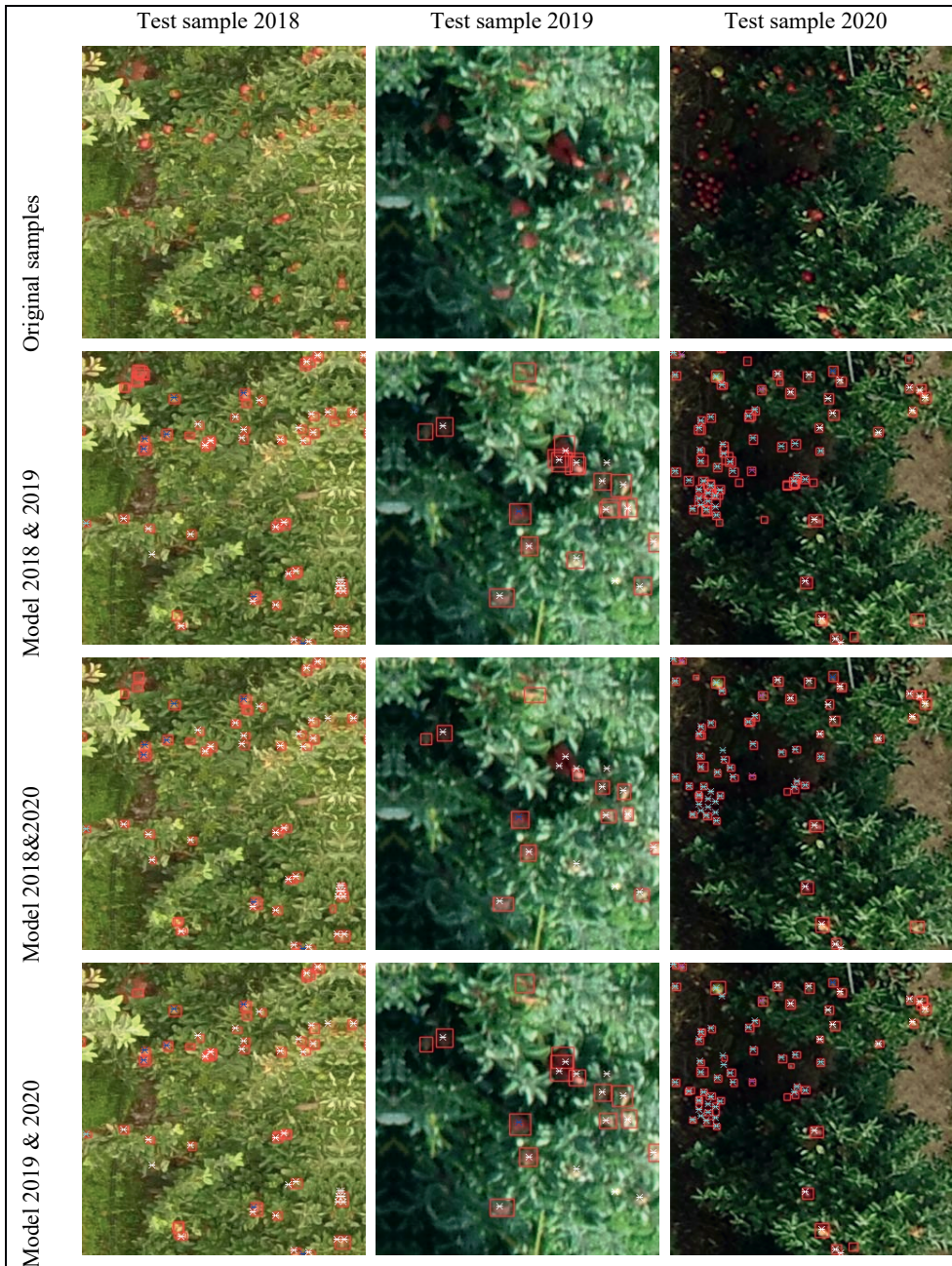




Fig. 5.14. Apple detection performance comparison of four YOLOv5s against manual annotation in various complex testset scenarios. Model 2018&2019: the YOLOv5s trained on datasets mixed from 2018 and 2019. Red bounding box: detection results of YOLOv5s; star marker: manual annotation of the 4 apple classes. Star markers with blue color: apples; white: occluded apples; cyan: apples on the ground; magenta: difficult class.

5.4.2. Apple assignment model

5.4.2.1. Calculate tree GPS position

With GPS positions of four corner trees in the orchard, all the tree coordinates were calculated using the method introduced in section 3.2.1. Prediction results were validated with ground truth, tree positions measured with RTK in the field. 101 trees in row5 were the test samples. High prediction accuracy was observed. The MRE of latitude and longitude predictions were 0.31×10^{-7} and 2.20×10^{-7} , respectively. This matches the fact that the measurement of the ground truth was conducted at the nearest position to the tree root rather than the exact root positions. Thus accuracy of longitude prediction was not as accurate as that of the latitude.

5.4.2.2. Delineate projected area

GPS position of the four corners of a projection area was calculated based on GSD, image GPS position and drone yaw of a corresponding UAV image. To examine the delineation accuracy, visual inspection was conducted by plotting the estimated area data on a satellite base map (Fig. 5.15). Trees that fall into the projection area were manually counted (Fig. 5.15c). The counting was compared against tree number that is visible in the corresponding UAV image (Fig. 5.15b). It yielded a maximum tree counting error of 1 tree per row. Generally speaking, the projection area was delineated precisely for the datasets 2018 and 2019. In the examination of image DJI_0138, only roots of the trees in row6 (count from left to right) are visible in the UAV image, and the exact tree number in this row is impossible to count (Fig. 5.15b). Yet these trees were still recognized in the projection area where the tree number was determined

for 7 (Fig. 5.15c). For the test in dataset 2020, the delineation accuracy was quite low. Produced projection areas even covered one additional tree row completely. Therefore, dataset 2020 was not used for further analysis. Both dataset 2018 and 2019 were used for further apple assignment study. In addition, predicted tree positions locate properly around the center of tree canopy areas (red points in Fig. 5.15c).

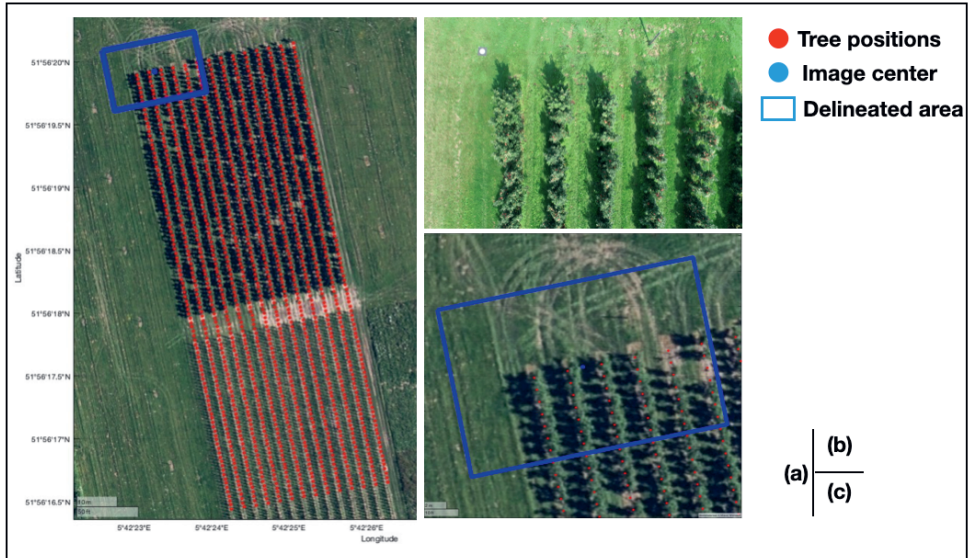


Fig. 5.15. Visualization of the estimated projection area of image DJI_0138 in dataset 2019. (a) estimation results; (b) image DJI_0138; (c) a zoomed-in view of the projection area. Border of the projection area is highlighted in blue. Red circles are the predicted GPS positions of all the trees in the orchard while blue circle is the center of both the image (b) and its corresponding projection area.

5.4.2.3. Locate trees in the image

The estimated projection area was further divided into small partitions to register pixels to real-world coordinates. Firstly, it was divided by using the same resolution of corresponding images. For instance, in the case of dataset 2019 (Table 5.1), the projection area was transformed to a grid with 5472×3648 resolution. This took 30 mins to produce one grid and it also burdened the upcoming computation. Thus the grid resolution was decreased to 2736×1824 for dataset 2019. It decreased two times for dataset 2018 as well. The computation time decreased to approximate 1min per image for both 2018 and 2019. Next, the estimated tree position in image-coordinate was increased two times for tree localization. Results suggested that, in general, for the images filled with trees, around 95 trees were recognized per image for dataset 2019. While the amount for dataset 2018 was approximately 135 trees per image.

Visual inspection was applied to evaluate the tree localization accuracy. Ideally, the estimated tree positions should be around the center of the canopy area or the root positions in the areas with a nadir view. However, it is challenging to make the inspection for the apple dataset 2018 and 2019. Because tree branches closely connect to adjacent trees and the leaves are heavily occluded (Fig. 5.15b). Hence, an apple flower dataset from a previous study (Zhang et al., 2023) was used to assist the validation. The dataset was collected by Phantom 4 RTK, in the same orchard as this study. It was during flowering period, the tree trunk was visible for majority of trees in the image. Tree localization in the flowering image shows good accuracy (Fig. 5.16). First, the tree number within the image was predicted accurately. Next, the relative position of the predicted tree position to canopy area or tree root shows spatial diversity across the whole image. Some predicted positions are slightly upper to the roots but lower than the center of the canopy area (Fig. 5.16a). Some predictions are located right at the root positions (Fig. 5.16d). Details of this distribution pattern were summarized (Table 5.5). From bottom to top part of the image, the distance between predicted tree positions and canopy center decreased first, then increased till the end. The cases that these two positions overlap happened at the upper part of the image. Regarding the relative position to the roots, the predictions locate lower in the vertical direction. This pattern shows across the whole image. On the contrary, these two positions overlap at bottom part. The ideal situation happened in the middle area of the image where the predictions locate right at the root and canopy center (area 2 (A2), A5 and A8 in Fig. 5.16).

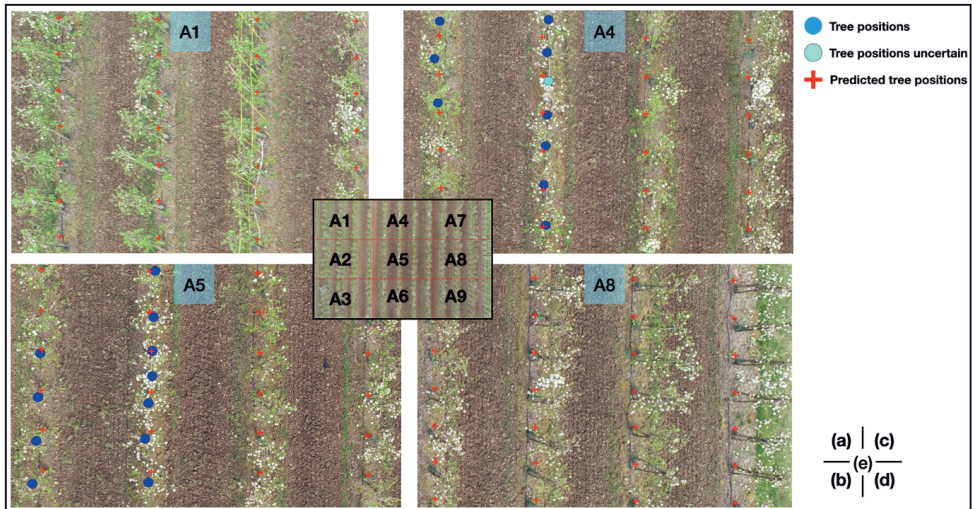


Fig. 5.16. Predicted tree positions in the image DJI_0038 in flower dataset 2020. Red plus symbols represent the estimated tree positions. Blue circles are manually identified tree positions (canopy center); cyan circles are the visual identification not sure. A1: area 1.

Table 5.5

Summary of the canopy area and root relative positions in the apple flower image taking the predicted tree positions as a reference. ‘↔’ indicates the same vertical position; ‘↑’ and ‘↓’ denote upper and lower vertical positions, respectively. The 9 cells of either canopy area or root distribution correspond to the 9 divisions in Fig. 5.16e one by one.

Canopy area distribution			Root distribution		
↑	↑, ↔	↑, ↔	↓	↔	↓
↓, ↔	↓, ↔	↓, ↔	↓, ↔	↔	↓, ↔
↓	↓	↓	↓, ↔	↔	↓, ↔

5.4.2.4. Assign apples to individual trees

Assignment of apples to individual trees is the only procedure that involves manual efforts in this study. Tree areas were identified by drawing rectangles with a fixed size. Detected apples from YOLOv5s that fall into a specific tree area are assigned to the corresponding trees. To evaluate the assignment performance, visual inspection was conducted by checking the integrity of trees in the rectangle areas. The assignment shows spatial diversity over the images in both 2018 and 2019 (Fig. 5.17). Trees located at the top (Fig. 5.17a and c) or bottom part (Fig. 5.17 b and d) of a row were segmented poorly. Only one or two trees close to the center area are recognized properly (Fig. 5.17b). Because of the heavy occlusion of tree branches and leaves, in some cases, it is impossible to tell the relative position of the predicted tree positions to the tree root or canopy area. Some trees leaning to the adjacent trees because of over fruit load (Fig. 5.17c). This make their canopy area center deviates from the root and further affect the tree area identification. Moreover, it is observed that some first and last trees (count from bottom to top) are not covered completely in the images. In general, trees were localized better in dataset 2018 than 2019. In 2019, trees situate at left area of the image (A1, A2 and A3) are not properly localized. The predictions are far from the potential root positions in the corresponding row (Fig. 5.17e). While in 2018, this distance is smaller (Fig. 5.17f).

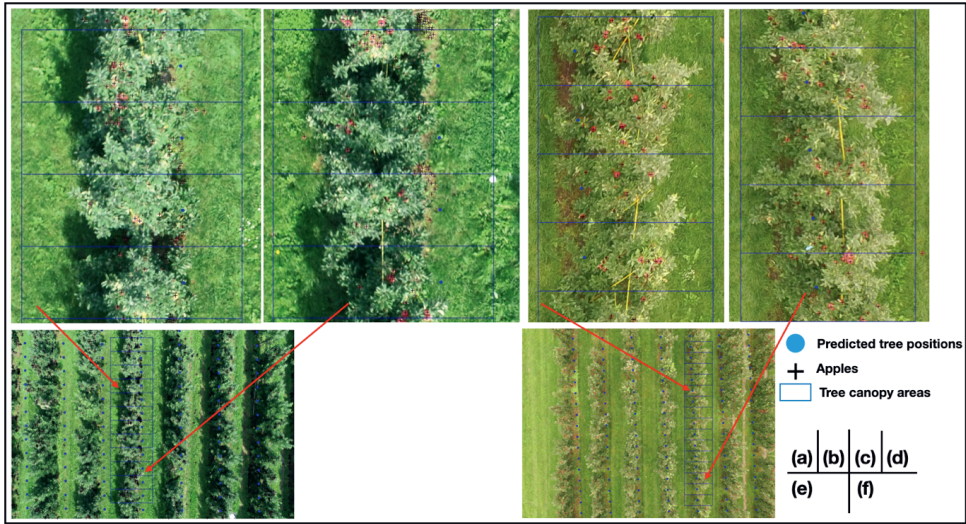


Fig. 5. 17. Apple assignment for the trees in row 5 in dataset 2018 (f) and 2019 (e). Upper (a and c) and lower parts (b and d) of the assignment are zoomed in. Black plus symbols are the detected apples derived from YOLOv5s; blue circles are the predicted tree positions; blue rectangles represent predicted individual tree areas.

5.4.3. Yield estimation

Ground truth was only recorded for row5 in the orchard. Therefore, two images encompassing nadir view of this row were randomly selected for yield estimation. Horizontally, trees in row5 situate in the middle area of the selected images (Fig. 5.17). On the basis of proposed manual tree area delineation derived apple assignment, no correlation was recognized between the visible apple amount in images and the exact apple yield recorded in the field (Fig. 5.18). Regarding the manual annotation as a benchmark, its correlation against the ground truth was first tested. No correlations were observed for both the annotations including and excluding apples on the ground. Apple detection models M2018 and M2019, which were trained on only dataset 2018 and 2019, respectively, yielded high detection accuracy (Fig. 5.12). They were selected for yield estimation and the confidence and IOU thresholds were set to 0.25 and 0.6, respectively. Detected apples from YOLOv5s comprise the apples on the ground. Results showed no correlation against the ground truth of row5 either. Yet, in the dataset 2018, YOLOv5s detections yielded an R^2 of 0.86 against manual annotation excluding apples on the ground and 0.88 to the annotation including apples on the ground (Fig. 5.18a). In the case study of 2019, its correlation against manual annotation including and excluding apples on the ground is 0.56 and 0.29 (R^2), respectively (Fig. 5.18b). In addition, for apple detection of row5 in the two selected images, it was observed that detection performance in 2018 was better than 2019. Main error emanated from

image 2019 is the misdetection of leaves. High illumination level existing in image 2019 induces leaves partly bright, and causes the model to misjudge these bright areas as apples.

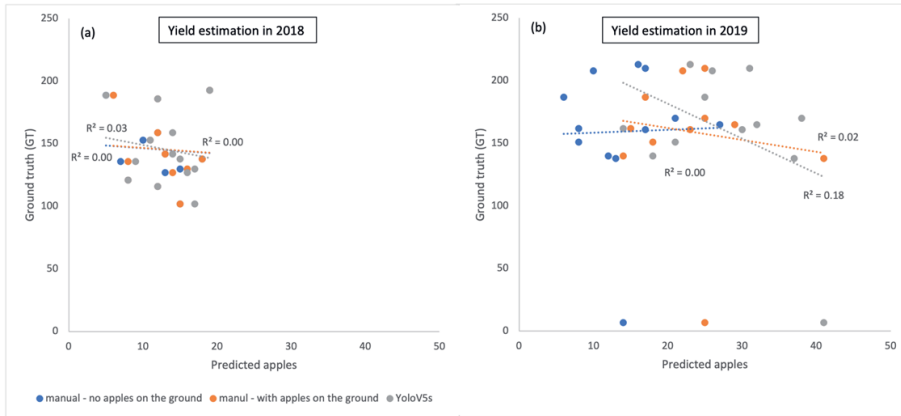


Fig. 5.18. Comparison of relationships between YOLOv5s apple counting and manual annotation per tree against in situ ground truth (GT) in 2018 (a) and 2019 (b). Samples are the trees in row5 that are covered in image DJI_0482, in the year 2018 (a) (N=13) and image DJI_0117, in the year 2019 (b) (N=12). Grey points show the correlation of YOLOv5s -based; orange and blue points show manual annotation with apples on the ground and without, respectively.

5.5. Discussion

5.5.1. Apple detection in single years

YOLOv5s was found to be proficient in the detection of small apple objects in aerial images. Its performance was tested with temporal UAV apple datasets across three consecutive years (Fig. 5.12). The baseline accuracy ranged from 0.69 to 0.78 (mAP50) which was similar to previous demonstration of YOLOv5s for litch late-autumn shoots detection (Liang et al., 2023). Highest detection accuracy in 2018 was slightly lower than the best results from other two years (Table 5.3). One reason is the contribution of apples on the ground. As seen in figure 5, this class of apples maintains a relatively complete shape feature which is easier to identify. While it only held approximate 10 percent of the whole dataset of 2018 which is much less than other two datasets (Fig. 5.6). Surprisingly, dataset 2020 comprises three times more labels than other years (Table 5.2) yet, its best test result was similar to 2019 (Fig. 5.12). It indicates that 5,515 original labels with no data enhancement are sufficiently large for the training of YOLOv5s (Table 5.2). The predefined four classes, apples, apples on the ground, occluded apples and difficult, were designed to fully understand the performance of YOLOv5s (Fig. 5.5). Thus the imbalanced distribution of these classes is acceptable. For the prediction of final yield, there is no need to conduct apple class classification. Yet, to quantify the effects of apples on the ground,

a test is encouraged where images and instances per class are well prepared. Model 2018 outperformed other two models in the detection of occluded apples (Fig. 5.13). Because dataset 2018 comprises the highest percentage of occluded apples (Fig. 5.6). Similarly, less instances of green apples and apples in relatively dark area within the tree structure made YOLOv5s produce poor detections in these two cases (Fig. 5.13). Including more instances for model training can be a solution.

Illumination verified to be the main challenge for YOLOv5s in detecting apples in UAV images. Generally, dataset 2019 suffers more illumination effects than other two datasets (Fig. 5.13). This justifies that the model 2018, which was trained on dataset 2018 only, yielded comparable performance for test sets 2018 and 2020 (Fig. 5.12). Because datasets 2018 and 2020 shared similar illumination conditions. Cross-test results showed that dataset 2019 suffers more from the issue of multiple predictions (Fig. 5.13). It highlights the illumination influence once again. Since uneven illumination produced more predictions with lower confidence. Setting optimal thresholds for confidence and IOU can mitigate this problem. Yet it affects the development of a generalized model for apple detection. Additionally, in dataset 2019, sunlight passes through the gaps in the tree leaves and branches and forms bright areas of various shapes in the shadow areas on the ground. These bright areas were very close to apples with light green or yellow color and produced more FPs.

Tree leaves in 2018 had abnormal colors ranging from light green to yellow even brown (Fig. 5.13). These colors are similar to apples that are not fully mature. Once these leaves are captured within dark areas at the anti-sunshine side or in the deeper internal structure of trees, they can form regular ellipses at their surfaces and interfere with the detection performance of deep learning algorithms, resulting in false positive predictions (Fig. 5.13). The unnormal color of leaves can be caused by fireblight disease or iron deficiency (Zhang et al., 2021). Thus one way to fix this is to utilize regular management. While the other solution is to apply an advanced modification strategy for YOLOv5s.

Annotation is one challenge in extreme small object detection owing to its high requirement for image quality and manual efforts. In the present study, it proceeds from two aspects: judging if an object is an apple and counting how many apples exactly fit in one apple cluster (Fig. 5.14). It is hard to guarantee that the space between apples and their bounding boxes is close to zero and that no apples were missing a label. The latter affects label consistency. Thus overall label accuracy is tough to ensure. Most studies utilized hand-held or ground vehicle-derived datasets which are beneficial in image resolution (Huang et al., 2022). Though a few studies used UAV for image acquisition, yet, the generated images are not real remote sensing images and are not representative. Since the UAVs were manually deployed to either proximal imaging, which is nearly static imaging (Zhang et al., 2022d), or low-altitude sensing (less than 9m altitude) (Liang et al., 2023) (Li et al., 2023b). They highly bank on manual interference and are not suitable for automatic monitoring on the whole orchard scale. Ultimately, in comparison

with the present study, better results of YOLOv5s baseline model demonstrated from studies employed these data collection strategies are explained (Huang et al., 2022; Li et al., 2023b).

5.5.2. Apple detection crosses three years

UAV imagery is beneficial in the development of a robust generalized detector in horticulture. Obtained results indicate that one UAV flight can produce sufficient scale variation for building up the dataset of apples enduring different degrees of occlusion (Fig. 5.14). As a single image already captures fruits under various conditions (Fig. 5.4), with the aid of complex tree structures and orchard circumstances (Li et al., 2023b). This ensures the richness of training sets and further improve the model capability in detecting new cases. Therefore, it clarifies the similar performance derived from model 2018 on test sets 2018 and 2020 (Fig. 5.12). It is anticipated that two UAV datasets embracing both cloudy and sunny illumination conditions are adequate for developing a generalized apple detector (Li et al., 2023b). As an illustration, model 2018&19 generated a similar performance within the test on dataset 2018 and 2020 (Fig. 5.12), where the difference was only 0.06 (mAP50) (Table 5.4). Since datasets 2018 and 2020 shared similar illumination conditions. Thus, though model 3-years was found to be the most powerful for apple detections across three years (Fig. 5.12), training YOLOv5s with two-year datasets is sufficient. Moreover, a generalized model is also affected by various orchard management strategies (Zhang et al., 2021). For instance, irregular management of the apples on the ground induces the model a poor performance in the detection of other apple classes, i.e., occluded apples. The poor performance of model 2019&20 on test set 2018 also proved this, as against its accuracy yielded from test sets 2019 and 2020 (Fig. 5.12). Because the majority of TNs was occluded apple (Fig. 5.14), and the dominant class in dataset 2020 is apples on the ground (Fig. 5.6).

5.5.3. Apple assignment

5.5.3.1. Calculate tree GPS position

The accuracy of tree GPS position calculation is almost perfect (Fig. 5.15). Since tree branches make RTK measurement at the exact root position impossible, the GT of tree GPS positions itself includes errors. The errors are 30 to 40 cm (distance between the real measurement position and root). This explains the deviation observed in longitude prediction. The tree rows were planted from South to North. Thus the errors in the GT do not affect the prediction accuracy of latitude. The good results from tree GPS position calculation provide a reliable reference or tree position inventory for assisting tree localization in the image coordinate system. It also shows an efficient way to map tree positions in modern orchards, where a strict and precise layout is designed for tree positions.

5.5.3.2. Delineate projected area

Regarding the drone yaw value stored in image metadata as the image bearing, the proposed method shows good performance in the delineation of areas projected by UAV images of 2018 and 2019 (Fig. 5.15). It also proves that assuming image GPS to be the position of the center pixel in the image is correct. Delineation accuracy in dataset 2020 was very poor, as mentioned in section 4.2.2. One main reason is the UAV platform difference (Table 5.1). Cameras of Phantom 3 pro and 4 RTK were almost at the same horizontal position with the drone gravity. This meets the prerequisites of the method proposed in this study (image GPS can be the position of the image center pixel). However, the camera equipped on M210 is far from the drone gravity which makes the calculation of projection area corners inaccurate. To fix this problem, an image GPS converter should be developed to eliminate errors caused by camera position. Another option is to determine the right pixel in the image which can represent the camera position in the real-world when the image was captured. Additionally, as seen in Fig. 5.15b, trees in some areas are closely connected which makes it hard to tell the tree number in original image. This leads to a less reliable accuracy calculation.

5.5.3.3. Locate trees in the image

The proposed tree identification method yielded notably high accuracy in tree amount prediction for aerial images (Fig. 5.16). Localization performance varies from different areas across the images and this regular distribution pattern was demonstrated (Table 5.5). This method benefits various UAV-derived applications, such as tree detection in complex environments (Osco et al., 2020a; Wu et al., 2020b). Predictions could be a reliable reference for improving computer vision-based detection accuracy.

Validation of the proposed tree localization method on an apple flowering dataset is adequate for the assessment of tree identification performance over ripening period. Apple trees in the same row are interlacing and touching each other where heavy occlusion of leaves and branches is observed (Fig. 5.17). It makes precise validation via visual inspection difficult. With consistent aerial image collection parameters and weather conditions, in theory, knowledge from one case study is transferable to another comparable study. Apart from using datasets from another growing stage, another option can be the dataset collected from a low-density orchard. It can be an orchard with either large tree spacing or the trees bear less leaf occlusion. This guarantees that the canopy area center and the tree roots are visible or evident in the images. Thus the visual inspection is precise.

Weather conditions have much less effect on the proposed tree localization method. Since the proposed method was based on geographic calculation instead of conventional object detections in images. Potential tree identification errors in this study could come from four aspects: differences among the

system design of UAVs (Table 5.1), projection area resolution, GSD and flying altitude. UAV system design directly affects the identification of a representative pixel of the GPS coordinate stored in the geotagged image metadata, as discussed in section 5.3.2. Thus the accuracy of both projection area delineation and tree localization was influenced. The second error type for tree localization arises from the projection area resolution. Present results were derived from the resolution that was half of the aerial image resolution. It increased the distance between representative points and tree positions in the real world. Thus tree positions were migrated a short distance in the images. Keeping the same resolution as the image significantly affects computational cost. Yet building a projection area grid with high resolution can improve localization accuracy. In the case that accuracy matters, a resolution higher than that of the image can produce precise projection, thus it is recommended. In this study, the utilized resolution was sufficient since it provided a proper reference for the delineation of tree areas.

Tree localization performance in dataset 2018 was better than 2019 (Fig. 5.17e and f). One potential reason is that larger GSD leads to higher accuracy. The GSD of 2019 (0.41 cm/pixel) is much smaller than that of 2018 (0.64 cm/pixel) (Table 5.1). While the GSD of flower dataset 2020 is 0.69 cm/pixel. This justifies the extremely good localization in flower dataset (Fig. 5.16) though a small GSD difference was observed between flower dataset 2020 and apple dataset 2018. Yet it is hard to make precise inspection in dataset 2018 due to heavy tree branch occlusion. To further validate it, a systematic field campaign design is encouraged for comparison in different GSDs that are derived from different flying altitudes. The timing should be spring or early summer when trees are not bearing leaves too much. Another reason can be the flying altitude itself rather than GSD value. Flower dataset 2020 applied a flying altitude of 25m which is much higher than those of apple dataset 2018 and 2019 (Table 5.1). Higher flying altitude can enhance the calculation accuracy of the four projection area corners. Thus the consequent tree localization accuracy is also improved. In addition, higher flying altitudes suffer less tree structural overlapping (Zhang et al., 2023) in the image and produce more trees with an independent view. It has potential to improve the final yield estimation accuracy. However, disadvantage is the resultant effects on apple detection. To tackle this, advance algorithm that is capable of detecting smaller objects derived from high-altitude aerial images needs to be developed. For certain cases, the altitude-derived trade-off between tree localization and fruit detection accuracy requires more attention.

5.5.4. Yield estimation

No correlation was observed between apple detections from YOLOv5s and the ground truth of row 5 in the orchard (Fig. 5.18). Manual annotation is supposed to be reliable for the estimation of visible apples in the images. However, it showed no correlation to the ground truth either using the proposed

apple assignment method. Errors originate in two aspects: apple detection accuracy and apple assignment performance. Obtained low correlation of YOLOv5s derived apple detections against manual annotation in 2019 verified the influence of illumination on apple detection one more time (Fig. 5.18b). In yield estimation of 2018, high correlation was received between YOLOv5s derived apple detections and manual annotation for trees in row 5 ($R^2 > 0.86$). And fine apple detection performance was already demonstrated (Fig. 5.12). Therefore the main error arises from the apple assignment.

In principle, the proposed apple assignment method is operable for the delineation of tree canopy area with a nadir-view (Fig. 5.16b) or the case that the canopy area center locates at the same vertical position as the roots (Fig. 5.16d). Though UAV images assembled in this study were under a camera setting of -90 gimbal pitch, the majority of trees in the images are not within nadir-view. For instance, only area A5 covers trees with a nadir-view (Fig. 5.16). While trees in other areas stand in a side-view. Trees locate at upper (A1, A4 and A7) and lower (A3, A6 and A9) part of the image are inappropriate for yield estimation. Because they suffer either vertical (nadir) or horizontal (angular) overlapping in the images (Zhang et al., 2023). In certain cases, trees also occluded each other making detected apples unassignable. Thus proposed apple assignment method was proven to be applicable only to a certain area in an aerial image. But the optimal area position in the image is fixed when flying parameters are consistent. In relation to yield estimation for an entire row, as expected, low correlation of the visible apples in the image against ground truth can be procured.

Usage of the summarized spatial distribution of canopy view (Table 5.5) depends on specific research focus. In this study, the optimal areas for yield estimation are in the middle of images, A2, A5 and A8 (Fig. 5.16). Because tree canopy areas situate at the same vertical positions as the predicted tree positions among these three areas. More importantly, tree canopy areas are relatively independent where branches occlude each other slightly. It makes the following yield analysis more precise for individual trees. Yet, it is noticed that areas A2 and A8 provide a side-view of the trees while area A5 is a nadir-view. The difference leads to dissimilar yield estimation results. Row5 in image 2018 comprised trees that fall into area A8 (Fig. 5.17f) while row5 in image 2019 contains area A5 (Fig. 5.17e). Thus present yield estimation of 2018 and 2019 is partly based on side-view and nadir-view, respectively. A comparison of these two situations on yield estimation is encouraged in the near future. Obtained results did not prove that side-view yield estimation is better than nadir-view.

The proposed apple assignment method is the only section that required manual efforts. It requires pre-definition of a segment position and the canopy area width. To fully automate the proposed framework, clustering methods are recommended (Zhang et al., 2022b). Optimal yield estimation areas are the same as the proposed apple assignment method. In addition, there is one requirement associated with orchard management to employ the yield estimation framework defined in this study. Crop load of the trees

needs to be supervised properly. It is noticed that trees with heavy fruit load tilt to adjacent trees (Fig. 5.17c). This makes the detected apples originally belong to a tree identified assigned to the adjacent trees which are closer to them in the image coordinate. It can also happen in the optimal area recognized in this study, A5 (Fig. 5.16). It is believed that this requirement is in line with the principle of precision horticulture, especially for the management of modern high-density orchards.

5.6. Conclusions

Present study proposed a novel automatic apple yield estimation mechanism based on single raw UAV RGB images. YOLOv5s was proven to be proficient in the detection of small apples in aerial images. Obtained results revealed that UAV images are beneficial in developing a generalized model due to their unique camera view. Experiments from YOLOv5s on apple detection across three years suggested that two temporal UAV RGB datasets are adequate for a generalized model. Proposed methods for fruit tree identification achieved great accuracy in tree counting. A good localization performance was observed as well. Effects of vertical and horizontal overlapping on the tree crown area delineation accuracy were well discussed. The spatial pattern of predicted tree positions was summarized and indicated the optimal area for single RGB images-based fruit yield estimation. No correlation between apples detected from aerial images and ground truth data was found at tree level. The main reason is the identification of individual tree crown areas. Yet, results showed great potential of proposed tree localization methods in tree-level apple yield estimation.

5.A. Appendix

Fig. 5.A.1 describes cross-test results of YOLOv5s trained on single-year datasets, in the test set 2019.

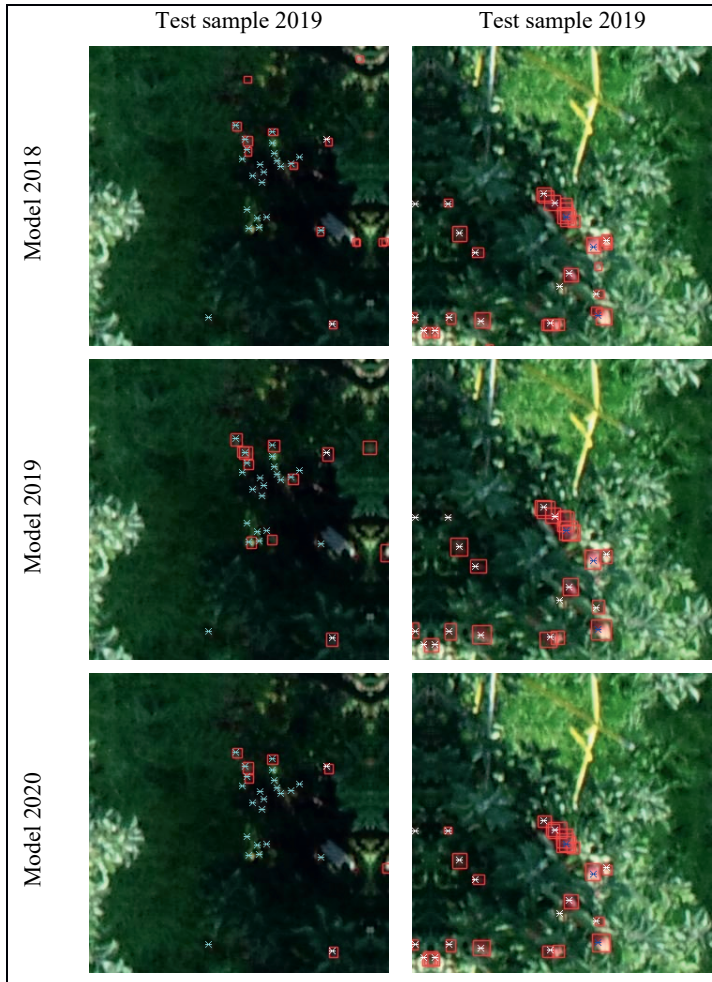


Fig. 5.A.1. Model2018: the YOLOv5s trained on dataset 2018. Red bounding box: detection results of YOLOv5s; star marker: manual annotation of the four apple classes. Star markers with blue color: apples; white: occluded apples; cyan: apples on the ground; magenta: difficult class.

6

Chapter 6

Synthesis

6.1. Main findings

In this thesis, the potential of single raw UAV RGB images in orchard management was evaluated. Its capability in two crop load estimation cases, apple flowering intensity and yield estimation, was tested against conventional benchmarks (methods derived from ground vehicle- and UAV-based color point clouds) using datasets crossing three consecutive years. In this chapter, obtained results from each individual topic are outlined and discussed in parallel with current research (Section 6.1). Next, further reflections including limitations of the present thesis (Section 6.2), challenges and prospects of UAV RGB imagery applied to agricultural applications are summarized (Section 6.3).

6.1.1 What are the research gaps and opportunities of UAV-derived monitoring in orchard management?

UAVs are groundbreaking monitoring platforms that will continue to grow and support orchard management (Chapter 2). The latest research focus, in the first half of 2023, shows a different pattern than earlier years (Zhang et al., 2019a). But this trend is consistent with the previous forecast, at the beginning of 2020, presented in Chapter 2:

- UAVs for resource efficiency management are currently satisfactory (Section 1.4.2). More efforts would need to be shifted to other applications such as yield estimation;
- Likewise, in the case of geometric trait calculation, promising results have been demonstrated by a growing body of literature and the utilized point clouds almost only derived from aerial RGB imagery (Section 1.4.1). However, it was expected that LiDAR point clouds would be the tendency (Dian et al., 2023). LiDAR point clouds would better deal with limitations held by colored point clouds such as the effects of illumination. Moreover, to further improve the performance of 3D representation, more systematic studies focusing on flying parameter optimization were encouraged;
- The urgency of tree-level yield estimation (Tang et al., 2023) and the remarkable strength of deep learning for this observation level (Section 1.4.3). This success has been gained from the advance of state-of-art algorithms such as YOLOv8 and transformers;
- In addition, the fields of disease detection (Choosumrong et al., 2023) (Section 1.4.3), spraying system development and optimization (Qi et al., 2023) (Section 1.4.4) and UAV customization (Alligier et al., 2023) (Section 1.4.4) will tend to grow. The harshness of fruit tree-related disease needs a fast and precise diagnosis. Whilst, innovative UAV-based spraying systems need to be established and optimized.

UAVs supply an efficient site-specific inventory for orchards. With respect to photogrammetry, currently, its GPS accuracy meets the requirement of spatial mapping at site level. Yet the way how it is stored in image metadata should be consistent crossing different models of UAVs, to facilitate tree-

level monitoring (Chapter 5). For example, the GPS recorded in one image captured by one UAV type can be regarded as the center pixel coordinate, which is different from another UAV type (Section 5.5.3.2). Moreover, good GPS accuracy still relies on added ground control points (GCP) and checkpoints which affects UAVs efficiency in terms of operation and data processing. The majority of existing UAV campaigns are semi-autonomous. From this aspect, customized design or development of UAVs should be further improved where advanced obstacle avoidance is integrated (Badrloo et al., 2022). Additionally, though UAV battery capacity enables normal surveys in small or middle-size orchards, it potentially limits UAV performance in real-time data processing. Since integrated data processing modules require additional power sources.

Aerial data acquisition, in comparison with ground-based stationary or mobile sensing platforms, comprises more parameters that affect data quality or final monitoring accuracy. The parameters can be flying altitudes (Chapter 4), camera angle and camera calibration. In other words, fine results obtained from existing studies are feasible under certain data collection strategies. From this facet, systematic fieldwork design involving various flying parameters should be conducted to understand their effects and develop strategies for optimal results (Raman et al., 2023a). From the aspect of environmental conditions, aerial data acquisition suffers from more complex illumination problems which are heterogeneous when covering the whole orchard. On the contrary, ground-based platforms mainly endure two situations: normal sunlight and shadow view. In addition, the situation of surveyed fruit trees and fruit cultivars should also be considered. For instance, different flowering intensity levels affect the UAV-based flower load estimation (Chapter 4). Therefore, to test the uncertainties arising from these factors, multi-flights are compulsory.

Artificial neural networks reform UAV achievements in orchard management. Benefits from advances in the computer vision community, object detection and classification become the most widely used approach in accomplishing orchard monitoring, either in 2D or 3D space (Yu et al., 2022). And the common data source is RGB images. One justification is that UAVs have an advantage in providing sufficient large and diverse datasets in an efficient way (Fig.5.12). The performance of state-of-art algorithms has been demonstrated in the orchard scenario such as YOLOv8 (Ahmed et al., 2023), attention mechanisms (Tang et al., 2023) and transformers (Li et al., 2023b). Even so, modifications to normal-size networks are encouraged rather than focusing on testing the latest deep learning algorithms, such as vision transformers. Since these algorithms usually need to be trained on extremely large datasets where a high computational resource is required. Otherwise, deeper networks cannot be trained properly. For point cloud data, colored or LiDAR-derived point clouds, this intelligent evolution was also gradually observed in orchard management (Yu et al., 2022). The main challenge comes from data annotation. Differing from the adoption of point clouds in building information modeling (BIM) (Yang et al., 2023), fruit trees suffer more complex structures and endure occlusion problems in some cases

(Chapter 3). Regarding data derived from multispectral or hyperspectral sensors, CNN has also been tested within images (Tang et al., 2023). Yet, most methods are still based on conventional spectral analysis.

Considerably more work will need to be done to establish generalized models. As discussed above, multiple flights can usefully produce sufficient large and diverse datasets in supporting model generalization. Yet, it is not recommended to start this with different fruit cultivars due to their high heterogeneity (Chen et al., 2017). By taking the same fruit cultivar, it is believed that datasets with different flying parameters and various weather conditions are sufficient for a well-established generalized model (Fig.4.11). In addition, researchers should be encouraged to share and build up publicly available datasets with a focus on the use of UAVs in orchard management (Zhang et al., 2022c).

6.1.2 How can apple flower load be spatially mapped from UAV-based colored point clouds?

Unstructured point cloud data in 3-dimensional (3D) space is believed to be the optimal alternative for the inspection of crop load on fruit trees. Chapter 3 - addressing flower load estimation at tree level - establishes a complete benchmark for the adoption of colored point clouds-derived methods where both aerial and ground-based platforms were employed. The results obtained revealed that point cloud-derived flower load estimation accuracy was higher than 0.65 (R^2) (Table 3.9). Even so, the present work could be a baseline for assisting ground-based robotics systems applied to automatic apple flower thinning.

Object classifiers or detectors developed from point cloud data structures, in agricultural domains, gradually advance towards intelligent understanding of small objects such as apples (Tsoulias et al., 2023) and wheat heads (Zou et al., 2023). Its accuracy is the main component that dominates the performance of the proposed flower load estimation method using point clouds (Table 3.7). Though the unsupervised machine learning method, hierarchical clustering, was proven to be optimal for apple flower cluster estimation, it was only validated with in-situ ground truth. Given the fact that on-tree flower load suffers heavy occlusion and that point cloud data is irregular and unordered, to a certain degree, obtained results are less well explainable. Since both ground reference data recorded in the field and the manual annotation made within raw point clouds, in agriculture, are indispensable for the validation and development of a robust model. In comparison with other small objects such as apples and oranges, apple flower annotation in 3D space proved challenging. This also makes the geometric features of point cloud data such as the curvature (Tsoulias et al., 2023) unsuitable for point-wise flower detection. Increasing the density of point clouds can be a solution to enhance the recognizability of flower-related points (Raman et al., 2023a). Once manual annotations are available, another clustering

method, DBSCAN (Vanbrabant et al., 2020b), is suggested for tests with presented flower load datasets aiming at further improving the obtained results. In addition, high-density point clouds benefit flower load estimation as well. This was already verified by the flower cluster estimation results that ground-based point clouds outperformed aerial point clouds (Table 3.8). Overall, to generalize the proposed method (Chapter 3) with another apple or stone fruit orchard, the density of point clouds and the in-situ flowering intensity level should be kept in mind.

Apple flower load predicted from color point clouds (Chapter 3) underperformed compared to single RGB images-based methods (Chapter 4). This was proven by the correlation between data-derived flower clusters and the ground reference data. After the successful implementation of flower load estimation with 2-dimensional data (Chapter 4), an alternative solution can be tested for Chapter 3. It is mainly based on a side-view projection of the color point cloud in the X-Y planes, as shown in Fig. 3.10. A dual view of each side of the tree rows should also be applied. It is expected that the detected flower cluster from this 2D side view endure less occlusion issues than that of single RGB images. Since this side view is comparable to ground-based sensing where the vertical (nadir) overlapping magnitude is much lower than aerial side-view imaging (Fig. 4.10b). Its flower load estimation accuracy also has potential to be higher than the aerial solution (Chapter 4) but lower than ground-based sensing approach (Zhou et al., 2023). Because the side view is projected from point clouds which are already digital representatives rather than the surveyed targets in the real world. To further enhance flower detection capability, CNN-based methods can be adopted (Dias et al., 2018a). The quick-shift method (Zou et al., 2023) is not suitable, in the case of apple flower detection, as the points of branches, leaves and flowers are mixed along the Y-axis (Fig. 3.10). Yet, it potentially produces an efficient segmentation of clusters in the vine row due to the special fruit-tree structure (Torres-Sánchez et al., 2021).

Point cloud data is predominant in calculating geometric characteristics for fruit trees (Teng et al., 2023; Zhang et al., 2020a). Main adoption in assisting tree-level flower load monitoring is the segmentation of individual trees: specifically, the completeness of tree segmentation. From this aspect, in 3D space, individual tree segmentation in orchards is proven to be more complex than that in forests, particularly in modern high-density orchards (Vinci et al., 2022). Small tree spacing such as 0.45m (pear trees) (Raman et al., 2023a) and 0.95m (apple trees) (Tsoulias et al., 2023) produces more interlacing branches between trees which retards tree segmentation accuracy and even makes the segmentation of individual trees impossible. One solution is drawing support from unique environmental settings such as sticking poles with distinguishable colors among trees within the same row (Chapter 3). In follow-up, methods such as MSAC can be used to identify the plane that the poles locate in for individual tree segmentation. Yet it is still tough to guarantee the segmented-tree completeness and additional manual efforts are involved for identification of the poles. To automate this method, one alternative is to detect the center position of the tree trunk first (Feng et al., 2022), instead of using the poles. Point clouds of each tree

can be assimilated to a regular 3D geometry such as a cylinder (Vinci et al., 2023) taking the trunk center as the 3D geometry center.

In operational scenarios, colored point clouds reconstructed from UAVs are suitable for peak blooming stage determination rather than assisting flower thinning in orchards. Supporting flower thinning requires high flower load estimation accuracy at tree-level while plot-level or row-level estimation (Vanbrabant et al., 2020b) still lacks quantitative information for the decision of how many flowers needs to be removed for a specific tree. Conversely, in orchards, identification of the peak blooming stage or monitoring flowering dynamics does not hold strict necessity towards this quantitative information (Zhou et al., 2023). Yet, in this case, the utilized point cloud density should be consistent by employing constant flying parameters such as flying height and overlap settings. Otherwise, the established flowering index for monitoring flowering dynamics might be weak. In addition, with the development of flowers, effects of the changes in foliar density on flower detection accuracy should be investigated to ensure flower index robustness. Though the aerial colored point clouds are affected by illumination conditions, LiDAR-derived point clouds could be unfeasible for the classification of stone fruits flowers due to the heavy occlusion of flower clusters. The attribute of reflection intensity in LiDAR point data is capable for the detection of small objects like oranges (Méndez et al., 2019) but shows limitations in small objects with complex structures like flowers (Malambo et al., 2019). As for supporting automatic fruit-picking (Zhao et al., 2020) or flower-thinning robotics, ground-based point clouds are better than aerial ones because of the camera view (Table 3.5). Even so, the data processing efficiency limits its application in real-time scenarios. From this aspect, 2D image-based solutions are expected to be a good solution (Bhattarai et al., 2023).

6.1.3 What is the feasibility of estimating the spatial distribution of flower load in apple orchards with single raw UAV images?

The spatial mapping of flower load in orchards requires crop load estimation at the tree level. High processing workflows can be avoided if the flower estimation is done directly on single UAV images. The spatial distribution of flower load from single RGB images can be estimated at a tree level in two steps: (1) the detection of flower or flower clusters in images and (2) the identification of which tree the detected flower or flower clusters developed from (Vanbrabant et al., 2020a). The proposed framework in Chapter 4 took the second task as the first step and further detected the flower clusters (Fig.4.6). Obtained results indicated its promising temporal monitoring capability in tree-level apple flowering intensity (Fig. 4.11) which outperformed the benchmark based on colored point clouds (Table 3.9) with respect to accuracy and efficiency.

The main motivation was to guarantee that flower cluster estimation could be assessed at a tree level and to further establish fine datasets for the examination of influential structural overlapping, especially horizontal (angular) overlapping. During the first stage of the proposed framework, individual trees were identified manually from the UAV images. To automate this module, advanced deep learning algorithms for tree trunk detection can be alternatives, such as YOLOv8 (Ahmed et al., 2023). Since the crop load, during flowering period, endure less occlusion problem than that in harvesting period, the tree trunk will be visible in aerial images. Yet, it is expected that the trunk detection accuracy for high-occlusion blooming trees would be low, such as the trees in the 2019 image dataset (Fig. 4.3). Moreover, detectors that regard an entire tree as one object are not recommended (Zhao et al., 2023a). Mainly because these detectors still concentrate on the trunk features and it is difficult to properly identify which tree the branches belong to. Though instance segmentation exhibits advantages in the detection of these details (Lucena et al., 2022), the existing body of research is limited to the segmentation of fruits (Li and Chen, 2022) or other objects with simple structures (Mahmud et al., 2023; Mo et al., 2021). Instance segmentation of trees with complex structures in agricultural environments such as orchards is yet being researched (Gibril et al., 2022).

Moreover, the effects of structural overlapping on tree-level crop load estimation are of utmost importance when single aerial RGB images are regarded as the only data source. Preliminary tests show these challenges in determining the flower load estimation on each individual tree (Section 4.4.4). Different flowering indices indicated dissimilar responses to structural overlapping while vertical (nadir) overlapping was proven to have more influence than horizontal overlapping. Later experiments further verified these findings and concluded a general pattern for structural overlapping exists in aerial images (Table 5.5). It is essential to conduct flower load estimation following this pattern, to produce precise estimation of flower clusters. Yet, the optimal image area (Fig.5. 16) for tree-level flower load estimation needs further systematic analysis. Moreover, it is noticed that aerial images captured under the nadir-view cameras provide a real nadir-view of trees only in the image center area. Yet, in comparison with RGB orthomosaics, how well the flower load estimation derived from these center areas is unclear. It is believed that its performance can be similar to or even better than that based on orthomosaics (Tubau Comas et al., 2019). And its main benefit would be efficiency as no conventional time-consuming photogrammetric processing such as SfM is involved.

Color thresholding is sufficient in supporting the extraction of flower features. However its scalability is poor as great limitations to illumination conditions are shown (Vanbrabant et al., 2020a). Given the fact that small objects of flowers suffer heavy occlusion during the peak blooming period, it is impractical to apply advanced deep learning-based object detectors such as Swin Transformer-involved detectors (Zhou et al., 2023). Still promising detection accuracy has been demonstrated in proximal sensing such as handheld smartphones and ground vehicles. The first challenge is small object detection

in aerial imaging where various object sizes, illumination conditions and occlusion levels subsist (Shen et al., 2022). From this aspect, the detector of disentangle your dense object (DDOD) and Cascade R-CNN can be alternatives (K.R et al., 2023). Yet, the detection of on-tree fruit flowers or flower clusters in agricultural environments is believed to be more complicated than the detection of persons and ground vehicles in aerial images. Another challenge is proceeding from image resolution. Higher flying altitudes of UAVs reduce spatial resolution for detection of apple flowers. While inadequate resolution limits data annotation accuracy and further diminishes the performance of deep learning algorithms. However, in case of mapping a specific area, high flying altitude leads to efficient data collection. Lower flying altitude (<10m) threatens drone safety and can require more manual control efforts (Zhang et al., 2022d). In conclusion, a trade-off between flower detection accuracy and data collection efficiency requires to be taken into account for certain applications. Studies focusing on the identification of optimal flying altitude for flower detection in aerial images should be repeated utilizing a systematic experimental design for a specific orchard.

With a fine resolution of aerial RGB images, state-of-the-art algorithms that involve attention mechanisms are prospective to further improve obtained flower cluster estimation accuracy. Such attention networks can be a Gaussian non-local mechanism (Jia et al., 2022) and a SE block (Liu et al., 2021). There are a few ideas that have been proposed to identify the specific flowering periods ranging from flower buds to end-open flowers (Koirala et al., 2020c; Zhou et al., 2023). Such efforts, yet, point at peak blooming time determination and the monitoring over a complete blooming season which benefits breeding program directly and also aids in understanding regional climate dynamics. In this case, flowering intensity quantification is not necessary, characterizing dynamics of image-derived flowering indicator can be sufficient. However, ground truth is highly required for validation. In terms of flowering intensity monitoring, proposed flower floridity calculation can be a more efficient solution. It is projected that its performance can be similar or even better than simply considering flower numbers based on its correlation to manual floridity estimation (Fig. 4.13). Yet, how sensitive the proposed floridity index responds to the seasonal blooming dynamics remains to be elucidated.

6.1.4 How can deep learning-derived spatial apple yield mapping be automated using single raw UAV images?

Like tree-level flower load estimation as presented in Chapter 3 and 4, the spatial mapping of apple fruit load also comprises a combined task of fruit detection and localization (Chapter 5). The localization highlights the task to geolocate detected fruits in real-world coordinates. Though the whole task can be directly accomplished with colored point clouds (Chapter 3) (Zine-El-Abidine et al., 2021) and orthophoto derived from aerial RGB images, the accuracy and efficiency are still not satisfactory. Inspired by the promising results demonstrated in Chapter 4, it was expected that single raw UAV RGB

images were feasible for apple yield prediction at tree level. Yet, the manual efforts entailed in the proposed framework (Section 4.3.1) need to be automated to further enhance its usefulness.

YOLOv5 was proven to be more accurate and robust to detect on-tree apples (Fig. 5.12) than pixel-based object detection methods such as color thresholding utilized in Section 4.3.1.3. Though the segmentation accuracy of flower-related pixels was not provided in Chapter 4, previous studies that used object-based methods, such as YOLOv4 (Yuan et al., 2022) and YOLOv5 (Chen et al., 2022d), for apple flower detection can also prove this. Thus it can be concluded that deep learning algorithms are indispensable to automate the object detection task in single RGB-based crop load estimation, either for apple flowers or fruits. It potentially mitigates the effects of illumination conditions on fruit detection accuracy at certain degree (Fig. 5.14).

Object detection in aerial images, in the case of fruit load estimation, mainly embraces issues from three aspects: various fruit sizes, color and shape (Fig. 5.5). Size variation is attributable to the differences in nutrient absorption by fruits and in the position where the fruits grow such as the canopy bottom and top parts. While the color variation is caused by different apple maturity stages and the effects of the illumination conditions. As the irregularity of apple shape, occlusion derived from leaves, branches and other apples is the main reason. Even so, YOLOv5 showed good performance to take these complexities into account. The results indicated that the majority of false positive predictions came from the effects of illumination conditions (Fig. 5.13) which is also the drawback of RGB cameras (Section 2.3.3). Surprisingly, YOLOv5s models trained with combinations of datasets from different years showed a relatively comparable performance (Fig. 5.12). This revealed that aerial images are advantageous in developing a generalized model. In other words, two UAV datasets can be adequate to cover sufficient data variability (Fig. 5.14). From this aspect, one potential issue can be multi-scale problems produced by datasets that include different flying altitudes. To ease this, adding an additional model like a transformer encoder to the basic YOLOv5 can be an alternative (Li et al., 2023b).

Aerial images enable each pixel in the 2D orthophoto and each point in the 3D space of point clouds to be geolocated. Likewise, it has been tested that each pixel in single raw RGB images can also be geolocated (Chapter 5). This directly automated the tree-level estimation issue presented in Chapter 4. Compared to the currently available fine GPS accuracy in UAVs (Chapter 2), the precision of pitch, yaw and roll values concerning both the gimbal and drone is the dominant factor towards tree localization accuracy using the proposed method (Section 5.3.2). Another factor can be the flying altitude which potentially affects the geographic calculation. To further quantify the effects discussed above and improve tree localization accuracy, a systematic design of the field campaign will be conducted. In addition, the proposed method provides a novel solution for the tree identification task as introduced in Chapter 2 and outstanding results were demonstrated (Fig.5.16). Since no computer vision

technique was included in the proposed tree localization method, it is not limited by weather conditions and is believed to be an efficient solution for real-time monitoring tasks in modern high-density orchards.

The occlusion magnitudes of apple flower and fruit load were different. This explains the low correlation between image-derived apple amount and corresponding ground reference data (Fig.5.18). In three consecutive years, starting from 2018, apple datasets suffer much more occlusion than flowers in the raw images. This visibility issue can be explored by applying different leaf-thinning strategies. It is hard to compare the occlusion issues. One solution is developing an occlusion index to quantify its effects. It can be the percentage of apple- or flower-related pixels to the whole tree pixels. And the flying parameters should be fixed, such as flying altitudes and camera angles. Another factor that affects the yield estimation accuracy can be the apples on the ground. Yet, in operational scenarios, they can be removed by regular management. But it can also help to understand the correlation between flower load and fruit load in the same growing season. It is interesting to conduct this investigation for yield prediction at the early stage, the flowering period. Yet the main factor that challenges the establishment of this model is the uncertainties proceeding from the June drop where apple fruitlets dropped naturally (Section 4.2.1).

The necessity of tree-level apple load estimation, in comparison with flower load estimation (Chapter 3), is less. Flower load estimation at the tree level produces a precise number of flower clusters per tree. With this information, excess flowers can be directly removed by operators, either an experienced person (Chapter 4) or an intelligent robotic platform (Bhattarai et al., 2023). By contrast, during harvest period, the key information is how many apples and how much yield (kg) are harvestable for the market. Thus the apple load estimated at row or plot level is sufficient. Likewise, in operational scenario, the crucial factor for guiding robotics to accomplish fruit-picking tasks is to localize and further classify the maturity of apples. Details concerning which tree the localized apples grow on are of less importance. Therefore, profits from tree-level apple load estimation can be determined as optimizing the placement of harvest containers (Osman et al., 2021) and monitoring the production capacity of individual trees which benefits the crop breeding program.

6.2 Limitations

On the basis of surveyed results on the opportunities of UAVs in orchard management (Chapter 2), tree-level crop load estimation was determined as the main research objective of the present thesis. A benchmark of UAV-based flower load estimation, in the case of apple orchards, was established first using colored point clouds (Chapter 3). And its performance was compared with ground-based colored point clouds to further understand its advantages and limitations. To improve the flower load estimation accuracy and efficiency, the feasibility of using single raw UAV RGB images was investigated (Chapter 4). Finally, an automatic geo-localization method of aerial image pixel was developed to enhance the framework built up in Chapter 4 and was tested for tree-level apple yield estimation (Chapter 5). Overall, though fine results have been already demonstrated, there are still limitations that can be refined in the near future.

There are two improvements which can be identified for the review work introduced in Chapter 2. First, the methodology comparison within the same application like the calculation of geometric features should be more specific. For example, relevant literature should be further categorized into various fruit species. Since different fruit trees hold diverse structures and suffer dissimilar leaf or fruit occlusion which leads to different responses to the sensors equipped on UAVs (Gene-Mola et al., 2021). Consequently, results derived from the same method or vegetation index are not comparable. On the other hand, the flying parameters should also be considered. Evidence indicates that parameters like flying altitudes affect UAV-based monitoring precision (Chapter 4). Lastly, a survey of relevant work published between 2020 and 2022 should be carried out. This can be a good reference to validate the predictions of future tendencies made in Chapter 2. It also provides new insights into the use of UAVs in orchard management.

The main limitation in Chapter 3 is the difference between ground- and UAV-based point cloud density. Given the fact that the point cloud density of UAVs used in the study was lower than ground-based (Table 3.5), the demonstrated comparison is not completely fair. Thus, adding more UAV flights or increasing the overlapping ratio to make the aerial point cloud density more comparable to ground-based is recommended. In the same case study, flower load estimation, as demonstrated in Chapter 4, one problem is also derived from data collection. Applied datasets comprise the variance in flying altitudes and weather conditions (Table 4.1) which potentially affects the analysis of obtained results. Though it provided a chance to investigate the effects of flying parameters, a more systematic design of the field campaigns is encouraged. In addition, no evaluation of the flower-related pixel segmentation was conducted in Chapter 4. This retards the identification of flower estimation errors. Color thresholding method is a pixel-level segmentation method. The building up of reference data in images

is labor-intensive. But this evaluation is still highly required. It can also help to further recognize the effects of structural overlapping on tree-level flower load estimation.

Annotation work in the apple detection part of Chapter 5 is challenging because of the difficulties caused by heavy leaf and fruit occlusions and illumination conditions (Fig.5.5). Current annotation was conducted by two operators and no overlapping was covered for the labeled images. It would be required to quantify the labeling variance between the annotation operators as the trained YOLOv5s performance can also be influenced. From this aspect, a fair comparison between manual labeling is recommended. Present apple detection work in Chapter 5 produced a baseline of YOLOv5s. Future work should focus on the modification of YOLOv5s basic model to enhance the detection of apples. A potential solution can be adding attention mechanisms into YOLOv5s. Regarding the apple assignment part, the main limitation is determined by the visibility of exact tree positions in the UAV images. Because of the heavy occlusion of leaves, it is hard to identify the precise tree positions by inspecting the tree root (Fig.5.11). Thus uncertainties exist during the evaluation of proposed tree localization method. To solve this, datasets that suffer less leaf occlusion issues are needed. The key is the visibility of tree roots in the images. Moreover, to explore the effects of flying altitudes on tree localization accuracy, multiple datasets collected under different flying altitudes are suggested.

6.3 Parallel with current research and outlook

Crop load estimation is one of the most important applications in UAV-driven orchard management (Chapter 2). The main findings derived from two case studies of crop load estimation in an apple orchard, flower load and apple fruit load estimation at tree level, are described in Section 6.1. Considerations initiated in the comparison among ground- and UAV-based colored point clouds for flower load estimation are further extended to multi-source sensing approaches (Section 6.3.1). It aims at filling gaps between the current practice of orchard management and future developments. Great potential of single raw UAV RGB images in tree-level crop load estimation has been fully demonstrated in Chapter 4 and 5. The remainder of this section places this finding in a wider context of orchard management. Its potential in supporting horticultural crop productivity and resource efficiency management, geometric trait calculation, disease detection and other applications is forecasted.

6.3.1 Multi-platform and multi-modal sensing for orchard management

Fruit trees in orchards struggle to receive individualized monitoring from one single sensing platform. The complexities arise from two main aspects. The first facet comes from the intensively cultivated module which makes it hard to precisely analyze the sensed information at tree level. The second aspect is the complex tree structure. In comparison with other horticultural crops like strawberries (Chen et al., 2019b) and cauliflower (Gunder et al., 2022), fruit trees hold vast structural characteristics in 3D space such as tree volume and height (Ganz et al., 2019). Jointly, the interlacing and touching branches of fruit trees retards the precision of individualized monitoring derived from one sensing platform (Zine-El-Abidine et al., 2021). On the other hand, it reveals the tendency and importance of a multi-platform sensing approach (Chapter 3).

The main advantages of multi-platform sensing are mutual cooperation and validation. Towards mutual cooperation, it refers to the combination of data derived from different platforms. It helps to get more insights into a specific orchard area by maximizing the amount of information gathered on fruit trees. Chapter 3, for instance, revealed the value of exploiting complementary properties of different types of point clouds. Aerial point clouds, in general, held sparser points than ground-derived point clouds, for the lower part of a tree canopy. This difference distinguishes the reliability of corresponding predictions such as apple flower load estimation (Zhang et al., 2022b). The key difference between aerial and ground-based platforms is the camera view. This makes them irreplaceable from each other. UAVs provide a unique solution for the inspection of the upper canopy area with various camera angles unreachable by a ground platform. While ground-based platforms hold a fair front-view of trees with higher spatial resolution. Thus, the combination of these two types of platforms is expected to be the only solution for a complete inspection of individual fruit trees. On the other hand, for regular orchard

management activities, ground-based platforms like tractors already regularly move through the orchard. Spatio-temporal optimization methods could assist in the efficient acquisition, in terms of timing, frequency, sensor type, of complementary data from sensors onboard UAV platforms. With the increasing spatial resolution of images from satellite-based platforms (e.g., PlanetScope), space-based observations are becoming a viable complementary source (Sandónis-Pozo et al., 2022). These are comprised of mainly optical multi-spectral images which would allow the characterization of the temporal development of the tree orchard canopies.

The distance to the target object differs among various sensing platforms which cause data to suffer different resolutions and precision, and further affect corresponding monitoring accuracy. Thus, in the same application scenario, results derived from these three types of platforms should be used to validate each other. On the other hand, comparison among conclusions resulting from different platforms benefits determination of the optimal approach. For example, in the case study of frost management in orchards, it is interesting to compare NDVI images derived from Sentinel-2 and Landsat-TM/ETM+/OLI (Zhu et al., 2021) with that produced by UAVs (Yuan and Choi, 2021) to further understand its effects on the predicted results.

Moreover, UAVs, in contrast with other platforms, are expected to be the key element in developing digital twin of the orchards (Nasirahmadi and Hensel, 2022). Orchard digital twin refers to a digital equivalent of the orchard in the real world of which it dynamically mirrors the states of individual trees over their lifetime (Verdouw et al., 2021). With this rich model, fruit yield and disease outbreaks can be predicted at an earlier stage. Multi-platform sensing meets its requirement for large volumes of spatial-temporal data (Chapter 2). Satellite data, in general, suffers limited spatial and spectral resolutions, and its temporal data is restricted by unfavorable re-visit time (Berni et al., 2009b). It fails to provide hourly or even daily data for the establishment of orchard digital twins. Concerning ground-based sensing platforms like ground vehicles, higher labor and time input per acre for data collection, compare with UAVs, is still the main bottleneck. Another fact is that ground vehicle-based sensing approach is not fully non-destructive. Its effects on soil compactness can also influence the growth of fruit trees. In summary, UAVs are believed to be the dominant tool in both multi-platform derived orchard management and the development of the orchard digital twin.

In addition, multi-modal sensing approaches are considered to be another trend in optimizing orchard management. There is a growing body of literature that compares predictions derived from different optical sensors (Chen et al., 2022a). For example, the comparison between UAV images-derived NDVI and LiDAR-based cross-sectional area for management zone identification (Martínez-Casasnovas et al., 2022), and that between LiDAR SLAM and UAV-SfM for peach branch detection (Teng et al., 2023). Similar to the usefulness of multi-platform approach, this comparison not only helps to determine the

optimal method but is fundamental for data fusion. Multi-source inputs proceeding from UAVs also benefit the modeling of complex cases, such as the prediction of fruit number reduction ratio caused by frost (Zhu et al., 2021). Moreover, the increasing investigations of point clouds derived from UAV-LiDAR (Dian et al., 2023; Raman et al., 2023b) indicate that the quality of colored point clouds comprising multispectral features can be improved. The combination of LiDAR-derived high-density point clouds and multispectral or thermal or hyperspectral point clouds is expected to provide new solutions for orchard management (Jurado et al., 2022). This inspection potentially produces the fruit-tree disease detection at intra-tree level. Fruit-tree disease holds the characteristics of heterogeneity crossing an entire tree (Ali et al., 2023). High-quality LiDAR point clouds, combined with spectral features, can enable disease detection in 3D space. It advances the follow-up disease control directly by providing precise 3D locations for operational robotics.

6.3.2 The potential of single raw UAV images in horticulture

Methods developed around single raw UAV RGB images were and will still be dominant solutions in the management of horticulture where crops are intensively cultivated and grown with intensive and individualized care. Conventional approaches, based on ground-based platforms, primarily use raw RGB images to accomplish inspection tasks directly due to the high spatial resolution derived from proximal sensing (Zhao et al., 2023b). Efficient collection of aerial geotagged images with a unique camera view like a nadir view enables orthomosaics (Apolo-Apolo et al., 2020b) and colored point clouds (Yuan et al., 2023) derived from aerial RGB images fast become popular data sources. Yet, evidence proved that the use of single raw UAV RGB images will reform this pattern and draw more attention to supporting horticulture management (Chapter 4 and 5).

The feasibility of geolocating each image pixel empowers high-resolution aerial images to predict apple yield at tree level skipping conventional photogrammetry methods such as SfM (Chapter 5). The proposed automatic crop load estimation framework is capable to be extended to other horticultural applications. In the case of monitoring crop load on trees, the summarized spatial pattern of structural overlapping should be paid attention to (Fig.6.1). It varies in the camera view such as a front view (Fig. 6.1a) and a side view (Fig. 6.1b). But, in general, the structural overlapping shows a gradual change in vertical and horizontal directions crossing the whole image. The variance produces different visibility of the whole tree structure. Thus, with consistent vertical or horizontal overlapping magnitude, a crop load estimation can be established (Chapter 4). The quantification of structural overlapping, from one perspective, benefits from the well-designed landscapes in orchards where fixed row and tree spacing are employed. Coupled with tree coordinates in the images, the estimation model can be automated and made robust. For a random image view in the footprint, besides the front and side view, crop load can be predicted as well. But the errors produced by structural overlapping are hard to quantify. In addition,

the proposed framework can be applied to other horticultural crops directly and fewer structural overlapping problems are involved. Since crops like cauliflower hold less complex structural features like height. For example, as for strawberry yield estimation, the proposed framework can replace orthomosaic-based methods (Chen et al., 2019b; de Oliveira et al., 2023) for data processing efficiency improvement and the detected strawberries are geolocated automatically in the real world.

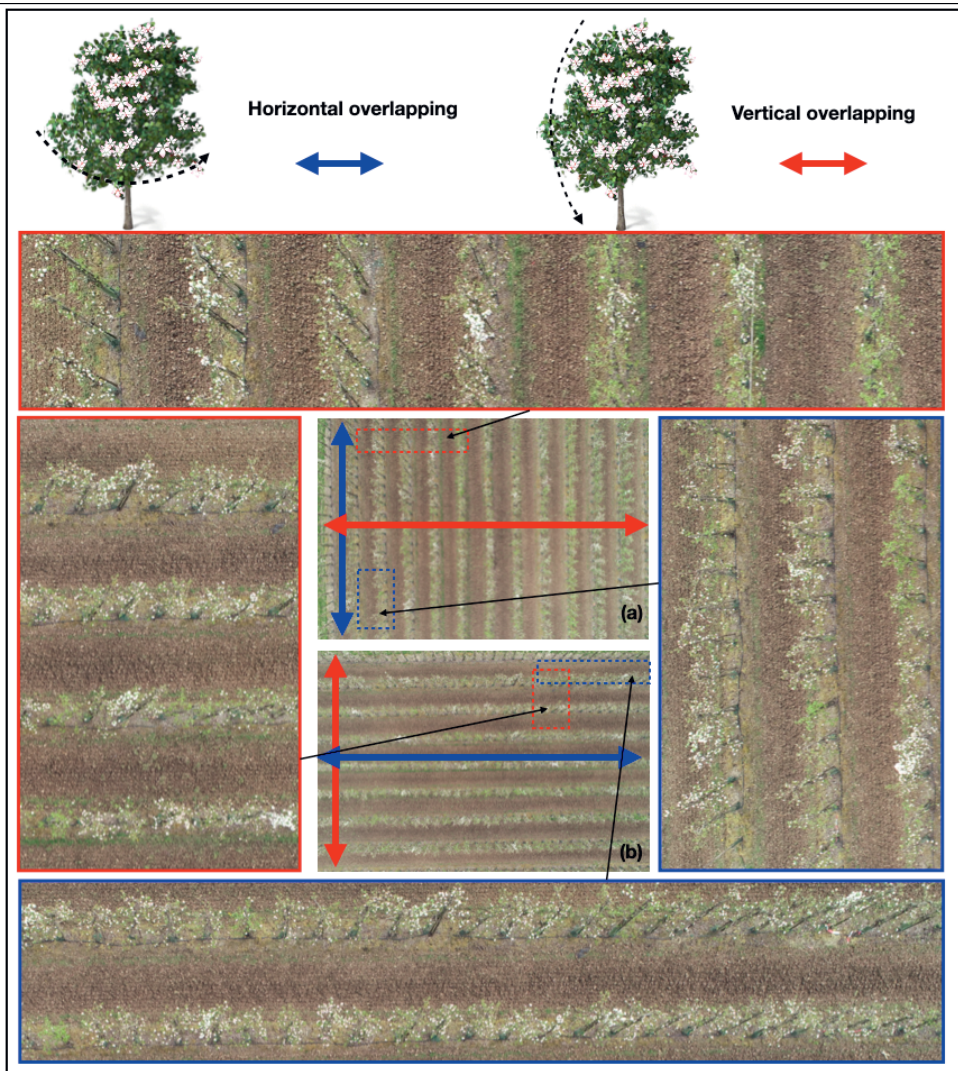


Fig. 6.1. Summary of the structural overlapping (vertical and horizontal overlapping) exists in the raw orchard images captured by a single UAV RGB camera. (a) a front view of the trees; (b) a side view of the trees. The present image samples were captured under a nadir camera view. Red arrows indicate the direction in which vertical (nadir) overlapping occurs, and corresponding samples with a zoomed view are highlighted with red borders. While blue arrows show the direction of horizontal (angular) overlapping, and corresponding samples are highlighted with blue borders.

Single raw RGB images can be used to directly calculate the geometric features of individual fruit trees. Current advancements in the calculation of tree geometric features like canopy area rely on RGB image-

derived orthophotos and colored point clouds (Chapter 2). While the proposed pixel-geolocate method (PGM) (Chapter 5) enables this calculation to be conducted with simple data sources, the raw RGB images. Fruit trees in aerial images generally hold two situations, a nadir view of the canopy (like the center area of Fig. 6.1a and b) and a side view of the whole tree. These two cases potentially lead to different geometric feature calculations. In the first case, canopy projection area (CPA), canopy diameter or width and height can be measured with a segmented canopy area (Mu et al., 2018). Conducting a precise measurement, instance segmentation is recommended (Zheng et al., 2022). To register the measured values into the real world, center pixel coordinate of the segmented canopy area can be regarded as the tree positions for spatial mapping using PGM. Since only the center area of aerial images holds the nadir view of trees (tree crown area), higher front overlapping or multiple flights are needed for the mapping of the whole orchards. Even so, the data processing efficiency is expected to be higher than conventional methods since only raw images are processed. As for the second case, trees display a side view, tree height, canopy volume and canopy width or height can be measured using PGM (Ganz et al., 2019). And instance segmentation methods of the trees are also suggested. However, in this case, the structural overlapping issue must be considered. As different overlapping levels affect the correlation between the pixel-wise and in-situ measurements of the geometrical features (Chapter 4). Regarding the tree registration, center pixel coordinate of the tree canopy or the coordinate of a pixel of the detected tree root can be used which depends on specific applications. Overall, for both cases, flying parameters like flying heights and camera angles should be taken as important variables for developing a geometric feature prediction model.

The PGM proposed in Chapter 5 can promote water stress estimation and disease detection at the intra-canopy level. Current practice in these two applications highly leans on orthomosaics produced by multispectral images (Selvaraj et al., 2020). The main restrictions are that the extracted spectral features come from a limited area of the trees such as the canopy or crown area (Zhao et al., 2017). Though previous studies already demonstrated the reliability of using vegetation indices such as the photochemical reflectance index (PRI) and NDVI (Ballester et al., 2018) as water stress indicators, it is still at tree level which indicates the status of an entire tree. In this context, PGM potentially provides the variance of water stress crossing the whole tree canopy for high-level inspection. Since spectral features of pixels can be registered in the real world, and more spectral features of fruit trees can be extracted from the side-view of the trees. Yet, to validate the PGM-based methods, high requirements for the collection of ground reference data are needed. Likewise, intra-canopy level inspection is also needed for disease detection. Fruit diseases like banana stem borer damage and *Fusarium wilt* in bananas produce symptoms on the leaves. It is not wise to diagnose the disease from only the canopy area which missing more spectral features from the side of the trees (Choosumrong et al., 2023). From this aspect, it is considered that PGM-derived intra-canopy disease detection would yield results with higher accuracy.

In addition, the key advantage of PGM-derived methods is believed to be their high-efficiency data processing which is required for real-time UAV-based orchard monitoring. The main body of existing methods only uses orthophoto or colored point clouds to geolocate the detection results (Chapter 2). This produces great demands for data transmission and computational sources. Yet, PGM only processes data in 2D space (raw RGB or multispectral images) shows great potential for UAV-derived real-time applications. It is expected to reform the application of UAV-sprayers (Piljek et al., 2022). With PGM-based tree detection and localizations, sprayer can make precise spraying for individual trees which saves pesticides and reduces environmental impacts at the same time. The precision can research intra-canopy or leaf level. Yet, a high standard for droplet distribution will be needed (Meng et al., 2022).

Illumination conditions still limit small object detection tasks in single raw aerial RGB images (Chapter 5). Advanced deep learning algorithms, in the computer vision community, showed fine performance in dealing with detection problems derived from multiscale aerial objects (Li et al., 2023a; Li et al., 2023b). Yet, it is urgent to develop a filter to mitigate illumination effects, especially for the adoption of PGM. One indirect solution can be multiple re-visits by UAVs. With one flight, PGM can produce a spatial map of the orchards where detailed information on individual trees is recorded. Another flight for the same orchard produces a map that exhibits different illumination conditions from the previous flight. Comparing these two temporal maps, the dynamics of spatial distribution of the illumination effects can be monitored and evaluated. Since PGM enables the mapping at leaf level, the illumination effects can be averaged for a better prediction. For example, in the case of apple yield prediction, one spatial map makes false positive predictions of leaves because of the effects of illumination. These predictions will be geolocated by PGM. While another spatial map, assuming it is produced at a different time, of apple yield might make false negatives for the false positive predictions produced by the previous map. The final predictions can be optimized by comparing these different predictions, based on coordinates predicted by PGM. Because of the data-processing efficiency of PGM, it is believed to be a good solution for reducing illumination effects. Yet, the influence of wind should also be considered. Accordingly, it is suggested to conduct these flights under less windy conditions.

The AI-driven precise monitoring of orchards and the development of orchard digital twins require large volumes of data. Its importance has been proven by the promotion derived from public datasets like MS-COCO, MNIST and ImageNet to the advanced deep learning algorithms. Consequently, algorithms applied to orchard management benefit from this advancement using transfer learning (Chapter 5). Though fruits like apples have already been covered by these datasets, the present features are far different from the practical in-field object features. Therefore, the complicated orchard environments make it necessary to build up publicly available orchard datasets of UAVs (Zhang et al., 2022c). The

challenges come from two aspects: the complexity of orchard environments and the variability of UAV flying parameters. To mitigate the first challenge, the datasets should be organized into proper crop categories. For example, it can be stone fruits and vineyards (Ariza-Sentís et al., 2023). Bounding box annotation of fruits or fruit trees is fundamental. If possible, pixel-level instance annotation should also be involved which is extremely important for modern high-density orchards. Both annotations should be conducted by the data uploader since they are more familiar with the present orchard environment. The second challenge is easier to solve. Clear documentation of the flying parameters should be included. These parameters, for instance, should comprise flying altitudes and camera angles. Overall, various weather conditions are also recommended. With the availability of the public UAV orchard datasets, the proposed PGM is believed to deeply reform the whole orchard management ranging from the geometric calculation, and crop productivity management, to disease detection and resource efficiency monitoring (Chapter 2).



References

- Abdulridha, J., Batuman, O., Ampatzidis, Y., 2019. UAV-Based Remote Sensing Technique to Detect Citrus Canker Disease Utilizing Hyperspectral Imaging and Machine Learning. *Remote Sens.* 11. <https://doi.org/10.3390/rs11111373>.
- Aggelopoulou, A.D., Bochtis, D., Fountas, S., Swain, K.C., Gemtos, T.A., Nanos, G.D., 2010. Yield prediction in apple orchards based on image processing. *Precis. Agric.* 12, 448-456. <https://doi.org/10.1007/s11119-010-9187-0>.
- Aggelopoulou, A.D., Bochtis, D., Fountas, S., Swain, K.C., Gemtos, T.A., Nanos, G.D., 2011. Yield prediction in apple orchards based on image processing. *Precision Agriculture* 12, 448-456. <https://doi.org/10.1007/s11119-010-9187-0>.
- Aggelopoulou, K.D., Wulfsohn, D., Fountas, S., Gemtos, T.A., Nanos, G.D., Blackmore, S., 2009. Spatial variation in yield and quality in a small apple orchard. *Precis. Agric.* 11, 538-556. <https://doi.org/10.1007/s11119-009-9146-9>.
- Ahmed, D., Sapkota, R., Churuvija, M., Karkee, M., 2023. Machine Vision-Based Crop-Load Estimation Using YOLOv8. arXiv preprint arXiv:2304.13282.
- Ali, Z.A., Yang, C., Israr, A., Zhu, Q., 2023. A Comprehensive Review of Scab Disease Detection on Rosaceae Family Fruits via UAV Imagery. *Drones* 7, 97.
- Alligier, R., Gianazza, D., Durand, N., Olive, X., 2023. Dual-Horizon Reciprocal Collision Avoidance for Aircraft and Unmanned Aerial Systems. *Journal of Intelligent & Robotic Systems* 107. <https://doi.org/10.1007/s10846-022-01782-2>.
- Ampatzidis, Y., Partel, V., Meyering, B., Albrecht, U., 2019. Citrus rootstock evaluation utilizing UAV-based remote sensing and artificial intelligence. *Comput. Electron. Agric.* 164. <https://doi.org/10.1016/j.compag.2019.104900>.
- Anifantis, A.S., Camposeo, S., Vivaldi, G.A., Santoro, F., Pascuzzi, S., 2019. Comparison of UAV Photogrammetry and 3D Modeling Techniques with Other Currently Used Methods for Estimation of the Tree Row Volume of a Super-High-Density Olive Orchard. *Agriculture-Basel* 9. <https://doi.org/10.3390/agriculture9110233>.
- Apolo-Apolo, O.E., Martinez-Guanter, J., Egea, G., Raja, P., Perez-Ruiz, M., 2020a. Deep learning techniques for estimation of the yield and size of citrus fruits using a UAV. *European Journal of Agronomy* 115. <https://doi.org/10.1016/j.eja.2020.126030>.
- Apolo-Apolo, O.E., Perez-Ruiz, M., Martinez-Guanter, J., Valente, J., 2020b. A Cloud-Based Environment for Generating Yield Estimation Maps From Apple Orchards Using UAV Imagery and a Deep Learning Technique. *Frontiers in Plant Science* 11. <https://doi.org/10.3389/fpls.2020.01086>.
- Arakawa, T., Tanaka, T., Kamio, S., 2023. Detection of On-tree Chestnut Fruits Using Deep Learning and RGB UAV Imagery for Estimation of Yield and Fruit Load. *Agronomy Journal*. <https://doi.org/10.1002/agj2.21330>.
- Ariza-Sentís, M., Vélez, S., Valente, J., 2023. Dataset on UAV RGB videos acquired over a vineyard including bunch labels for object detection and tracking. *Data in Brief* 46, 108848. <https://doi.org/10.1016/j.dib.2022.108848>.
- Arredondo Valdés, R., Delgado Ortiz, J.C., Beltrán Beache, M., Anguiano Cabello, J., Cerna Chávez, E., Rodríguez Pagaza, Y., Ochoa Fuentes, Y.M., 2016. A review of techniques for detecting

- Huanglongbing (greening) in citrus. *Can J Microbiol* 62, 803-811.<https://doi.org/10.1139/cjm-2016-0022>.
- Avola, G., Di Gennaro, S.F., Cantini, C., Riggi, E., Muratore, F., Tornambe, C., Matese, A., 2019. Remotely Sensed Vegetation Indices to Discriminate Field-Grown Olive Cultivars. *Remote Sensing* 11.<https://doi.org/10.3390/rs111101242>.
- Badrloo, S., Varshosaz, M., Pirasteh, S., Li, J., 2022. Image-Based Obstacle Detection Methods for the Safe Navigation of Unmanned Vehicles: A Review. *Remote Sensing* 14, 3824.
- Bai, T., Zhang, N., Mercatoris, B., Chen, Y., 2019. Jujube yield prediction method combining Landsat 8 Vegetation Index and the phenological length. *Computers and Electronics in Agriculture* 162, 1011-1027.<https://doi.org/https://doi.org/10.1016/j.compag.2019.05.035>.
- Bai, X., Li, Z., Li, W., Zhao, Y., Li, M., Chen, H., Wei, S., Jiang, Y., Yang, G., Zhu, X., 2021. Comparison of Machine-Learning and CASA Models for Predicting Apple Fruit Yields from Time-Series Planet Imageries. *Remote Sensing* 13, 3073.
- Ballester, C., Intrigliolo, D.S., Castel, J.R., Jiménez-Bello, M.A., 2013. Usefulness of thermography for plant water stress detection in citrus and persimmon trees. *Agricultural and forest meteorology*. 168, 120-129.<https://doi.org/10.1016/j.agrformet.2012.08.005>.
- Ballester, C., Zarco-Tejada, P., Nicolas, E., Alarcon, J., Fereres, E., Intrigliolo, D., Gonzalez-Dugo, V., 2018. Evaluating the performance of xanthophyll, chlorophyll and structure-sensitive spectral indices to detect water stress in five fruit tree species. *Precis. Agric.* 19, 178-193.<https://doi.org/10.1007/s11119-017-9512-y>.
- Barbagallo, S., Consoli, S., Russo, A., 2009. A one-layer satellite surface energy balance for estimating evapotranspiration rates and crop water stress indexes. *Sensors (Basel)* 9, 1-21.<https://doi.org/10.3390/s90100001>.
- Bargoti, S., Underwood, J., 2016. Image Segmentation for Fruit Detection and Yield Estimation in Apple Orchards. *Journal of Field Robotics* 34.<https://doi.org/10.1002/rob.21699>.
- Barrows, C., Bulanon, D.M., 2017. Development of a low-cost multispectral camera for aerial crop monitoring. *Journal of Unmanned Vehicle Systems* 5, 192-200.<https://doi.org/10.1139/juvs-2017-0008>.
- Bebber, D.P., Gurr, S.J., 2015. Crop-destroying fungal and oomycete pathogens challenge food security. *Fungal Genetics and Biology* 74, 62-64.<https://doi.org/https://doi.org/10.1016/j.fgb.2014.10.012>.
- Belfanti, E., Silfverberg-Dilworth, E., Tartarini, S., Patocchi, A., Barbieri, M., Zhu, J., Vinatzer, B.A., Gianfranceschi, L., Gessler, C., Sansavini, S., 2004. The HcrVf2 gene from a wild apple confers scab resistance to a transgenic cultivated variety. *Proc. Natl. Acad. Sci. U. S. A.* 101, 886-890.<https://doi.org/10.1073/pnas.0304808101>.
- Ben Sadok, I., Moutier, N., Garcia, G., Dosba, F., Grati-Kamoun, N., Rebai, A., Khadari, B., Costes, E., 2012. Genetic determinism of the vegetative and reproductive traits in an F1 olive tree progeny. *Tree Genetics & Genomes* 9, 205-221.<https://doi.org/10.1007/s11295-012-0548-x>.
- Berni, J.A.J., Zarco-Tejada, P.J., Sepulcre-Canto, G., Fereres, E., Villalobos, F., 2009a. Mapping canopy conductance and CWSI in olive orchards using high resolution thermal remote sensing imagery. *Remote Sens. Environ.* 113, 2380-2388.<https://doi.org/10.1016/j.rse.2009.06.018>.

References

- Berni, J.A.J., Zarco-Tejada, P.J., Suarez, L., Fereres, E., 2009b. Thermal and Narrowband Multispectral Remote Sensing for Vegetation Monitoring From an Unmanned Aerial Vehicle. *Ieee Transactions on Geoscience and Remote Sensing* 47, 722-738.<https://doi.org/10.1109/tgrs.2008.2010457>.
- Bhattarai, U., Karkee, M., 2022. A weakly-supervised approach for flower/fruit counting in apple orchards. *Computers in Industry* 138, 103635.<https://doi.org/https://doi.org/10.1016/j.compind.2022.103635>.
- Bhattarai, U., Zhang, Q., Karkee, M., 2023. Design, Integration, and Field Evaluation of a Robotic Blossom Thinning System for Tree Fruit Crops. arXiv preprint arXiv:2304.04919.
- Bleasdale, A.J., Blackburn, G.A., Whyatt, J.D., 2022. Feasibility of detecting apple scab infections using low-cost sensors and interpreting radiation interactions with scab lesions. *International Journal of Remote Sensing* 43, 4984-5005.<https://doi.org/10.1080/01431161.2022.2122895>.
- Bound, S., 2018. Precision Crop Load Management of Apple (*Malus x domestica* Borkh.) without Chemicals. *Horticulturae* 5.<https://doi.org/10.3390/horticulturae5010003>.
- Brinkhoff, J., Robson, A.J., 2020. Macadamia Orchard Planting Year and Area Estimation at a National Scale. *Remote Sensing* 12, 2245.
- Bulanon, D.M., Lonai, J., Skovgard, H., Fallahi, E., 2016. Evaluation of Different Irrigation Methods for an Apple Orchard Using an Aerial Imaging System. *Isprs International Journal of Geo-Information* 5.<https://doi.org/10.3390/ijgi5060079>.
- Calderon, R., Navas-Cortes, J.A., Lucena, C., Zarco-Tejada, P.J., 2013. High-resolution airborne hyperspectral and thermal imagery for early, detection of Verticillium wilt of olive using fluorescence, temperature and narrow-band spectral indices. *Remote Sensing of Environment* 139, 231-245.<https://doi.org/10.1016/j.rse.2013.07.031>.
- Campos, J., Llop, J., Gallart, M., García-Ruiz, F., Gras, A., Salcedo, R., Gil, E., 2019. Development of canopy vigour maps using UAV for site-specific management during vineyard spraying process. *Precis. Agric.*<https://doi.org/10.1007/s11119-019-09643-z>.
- CaraDonna, P.J., Iler, A.M., Inouye, D.W., 2014. Shifts in flowering phenology reshape a subalpine plant community. *Proceedings of the National Academy of Sciences* 111, 4916-4921.<https://doi.org/10.1073/pnas.1323073111>.
- Caruso, G., Zarco-Tejada, P.J., Gonzalez-Dugo, V., Moriondo, M., Tozzini, L., Palai, G., Rallo, G., Hornero, A., Primicerio, J., Gucci, R., 2019. High-resolution imagery acquired from an unmanned platform to estimate biophysical and geometrical parameters of olive trees under different irrigation regimes. *PLoS One* 14, e0210804.<https://doi.org/10.1371/journal.pone.0210804>.
- Castillo-Ruiz, F.J., Jiménez-Jiménez, F., Blanco-Roldán, G.L., Sola-Guirado, R.R., Agüera-Vega, J., Castro-García, S., 2015. Analysis of fruit and oil quantity and quality distribution in high-density olive trees in order to improve the mechanical harvesting process. *Spanish Journal of Agricultural Research* 13.<https://doi.org/10.5424/sjar/2015132-6513>.
- Catania, P., Roma, E., Orlando, S., Vallone, M., 2023. Evaluation of Multispectral Data Acquired from UAV Platform in Olive Orchard. *Horticulturae* 9, 133.
- Chen, B., Jin, Y.F., Brown, P., 2019a. An enhanced bloom index for quantifying floral phenology using multi-scale remote sensing observations. *Isprs Journal of Photogrammetry and Remote Sensing* 156, 108-120.<https://doi.org/10.1016/j.isprsjsprs.2019.08.006>.

- Chen, R., Zhang, C., Xu, B., Zhu, Y., Zhao, F., Han, S., Yang, G., Yang, H., 2022a. Predicting individual apple tree yield using UAV multi-source remote sensing data and ensemble learning. *Computers and Electronics in Agriculture* 201, 107275.
- Chen, R.Q., Zhang, C.J., Xu, B., Zhu, Y.H., Zhao, F., Han, S.Y., Yang, G.J., Yang, H., 2022b. Predicting individual apple tree yield using UAV multi-source remote sensing data and ensemble learning. *COMPUTERS AND ELECTRONICS IN AGRICULTURE* 201.<https://doi.org/10.1016/j.compag.2022.107275>.
- Chen, S.W., Shivakumar, S.S., Dcunha, S., Das, J., Okon, E., Qu, C., Taylor, C.J., Kumar, V., 2017. Counting Apples and Oranges With Deep Learning: A Data-Driven Approach. *IEEE Robotics and Automation Letters* 2, 781-788.<https://doi.org/10.1109/lra.2017.2651944>.
- Chen, Y., Lee, W.S., Gan, H., Peres, N., Fraisse, C., Zhang, Y.C., He, Y., 2019b. Strawberry Yield Prediction Based on a Deep Neural Network Using High-Resolution Aerial Orthoimages. *Remote Sensing* 11.<https://doi.org/10.3390/rs11131584>.
- Chen, Y.Y., Hou, C.J., Tang, Y., Zhuang, J.J., Lin, J.T., He, Y., Guo, Q.W., Zhong, Z.Y., Lei, H., Luo, S.M., 2019c. Article Citrus Tree Segmentation from UAV Images Based on Monocular Machine Vision in a Natural Orchard Environment. *Sensors* 19.<https://doi.org/10.3390/s19245558>.
- Chen, Z., Su, R., Wang, Y., Chen, G., Wang, Z., Yin, P., Wang, J., 2022c. Automatic Estimation of Apple Orchard Blooming Levels Using the Improved YOLOv5, *Agronomy*.<https://doi.org/10.3390/agronomy12102483>.
- Chen, Z.Y., Su, R., Wang, Y.L., Chen, G.F., Wang, Z.Q., Yin, P.J., Wang, J.X., 2022d. Automatic Estimation of Apple Orchard Blooming Levels Using the Improved YOLOv5. *Agronomy-Basel* 12.<https://doi.org/10.3390/agronomy12102483>.
- Cheng, H., Damerow, L., Sun, Y.R., Blanke, M., 2017. Early Yield Prediction Using Image Analysis of Apple Fruit and Tree Canopy Features with Neural Networks. *Journal of Imaging* 3.<https://doi.org/10.3390/jimaging3010006>.
- Choosumrong, S., Hataitara, R., Sujipuli, K., Weerawatanakorn, M., Preechaharn, A., Premjet, D., Laywisadkul, S., Raghavan, V., Panumonwatee, G., 2023. Bananas diseases and insect infestations monitoring using multi-spectral camera RTK UAV images. *Spatial Information Research*.<https://doi.org/10.1007/s41324-022-00504-y>.
- Cibuk, M., Budak, U., Guo, Y.H., Ince, M.C., Sengur, A., 2019. Efficient deep features selections and classification for flower species recognition. *Measurement* 137, 7-13.<https://doi.org/10.1016/j.measurement.2019.01.041>.
- Colaco, A.F., Molin, J.P., Rosell-Polo, J.R., Escola, A., 2018. Application of light detection and ranging and ultrasonic sensors to high-throughput phenotyping and precision horticulture: current status and challenges. *Hortic Res* 5, 35.<https://doi.org/10.1038/s41438-018-0043-0>.
- Couvreur, V., Kandelous, M.M., Sanden, B.L., Lampinen, B.D., Hopmans, J.W., 2016. Downscaling transpiration rate from field to tree scale. *Agric. For. Meteorol.* 221, 71-77.<https://doi.org/10.1016/j.agrformet.2016.02.008>.
- Crtomir, R., Urska, C., Stanislav, T., Denis, S., Karmen, P., Pavlovic, M., Marjan, V., 2012. Application of Neural Networks and Image Visualization for Early Forecast of Apple Yield. *Erwerbs-Obstbau* 54, 69-76.<https://doi.org/10.1007/s10341-012-0162-y>.

References

- DadrasJavan, F., Samadzadegan, F., Pourazar, S.H.S., Fazeli, H., 2019. UAV-based multispectral imagery for fast Citrus Greening detection. *Journal of Plant Diseases and Protection* 126, 307-318.<https://doi.org/10.1007/s41348-019-00234-8>.
- Das, J., Cross, G., Qu, C., Makineni, A., Tokekar, P., Mulgaonkar, Y., Kumar, V., 2015. Devices, systems, and methods for automated monitoring enabling precision agriculture, 2015 IEEE International Conference on Automation Science and Engineering (CASE), pp. 462-469.<https://doi.org/10.1109/CoASE.2015.7294123>.
- de Castro, A., Jiménez-Brenes, F., Torres-Sánchez, J., Peña, J., Borra-Serrano, I., López-Granados, F., 2018. 3-D Characterization of Vineyards Using a Novel UAV Imagery-Based OBIA Procedure for Precision Viticulture Applications. *Remote Sens.* 10.<https://doi.org/10.3390/rs10040584>.
- de Castro, A.I., Rallo, P., Suarez, M.P., Torres-Sanchez, J., Casanova, L., Jimenez-Brenes, F.M., Morales-Sillero, A., Jimenez, M.R., Lopez-Granados, F., 2019. High-Throughput System for the Early Quantification of Major Architectural Traits in Olive Breeding Trials Using UAV Images and OBIA Techniques. *Frontiers in Plant Science* 10.<https://doi.org/10.3389/fpls.2019.01472>.
- De la Rosa, R., León, L., Guerrero, N., Rallo, L., Barranco, D., 2007. Preliminary results of an olive cultivar trial at high density. *Australian Journal of Agricultural Research* 58.<https://doi.org/10.1071/ar06265>.
- de Oliveira, L.S., Castoldi, R., Martins, G.D., Medeiros, M.H., 2023. Estimation of Strawberry Crop Productivity by Machine Learning Algorithms Using Data from Multispectral Images. *Agronomy-Basel* 13.<https://doi.org/10.3390/agronomy13051229>.
- Delalieux, S., Zarco-Tejada, P.J., Tits, L., Bello, M.A.J., Intrigliolo, D.S., Somers, B., 2014. Unmixing-Based Fusion of Hyperspatial and Hyperspectral Airborne Imagery for Early Detection of Vegetation Stress. *IEEE Journal of Selected Topics in Applied Earth Observations and Remote Sensing* 7, 2571-2582.<https://doi.org/10.1109/jstars.2014.2330352>.
- Dennis, F.G., Jr., 2000. The history of fruit thinning. *Plant Growth Regulation* 31, 1-16.<https://doi.org/10.1023/A:1006330009160>.
- Di Gennaro, S.F., Toscano, P., Cinat, P., Berton, A., Matese, A., 2019. A Low-Cost and Unsupervised Image Recognition Methodology for Yield Estimation in a Vineyard. *Front Plant Sci* 10, 559.<https://doi.org/10.3389/fpls.2019.00559>.
- Dian, Y., Liu, X.Y., Hu, L., Zhang, J.Z., Hu, C.E., Liu, Y.Z., Zhang, J.X., Zhang, W.B., Hu, Q.Q., Zhang, Y.H., Fang, Y.N., Zhou, J.J., 2023. Characteristics of photosynthesis and vertical canopy architecture of citrus trees under two labor-saving cultivation modes using unmanned aerial vehicle (UAV)-based LiDAR data in citrus orchards. *Horticulture Research* 10.<https://doi.org/10.1093/hr/uhad018>.
- Dias, P.A., Tabb, A., Medeiros, H., 2018a. Apple flower detection using deep convolutional networks. *Computers in Industry* 99, 17-28.<https://doi.org/https://doi.org/10.1016/j.compind.2018.03.010>.
- Dias, P.A., Tabb, A., Medeiros, H., 2018b. Multispecies Fruit Flower Detection Using a Refined Semantic Segmentation Network. *Ieee Robotics and Automation Letters* 3, 3003-3010.<https://doi.org/10.1109/lra.2018.2849498>.
- Díaz-Varela, R., de la Rosa, R., León, L., Zarco-Tejada, P., 2015. High-Resolution Airborne UAV Imagery to Assess Olive Tree Crown Parameters Using 3D Photo Reconstruction: Application in Breeding Trials. *Remote Sens.* 7, 4213-4232.<https://doi.org/10.3390/rs70404213>.

- Dong, X.Y., Zhang, Z.C., Yu, R.Y., Tian, Q.J., Zhu, X.C., 2020. Extraction of Information about Individual Trees from High-Spatial-Resolution UAV-Acquired Images of an Orchard. *REMOTE SENSING* 12.<https://doi.org/10.3390/rs12010133>.
- Duan, S., Jia, H., Pang, Z., Teper, D., White, F., Jones, J., Zhou, C., Wang, N., 2018. Functional characterization of the citrus canker susceptibility gene CsLOB1. *Mol Plant Pathol*.<https://doi.org/10.1111/mpp.12667>.
- Duarte, L., Silva, P., Teodoro, A., 2018. Development of a QGIS Plugin to Obtain Parameters and Elements of Plantation Trees and Vineyards with Aerial Photographs. *ISPRS International Journal of Geo-Information* 7.<https://doi.org/10.3390/ijgi7030109>.
- Egea, G., Padilla-Díaz, C.M., Martínez-Guanter, J., Fernández, J.E., Pérez-Ruiz, M., 2017. Assessing a crop water stress index derived from aerial thermal imaging and infrared thermometry in super-high density olive orchards. *Agric. Water Manage.* 187, 210-221.<https://doi.org/10.1016/j.agwat.2017.03.030>.
- Escollà, A., Martínez-Casasnovas, J.A., Rufat, J., Arnó, J., Arbonés, A., Sebé, F., Pascual, M., Gregorio, E., Rosell-Polo, J.R., 2016. Mobile terrestrial laser scanner applications in precision fruticulture/horticulture and tools to extract information from canopy point clouds. *Precis. Agric.* 18, 111-132.<https://doi.org/10.1007/s11119-016-9474-5>.
- Falagas, M.E., Pitsouni, E.I., Malietzis, G.A., Pappas, G., 2008. Comparison of PubMed, Scopus, Web of Science, and Google Scholar: strengths and weaknesses. *Faseb Journal* 22, 338-342.<https://doi.org/10.1096/fj.07-9492LSF>.
- FAO, 2021. FAOSTAT.
- Farjon, G., Krikeb, O., Bar Hiller, A., Alchanatis, V., 2020. Detection and counting of flowers on apple trees for better chemical thinning decisions. *Precision Agriculture* 21, 503-521.<https://doi.org/10.1007/s11119-019-09679-1>.
- Felderhof, L., Gillieson, D., 2011. Near-infrared imagery from unmanned aerial systems and satellites can be used to specify fertilizer application rates in tree crops. *Canadian Journal of Remote Sensing* 37, 376-386.<https://doi.org/10.5589/m11-046>.
- Feng, B.K., Nie, S., Wang, C., Xi, X.H., Wang, J.L., Zhou, G.Q., Wang, H.Y., 2022. Exploring the Potential of UAV LiDAR Data for Trunk Point Extraction and Direct DBH Measurement. *Remote Sensing* 14.<https://doi.org/10.3390/rs14122753>.
- Fernandez, T., Perez, J.L., Cardenal, J., Gomez, J.M., Colomo, C., Delgado, J., 2016. Analysis of Landslide Evolution Affecting Olive Groves Using UAV and Photogrammetric Techniques. *Remote Sensing* 8.<https://doi.org/10.3390/rs8100837>.
- Forshey, C., 1986. Chemical fruit thinning of apples.
- Friedli, M., Kirchgessner, N., Grieder, C., Liebisch, F., Mannale, M., Walter, A., 2016. Terrestrial 3D laser scanning to track the increase in canopy height of both monocot and dicot crop species under field conditions. *Plant Methods* 12, 9.<https://doi.org/10.1186/s13007-016-0109-7>.
- Fu, L., Majeed, Y., Zhang, X., Karkee, M., Zhang, Q., 2020. Faster R-CNN-based apple detection in dense-foliage fruiting-wall trees using RGB and depth features for robotic harvesting. *Biosystems Engineering* 197, 245-256.<https://doi.org/https://doi.org/10.1016/j.biosystemseng.2020.07.007>.

References

- Ganz, S., Käber, Y., Adler, P., 2019. Measuring Tree Height with Remote Sensing—A Comparison of Photogrammetric and LiDAR Data with Different Field Measurements. *Forests* 10, 694.
- Gao, F., Fang, W., Sun, X., Wu, Z., Zhao, G., Li, G., Li, R., Fu, L., Zhang, Q., 2022. A novel apple fruit detection and counting methodology based on deep learning and trunk tracking in modern orchard. *Computers and Electronics in Agriculture* 197, 107000. <https://doi.org/https://doi.org/10.1016/j.compag.2022.107000>.
- Gao, P., Zhang, Y., Zhang, L., Noguchi, R., Ahamed, T., 2019. Development of a Recognition System for Spraying Areas from Unmanned Aerial Vehicles Using a Machine Learning Approach. *Sensors (Basel)* 19. <https://doi.org/10.3390/s19020313>.
- Garcia-Ruiz, F., Sankaran, S., Maja, J.M., Lee, W.S., Rasmussen, J., Ehsani, R., 2013. Comparison of two aerial imaging platforms for identification of Huanglongbing-infected citrus trees. *Comput. Electron. Agric.* 91, 106-115. <https://doi.org/10.1016/j.compag.2012.12.002>.
- Garza, B.N., Ancona, V., Enciso, J., Perotto-Baldivieso, H.L., Kunta, M., Simpson, C., 2020. Quantifying Citrus Tree Health Using True Color UAV Images. *Remote Sensing* 12. <https://doi.org/10.3390/rs12010170>.
- Gene-Mola, J., Gregorio, E., Guevara, J., Auat, F., Sanz-Cortiella, R., Escola, A., Llorens, J., Morros, J.R., Ruiz-Hidalgo, J., Vilaplana, V., Rosell-Polo, J.R., 2019a. Fruit detection in an apple orchard using a mobile terrestrial laser scanner. *Biosystems Engineering* 187, 171-184. <https://doi.org/10.1016/j.biosystemseng.2019.08.017>.
- Gene-Mola, J., Sanz-Cortiella, R., Rosell-Polo, J.R., Escola, A., Gregorio, E., 2021. In-field apple size estimation using photogrammetry-derived 3D point clouds: Comparison of 4 different methods considering fruit occlusions. *Computers and Electronics in Agriculture* 188. <https://doi.org/10.1016/j.compag.2021.106343>.
- Gené-Mola, J., Sanz-Cortiella, R., Rosell-Polo, J.R., Morros, J.-R., Ruiz-Hidalgo, J., Vilaplana, V., Gregorio, E., 2020. Fruit detection and 3D location using instance segmentation neural networks and structure-from-motion photogrammetry. *Computers and Electronics in Agriculture* 169, 105165. <https://doi.org/https://doi.org/10.1016/j.compag.2019.105165>.
- Gene-Mola, J., Vilaplana, V., Rosell-Polo, J.R., Morros, J.R., Ruiz-Hidalgo, J., Gregorio, E., 2019b. Multi-modal deep learning for Fuji apple detection using RGB-D cameras and their radiometric capabilities. *Computers and Electronics in Agriculture* 162, 689-698. <https://doi.org/10.1016/j.compag.2019.05.016>.
- Gibril, M.B.A., Shafri, H.Z.M., Shanableh, A., Al-Ruzouq, R., Wayayok, A., bin Hashim, S.J., Sachit, M.S., 2022. Deep convolutional neural networks and Swin transformer-based frameworks for individual date palm tree detection and mapping from large-scale UAV images. *Geocarto International* 37, 18569-18599. <https://doi.org/10.1080/10106049.2022.2142966>.
- Girona, J., 2002. REGULATED DEFICIT IRRIGATION IN PEACH. A GLOBAL ANALYSIS, 592 ed. International Society for Horticultural Science (ISHS), Leuven, Belgium, pp. 335-342. <https://doi.org/10.17660/ActaHortic.2002.592.47>.
- Glozer, K., Hasey, J., 2006. Mechanical Thinning in Cling Peach. 41, 995D. <https://doi.org/10.21273/hortsci.41.4.995d>.
- Gomez-Candon, D., Virlet, N., Labbe, S., Jolivot, A., Regnard, J.L., 2016. Field phenotyping of water stress at tree scale by UAV-sensed imagery: new insights for thermal acquisition and calibration. *Precis. Agric.* 17, 786-800. <https://doi.org/10.1007/s11119-016-9449-6>.

- Gongal, A., Silwal, A., Amatya, S., Karkee, M., Zhang, Q., Lewis, K., 2016. Apple crop-load estimation with over-the-row machine vision system. *Computers and Electronics in Agriculture* 120, 26-35. <https://doi.org/https://doi.org/10.1016/j.compag.2015.10.022>.
- Gonzalez-Dugo, V., Zarco-Tejada, P., Nicolas, E., Nortes, P.A., Alarcon, J.J., Intrigliolo, D.S., Fereres, E., 2013. Using high resolution UAV thermal imagery to assess the variability in the water status of five fruit tree species within a commercial orchard. *Precis. Agric.* 14, 660-678. <https://doi.org/10.1007/s11119-013-9322-9>.
- Gonzalez-Dugo, V., Zarco-Tejada, P.J., Fereres, E., 2014. Applicability and limitations of using the crop water stress index as an indicator of water deficits in citrus orchards. *Agric. For. Meteorol.* 198, 94-104. <https://doi.org/10.1016/j.agrformet.2014.08.003>.
- Greene, D., Costa, G., 2013. FRUIT THINNING IN POME- AND STONE-FRUIT: STATE OF THE ART, 998 ed. International Society for Horticultural Science (ISHS), Leuven, Belgium, pp. 93-102. <https://doi.org/10.17660/ActaHortic.2013.998.10>.
- Guillen-Climent, M.L., Zarco-Tejada, P.J., Berni, J.A.J., North, P.R.J., Villalobos, F.J., 2012. Mapping radiation interception in row-structured orchards using 3D simulation and high-resolution airborne imagery acquired from a UAV. *Precis. Agric.* 13, 473-500. <https://doi.org/10.1007/s11119-012-9263-8>.
- Guillen-Climent, M.L., Zarco-Tejada, P.J., Villalobos, F.J., 2014. Estimating Radiation Interception in Heterogeneous Orchards Using High Spatial Resolution Airborne Imagery. *Ieee Geoscience and Remote Sensing Letters* 11, 579-583. <https://doi.org/10.1109/lgrs.2013.2284660>.
- Gunder, M., Yamati, F.R.I., Kierdorf, J., Roscher, R., Mahlein, A.K., Bauckhage, C., 2022. Agricultural plant cataloging and establishment of a data framework from UAV-based crop images by computer vision. *Gigascience* 11. <https://doi.org/10.1093/gigascience/giac054>.
- Hadas, E., Jozkow, G., Walicka, A., Borkowski, A., 2019. Apple orchard inventory with a LiDAR equipped unmanned aerial system. *International Journal of Applied Earth Observation and Geoinformation* 82. <https://doi.org/10.1016/j.jag.2019.101911>.
- Halavatau, S., Halavatau, N.V., 2001. Food Security Strategies for the Kingdom of Tonga. United Nations Centre for Alleviation of Poverty Through Secondary Crops' Development in Asia and the Pacific (CAPSA), Working Papers.
- Handique, B.K., Khan, A.Q., Goswami, C., Prashnani, M., Gupta, C., Raju, P.L.N., 2017. Crop Discrimination Using Multispectral Sensor Onboard Unmanned Aerial Vehicle. *Proc. Nat. Acad. Sci. India A* 87, 713-719. <https://doi.org/10.1007/s40010-017-0443-9>.
- Ho, B., Kocer, B.B., Kovac, M., 2022. Vision based crown loss estimation for individual trees with remote aerial robots. *ISPRS Journal of Photogrammetry and Remote Sensing* 188, 75-88. <https://doi.org/https://doi.org/10.1016/j.isprsjprs.2022.04.002>.
- Hobart, M., Pflanz, M., Weltzien, C., Schirrmann, M., 2020. Growth Height Determination of Tree Walls for Precise Monitoring in Apple Fruit Production Using UAV Photogrammetry. *Remote Sensing* 12. <https://doi.org/10.3390/rs12101656>.
- Hocevar, M., Sirok, B., Godesa, T., Stopar, M., 2014. Flowering estimation in apple orchards by image analysis. *Precision Agriculture* 15, 466-478. <https://doi.org/10.1007/s11119-013-9341-6>.
- Horton, R., Cano, E., Bulanon, D., Fallahi, E., 2017. Peach Flower Monitoring Using Aerial Multispectral Imaging. *Journal of Imaging* 3. <https://doi.org/10.3390/jimaging3010002>.

References

- Hou, C.J., Tang, Y., Luo, S.M., Lin, J.T., He, Y., Zhuang, J.J., Huang, W.F., 2019. Optimization of control parameters of droplet density in citrus trees using UAVs and the Taguchi method. *International Journal of Agricultural and Biological Engineering* 12, 1-9.<https://doi.org/10.25165/j.ijabe.20191204.4139>.
- Hovenden, M.J., Wills, K.E., Vander Schoor, J.K., Williams, A.L., Newton, P.C.D., 2008. Flowering phenology in a species-rich temperate grassland is sensitive to warming but not elevated CO₂. *New Phytologist* 178, 815-822.<https://doi.org/https://doi.org/10.1111/j.1469-8137.2008.02419.x>.
- Huang, H.Q., Huang, T.B., Li, Z., Lyu, S.L., Hong, T., 2022. Design of Citrus Fruit Detection System Based on Mobile Platform and Edge Computer Device. *SENSORS* 22.<https://doi.org/10.3390/s22010059>.
- Hycza, T., Kupidura, P., 2021. Methods for separating orchards from forest using airborne LiDAR. *Annals of Forest Science* 78.<https://doi.org/10.1007/s13595-021-01116-6>.
- Iatrou, G., Mourelatos, S., Zartaloudis, Z., Iatrou, M., Gewehr, S., Kalaitzopoulou, S., 2016. REMOTE SENSING FOR THE MANAGEMENT OF VERTICILLIUM WILT OF OLIVE. *Fresenius Environmental Bulletin* 25, 3622-3628.
- Idso, S.B., Jackson, R.D., Reginato, R.J., 1978. Extending the 'Degree Day' Concept of Plant Phenological Development to Include Water Stress Effects. *Ecology* 59, 431-433.<https://doi.org/10.2307/1936570>.
- Ishida, T., Kurihara, J., Viray, F.A., Namuco, S.B., Paringit, E.C., Perez, G.J., Takahashi, Y., Marciano, J.J., 2018. A novel approach for vegetation classification using UAV-based hyperspectral imaging. *Comput. Electron. Agric.* 144, 80-85.<https://doi.org/10.1016/j.compag.2017.11.027>.
- Jackson, R.D., Idso, S.B., Reginato, R.J., Pinter Jr, P.J., 1981. Canopy temperature as a crop water stress indicator. *Water Resources Research* 17, 1133-1138.<https://doi.org/10.1029/WR017i004p01133>.
- Janowski, A., Kazmierczak, R., Kowalczyk, C., Szulwic, J., 2021. Detecting Apples in the Wild: Potential for Harvest Quantity Estimation. *Sustainability* 13.<https://doi.org/10.3390/su13148054>.
- Jarolmasjed, S., Sankaran, S., Marzougui, A., Kostick, S., Si, Y., Quiros Vargas, J.J., Evans, K., 2019. High-Throughput Phenotyping of Fire Blight Disease Symptoms Using Sensing Techniques in Apple. *Front Plant Sci* 10, 576.<https://doi.org/10.3389/fpls.2019.00576>.
- Ji, J., Zhu, X., Ma, H., Wang, H., Jin, X., Zhao, K., 2021. APPLE FRUIT RECOGNITION BASED ON A DEEP LEARNING ALGORITHM USING AN IMPROVED LIGHTWEIGHT NETWORK. *Applied Engineering in Agriculture* 37, 123-134.<https://doi.org/10.13031/aea.14041>.
- Jia, W.K., Zhang, Z.H., Shao, W.J., Ji, Z., Hou, S.J., 2022. RS-Net: robust segmentation of green overlapped apples. *Precision Agriculture* 23, 492-513.<https://doi.org/10.1007/s11119-021-09846-3>.
- Jimenez-Brenes, F.M., Lopez-Granados, F., de Castro, A.I., Torres-Sanchez, J., Serrano, N., Pena, J.M., 2017. Quantifying pruning impacts on olive tree architecture and annual canopy growth by using UAV-based 3D modelling. *Plant Methods* 13.<https://doi.org/10.1186/s13007-017-0205-3>.
- Jimenez-Brenes, F.M., Lopez-Granados, F., Torres-Sanchez, J., Pena, J.M., Ramirez, P., Castillejo-Gonzalez, I.L., de Castro, A.I., 2019. Automatic UAV-based detection of *Cynodon dactylon* for site-specific vineyard management. *PLoS One* 14, e0218132.<https://doi.org/10.1371/journal.pone.0218132>.
- Johansen, K., Raharjo, T., McCabe, M.F., 2018. Using Multi-Spectral UAV Imagery to Extract Tree Crop Structural Properties and Assess Pruning Effects. *Remote Sensing* 10, 21.<https://doi.org/10.3390/rs10060854>.

- Jones, H.G., 2013. *Plants and microclimate: a quantitative approach to environmental plant physiology*. Cambridge university press.
- Jorge, J., Vallbe, M., Soler, J.A., 2019. Detection of irrigation inhomogeneities in an olive grove using the NDRE vegetation index obtained from UAV images. *European Journal of Remote Sensing* 52, 169-177.<https://doi.org/10.1080/22797254.2019.1572459>.
- Jurado, J.M., López, A., Pádua, L., Sousa, J.J., 2022. Remote sensing image fusion on 3D scenarios: A review of applications for agriculture and forestry. *International Journal of Applied Earth Observation and Geoinformation* 112, 102856.<https://doi.org/https://doi.org/10.1016/j.jag.2022.102856>.
- K.R, A., A.K, K., B, S.S., K, P.P., Dhareshwar, C.V., Johnson, D.G., 2023. Manipal-UAV person detection dataset: A step towards benchmarking dataset and algorithms for small object detection. *ISPRS Journal of Photogrammetry and Remote Sensing* 195, 77-89.<https://doi.org/https://doi.org/10.1016/j.isprsjprs.2022.11.008>.
- Kamilaris, A., Prenafeta-Boldú, F.X., 2018. Deep learning in agriculture: A survey. *Computers and Electronics in Agriculture* 147, 70-90.<https://doi.org/https://doi.org/10.1016/j.compag.2018.02.016>.
- Kanwal, Z., Basit, A., Jawad, M., Ullah, I., Sanjrani, A.A., 2019. Overlapped Apple Fruit Yield Estimation using Pixel Classification and Hough Transform. *International Journal of Advanced Computer Science and Applications* 10, 567-573.
- Karydas, C., Gewehr, S., Iatrou, M., Iatrou, G., Mourelatos, S., 2017. Olive Plantation Mapping on a Sub-Tree Scale with Object-Based Image Analysis of Multispectral UAV Data; Operational Potential in Tree Stress Monitoring. *Journal of Imaging* 3.<https://doi.org/10.3390/jimaging3040057>.
- Kestur, R., Angural, A., Bashir, B., Omkar, S.N., Anand, G., Meenavathi, M.B., 2018. Tree Crown Detection, Delineation and Counting in UAV Remote Sensed Images: A Neural Network Based Spectral-Spatial Method. *J. Indian Soc. Remote Sens.* 46, 991-1004.<https://doi.org/10.1007/s12524-018-0756-4>.
- Khan, M.A., Akram, T., Sharif, M., Awais, M., Javed, K., Ali, H., Saba, T., 2018. CCDF: Automatic system for segmentation and recognition of fruit crops diseases based on correlation coefficient and deep CNN features. *Comput. Electron. Agric.* 155, 220-236.<https://doi.org/10.1016/j.compag.2018.10.013>.
- Koc-San, D., Selim, S., Aslan, N., San, B.T., 2018. Automatic citrus tree extraction from UAV images and digital surface models using circular Hough transform. *Comput. Electron. Agric.* 150, 289-301.<https://doi.org/10.1016/j.compag.2018.05.001>.
- Koirala, A., Walsh, K.B., Wang, Z., Anderson, N., 2020a. Deep Learning for Mango (*Mangifera indica*) Panicle Stage Classification. *Agronomy* 10, 143.
- Koirala, A., Walsh, K.B., Wang, Z., McCarthy, C., 2019. Deep learning – Method overview and review of use for fruit detection and yield estimation. *Computers and Electronics in Agriculture* 162, 219-234.<https://doi.org/https://doi.org/10.1016/j.compag.2019.04.017>.
- Koirala, A., Walsh, K.B., Wang, Z.L., Anderson, N., 2020b. Deep Learning for Mango (*Mangifera indica*) Panicle Stage Classification. *Agronomy-Basel* 10, 21.<https://doi.org/10.3390/agronomy10010143>.
- Koirala, A., Walsh, K.B., Wang, Z.L., Anderson, N., 2020c. Deep Learning for Mango (*Mangifera indica*) Panicle Stage Classification. *Agronomy-Basel* 10.<https://doi.org/10.3390/agronomy10010143>.

References

- Lee, J., Gadsden, S.A., Biglarbegian, M., Cline, J.A., 2022. Smart Agriculture: A Fruit Flower Cluster Detection Strategy in Apple Orchards Using Machine Vision and Learning. *APPLIED SCIENCES-BASEL* 12.<https://doi.org/10.3390/app122211420>.
- Leroux, C., Tisseyre, B., 2019. How to measure and report within-field variability: a review of common indicators and their sensitivity. *Precision Agriculture* 20, 562-590.<https://doi.org/10.1007/s11119-018-9598-x>.
- Li, B., Chen, C., 2022. Location of Fruits by Counting: A Point-to-Point Approach. *Agronomy* 12, 2863.
- Li, D.H., Sun, X.X., Jia, Y.H., Yao, Z.W., Lin, P.Y., Chen, Y.Y., Zhou, H.B., Zhou, Z.Q., Wu, K.X., Shi, L.L., Li, J., 2023a. A longan yield estimation approach based on UAV images and deep learning. *Frontiers in Plant Science* 14.<https://doi.org/10.3389/fpls.2023.1132909>.
- Li, G., Fu, L., Gao, C., Fang, W., Zhao, G., Shi, F., Dhupia, J., Zhao, K., Li, R., Cui, Y., 2022. Multi-class detection of kiwifruit flower and its distribution identification in orchard based on YOLOv5l and Euclidean distance. *Computers and Electronics in Agriculture* 201, 107342.<https://doi.org/10.1016/j.compag.2022.107342>.
- Li, Y.P., Rao, Y., Jin, X., Jiang, Z.H., Wang, Y.W., Wang, T., Wang, F.Y., Luo, Q., Liu, L., 2023b. YOLOv5s-FP: A Novel Method for In-Field Pear Detection Using a Transformer Encoder and Multi-Scale Collaboration Perception. *SENSORS* 23.<https://doi.org/10.3390/s23010030>.
- Liakos, V., Tagarakis, A., Aggelopoulou, K., Fountas, S., Nanos, G.D., Gemtos, T., 2017. In-season prediction of yield variability in an apple orchard. *European Journal of Horticultural Science* 82, 251-259.<https://doi.org/10.17660/eJHS.2017/82.5.5>.
- Liang, J.T., Chen, X., Liang, C.J., Long, T., Tang, X.Y., Shi, Z.M., Zhou, M., Zhao, J., Lan, Y.B., Long, Y.B., 2023. A detection approach for late-autumn shoots of litchi based on unmanned aerial vehicle (UAV) remote sensing. *COMPUTERS AND ELECTRONICS IN AGRICULTURE* 204.<https://doi.org/10.1016/j.compag.2022.107535>.
- Lima-Cueto, F.J., Blanco-Sepulveda, R., Gomez-Moreno, M.L., Galacho-Jimenez, F.B., 2019. Using Vegetation Indices and a UAV Imaging Platform to Quantify the Density of Vegetation Ground Cover in Olive Groves (*Olea Europaea* L.) in Southern Spain. *Remote Sensing* 11.<https://doi.org/10.3390/rs11212564>.
- Lin, J., Li, J., Yang, Z., Lu, H., Ding, Y., Cui, H., 2022. Estimating litchi flower number using a multicolumn convolutional neural network based on a density map. *Precision Agriculture* 23, 1226-1247.<https://doi.org/10.1007/s11119-022-09882-7>.
- Lin, P., Lee, W.S., Chen, Y.M., Peres, N., Fraisse, C., 2020. A deep-level region-based visual representation architecture for detecting strawberry flowers in an outdoor field. *Precision Agriculture* 21, 387-402.<https://doi.org/10.1007/s11119-019-09673-7>.
- Lin, T.-Y., Maire, M., Belongie, S., Hays, J., Perona, P., Ramanan, D., Dollár, P., Zitnick, C.L., 2014. Microsoft coco: Common objects in context, *Computer Vision–ECCV 2014: 13th European Conference, Zurich, Switzerland, September 6-12, 2014, Proceedings, Part V* 13. Springer, pp. 740-755.
- Linker, R., Cohen, O., Naor, A., 2012. Determination of the number of green apples in RGB images recorded in orchards. *Computers and Electronics in Agriculture* 81, 45-57.<https://doi.org/10.1016/j.compag.2011.11.007>.
- Liu, X.F., Lyu, Q., He, S.L., Yi, S.L., Hu, D.Y., Wang, Z.T., Xie, R.J., Zheng, Y.Q., Deng, L., 2016. Estimation of carbon and nitrogen contents in citrus canopy by low-altitude remote sensing.

- International Journal of Agricultural and Biological Engineering 9, 149-157.<https://doi.org/10.3965/j.ijabe.20160905.2246>.
- Liu, X.J., Wu, X.T., Peng, Y., Mo, J.C., Fang, S.H., Gong, Y., Zhu, R.N., Wang, J., Zhang, C.R., 2023. Application of UAV-retrieved canopy spectra for remote evaluation of rice full heading date. *Science of Remote Sensing* 7.<https://doi.org/10.1016/j.srs.2023.100090>.
- Liu, Y.K., Yang, G.P., Huang, Y.W., Yin, Y.L., 2021. SE-Mask R-CNN: An improved Mask R-CNN for apple detection and segmentation. *Journal of Intelligent & Fuzzy Systems* 41, 6715-6725.<https://doi.org/10.3233/jifs-210597>.
- Lombardi, E., Rodríguez-Puerta, F., Santini, F., Chambel, M.R., Climent, J., Resco de Dios, V., Voltas, J., 2022. UAV-LiDAR and RGB Imagery Reveal Large Intraspecific Variation in Tree-Level Morphometric Traits across Different Pine Species Evaluated in Common Gardens. *Remote Sensing* 14, 5904.
- Lopez-Granados, F., Torres-Sanchez, J., Jimenez-Brenes, F.M., Arquero, O., Lovera, M., de Castro, A.I., 2019a. An efficient RGB-UAV-based platform for field almond tree phenotyping: 3-D architecture and flowering traits. *Plant Methods* 15, 16.<https://doi.org/10.1186/s13007-019-0547-0>.
- Lopez-Granados, F., Torres-Sanchez, J., Jimenez-Brenes, F.M., Arquero, O., Lovera, M., de Castro, A.I., 2019b. An efficient RGB-UAV-based platform for field almond tree phenotyping: 3-D architecture and flowering traits. *Plant Methods* 15.<https://doi.org/10.1186/s13007-019-0547-0>.
- Lu, J., Lin, W., Chen, P., Lan, Y., Deng, X., Niu, H., Mo, J., Li, J., Luo, S., 2021. Research on Lightweight Citrus Flowering Rate Statistical Model Combined with Anchor Frame Clustering Optimization. *Sensors* 21, 7929.
- Lucena, F., Breunig, F.M., Kux, H., 2022. The Combined Use of UAV-Based RGB and DEM Images for the Detection and Delineation of Orange Tree Crowns with Mask R-CNN: An Approach of Labeling and Unified Framework. *Future Internet* 14, 275.
- Lyu, H.K., Park, C.H., Han, D.H., Kwak, S.W., Choi, B., 2018. Orchard Free Space and Center Line Estimation Using Naive Bayesian Classifier for Unmanned Ground Self-Driving Vehicle. *Symmetry-Basel* 10.<https://doi.org/10.3390/sym10090355>.
- Machovina, B.L., Feeley, K.J., Machovina, B.J., 2016. UAV remote sensing of spatial variation in banana production. *Crop & Pasture Science* 67, 1281-1287.<https://doi.org/10.1071/cp16135>.
- Mahmud, M.S., He, L., Zahid, A., Heinemann, P., Choi, D., Krawczyk, G., Zhu, H., 2023. Detection and infected area segmentation of apple fire blight using image processing and deep transfer learning for site-specific management. *Computers and Electronics in Agriculture* 209, 107862.<https://doi.org/https://doi.org/10.1016/j.compag.2023.107862>.
- Malambo, L., Popescu, S.C., Horne, D.W., Pugh, N.A., Rooney, W.L., 2019. Automated detection and measurement of individual sorghum panicles using density-based clustering of terrestrial lidar data. *Isprs Journal of Photogrammetry and Remote Sensing* 149, 1-13.<https://doi.org/10.1016/j.isprsjprs.2018.12.015>.
- Marques, P., Padua, L., Adao, T., Hruska, J., Peres, E., Sousa, A., Sousa, J.J., 2019. UAV-Based Automatic Detection and Monitoring of Chestnut Trees. *Remote Sensing* 11.<https://doi.org/10.3390/rs11070855>.
- Marris, E., 2013. Drones in science: Fly, and bring me data. *Nature* 498, 156-158.<https://doi.org/10.1038/498156a>.

References

- Martínez-Casasnovas, J.A., Sandoñis-Pozo, L., Escolà, A., Arnó, J., Llorens, J., 2022. Delineation of Management Zones in Hedgerow Almond Orchards Based on Vegetation Indices from UAV Images Validated by LiDAR-Derived Canopy Parameters. *Agronomy* 12, 102.
- Martínez-Guanter, J., Agüera, P., Agüera, J., Pérez-Ruiz, M., 2019. Spray and economics assessment of a UAV-based ultra-low-volume application in olive and citrus orchards. *Precis. Agric.* <https://doi.org/10.1007/s11119-019-09665-7>.
- Matese, A., Di Gennaro, S.F., Santesteban, L.G., 2019. Methods to compare the spatial variability of UAV-based spectral and geometric information with ground autocorrelated data. A case of study for precision viticulture. *Comput. Electron. Agric.* 162, 931-940. <https://doi.org/10.1016/j.compag.2019.05.038>.
- Méndez, V., Pérez-Romero, A., Sola-Guirado, R., Miranda-Fuentes, A., Manzano-Agugliaro, F., Zapata-Sierra, A., Rodríguez-Lizana, A., 2019. In-Field Estimation of Orange Number and Size by 3D Laser Scanning. *Agronomy* 9, 885.
- Mendez-Vazquez, L.J., Lira-Noriega, A., Lasa-Covarrubias, R., Cerdeira-Estrada, S., 2019. Delineation of site-specific management zones for pest control purposes: Exploring precision agriculture and species distribution modeling approaches. *Computers and Electronics in Agriculture* 167. <https://doi.org/10.1016/j.compag.2019.105101>.
- Meng, Y., Zhong, W., Liu, Y., Wang, M., Lan, Y., 2022. Droplet distribution of an autonomous UAV-based sprayer in citrus tree canopy, *Journal of Physics: Conference Series*. IOP Publishing, p. 012022.
- Meng, Y.H., Su, J.Y., Song, J.L., Chen, W.H., Lan, Y.B., 2020. Experimental evaluation of UAV spraying for peach trees of different shapes: Effects of operational parameters on droplet distribution. *Computers and Electronics in Agriculture* 170. <https://doi.org/10.1016/j.compag.2020.105282>.
- Mesas-Carrascosa, F.J., Perez-Porras, F., de Larriva, J.E.M., Frau, C.M., Agüera-Vega, F., Carvajal-Ramirez, F., Martínez-Carricondo, P., García-Ferrer, A., 2018. Drift Correction of Lightweight Microbolometer Thermal Sensors On-Board Unmanned Aerial Vehicles. *Remote Sens.* 10. <https://doi.org/10.3390/rs10040615>.
- Methley, A.M., Campbell, S., Chew-Graham, C., McNally, R., Cheraghi-Sohi, S., 2014. PICO, PICOS and SPIDER: a comparison study of specificity and sensitivity in three search tools for qualitative systematic reviews. *Bmc Health Services Research* 14. <https://doi.org/10.1186/s12913-014-0579-0>.
- Mills, L., Flemmer, R., Flemmer, C., Bakker, H., 2019. Prediction of kiwifruit orchard characteristics from satellite images. *Precision Agriculture* 20, 911-925. <https://doi.org/10.1007/s11119-018-09622-w>.
- Miranda-Fuentes, A., Llorens, J., Gamarra-Diezma, J.L., Gil-Ribes, J.A., Gil, E., 2015. Towards an optimized method of olive tree crown volume measurement. *Sensors (Basel)* 15, 3671-3687. <https://doi.org/10.3390/s150203671>.
- Mitchell, P.D., 1986. Pear Fruit Growth and the Use of Diameter to Estimate Fruit Volume and Weight. *HortScience* 21, 1003-1005. <https://doi.org/10.21273/HORTSCI.21.4.1003>.
- Mo, J., Lan, Y., Yang, D., Wen, F., Qiu, H., Chen, X., Deng, X., 2021. Deep Learning-Based Instance Segmentation Method of Litchi Canopy from UAV-Acquired Images. *Remote Sensing* 13, 3919.
- Moorthy, I., Miller, J.R., Berni, J.A.J., Zarco-Tejada, P., Hu, B., Chen, J., 2011. Field characterization of olive (*Olea europaea* L.) tree crown architecture using terrestrial laser scanning data. *Agric. For. Meteorol.* 151, 204-214. <https://doi.org/10.1016/j.agrformet.2010.10.005>.

- Mu, X., He, L., Heinemann, P., Schupp, J., Karkee, M., 2023. Mask R-CNN based apple flower detection and king flower identification for precision pollination. *Smart Agricultural Technology* 4, 100151. <https://doi.org/https://doi.org/10.1016/j.atech.2022.100151>.
- Mu, Y., Fujii, Y., Takata, D., Zheng, B.Y., Noshita, K., Honda, K., Ninomiya, S., Guo, W., 2018. Characterization of peach tree crown by using high-resolution images from an unmanned aerial vehicle. *Horticulture Research* 5. <https://doi.org/10.1038/s41438-018-0097-z>.
- Nasirahmadi, A., Hensel, O., 2022. Toward the Next Generation of Digitalization in Agriculture Based on Digital Twin Paradigm. *Sensors* 22. <https://doi.org/10.3390/s22020498>.
- Neupane, B., Horanont, T., Hung, N.D., 2019. Deep learning based banana plant detection and counting using high-resolution red-green-blue (RGB) images collected from unmanned aerial vehicle (UAV). *Plos One* 14. <https://doi.org/10.1371/journal.pone.0223906>.
- Nguyen, T.T., Vandevoorde, K., Wouters, N., Kayacan, E., De Baerdemaeker, J.G., Saeys, W., 2016. Detection of red and bicoloured apples on tree with an RGB-D camera. *Biosystems Engineering* 146, 33-44. <https://doi.org/10.1016/j.biosystemseng.2016.01.007>.
- O'Neill, W.T., Henderson, J., Pattemore, J.A., O'Dwyer, C., Perry, S., Beasley, D.R., Tan, Y.P., Smyth, A.L., Goosem, C.H., Thomson, K.M., Hobbs, R.L., Grice, K.R.E., Trevorrow, P., Vawdrey, L.L., Pathania, N., Shivas, R.G., 2016. Detection of *Fusarium oxysporum* f. sp. *cubense* tropical race 4 strain in northern Queensland. *Australas. Plant Dis. Notes* 11, 3. <https://doi.org/10.1007/s13314-016-0218-1>.
- Ok, A.O., Ozdarici-Ok, A., 2018a. 2-D delineation of individual citrus trees from UAV-based dense photogrammetric surface models. *Int. J. Digit. Earth* 11, 583-608. <https://doi.org/10.1080/17538947.2017.1337820>.
- Ok, A.O., Ozdarici-Ok, A., 2018b. Combining Orientation Symmetry and LM Cues for the Detection of Citrus Trees in Orchards From a Digital Surface Model. *Ieee Geoscience and Remote Sensing Letters* 15, 1817-1821. <https://doi.org/10.1109/lgrs.2018.2865003>.
- Ortega-Farías, S., Ortega-Salazar, S., Poblete, T., Kilic, A., Allen, R., Poblete-Echeverría, C., Ahumada-Orellana, L., Zuñiga, M., Sepúlveda, D., 2016. Estimation of Energy Balance Components over a Drip-Irrigated Olive Orchard Using Thermal and Multispectral Cameras Placed on a Helicopter-Based Unmanned Aerial Vehicle (UAV). *Remote Sensing* 8. <https://doi.org/10.3390/rs8080638>.
- Osco, L.P., Arruda, M.d.S.d., Marcato Junior, J., da Silva, N.B., Ramos, A.P.M., Moryia, É.A.S., Imai, N.N., Pereira, D.R., Creste, J.E., Matsubara, E.T., Li, J., Gonçalves, W.N., 2020a. A convolutional neural network approach for counting and geolocating citrus-trees in UAV multispectral imagery. *ISPRS Journal of Photogrammetry and Remote Sensing* 160, 97-106. <https://doi.org/https://doi.org/10.1016/j.isprsjprs.2019.12.010>.
- Osco, L.P., de Arruda, M.D., Marcato, J., da Silva, N.B., Ramos, A.P.M., Moryia, E.A.S., Imai, N.N., Pereira, D.R., Creste, J.E., Matsubara, E.T., Li, J., Goncalves, W.N., 2020b. A convolutional neural network approach for counting and geolocating citrus-trees in UAV multispectral imagery. *ISPRS-J. Photogramm. Remote Sens.* 160, 97-106. <https://doi.org/10.1016/j.isprsjprs.2019.12.010>.
- Osco, L.P., Marques Ramos, A.P., Saito Moriya, É.A., de Souza, M., Marcato Junior, J., Matsubara, E.T., Imai, N.N., Creste, J.E., 2019a. Improvement of leaf nitrogen content inference in Valencia-orange trees applying spectral analysis algorithms in UAV mounted-sensor images. *International Journal of Applied Earth Observation and Geoinformation* 83. <https://doi.org/10.1016/j.jag.2019.101907>.
- Osco, L.P., Ramos, A.P.M., Pereira, D.R., Moriya, E.A.S., Imai, N.N., Matsubara, E.T., Estrabis, N., de Souza, M., Marcato, J., Goncalves, W.N., Li, J., Liesenberg, V., Creste, J.E., 2019b. Predicting Canopy

References

- Nitrogen Content in Citrus-Trees Using Random Forest Algorithm Associated to Spectral Vegetation Indices from UAV-Imagery. *Remote Sensing* 11.<https://doi.org/10.3390/rs11242925>.
- Osman, Y., Dennis, R., Elgazzar, K., 2021. Yield Estimation and Visualization Solution for Precision Agriculture. *Sensors* 21.<https://doi.org/10.3390/s21196657>.
- Ozden, C., 2021. Apple leaf disease detection and classification based on transfer learning. *Turkish Journal of Agriculture and Forestry* 45, 775-783.<https://doi.org/10.3906/tar-2010-100>.
- Pan, L., Zhang, W., Zhu, N., Mao, S., Tu, K., 2014. Early detection and classification of pathogenic fungal disease in post-harvest strawberry fruit by electronic nose and gas chromatography–mass spectrometry. *Food Research International* 62, 162-168.<https://doi.org/10.1016/j.foodres.2014.02.020>.
- Panda, S.S., Hoogenboom, G., Paz, J.O., 2010. Remote Sensing and Geospatial Technological Applications for Site-specific Management of Fruit and Nut Crops: A Review. *Remote Sens.* 2, 1973-1997.<https://doi.org/10.3390/rs2081973>.
- Park, S., Ryu, D., Fuentes, S., Chung, H., Hernyandez-Montes, E., O'Connell, M., 2017. Adaptive Estimation of Crop Water Stress in Nectarine and Peach Orchards Using High-Resolution Imagery from an Unmanned Aerial Vehicle (UAV). *Remote Sensing* 9.<https://doi.org/10.3390/rs9080828>.
- Pathak, H.S., Brown, P., Best, T., 2019. A systematic literature review of the factors affecting the precision agriculture adoption process. *Precision Agriculture* 20, 1292-1316.<https://doi.org/10.1007/s11119-019-09653-x>.
- Peng, H., Shao, Y., Chen, K., Deng, Y., Xue, C., 2018. Research on Multi-class Fruits Recognition Based on Machine Vision and SVM. *IFAC-PapersOnLine* 51, 817-821.<https://doi.org/https://doi.org/10.1016/j.ifacol.2018.08.094>.
- Perry, E.M., Dezzani, R.J., Seavert, C.F., Pierce, F.J., 2009. Spatial variation in tree characteristics and yield in a pear orchard. *Precis. Agric.* 11, 42-60.<https://doi.org/10.1007/s11119-009-9113-5>.
- Perry, E.M., Dezzani, R.J., Seavert, C.F., Pierce, F.J., 2010. Spatial variation in tree characteristics and yield in a pear orchard. *Precision Agriculture* 11, 42-60.<https://doi.org/10.1007/s11119-009-9113-5>.
- Perry, E.M., Goodwin, I., Cornwall, D., 2018. Remote Sensing Using Canopy and Leaf Reflectance for Estimating Nitrogen Status in Red-blush Pears. *Hortscience* 53, 78-83.<https://doi.org/10.21273/hortsci12391-17>.
- Pichon, L., Leroux, C., Macombe, C., Taylor, J., Tisseyre, B., 2019. What relevant information can be identified by experts on unmanned aerial vehicles' visible images for precision viticulture? *Precis. Agric.* 20, 278-294.<https://doi.org/10.1007/s11119-019-09634-0>.
- Piljek, P., Pranjić, M., Kotarski, D., Petanjek, T., 2022. Autonomous Aerial Robotic System for Smart Spraying Tasks: Potentials and Limitations, *Digital Agriculture, Methods and Applications*. IntechOpen.
- Pourazar, H., Samadzadegan, F., Javan, F.D., 2019. Aerial multispectral imagery for plant disease detection: radiometric calibration necessity assessment. *European Journal of Remote Sensing* 52, 17-31.<https://doi.org/10.1080/22797254.2019.1642143>.
- Qi, P., Zhang, L.T., Wang, Z.C., Han, H., Mueller, J., Li, T., Wang, C.L., Huang, Z., He, M., Liu, Y.J., He, X.K., 2023. Effect of Operational Parameters of Unmanned Aerial Vehicle (UAV) on Droplet Deposition in Trellised Pear Orchard. *Drones* 7.<https://doi.org/10.3390/drones7010057>.

- Qian, J.P., Xing, B., Wu, X.M., Chen, M.X., Wang, Y.A., 2018. A smartphone-based apple yield estimation application using imaging features and the ANN method in mature period. *Scientia Agricola* 75, 273-280.<https://doi.org/10.1590/1678-992x-2016-0152>.
- Qureshi, J.A., Kostyk, B.C., Stansly, P.A., 2017. Single and Multiple Modes of Action Insecticides for Control of Asian Citrus Psyllid and Citrus Leafminer. *HortScience* 52, 732-735.<https://doi.org/10.21273/hortsci11726-17>.
- Racszó, J., 2006. Crop Load, Fruit Thinning and their Effects on Fruit Quality of Apple (*Malus domestica* Borkh.). *JOURNAL OF AGRICULTURAL SCIENCES* 24.<https://doi.org/10.34101/actaagrar/24/3221>.
- Rahman, M., Robson, A., Bristow, M., 2018a. Exploring the Potential of High Resolution WorldView-3 Imagery for Estimating Yield of Mango. *Remote Sens.* 10.<https://doi.org/10.3390/rs10121866>.
- Rahman, M.M., Robson, A., Bristow, M., 2018b. Exploring the Potential of High Resolution WorldView-3 Imagery for Estimating Yield of Mango. *Remote Sensing* 10, 1866.
- Raman, M.G., Carlos, E.F., Sankaran, S., 2022. Optimization and Evaluation of Sensor Angles for Precise Assessment of Architectural Traits in Peach Trees. *SENSORS* 22.<https://doi.org/10.3390/s22124619>.
- Raman, M.G., Marzougui, A., Teh, S.L., York, Z.B., Evans, K.M., Sankaran, S., 2023a. Rapid Assessment of Architectural Traits in Pear Rootstock Breeding Program Using Remote Sensing Techniques. *Remote Sensing* 15, 1483.
- Raman, M.G., Marzougui, A., Teh, S.L., York, Z.B., Evans, K.M., Sankaran, S., 2023b. Rapid Assessment of Architectural Traits in Pear Rootstock Breeding Program Using Remote Sensing Techniques. *Remote Sensing* 15.<https://doi.org/10.3390/rs15061483>.
- Rom, C.R., 1991. Light Thresholds for Apple Tree Canopy Growth and Development. 26, 989.<https://doi.org/10.21273/hortsci.26.8.989>.
- Romero-Trigueros, C., Nortes, P.A., Alarcon, J.J., Hunink, J.E., Parra, M., Contreras, S., Droogers, P., Nicolas, E., 2017. Effects of saline reclaimed waters and deficit irrigation on Citrus physiology assessed by UAV remote sensing. *Agric. Water Manage.* 183, 60-69.<https://doi.org/10.1016/j.agwat.2016.09.014>.
- Sabzi, S., Abbaspour-Gilandeh, Y., Garcia-Mateos, G., Ruiz-Canales, A., Molina-Martinez, J.M., 2018. Segmentation of Apples in Aerial Images under Sixteen Different Lighting Conditions Using Color and Texture for Optimal Irrigation. *Water* 10.<https://doi.org/10.3390/w10111634>.
- Salami, E., Gallardo, A., Skorobogatov, G., Barrado, C., 2019. On-the-Fly Olive Trees Counting Using a UAS and Cloud Services. *Remote Sens.* 11.<https://doi.org/10.3390/rs11030316>.
- Saldana Ochoa, K., Guo, Z., 2019. A framework for the management of agricultural resources with automated aerial imagery detection. *Comput. Electron. Agric.* 162, 53-69.<https://doi.org/10.1016/j.compag.2019.03.028>.
- Salgadoe, A., Robson, A., Lamb, D., Dann, E., Searle, C., 2018. Quantifying the Severity of Phytophthora Root Rot Disease in Avocado Trees Using Image Analysis. *Remote Sens.* 10.<https://doi.org/10.3390/rs10020226>.
- Salm, H., Geider, K., 2004. Real-time PCR for detection and quantification of *Erwinia amylovora*, the causal agent of fireblight. *Plant Pathology* 53, 602-610.<https://doi.org/10.1111/j.1365-3059.2004.01066.x>.

References

- Sanders, K.F., 2005. Orange Harvesting Systems Review. *Biosystems Engineering* 90, 115-125.<https://doi.org/https://doi.org/10.1016/j.biosystemseng.2004.10.006>.
- Sandonís-Pozo, L., Llorens, J., Escolà, A., Arnó, J., Pascual, M., Martínez-Casasnovas, J.A., 2022. Satellite multispectral indices to estimate canopy parameters and within-field management zones in super-intensive almond orchards. *Precision Agriculture* 23, 2040-2062.<https://doi.org/10.1007/s11119-022-09956-6>.
- Şandric, I., Irimia, R., Petropoulos, G.P., Anand, A., Srivastava, P.K., Pleşoianu, A., Faraslis, I., Stateras, D., Kalivas, D., 2022. Tree's detection & health's assessment from ultra-high resolution UAV imagery and deep learning. *Geocarto International*, 1-21.
- Sankaran, S., Mishra, A., Maja, J.M., Ehsani, R., 2011. Visible-near infrared spectroscopy for detection of Huanglongbing in citrus orchards. *Comput. Electron. Agric.* 77, 127-134.<https://doi.org/10.1016/j.compag.2011.03.004>.
- Sarron, J., Malézieux, É., Sané, C., Faye, É., 2018a. Mango Yield Mapping at the Orchard Scale Based on Tree Structure and Land Cover Assessed by UAV. *Remote Sens.* 10.<https://doi.org/10.3390/rs10121900>.
- Sarron, J., Malezieux, E., Sane, C.A.B., Faye, E., 2018b. Mango Yield Mapping at the Orchard Scale Based on Tree Structure and Land Cover Assessed by UAV. *REMOTE SENSING* 10.<https://doi.org/10.3390/rs10121900>.
- Scalisi, A., McClymont, L., Underwood, J., Morton, P., Scheduling, S., Goodwin, I., 2021. Reliability of a commercial platform for estimating flower cluster and fruit number, yield, tree geometry and light interception in apple trees under different rootstocks and row orientations. *Computers and Electronics in Agriculture* 191, 106519.<https://doi.org/https://doi.org/10.1016/j.compag.2021.106519>.
- Selvaraj, M.G., Vergara, A., Montenegro, F., Ruiz, H.A., Safari, N., Raymaekers, D., Ocimati, W., Ntamwira, J., Tits, L., Omondi, A.B., Blomme, G., 2020. Detection of banana plants and their major diseases through aerial images and machine learning methods: A case study in DR Congo and Republic of Benin. *Isprs Journal of Photogrammetry and Remote Sensing* 169, 110-124.<https://doi.org/10.1016/j.isprsiprs.2020.08.025>.
- Sepulcre-Canto, G., Zarco-Tejada, P.J., Jimenez-Munoz, J.C., Sobrino, J.A., Soriano, M.A., Fereres, E., Vega, V., Pastor, M., 2007. Monitoring yield and fruit quality parameters in open-canopy tree crops under water stress. Implications for ASTER. *Remote Sensing of Environment* 107, 455-470.<https://doi.org/10.1016/j.rse.2006.09.014>.
- Shackel, K.A., Ahmadi, H., Biasi, W., Buchner, R., Goldhamer, D., Gurusinge, S., Hasey, J., Kester, D., Krueger, B., Lampinen, B., McGourty, G., Micke, W., Mitcham, E., Olson, B., Pelletrau, K., Philips, H., Ramos, D., Schwankl, L., Sibbett, S., Snyder, R., Southwick, S., Stevenson, M., Thorpe, M., Weinbaum, S., Yeager, J., 1997. Plant Water Status as an Index of Irrigation Need in Deciduous Fruit Trees. *HortTechnology* 7, 23-29.<https://doi.org/10.21273/horttech.7.1.23>.
- Shakoor, N., Lee, S., Mockler, T.C., 2017. High throughput phenotyping to accelerate crop breeding and monitoring of diseases in the field. *Curr Opin Plant Biol* 38, 184-192.<https://doi.org/10.1016/j.pbi.2017.05.006>.
- Shen, Y.Y., Liu, D., Zhang, F.Z., Zhang, Q.L., 2022. Fast and accurate multi-class geospatial object detection with large-size remote sensing imagery using CNN and Truncated NMS. *ISPRS JOURNAL OF PHOTOGRAMMETRY AND REMOTE SENSING* 191, 235-249.<https://doi.org/10.1016/j.isprsiprs.2022.07.019>.

- Shim, H., Min, Y., Hong, S., Kwon, M., Kini, D., Kim, H., Choi, Y., Lee, S., Yang, J., 2004. Nucleotide sequences of a Korean isolate of apple stem grooving virus associated with black necrotic leaf spot disease on pear (*Pyrus pyrifolia*). *Molecules and Cells* 18, 192-199.
- Sola-Guirado, R.R., Castillo-Ruiz, F.J., Jimenez-Jimenez, F., Blanco-Roldan, G.L., Castro-Garcia, S., Gil-Ribes, J.A., 2017. Olive Actual "on Year" Yield Forecast Tool Based on the Tree Canopy Geometry Using UAS Imagery. *Sensors (Basel)* 17.<https://doi.org/10.3390/s17081743>.
- Somers, B., Delalieux, S., Verstraeten, W., Eynde, A., Barry, G., Coppin, P., 2010. The Contribution of the Fruit Component to the Hyperspectral Citrus Canopy Signal. *Photogrammetric Engineering & Remote Sensing* 76, 37-47.<https://doi.org/10.14358/PERS.76.1.37>.
- Srivastava, S., Sadistap, S., 2017. Non-destructive sensing methods for quality assessment of on-tree fruits: a review. *Journal of Food Measurement and Characterization* 12, 497-526.<https://doi.org/10.1007/s11694-017-9663-6>.
- Srivastava, S., Sadistap, S., 2018. Non-destructive sensing methods for quality assessment of on-tree fruits: a review. *Journal of Food Measurement and Characterization* 12, 497-526.<https://doi.org/10.1007/s11694-017-9663-6>.
- Stagakis, S., Gonzalez-Dugo, V., Cid, P., Guillen-Climent, M.L., Zarco-Tejada, P.J., 2012. Monitoring water stress and fruit quality in an orange orchard under regulated deficit irrigation using narrow-band structural and physiological remote sensing indices. *ISPRS-J. Photogramm. Remote Sens.* 71, 47-61.<https://doi.org/10.1016/j.isprsjprs.2012.05.003>.
- Stajanko, D., Rakun, J., Blanke, M., 2009a. Modelling Apple Fruit Yield Using Image Analysis for Fruit Colour, Shape and Texture. *European Journal of Horticultural Science* 74, 260-267.
- Stajanko, D., Rakun, J., Blanke, M., 2009b. Modelling apple fruit yield using image analysis for fruit colour, shape and texture. *European Journal of Horticultural Science* 74, 260-267.
- Stefas, N., Bayram, H., Isler, V., 2019. Vision-based monitoring of orchards with UAVs. *Comput. Electron. Agric.* 163.<https://doi.org/10.1016/j.compag.2019.05.023>.
- Stella, A., Caliendo, G., Melgani, F., Goller, R., Barazzuol, M., La Porta, N., 2017. Leaf Wetness Evaluation Using Artificial Neural Network for Improving Apple Scab Fight. *Environments* 4.<https://doi.org/10.3390/environments4020042>.
- Su, J.Y., Liu, C.J., Coombes, M., Hu, X.P., Wang, C.H., Xu, X.M., Li, Q.D., Guo, L., Chen, W.H., 2018. Wheat yellow rust monitoring by learning from multispectral UAV aerial imagery. *Comput. Electron. Agric.* 155, 157-166.<https://doi.org/10.1016/j.compag.2018.10.017>.
- Suarez, L., Zarco-Tejada, P.J., Gonzalez-Dugo, V., Berni, J.A.J., Sagardoy, R., Morales, F., Fereres, E., 2010. Detecting water stress effects on fruit quality in orchards with time-series PRI airborne imagery. *Remote Sensing of Environment* 114, 286-298.<https://doi.org/10.1016/j.rse.2009.09.006>.
- Sun, G.X., Wang, X.C., Ding, Y.Q., Lu, W., Sun, Y., 2019. Remote Measurement of Apple Orchard Canopy Information Using Unmanned Aerial Vehicle Photogrammetry. *Agronomy-Basel* 9.<https://doi.org/10.3390/agronomy9110774>.
- Sun, G.X., Wang, X.C., Yang, H.H., Zhang, X.J., 2020. A Canopy Information Measurement Method for Modern Standardized Apple Orchards Based on UAV Multimodal Information. *SENSORS* 20.<https://doi.org/10.3390/s20102985>.

References

- Sun, K., Wang, X., Liu, S., Liu, C., 2021. Apple, peach, and pear flower detection using semantic segmentation network and shape constraint level set. *Computers and Electronics in Agriculture* 185. <https://doi.org/10.1016/j.compag.2021.106150>.
- Suo, G.-D., Xie, Y.-S., Zhang, Y., Cai, M.-Y., Wang, X.-S., Chuai, J.-F., 2016. Crop load management (CLM) for sustainable apple production in China. *Scientia Horticulturae* 211, 213-219. <https://doi.org/https://doi.org/10.1016/j.scienta.2016.08.029>.
- Suo, G.-D., Xie, Y.-S., Zhang, Y., Luo, H., 2019. Long-term effects of different surface mulching techniques on soil water and fruit yield in an apple orchard on the Loess Plateau of China. *Scientia Horticulturae* 246, 643-651. <https://doi.org/10.1016/j.scienta.2018.11.028>.
- Tang, M.M., Sadowski, D.L., Peng, C., Vougioukas, S.G., Klever, B., Khalsa, S.D.S., Brown, P.H., Jin, Y.F., 2023. Tree-level almond yield estimation from high resolution aerial imagery with convolutional neural network. *Frontiers in Plant Science* 14. <https://doi.org/10.3389/fpls.2023.1070699>.
- Tang, Y., Hou, C.J., Luo, S.M., Lin, J.T., Yang, Z., Huang, W.F., 2018. Effects of operation height and tree shape on droplet deposition in citrus trees using an unmanned aerial vehicle. *Comput. Electron. Agric.* 148, 1-7. <https://doi.org/10.1016/j.compag.2018.02.026>.
- Teng, P.C., Zhang, Y., Yamane, T., Kogoshi, M., Yoshida, T., Ota, T., Nakagawa, J., 2023. Accuracy Evaluation and Branch Detection Method of 3D Modeling Using Backpack 3D Lidar SLAM and UAV-SfM for Peach Trees during the Pruning Period in Winter. *Remote Sensing* 15. <https://doi.org/10.3390/rs15020408>.
- Tian, G., Liu, J., Zhao, H., Yang, W., 2022. Small object detection via dual inspection mechanism for UAV visual images. *Applied Intelligence* 52, 4244-4257. <https://doi.org/10.1007/s10489-021-02512-1>.
- Tian, Y.N., Yang, G.D., Wang, Z., Li, E., Liang, Z.Z., 2020. Instance segmentation of apple flowers using the improved mask R-CNN model. *Biosystems Engineering* 193, 264-278. <https://doi.org/10.1016/j.biosystemseng.2020.03.008>.
- Torres-Sanchez, J., de Castro, A.I., Pena, J.M., Jimenez-Brenes, F.M., Arquero, O., Lovera, M., Lopez-Granados, F., 2018a. Mapping the 3D structure of almond trees using UAV acquired photogrammetric point clouds and object-based image analysis. *Biosystems Engineering* 176, 172-184. <https://doi.org/10.1016/j.biosystemseng.2018.10.018>.
- Torres-Sanchez, J., Lopez-Granados, F., Borra-Serrano, I., Pena, J.M., 2018b. Assessing UAV-collected image overlap influence on computation time and digital surface model accuracy in olive orchards. *Precis. Agric.* 19, 115-133. <https://doi.org/10.1007/s11119-017-9502-0>.
- Torres-Sanchez, J., Lopez-Granados, F., Serrano, N., Arquero, O., Pena, J.M., 2015. High-Throughput 3-D Monitoring of Agricultural-Tree Plantations with Unmanned Aerial Vehicle (UAV) Technology. *PLoS One* 10, e0130479. <https://doi.org/10.1371/journal.pone.0130479>.
- Torres-Sánchez, J., Mesas-Carrascosa, F.J., Santesteban, L.-G., Jiménez-Brenes, F.M., Oneka, O., Villallop, A., Loidi, M., López-Granados, F., 2021. Grape Cluster Detection Using UAV Photogrammetric Point Clouds as a Low-Cost Tool for Yield Forecasting in Vineyards. *Sensors* 21, 3083.
- Tsoulias, N., Paraforos, D.S., Xanthopoulos, G., Zude-Sasse, M., 2020. Apple Shape Detection Based on Geometric and Radiometric Features Using a LiDAR Laser Scanner. *Remote Sensing* 12. <https://doi.org/10.3390/rs12152481>.

- Tsoulias, N., Saha, K.K., Zude-Sasse, M., 2023. In-situ fruit analysis by means of LiDAR 3D point cloud of normalized difference vegetation index (NDVI). *Computers and Electronics in Agriculture* 205. <https://doi.org/10.1016/j.compag.2022.107611>.
- Tu, Y.-H., Phinn, S., Johansen, K., Robson, A., 2018. Assessing Radiometric Correction Approaches for Multi-Spectral UAS Imagery for Horticultural Applications. *Remote Sens.* 10. <https://doi.org/10.3390/rs10111684>.
- Tu, Y.H., Johansen, K., Phinn, S., Robson, A., 2019. Measuring Canopy Structure and Condition Using Multi-Spectral UAS Imagery in a Horticultural Environment. *Remote Sensing* 11. <https://doi.org/10.3390/rs11030269>.
- Tubau Comas, A., Valente, J., Kooistra, L., 2019. AUTOMATIC APPLE TREE BLOSSOM ESTIMATION FROM UAV RGB IMAGERY. *Int. Arch. Photogramm. Remote Sens. Spatial Inf. Sci. XLII-2/W13*, 631-635. <https://doi.org/10.5194/isprs-archives-XLII-2-W13-631-2019>.
- Underwood, J.P., Hung, C., Whelan, B., Sukkarieh, S., 2016. Mapping almond orchard canopy volume, flowers, fruit and yield using lidar and vision sensors. *Computers and Electronics in Agriculture* 130, 83-96. <https://doi.org/https://doi.org/10.1016/j.compag.2016.09.014>.
- Uribeetxebarria, A., Martínez-Casasnovas, J.A., Tisseyre, B., Guillaume, S., Escolà, A., Rosell-Polo, J.R., Arnó, J., 2019. Assessing ranked set sampling and ancillary data to improve fruit load estimates in peach orchards. *Comput. Electron. Agric.* 164. <https://doi.org/10.1016/j.compag.2019.104931>.
- Usha, K., Singh, B., 2013. Potential applications of remote sensing in horticulture—A review. *Scientia Horticulturae* 153, 71-83. <https://doi.org/10.1016/j.scienta.2013.01.008>.
- Valente, J., Almeida, R., Kooistra, L., 2019. A Comprehensive Study of the Potential Application of Flying Ethylene-Sensitive Sensors for Ripeness Detection in Apple Orchards. *Sensors (Basel)* 19. <https://doi.org/10.3390/s19020372>.
- Van Beek, J., Tits, L., Somers, B., Coppin, P., 2013. Stem Water Potential Monitoring in Pear Orchards through WorldView-2 Multispectral Imagery. *Remote Sensing* 5, 6647-6666. <https://doi.org/10.3390/rs5126647>.
- Van Beek, J., Tits, L., Somers, B., Deckers, T., Verjans, W., Bylemans, D., Janssens, P., Coppin, P., 2015. Temporal Dependency of Yield and Quality Estimation through Spectral Vegetation Indices in Pear Orchards, *Remote Sensing*, pp. 9886-9903. <https://doi.org/10.3390/rs70809886>.
- van der Wal, T., Abma, B., Viguria, A., Prévinaire, E., Zarco-Tejada, P.J., Serruys, P., van Valkengoed, E., van der Voet, P., 2013. *Fieldcopter: unmanned aerial systems for crop monitoring services*. Wageningen Academic Publishers, Wageningen, pp. 169-175.
- van Dijk, M., Morley, T., Rau, M.L., Saghai, Y., 2021. A meta-analysis of projected global food demand and population at risk of hunger for the period 2010–2050. *Nature Food* 2, 494-501. <https://doi.org/10.1038/s43016-021-00322-9>.
- Vanbrabant, Y., Delalieux, S., Tits, L., Pauly, K., Vandermaesen, J., Somers, B., 2020a. Pear Flower Cluster Quantification Using RGB Drone Imagery. *Agronomy-Basel* 10. <https://doi.org/10.3390/agronomy10030407>.
- Vanbrabant, Y., Delalieux, S., Tits, L., Pauly, K., Vandermaesen, J., Somers, B., 2020b. Pear Flower Cluster Quantification Using RGB Drone Imagery. *Agronomy* 10, 407.

References

- Vanbrabant, Y., Tits, L., Delalieux, S., Pauly, K., Verjans, W., Somers, B., 2019. Multitemporal Chlorophyll Mapping in Pome Fruit Orchards from Remotely Piloted Aircraft Systems. *Remote Sens.* 11. <https://doi.org/10.3390/rs11121468>.
- Vélez, S., Ariza-Sentís, M., Valente, J., 2023. Mapping the spatial variability of Botrytis bunch rot risk in vineyards using UAV multispectral imagery. *European Journal of Agronomy* 142, 126691.
- Verdouw, C., Tekinerdogan, B., Beulens, A., Wolfert, S., 2021. Digital twins in smart farming. *Agricultural Systems* 189, 103046. <https://doi.org/https://doi.org/10.1016/j.agry.2020.103046>.
- Vinci, A., Brigante, R., Traini, C., Farinelli, D., 2023. Geometrical Characterization of Hazelnut Trees in an Intensive Orchard by an Unmanned Aerial Vehicle (UAV) for Precision Agriculture Applications. *Remote Sensing* 15, 541.
- Vinci, A., Traini, C., Farinelli, D., Brigante, R., 2022. Assessment of the geometrical characteristics of hazelnut intensive orchard by an Unmanned Aerial Vehicle (UAV), 2022 IEEE Workshop on Metrology for Agriculture and Forestry (MetroAgriFor), pp. 218-222. <https://doi.org/10.1109/MetroAgriFor55389.2022.9964832>.
- Wang, C.L., Wang, Y.W., Liu, S.C., Lin, G.C., He, P., Zhang, Z.G., Zhou, Y., 2022. Study on Pear Flowers Detection Performance of YOLO-PEFL Model Trained With Synthetic Target Images. *Front. Plant Sci.* 13. <https://doi.org/10.3389/fpls.2022.911473>.
- Wang, D.D., He, D.J., 2021. Channel pruned YOLO V5s-based deep learning approach for rapid and accurate apple fruitlet detection before fruit thinning. *Biosystems Engineering* 210, 271-281. <https://doi.org/10.1016/j.biosystemseng.2021.08.015>.
- Wang, X., Tang, J., Whitty, M., 2020. Side-view apple flower mapping using edge-based fully convolutional networks for variable rate chemical thinning. *Computers and Electronics in Agriculture* 178. <https://doi.org/10.1016/j.compag.2020.105673>.
- Wang, X., Tang, J., Whitty, M., 2021a. DeepPhenology: Estimation of apple flower phenology distributions based on deep learning. *Computers and Electronics in Agriculture* 185. <https://doi.org/10.1016/j.compag.2021.106123>.
- Wang, X., Tang, J.L., Whitty, M., 2021b. DeepPhenology: Estimation of apple flower phenology distributions based on deep learning. *Computers and Electronics in Agriculture* 185, 15. <https://doi.org/10.1016/j.compag.2021.106123>.
- Wang, Z., Underwood, J., Walsh, K.B., 2018a. Machine vision assessment of mango orchard flowering. *Comput. Electron. Agric.* 151, 501-511. <https://doi.org/10.1016/j.compag.2018.06.040>.
- Wang, Z.L., Underwood, J., Walsh, K.B., 2018b. Machine vision assessment of mango orchard flowering. *Computers and Electronics in Agriculture* 151, 501-511. <https://doi.org/10.1016/j.compag.2018.06.040>.
- West, P., 2009. *Tree and forest measurement: 2nd edition*.
- Woodward, T.J., Clearwater, M.J., 2012. Spatial variation in 'Hayward' kiwifruit fruit size and orchard yield within a growing region across seasons. *New Zealand Journal of Crop and Horticultural Science* 40, 187-199. <https://doi.org/10.1080/01140671.2011.639377>.
- Wouters, N., De Ketelaere, B., Deckers, T., De Baerdemaeker, J., Saeys, W., 2015. Multispectral detection of floral buds for automated thinning of pear. *Computers and Electronics in Agriculture* 113, 93-103. <https://doi.org/10.1016/j.compag.2015.01.015>.

- Wu, D., Lv, S., Jiang, M., Song, H., 2020a. Using channel pruning-based YOLO v4 deep learning algorithm for the real-time and accurate detection of apple flowers in natural environments. *Computers and Electronics in Agriculture* 178. <https://doi.org/10.1016/j.compag.2020.105742>.
- Wu, J.T., Yang, G.J., Yang, H., Zhu, Y.H., Li, Z.H., Lei, L., Zhao, C.J., 2020b. Extracting apple tree crown information from remote imagery using deep learning. *COMPUTERS AND ELECTRONICS IN AGRICULTURE* 174. <https://doi.org/10.1016/j.compag.2020.105504>.
- Wulfsohn, D., Zamora, F.A., Tellez, C.P., Lagos, I.Z., Garcia-Finana, M., 2012. Multilevel systematic sampling to estimate total fruit number for yield forecasts. *Precision Agriculture* 13, 256-275. <https://doi.org/10.1007/s11119-011-9245-2>.
- Xia, X., Chai, X., Zhang, N., Sun, T., 2021. Visual classification of apple bud-types via attention-guided data enrichment network. *Computers and Electronics in Agriculture* 191, 106504. <https://doi.org/https://doi.org/10.1016/j.compag.2021.106504>.
- Xia, X., Chai, X.J., Zhang, N., Zhang, Z., Sun, Q.X., Sun, T., 2022. Culling Double Counting in Sequence Images for Fruit Yield Estimation. *Agronomy-Basel* 12. <https://doi.org/10.3390/agronomy12020440>.
- Xue, J., Fan, Y., Su, B., Fuentes, S., 2019. Assessment of canopy vigor information from kiwifruit plants based on a digital surface model from unmanned aerial vehicle imagery. *Int. J. Agric. Biol. Eng.* 12, 165-171. <https://doi.org/10.25165/j.ijabe.20191201.4634>.
- Yang, S., Hou, M., Li, S., 2023. Three-Dimensional Point Cloud Semantic Segmentation for Cultural Heritage: A Comprehensive Review. *Remote Sensing* 15, 548.
- Yu, T., Hu, C.H., Xie, Y.N., Liu, J.Z., Li, P.P., 2022. Mature pomegranate fruit detection and location combining improved F-PointNet with 3D point cloud clustering in orchard. *Computers and Electronics in Agriculture* 200. <https://doi.org/10.1016/j.compag.2022.107233>.
- Yuan, W., Choi, D., Bolkas, D., Heinemann, P.H., He, L., 2022. Sensitivity examination of YOLOv4 regarding test image distortion and training dataset attribute for apple flower bud classification. *International Journal of Remote Sensing* 43, 3106-3130.
- Yuan, W., Hua, W., Heinemann, P.H., He, L., 2023. UAV Photogrammetry-Based Apple Orchard Blossom Density Estimation and Mapping. *Horticulturae* 9, 266.
- Yuan, W.N., Choi, D., 2021. UAV-Based Heating Requirement Determination for Frost Management in Apple Orchard. *Remote Sensing* 13. <https://doi.org/10.3390/rs13020273>.
- Zarco-Tejada, P.J., Diaz-Varela, R., Angileri, V., Loudjani, P., 2014. Tree height quantification using very high resolution imagery acquired from an unmanned aerial vehicle (UAV) and automatic 3D photo-reconstruction methods. *European Journal of Agronomy* 55, 89-99. <https://doi.org/10.1016/j.eja.2014.01.004>.
- Zarco-Tejada, P.J., Gonzalez-Dugo, V., Berni, J.A.J., 2012. Fluorescence, temperature and narrow-band indices acquired from a UAV platform for water stress detection using a micro-hyperspectral imager and a thermal camera. *Remote Sens. Environ.* 117, 322-337. <https://doi.org/10.1016/j.rse.2011.10.007>.
- Zarco-Tejada, P.J., Morales, A., Testi, L., Villalobos, F.J., 2013. Spatio-temporal patterns of chlorophyll fluorescence and physiological and structural indices acquired from hyperspectral imagery as compared with carbon fluxes measured with eddy covariance. *Remote Sens. Environ.* 133, 102-115. <https://doi.org/10.1016/j.rse.2013.02.003>.

References

- Zhang, C., Kang, F., Wang, Y., 2022a. An Improved Apple Object Detection Method Based on Lightweight YOLOv4 in Complex Backgrounds. *Remote Sensing* 14, 4150.
- Zhang, C., Kovacs, J.M., 2012. The application of small unmanned aerial systems for precision agriculture: a review. *Precis. Agric.* 13, 693-712. <https://doi.org/10.1007/s11119-012-9274-5>.
- Zhang, C., Mouton, C., Valente, J., Kooistra, L., van Ooteghem, R., de Hoog, D., van Daltsen, P., Frans de Jong, P., 2022b. Automatic flower cluster estimation in apple orchards using aerial and ground based point clouds. *Biosystems Engineering* 221, 164-180. <https://doi.org/https://doi.org/10.1016/j.biosystemseng.2022.05.004>.
- Zhang, C., Valente, J., Kooistra, L., Guo, L., Wang, W., 2019a. Opportunities of uavs in orchard management. *The International Archives of Photogrammetry, Remote Sensing and Spatial Information Sciences* 42, 673-680.
- Zhang, C., Valente, J., Kooistra, L., Guo, L., Wang, W., 2019b. OPPORTUNITIES OF UAVS IN ORCHARD MANAGEMENT. *Int. Arch. Photogramm. Remote Sens. Spatial Inf. Sci.* XLII-2/W13, 673-680. <https://doi.org/10.5194/isprs-archives-XLII-2-W13-673-2019>.
- Zhang, C., Valente, J., Kooistra, L., Guo, L., Wang, W., 2021. Orchard management with small unmanned aerial vehicles: a survey of sensing and analysis approaches. *Precision Agriculture* 22, 2007-2052. <https://doi.org/10.1007/s11119-021-09813-y>.
- Zhang, C., Valente, J., van Daltsen, P., Kooistra, L., 2022c. Data on three-year flowering intensity monitoring in an apple orchard.
- Zhang, C., Valente, J., Wang, W., Guo, L., Tubau Comas, A., van Daltsen, P., Rijk, B., Kooistra, L., 2023. Feasibility assessment of tree-level flower intensity quantification from UAV RGB imagery: A triennial study in an apple orchard. *ISPRS Journal of Photogrammetry and Remote Sensing* 197, 256-273. <https://doi.org/https://doi.org/10.1016/j.isprsjprs.2023.02.003>.
- Zhang, C.J., Yang, G.J., Jiang, Y.Y., Xu, B., Li, X., Zhu, Y.H., Lei, L., Chen, R.Q., Dong, Z., Yang, H., 2020a. Apple Tree Branch Information Extraction from Terrestrial Laser Scanning and Backpack-LiDAR. *Remote Sensing* 12. <https://doi.org/10.3390/rs12213592>.
- Zhang, C.Y., Craine, W.A., McGee, R.J., Vandemark, G.J., Davis, J.B., Brown, J., Hulbert, S.H., Sankaran, S., 2020b. Image-Based Phenotyping of Flowering Intensity in Cool-Season Crops. *Sensors* 20. <https://doi.org/10.3390/s20051450>.
- Zhang, P., Deng, L., Lyu, Q., He, S.L., Yi, S.L., Liu, Y., Yu, Y.X., Pan, H.Y., 2016. Effects of citrus tree-shape and spraying height of small unmanned aerial vehicle on droplet distribution. 9, 45-52. <https://doi.org/10.3965/j.ijabe.20160904.2178>.
- Zhang, P., Wang, K.J., Lyu, Q., He, S.L., Yi, S.L., Xie, R.J., Zheng, Y.Q., Ma, Y.Y., Deng, L., 2017. DROPLET DISTRIBUTION AND CONTROL AGAINST CITRUS LEAFMINER WITH UAV SPRAYING. *Int. J. Robot. Autom.* 32, 299-307. <https://doi.org/10.2316/Journal.206.2017.3.206-4980>.
- Zhang, Y.C., Zhang, W.B., Yu, J.Y., He, L.Y., Chen, J.N., He, Y., 2022d. Complete and accurate holly fruits counting using YOLOX object detection. *COMPUTERS AND ELECTRONICS IN AGRICULTURE* 198. <https://doi.org/10.1016/j.compag.2022.107062>.
- Zhao, G., Yang, R., Jing, X., Zhang, H., Wu, Z., Sun, X., Jiang, H., Li, R., Wei, X., Fountas, S., Zhang, H., Fu, L., 2023a. Phenotyping of individual apple tree in modern orchard with novel smartphone-based heterogeneous binocular vision and YOLOv5s. *Computers and Electronics in Agriculture* 209, 107814. <https://doi.org/https://doi.org/10.1016/j.compag.2023.107814>.

- Zhao, G.A., Yang, R.Z., Jing, X.D., Zhang, H.S., Wu, Z.C., Sun, X.M., Jiang, H.H., Li, R., Wei, X.F., Fountas, S., Zhang, H.J., Fu, L.S., 2023b. Phenotyping of individual apple tree in modern orchard with novel smartphone-based heterogeneous binocular vision and YOLOv5s. *Computers and Electronics in Agriculture* 209. <https://doi.org/10.1016/j.compag.2023.107814>.
- Zhao, T.B., Stark, B., Chen, Y.Q., Ray, A.L., Doll, D., 2017. Challenges in Water Stress Quantification Using Small Unmanned Aerial System (sUAS): Lessons from a Growing Season of Almond. *Journal of Intelligent & Robotic Systems* 88, 721-735. <https://doi.org/10.1007/s10846-017-0513-x>.
- Zhao, X.K., Li, H., Zhu, Q.B., Huang, M., Guo, Y., Qin, J.W., 2020. Automatic sweet pepper detection based on point cloud images using subtractive clustering. *International Journal of Agricultural and Biological Engineering* 13, 154-160. <https://doi.org/10.25165/j.ijabe.20201303.5460>.
- Zhen, Z., Quackenbush, L.J., Zhang, L., 2016. Trends in Automatic Individual Tree Crown Detection and Delineation—Evolution of LiDAR Data. *Remote Sensing* 8, 333.
- Zheng, C.W., Abd-Elrahman, A., Whitaker, V.M., Dalid, C., 2022. Deep Learning for Strawberry Canopy Delineation and Biomass Prediction from High-Resolution Images. *Plant Phenomics* 2022. <https://doi.org/10.34133/2022/9850486>.
- Zhou, R., Damerow, L., Sun, Y., Blanke, M.M., 2012. Using colour features of cv. ‘Gala’ apple fruits in an orchard in image processing to predict yield. *Precision Agriculture* 13, 568-580. <https://doi.org/10.1007/s11119-012-9269-2>.
- Zhou, X., Sun, G., Xu, N., Zhang, X., Cai, J., Yuan, Y., Huang, Y., 2023. A Method of Modern Standardized Apple Orchard Flowering Monitoring Based on S-YOLO. *Agriculture* 13, 380.
- Zhu, Y., Yang, G., Yang, H., Zhao, F., Han, S., Chen, R., Zhang, C., Yang, X., Liu, M., Cheng, J., Zhao, C., 2021. Estimation of Apple Flowering Frost Loss for Fruit Yield Based on Gridded Meteorological and Remote Sensing Data in Luochuan, Shaanxi Province, China. *Remote Sensing* 13. <https://doi.org/10.3390/rs13091630>.
- Zhu, Y.H., Yang, G.J., Yang, H., Wu, J.T., Lei, L., Zhao, F., Fan, L.L., Zhao, C.J., 2020. Identification of Apple Orchard Planting Year Based on Spatiotemporally Fused Satellite Images and Clustering Analysis of Foliage Phenophase. *Remote Sensing* 12. <https://doi.org/10.3390/rs12071199>.
- Zine-El-Abidine, M., Dutagaci, H., Galopin, G., Rousseau, D., 2021. Assigning apples to individual trees in dense orchards using 3D colour point clouds. *Biosystems Engineering* 209, 30-52. <https://doi.org/10.1016/j.biosystemseng.2021.06.015>.
- Zou, R., Zhang, Y., Chen, J., Li, J.Y., Dai, W.J., Mu, S.L., 2023. Density estimation method of mature wheat based on point cloud segmentation and clustering. *Computers and Electronics in Agriculture* 205. <https://doi.org/10.1016/j.compag.2023.107626>.

A large, white, stylized letter 'S' is centered on a dark, textured, splattered background. The background consists of various shades of gray and black, with a rough, ink-splattered appearance. The letter 'S' is a simple, clean, sans-serif font. The overall composition is high-contrast and abstract.

Summary

Orchards oblige site-specific management throughout the entire growing season of fruit crops, from flowering, fruitlet development, ripening and harvest, to tree dormancy period. This precision management is essential for agricultural production enhancement and environmental impact mitigation. Advances in sensor miniaturization are increasing the global popularity of unmanned aerial vehicles (UAVs) in various agricultural applications. Existing research recognizes the critical role played by UAVs in orchard management, i.e., water stress monitoring and geometric traits measurement. Yet, these studies are limited with regard to crop load estimation. Crop load in orchards generally comprises flowers and mature fruits of fruit trees. Estimation of flowering intensity for individual trees directs growers to regulate crop load precisely during flower thinning. It aids chemical usage optimization and manual labor reduction. While yield estimation in orchards directly benefits market strategy making and logistics optimization, such as labor force, harvest containers and gathering path. Limited studies applied conventional UAV photogrammetry techniques that are based on structure from motion (SfM) in crop load estimation. They are generally resource consuming and the performance is unsatisfactory. Crop load estimation directly derived from 2-dimensional images overall is efficient and accurate. Recent advancement has proven the superiority of computer vision in flower or fruit detection at image level. Such approaches, however, only recognize how many flowers or fruits are visible in images. The link between the fine detections from images and the exact number of flowers or fruits in trees is not built up. Faced with problems identified above, the main research objectives of present thesis are: (1) examining the feasibility of crop load estimation in orchards with single raw UAV RGB images (2) identifying the distinctions of crop load estimation based on single UAV RGB images to the estimation emanates from SfM-derived methods.

First, current status of UAV-derived practice in orchard management was reviewed, to examine the potential technologies of UAVs. Chapter 2 provides a comprehensive literature review focused on achievements to date and shortcomings to be addressed. Sensing system architecture focusing on UAVs and sensors was summarized. Then up-to-date applications supported by UAVs were described, focusing on the diversity of data-processing techniques, monitoring efficiency and accuracy. Results showed that UAV derived orchard management (UAV-OM) is yet in its infancy. One limitation is the flying time due to current accomplishment in battery capacity. Multi-sensor data fusion could be promising in practice. However, it was not yet investigated. Statistical study to determine the optimal data acquisition parameters and understand their effects for specific research is encouraged. Applications for resource efficiency and geometric traits are relatively mature. High correlations between various UAV-derived indices and target physiological traits measured manually were observed. Yet model generalization, data processing efficiency and automation are still challenging. The

Summary

combination of artificial intelligence and remote sensing sciences is expected to close these research gaps. Crop load estimation, especially the estimation at tree level, will become an increasingly important area.

As a benchmark, the performance of conventional UAV photogrammetry method based on colored point clouds in crop load estimation was evaluated (Chapter 3). Apple flowering intensity estimation was taken as a case study. The potential of UAV-derived point clouds was first examined. Its performance was compared with ground vehicle-derived point clouds. To improve flowering intensity estimation accuracy, a framework combining UAV and ground-based RGB image data was proposed. It is based on SfM, and presents automatic point cloud handling techniques as well as automated unsupervised flowering intensity estimation methods. Two linear regression models based on unsupervised machine learning methods were trained and validated from the framework. Predicting flowering intensity in the orchard with both models having $R^2 > 0.65$, $RRMSE < 20\%$ and $p\text{-stat} < 0.005$ for the correlation between the image-derived flower index and the flower cluster number counted in field. It provides a novel strategy for guiding flower thinning using UAV imagery and location data. Moreover, the proposed methods also reveal the flexibility of intra-tree inspection by checking its sub-volumes.

Chapter 4 examines the feasibility of crop load estimation with single raw aerial images. It also focused on flowering intensity estimation aiming at a complete comparison with the benchmark solution that is based on colored point clouds. In three consecutive years, starting from 2018 to 2020, high-resolution UAV images of apple flowering trees and in-field ground truth (GT) data were collected. Flower-associated pixels were first extracted for individual trees using a pixel-based classification method, the color thresholding. Next, three flowering indices retrieved from UAV were evaluated, the index percentage (IPG), index pixel (IP), and index area (IA). Finally, linear correlation of the flowering indices to flower cluster number and expert-assessed floridity recorded in the field were calculated. Results indicated that IPG yielded the highest correlation to flower cluster ($R^2 = 0.93$, $RMSE = 8$) and floridity estimation ($R^2 = 0.78$, $RMSE = 0.9$). A UAV-based floridity scoring method was also designed for automatic estimation tasks in practice, and a comparable and even better performance to the expert-based approach was demonstrated. Furthermore, effects of vertical (nadir) and horizontal (angular) overlapping of flower clusters within the canopy were evaluated, showing excellent capacity to improve the estimation accuracy. Obtained results reveal the potential of single raw UAV RGB images in crop load estimation. Skipping conventional labor-intensive photogrammetric method, i.e., SfM, proposed framework outperforms the benchmark solution in terms of both accuracy and efficiency.

Chapter 5 further evaluates the performance of single raw UAV RGB images in crop load estimation for the other scenario, yield estimation at tree level. In three consecutive years (starting from 2018), UAV images and in-field GT data were collected during the harvest period of apples. First, a lightweight

YOLOv5s model was trained and validated to detect and count apples in original aerial images. Detected apples were delineated with bounding boxes and center-pixel positions of the bounding boxes in the image were treated as apple positions. Next, an automatic resourceless photogrammetric approach was designed for linking the detected apples with the trees they belong to: (1) GPS positions of all the trees in the orchard were first predicted basing on pre-measured positions of trees locate at the four corners of the orchard. (2) GPS positions of image-projected area corners were calculated by a great-circle-based method where metadata of the image was fed as inputs. With these first two steps, apple trees within the projected area were identified. (3) all the pixels in the image were registered in the real-world coordinate using a coordinate convert method proposed in this study. Based on output of Step 3 and positions of the trees that are covered by the image (in the projected area), image pixels that can represent these covered trees are recognized. (4) Finally, detected apples were assigned to individual trees employing the predicted tree positions in photo coordinates. Apple detection results showed that YOLOv5s is capable of small object detection in aerial images. Complex illumination conditions, high occlusion levels, and small and dense recognition apples prevail in UAV images. It revealed that these challenging image features enable YOLOv5s trained with aerial images more generalized when cross-test was conducted over different datasets. In addition, proposed apple tree localization method yielded a high accuracy in apple tree counting. The localization performance exhibits spatial variations across the whole image. It demonstrated the great potential of single raw UAV images in automatic tree-level apple yield estimation.

Chapter 6 provides a synthesis of the present thesis which reveals that: (1) UAV-derived orchard management is still in its infancy with certain application scenarios that need to be explored, a robust generalized model is drawing more attention; (2) It is feasible to estimate apple flowering intensity at tree level with single UAV RGB images while the effects of vertical (nadir) and horizontal (angular) overlapping need to be held in mind; (3) It is practicable to geo-locate computer vision-derived object detections with single UAV RGB images and to further achieve apple yield estimation at tree level.

A

Acknowledgments

Time flies over individuals, but leaves luxuriant shadows behind.

I am grateful for the supervision of my PhD project from my promotor, Lammert. Thank you so much for the guidance over both work and life. Starting from English writing to research-plan making, to results analysis, and to scientific article preparation, you showed me the way of fishing rather than providing the fish directly. I appreciate your professional skills and patience, and I am more confident in becoming an independent researcher. Thank you. I shared with you the definition of a supervisor or teacher. Your actions proved the correctness of that. I feel honored by the attention and time you have dedicated to helping me balance work and life. Thanks for the walk in the snow and the agricultural activities in the garden! Such a nice memory! I am so lucky that you will still be there in the upcoming postdoctoral journey! Let us enjoy it!

Good morning, Prof. Wang, thank you for the support towards my PhD study. It is a pity that you could not be around in the past years which makes you a virtual promotor. But your scientific suggestions and words on how to arrange things in life guide me. You showed me the basic characteristics of being a researcher. It empowers me to start and accomplish my PhD project. You gave me full trust and freedom to conduct the research which raised me a lot. You always stand at my side to consider things. Your understanding surprises me! I am so appreciate it. Hope to see you during my defense. Take care!

Next, I give thanks to my co-promoters, Joao and Leifeng. You are really a fresh-air producer, Joao. There are always innovative ideas from your side which inspires me. With these suggestions, I observed improvements in my research quality. Thanks. And thank you for the help with data collection and data analysis. Leifeng, though you are busy with your research, your attention to my study is appreciative.

Claudius, I regard you as a fake promotor in my supervision team. In the aspects of both work and life, you are my strong backing. Your experience in PhD management makes my study more efficient. Tips given by you were stored well in my mind. As a good friend, with your help, you cannot imagine how easy my life in holland has become. You are my emergency contact person ha! Too much to write down on your role in me. I am so lucky to have you. Xiaoqian, thanks for your trust and support as a sister. Aren't you surprised how quickly we became good friends beyond friendship? Thanks for your endless attention. I wish to have more dumplings from you! Let us enjoy the new life of we three, starting in 2023, together with Claudius.

Acknowledgments

Next, I appreciate the support of Mingjun, Zhang. Your efforts to the PhD in CAAS program can not be ignored. Thank you for your honest and direct suggestions. You fully stand at our sides to arrange things. Thank you. You are the one! Prof. Dazhou Zhu, thank you for your supervision during my master study in CAAS and the guidance during my PhD study. You showed me your attitude towards science which affects me so much. And because of this, I decided to do a PhD. At this moment, I think you agree with this decision already, haha. Knowledge from you supports me throughout the whole academy journey. Making real contributions to science has become my principle as well. Thank you! Lingang Lu, thanks for your help with the arrangement at the beginning of my PhD. It is Lin and you make me confident to face difficulties in life. Hope to see you in one year. Jiazhang Huang, thank you for your trust and the recommendation for doing a CAAS PhD. Though I did not go that way, I appreciate your understanding. Xiaohong Wang, thank you for helping me with the introduction to the development of Chinese pasture. Xiaocui, thank you for your support from AII side. Daily financial management is boring, yet, you are always patient to help me!

Ground truth collection in the field costs time. Thank Pieter for helping me with this data. Though you are always busy, work related to my PhD study was always well arranged. I appreciate your efforts, thank you. In addition, I like to give my thanks to the MSc students I supervised, Tiaan, Stefan, Haris and Lars. You showed me many interesting ideas and highlighted the importance of communication.

Colleagues are companions in the long journey of a career. I am lucky to have you in GRS. Thank you for the funny talks by our coffee machine. Yes, the talks were with you: Aldo, Sytze, Jan, Lukasz, Ron, Marcello, Hilmy, Ron, Na, Panpan, Na Wang, Ilan, Alex, Karimon, Quanxing and Anne-juul. But I still hold my opinion that Harm speaks the fastest English. Filling out forms is always challenging for a PhD candidate. Thank you for your patience and detailed introduction, Antoinette, Gerlinde and Truus. I really appreciate your efforts to the group, it is like a lubricant. Martin, thank you for the help at the beginning of my PhD. I really enjoyed the lunchtime when Devis and you were there. Thank Kirsten and Alexander for the new air to the group. I appreciate our lunch and birthday cake culture, let us keep it. You are always there, for a relaxing lunch talk, thank you: Johannes, Nandika, Alemu, Layla, Natalla, Arno and Sietse. You came less, Ximena. Bart, we should go to the Eastern Express more. Alvaro, we should organize the next dumpling party. Thank you for your accompany, Yaowu, Zhen and Kaiwen. Yaowu, thank you for your various noodles making. Thank the nice drinks from Huahua. Mecki, I am so happy for your success in quitting the thing starting with the English letter c. Frida, Onder de Linden, I will be in the next time, I promise. Dainius, thanks a lot! You helped me a lot! Daniela, you know, I can always ask you when things are not clear to me, thank you. Robert and Diego, thank you for your help with deep learning, my appointments with you pop up randomly. Hasib, thanks for your introduction of how the GPS works in drone, and your time during the knowledge transfer period. Andrei and Sabina, thanks for the time in Romania, I had a great time there, all the best! Sebastian, to

be honest, I prefer the fried bananas to the mushrooms from the East. Thank you bro. Deborah, I am so thankful for the nice food, we three always have a good time. Thank you for your texts. Julia, nice to meet you. Jens, thanks for the nice time, the nice time, and hope you achieve the goal of quitting something before 30. Magdalena, thanks for boarding my ship, let us go to the sea. Thanks for listening to my random thoughts.

Friends constantly assist your work in an indirect way. Siyuan, *caiji*, thank you. There should be some words for you, but it is not suitable for the public. Stefanie, you are my first Dutch friend. Thank you for designing and painting the thesis cover. Cheers for our friendship which is already more than 5 years. Sander and Meng, what to say, thank you for our gathering time which is always nice, nice food, nice talk, thank you. You and Wouter, thank you for the nice time, let us have more fun with Tesla. Mink, t man, thank you for your always online, let us see how to deal with Nijmegen. Thanks for the story of Asserpark, Anna, Nikki and Shassy, thank you for the hotpot time, we should go out of holland. Thank Hang Zhou, for the help with thesis cover editing, look forward to meeting you in UK. Yaoyao Wang, thanks for your personal time, during and after your graduation. Zulin and Chengcheng, I am curious about how much you won from me in card games, thanks for the regular meet-ups. Thank you Xiaxia, for helping me with language learning and culture understanding. Li Kang and Daoyuan, thank you for the 10 packages, I like our relaxing time. Barbara, thank you for the lovely time we spent together, all the best. Jiaqi, good luck with the next. Thank you for the support, Yifan, Xiulu and Fang, it is an interesting story. Qian Li, thank you for the introduction and arrangement at the beginning of my PhD study, honestly, you did a lot, thank you. Marcio, thank you for the time in 2019, please, come back and finish your PhD. Thank you, the friends in CAAS program, Jianing, Moyong, Zhenbiao, Mingzhu, Mengshuai, Qitong and Xiangxiao. Teacher Wang, Yi Wang, thank you for your help with our shared student room and the bed moving. Thanks for the summer holiday gifts, Haozhou, thanks for your greetings. Yongan Jian, long time no see, thank you for your accompany, see you in Taiwan or Beijing, let us see.

There are also close friends and families who live far from you. Thank you for the calls that popped up during any time of a day. Huaidong, thanks for your crazy words and actions, for your drunk calls. Thanks for the support from Shaoshuai, Jue, Fuyu. Thank you, the big brother, Zhen, your experience shared with me makes my life easier. Thank you for the laptop from Aoxuan, and thank you for the greetings from Xueying. Hongyu, how is life? Thank you for the trust, Bing, Saner. Thank my sister, Nuan, for your attention and help in assisting my study! Thank for the Wechat calls, Wei!

The words should be placed at the beginning, to my parents:

“感谢爹娘坚强的后盾！

感谢您们理解与支持！

感谢您们无闻的付出！

感恩您们陪伴与分享！”

About the author



Chenglong Zhang was born in 1992 in Jilin, Jilin province, China. The hometown is mountainous and is with fresh air. In 2003, he moved to North China, Daqing, Heilongjiang province. During the study in high school, physics and chemistry became his preferred domains. Meanwhile, history, literature and philosophy also call his attention.

Chenglong started a Bachelor of Agricultural Electrification and Automation at Heilongjiang Bayi Agricultural University in 2011. Following his interests in physics, circuit design and automatic control technology were his main focus during the bachelor study. His bachelor thesis topic is *an automatic packaging system for food production*. An automatic system was designed at theory level with programmable logic controller. It was also during that period, he started the use of Matlab.

His MSc study was conducted at the Institute of Food and Nutrition Development, Ministry of Agriculture which is located in Beijing, in 2015. Machine vision was new and quickly aroused his interest in learning. His MSc project was about *the fast detection of worms inside vegetable soybeans*. With the supervision of Prof. Dazhou Zhu, the use of conventional morphology features helped him achieve the detection tasks. Though the obtained results were fine, he knew the complete workflow of a machine vision-based solution. In the last year of his MSc study, he published his first scientific article which was written in Chinese.

After finishing the MSc, in 2018, he started his journey of doing a PhD study at Wageningen University & Research in the Netherlands. His PhD project was also the application of machine vision, and computer vision technology in agriculture. The main difference is that the RGB camera was equipped with a drone in the sky rather than the camera set in the laboratory. He has been developing multidisciplinary research projects involving information visualization and deep learning. Sustainable agriculture and friendly environmental monitoring are his current research focus. With the experience of UAVs, he likes to apply advanced remote sensing technology to further enhance the development in these two fields.

Peer-reviewed Journal Publications

- Zhang, C., Mouton, C., Valente, J., Kooistra, L., van Ooteghem, R., de Hoog, D., van Daltsen, P., Frans de Jong, P., 2022. Automatic flower cluster estimation in apple orchards using aerial and ground based point clouds. *Biosystems Engineering* 221, 164-180.
- Zhang, C., Valente, J., Kooistra, L., Guo, L., Wang, W., 2021. Orchard management with small unmanned aerial vehicles: A survey of sensing and analysis approaches. *Precision Agriculture* 22, 2007-2052.
- Zhang, C., Valente, J., Wang, W., Guo, L., Tubau Comas, A., van Daltsen, P., Rijk, B., Kooistra, L., 2023a. Feasibility assessment of tree-level flower intensity quantification from UAV RGB imagery: A triennial study in an apple orchard. *ISPRS Journal of Photogrammetry and Remote Sensing* 197, 256-273.
- Zhang, C., Valente, J., Wang, W., van Daltsen, P., de Jong, P.F., Rijk, B., Kooistra, L., 2023b. Data on three-year flowering intensity monitoring in an apple orchard: A collection of RGB images acquired from unmanned aerial vehicles. *Data in Brief* 49, 109356.

Other scientific Publications

- Zhang, C., Valente, J., Kooistra, L., Guo, L., Wang, W., 2019. Opportunities of uavs in orchard management. *The International Archives of Photogrammetry, Remote Sensing and Spatial Information Sciences* 42, 673-680.

PE&RC Training and Education Statement

With the training and education activities listed below the PhD candidate has complied with the requirements set by the C.T. de Wit Graduate School for Production Ecology and Resource Conservation (PE&RC) which comprises of a minimum total of 32 ECTS (= 22 weeks of activities)



Review/project proposal (9 ECTS)

- Orchard management with small unmanned aerial vehicles: A survey of sensing and analysis approaches
- Spatial and temporal yield estimation and prediction for orchard management using high-resolution UAV- based imagery technology

Post-graduate courses (4.5 ECTS)

- GIS in practice; PE&RC (2019)
- Neural networks and deep learning; DeepLearning.AI (2021)

Deficiency, refresh, brush-up courses (3 ECTS)

- Advanced earth observation; GRS-WUR (2019)

Competence strengthening/skills courses (6.3 ECTS)

- Efficient and effective academic development; China; PE&RC (2018)
- Scientific writing; WGS (2019)
- Project and time management; WGS (2019)

PE&RC Annual meetings, seminars and the PE&RC weekend (2.7 ECTS)

- PE&RC Weekend for first years (2019)
- PE&RC Day (2019, 2022)
- PE&RC Weekend for midterm years (2021)
- PE&RC Weekend for last years (2022)

Discussion groups/local seminars or scientific meetings (6 ECTS)

- Remote sensing thematic group meeting (2019/2023)
- Agro-food robotics platform (2019/2023)
- INF Lunch seminar (2020/2023)

International symposia, workshops and conferences (8.9 ECTS)

- UAV-g Unmanned aerial vehicles in geometrics; Enschede, the Netherlands (2019)
- NCG Symposium; Wageningen, the Netherlands (2022)
- 40th EARSel; Wageningen, the Netherlands (2021)
- 41th EARSel; Paphos, Cyprus (2022)
- 42th EARSel; Bucharest, Romania (2023)

BSc/MSc thesis supervision (3 ECTS)

- Stepping towards real-time detection and tracking of apples using deep learning
- Counting apples: deep learning-based fruit yield estimation from high-resolution UAV imagery
- Developing a deep learning algorithm that optimizes orchard apple detection in UAV-acquired RGB images

The research described in this thesis was financially supported by the SPECTORS project [grant number 143081] in the Netherlands, which is funded by the European cooperation program INTERREG Deutschland-Nederland. The work has partially been funded by the Wageningen University – Chinese Academy of Agricultural Sciences joint Ph.D. Programme.

Financial support from Wageningen University for printing this thesis is gratefully acknowledged.

Cover design by Stefanie Hulst & Hang Zhou

